Processing and Formulation Insights for Designing Quality into Lyophilised Biopharmaceuticals

By Karen E. Beech

Thesis submitted to the University of Nottingham
for the degree of Doctor of Philosophy

July 2015

Abstract

This thesis makes an original contribution to the field of formulation development by providing new experimental data and insights into the effect of processing and formulation conditions on the quality of lyophilised biopharmaceuticals.

The quality attributes of lyophilised products include: a quick reconstitution time, product elegance and protein stability, which are known to be affected by processing and formulation parameters. However, choice of formulation excipients or processing conditions often relies on previous experience rather than mechanistic insight. The motivation of this thesis was therefore to provide a greater understanding of how process variables and excipient choice affect these quality attributes.

Bovine serum albumin (BSA) and immunoglobulin G (IgG) were used as model proteins to investigate formulation conditions, which included the excipient, the lyophilisation cooling profile and duration of the annealing step. BSA was also used as a model protein to explore the effects of sucrose and arginine as lyoprotectants. Unique to this study was the investigation of arginine salts as lyoprotectants, wherein the counterions were dicarboxylic acids with increasing chain length.

Two key results regarding quality attributes were observed. Firstly, characterisation of the lyophilised structure established that there was an optimal annealing time, beyond which there was an increase in primary drying time, batch heterogeneity and variable moisture content. Secondly, a relationship was found between decreasing dicarboxylic acid chain length and improved protein stability.

To explain these findings, two mechanisms are proposed that account for ice crystal growth during annealing and the observed changes in protein stability at the molecular level. Significantly, this research provides insights for future formulation development studies.

Acknowledgements

I would like to express my gratitude and thanks to my academic supervisors, Stephanie Allen and Jonathan Burley, for their support and advice throughout my PhD project. I would also like to thank my industrial supervisors, Jamie Biddlecombe and Chris van der Walle, for all their advice, as well as their time and patience while I was working in MedImmune, Cambridge.

I would like to thank Lee Stevens in Chemical Engineering for all his help throughout my PhD with the nitrogen adsorption isotherms and mercury intrusion porosimeter. Also, I would like to thank Sean Rigby for his input throughout the project.

A special thanks goes to Mahammad (Mo) Ahmed in MedImmune for all his help with the freeze dryers, Karl Fisher, MFI, DLS and freeze drying microscope stage. Without his patience I would probably not have half the experimental work that I do today. At MedImmune I would also like to thank the Formulation Sciences Team, especially Shahid Uddin, and the do Ó brothers, Nuno and Joao, for all their help.

My appreciation and gratitude goes to Andrea Domingues Gonçalves for all her help throughout my PhD. Her support and advice have been invaluable and I thank her for all the time she has spent helping me with my project.

My gratitude goes to the Nottingham Nanotechnology and Nanoscience Centre (NNNC) for access to the confocal Raman microscope and to Martin Corfield in the Faculty of Engineering for running the samples on the Micro-CT.

A big thank you goes to the Boots Science Building technicians Paul Cooling, Christy Grainger-Boultby and Tom Booth for all their help with training and equipment. I would also like to thank Keith Dinsdale in the Wolfson building for his help with the mercury porosimeter and DMA, which allowed me to complete my work in the last few months of my PhD despite

their heavy use.

I would like to thank Aalae Alkhalil and Andrew Megarry for their advice during the start of my PhD and also Delyan Ivanov for his help with ImageJ. I would also like to thank my friends at university especially Vanessa Loczenski, Yewande Oni, Arran Basra, Hiteshri Makwana and Gabrielle Milson for their friendship and support.

Finally, I would like to thank everyone in the LBSA and the Targeted Therapeutics CDT, especially Claudia Matz and Cameron Alexander, for their support and encouragement. I would also like to acknowledge AstraZeneca and the EPSRC (grant EP/D501849/1) for their financial support for this project.

This thesis is dedicated to Matthew Alvey and my family for their unconditional love and support. Thank you.

Contents

Abstract i
Acknowledgements iii
Contents v
List of Figures viii
List of Tables xi
List of Abbreviations xiii

1 Introduction 1
1.1 The lyophilisation process . . . 3
1.1.1 Instrumentation . . . 4
1.1.2 The freezing step . . . 6
1.1.3 Modifications to the freezing step . . . 8
1.1.4 Primary and secondary drying . . . 12
1.2 Protein structure and stability . . . 18
1.2.1 The three-dimensional structure of proteins . . . 18
1.2.2 Stresses created during lyophilisation . . . 22
1.2.3 Maintaining protein stability . . . 24
1.3 A Quality by design approach . . . 30

2 Thesis Aims and Objectives 33
3 Instrumental Methods 35
3.1 Determining formulation properties . . . 36
3.1.1 Differential Scanning Calorimetry (DSC) . . . 36
3.1.2 Freeze drying microscopy . . . 38
3.2 Solid state characterisation . . . 40
3.2.1 Karl Fisher titration . . . 40
3.2.2 X-ray powder diffraction (XRPD) . . . 42
3.2.3 Dynamic mechanical analysis (DMA) . . . 43
3.3 Physical characterisation . . . 46
3.3.1 Inspection of lyophilised cakes . . . 46
3.3.2 Scanning electron microscopy (SEM) . . . 47
3.3.3 Gas adsorption isotherms . . . 48
3.3.4 Mercury intrusion porosimetry (MIP) . . . 54
3.3.5 X-ray microtomography (Micro-CT) . . . 57

3.4 Characterising protein aggregates 60
3.4.1 IR and Raman spectroscopy 60
3.4.2 Size exclusion chromatography (SEC) 64
3.4.3 Micro-Flow Imaging (MFI) 66

4 Insights into the Influence of the Cooling Profile on the Reconstitution Times of Lyophilised Protein Formulations 69
4.1 Introduction 71
4.1.1 The influence of the cooling profile on reconstitution time 73
4.1.2 Sucrose as a lyoprotectant 74
4.1.3 Model proteins 75
4.1.4 Chapter motivation 77
4.2 Materials and Methods 79
4.2.1 Materials 79
4.2.2 Methods 79
4.3 Results 85
4.3.1 Tg′, Tc and product collapse 85
4.3.2 Reconstitution time 88
4.3.3 Cake structure 90
4.3.4 Secondary structure analysis by FTIR 98
4.4 Discussion 102
4.4.1 Influence of protein concentration on reconstitution time 104
4.4.2 Influence of cake structure on reconstitution time . . 105
4.5 Conclusions 109

5 Insights into the Influence of Annealing Duration and Formulation on Lyophilised Protein Cake Structural Properties 111
5.1 Introduction 113
5.1.1 Properties of the cake structure 113
5.1.2 Improving excipient diversity through arginine salts . 114
5.1.3 Dicarboxylic acids as arginine counterions 115
5.1.4 Chapter motivation 120
5.2 Materials and Methods 121
5.2.1 Materials 121
5.2.2 Methods 121
5.3 Results 125
5.3.1 Notes on manufacture 125
5.3.2 Primary drying time and moisture content 126
5.3.3 Cake appearance and solid state characterisation . . 130
5.3.4 Cake surface area and bulk density measurements . . 135

5.3.5 Pore size and distribution . . . 138
5.3.6 Reconstitution time . . . 148
5.3.7 Cake properties of mAb1 . . . 149
5.4 Discussion . . . 151
5.4.1 Arginine-dicarboxylic acids as excipients . . . 151
5.4.2 Proposed mechanism for ice crystal growth during annealing . . . 152
5.5 Conclusion . . . 158

6 Insights into the Influence of the Annealing Duration and Formulation on Lyophilised Protein Stability 161
6.1 Introduction . . . 163
6.1.1 The formation of protein aggregates . . . 163
6.1.2 Protein stability in sucrose and arginine formulations 165
6.1.3 Chapter motivation . . . 168
6.2 Materials and methods . . . 170
6.2.1 Materials . . . 170
6.2.2 Methods . . . 170
6.3 Results . . . 175
6.3.1 Soluble aggregates . . . 175
6.3.2 Subvisible particles (SVP) . . . 179
6.3.3 Visible particles . . . 182
6.3.4 Protein conformational changes . . . 183
6.3.5 Phase separation using Raman spectroscopy . . . 190
6.4 Discussion . . . 195
6.4.1 Proposed mechanism for arginine-dicarboxylic acid stabilising effects . . . 195
6.4.2 The impact of annealing duration on protein stability 198
6.4.3 Phase separation in lyophilised cakes . . . 199
6.5 Conclusion . . . 201

7 Final Conclusion 203
7.1 Future outlook . . . 206

Appendix A 211

Appendix B 221

Appendix C 235

Bibliography 241

List of Figures

1.1 The phase diagram of water 3
1.2 A typical lyophilisation cycle 4
1.3 A typical bench-top freeze dryer 5
1.4 The enthalpy and volume of amorphous glasses 8
1.5 Mechanisms of recrystallisation 10
1.6 Heat and mass transfer within a vial 14
1.7 The three-dimensional structure of proteins 20
1.8 The preferential exclusion theory 25
1.9 The water replacement hypothesis 26
1.10 Vitrification of the protein formulation 27

3.1 A schematic drawing of a DSC 36
3.2 The Tg′ of a formulation 37
3.3 The set up employed for the freeze drying microscope 39
3.4 The collapse temperature 39
3.5 A Karl Fisher titration cell 41
3.6 A schematic diagram of an XRPD 43
3.7 A schematic diagram of a DMA 45
3.8 The resulting traces from a DMA experiment 45
3.9 The physical appearance of lyophilised cakes 46
3.10 A schematic of an SEM 47
3.11 The adsorption process 49
3.12 Types of adsorption isotherms 53
3.13 Diagram of a powder penetrometer 55
3.14 Different types of pore structure 57
3.15 A set up for a micro-CT 58
3.16 Jablonski diagram 61
3.17 Elution through an SEC column 65
3.18 A schematic diagram of MFI 67

4.1 The chemical structure of sucrose 75
4.2 The structure of IgG 77
4.3 The primary drying temperatures 86
4.4 Lyophilised cake appearance 88
4.5 The reconstitution times of lyophilised protein cakes 89
4.6 SEM images of lyophilised cakes 91
4.7 The BET SSA and residual moisture contents of lyophilised BSA cakes 93

4.8 The pore size distributions of lyophilised BSA cakes 95
4.9 The bulk density of BSA formulations 97
4.10 The total pore volume of BSA formulations 97
4.11 The second derivative FTIR spectra of lyophilised cakes . . . 99
4.12 Macromolecular crowding 105

5.1 The chemical structure of arginine. 115
5.2 The residual moisture contents for the lyophilisation cycles . 129
5.3 BSA cake appearance 131
5.4 SEM images of lyophilised BSA sucrose cakes 133
5.5 SEM images of lyophilised BSA arginine-C4 cakes 134
5.6 The BET SSA of lyophilised BSA formulations by annealing duration 136
5.7 The BET SSA of combined measurements by formulation . . 137
5.8 The pore size distribution of BSA formulations 139
5.9 The total pore volume of BSA formulations 141
5.10 Micro-CT of BSA arginine-C4 without annealing 142
5.11 Micro-CT of BSA arginine-C4 with two hour annealing duration 143
5.12 Micro-CT of BSA arginine-C4 with a four hour annealing duration 144
5.13 The calculated porosity of 2D Micro-CT slices 145
5.14 A 3D rendering of micro-CT images 147
5.15 The reconstitution times of BSA formulations 148
5.16 The BET SSA, reconstitution times and pore size distributions of lyophilised mAb1 150

6.1 A scheme for visible particle formation 165
6.2 A recently proposed mechanism of arginine aggregation suppressing effects 168
6.3 Spectral processing for Raman analysis 174
6.4 The monomer content of BSA by SEC 175
6.5 The soluble aggregation rate of BSA formulations 178
6.6 SVP in reconstituted BSA formulations 180
6.7 SVP in reconstituted mAb1 formulation 181
6.8 The opacity of reconstituted mAb1 solutions 183
6.9 The second derivative IR spectra of BSA with sucrose 184
6.10 The second derivative IR spectra of mAb1 185
6.11 Principal component loadings 187
6.12 The distribution of PC scores by formulation 188
6.13 The amide I region of PC loadings 189
6.14 The distribution of PC 4 190
6.15 A map of PC 2 and PC 4 scores for a lyophilised BSA sucrose cake 192
6.16 Raman spectra from the BSA sucrose cake 194

A.1 The formazin standards for assessing opalescence 211
A.2 FTIR spectral processing 214

A.3 The DSC traces of BSA and mAb1 215
A.4 XRPD of lyophilised BSA 216
A.5 Nitrogen adsorption isotherms of reference and lyophilised material 217
A.6 An SEM image of pores in quench cooled samples 219

B.1 The macro for image processing 221
B.2 The thermocouple data for lyophilisation cycles 222
B.3 SEM images of lyophilised BSA arginine-C5 cakes 223
B.4 SEM images of lyophilised BSA arginine-C6 cakes 224
B.5 SEM images of lyophilised BSA arginine-C7 cakes 225
B.6 XRPD as received materials 226
B.7 XRPD of lyophilised protein formulations 227
B.8 XRPD of lyophilised excipients 228
B.9 XRPD of lyophilised excipients after storage 229
B.10 The pore size distribution less than 5 μm 232
B.11 Images of mAb1 cakes after lyophilisation using different annealing durations. 233
B.12 An SEM image of mAb1 234

C.1 The monomer content of lyophilised BSA 235
C.2 MFI of refrigerated BSA after 12 weeks 237
C.3 IR spectra of arginine-dicarboxylic acid formulations 238
C.4 Raman spectra of arginine-dicarboxylic acid formulations . . 239

List of Tables

1.1 The quality attributes of a lyophilised biopharmaceuticals . . 32

3.1 Peak positions in the IR amide I band 62

4.1 The reconstitution guidelines of FDA approved mAbs 72
4.2 The lyophilisation cooling profiles 81
4.3 Tg′ and Tc values of BSA and mAb1 formulations 85
4.4 The correlation coefficients of lyophilised and reconstituted samples 101

5.1 The chemical structures of dicaboxylic acids 117
5.2 Inactive ingredient search for excipients of interest 119
5.3 The pH of BSA containing formulations. 125
5.4 Tg′ and Tc of lyophilised cakes 126
5.5 The primary drying times of annealed cycles 128
5.6 Tg of lyophilised BSA formulations 135
5.7 The bulk density of BSA formulations 138

6.1 The n values from SEC 176

A.1 The Tc temperature profile 212
A.2 The MIP pressure range 213
A.3 BET Constants for BSA and mAb1 formulations 218
A.4 Error of the BET fit for BSA and mAb1 formulations 218

B.1 BET Constants for sucrose and arginine formulations 230
B.2 Error of the BET fit for sucrose and arginine formulations . 231
B.3 The bulk density and total pore volume of lyophilised mAb1 234

C.1 The elution times of protein formulations by SEC 236
C.2 SVP of formulations prior to lyophilisation 236

List of Abbreviations

BET	Brunauer, Emmett & Teller
BSA	Bovine serum albumin
BP	British Pharmacopoeia
C4	Succinic acid
C5	Glutaric acid
C6	Adipic acid
C7	Pimelic acid
CIN	Controlled ice nucleation
DMA	Dynamic mechanical analysis
DSC	Differential scanning calorimetry
EMA	European Medicines Agency
IgG	Immunoglobulin G
FDA	U.S. Food and Drug Administration
FTIR	Fourier transorm infrared (spectroscopy)
IR	Infrared
mAb	Monoclonal antibody
MFI	Microflow imaging
Micro-CT	X-ray microtomography
MIP	Mercury intrusion porosimetry
PAT	Process Analytical Technology
PCA	Principal component analysis
PC	Principal component
QbD	Quality by design
SA	Soluble aggregates
SEC	Size exclusion chromatography
SSA	Specific surface area
SVP	Subvisible particles
Tc	Collapse temperature
Tg	Glass transition temperature
Tg′	Glass transition temperature of freeze concentrate
USP	United States Pharmacopoeia
VP	Visible particles
XRPD	X-ray powder diffraction

1 Introduction

Biopharmaceuticals are therapeutic agents in which the active component is a biological species and typically mimics the structure of a compound within the body (Nagle *et al.*, 2008). As such, they can range from simple peptides, proteins, and nucleic acids to more complex systems such as viruses and bacteria (Joshi *et al.*, 2010). The function of these macromolecules is dictated by their structure. Degradation of the structure can result in low biological activity, aggregation and immunological reactions (Arakawa *et al.*, 2001, Hermeling *et al.*, 2004). As physical and chemical degradation processes are often mediated by the presence of water, a solid dosage form is often favoured for maintaining the integrity and stability of a biopharmaceutical.

Lyophilisation can be used to dry biopharmaceuticals and, with the benefit of using low rather than high temperatures, lyophilisation is currently the most commonly used method for drying biopharmaceuticals (Wang, 2000). The process of lyophilisation is relatively straightforward and involves the freezing of a solution and application of a vacuum to sublime ice, thus drying the product.

The greatest concern in the development and commercialisation of a

biopharmaceutical is its safety and efficacy. Accordingly, regulatory considerations must be satisfied. In 2002, the US Food and Drug Administration (FDA) adopted a 'quality by design' (QbD) approach for manufacturing pharmaceuticals, whereby the product performance and quality attributes of the final product must be identified prior to manufacture. Following this approach, the formulation and processing strategies can be tailored to meet these requirements. However, this requires an understanding of how formulation and processing parameters affect the final product quality. Although progress has been made in the last ten years to refine our understanding of the relationship between process, formulation and quality attributes for lyophilised biopharmaceuticals, a comprehensive understanding at a mechanistic level remains elusive.

There are several excellent general reviews regarding lyophilisation (Franks, 1998, Kasper *et al.*, 2013b, Wang, 2000), alternate drying technologies (Walters *et al.*, 2014), excipient selection (Ohtake *et al.*, 2011, Wang, 2000) and protein stability (Chang and Pikal, 2009, Wang, 1999, 2005), although a detailed review is beyond the scope of this thesis. The present introduction is intended to give a brief overview on current lyophilisation process technology and the challenges faced when maintaining protein stability during lyophilisation and storage. Furthermore, the concept of QbD is discussed.

1.1 The lyophilisation process

For over one thousand years Peruvian Incas have dried potatoes to form a conserved powder using the high altitudes and low temperatures of the Andes (Salaman *et al.*, 1985). Today, although the technology has changed, the process of lyophilisation (also known as freeze drying) remains fundamentally the same. In its simplest form, lyophilisation can be considered as a two step process and has been illustrated in Figure 1.1. Initially the wet material (or solution) is frozen (arrow A) after which a vacuum is applied to reduce the pressure of the system (arrow B) leading to sublimation of ice which eventually leads to a dried product.

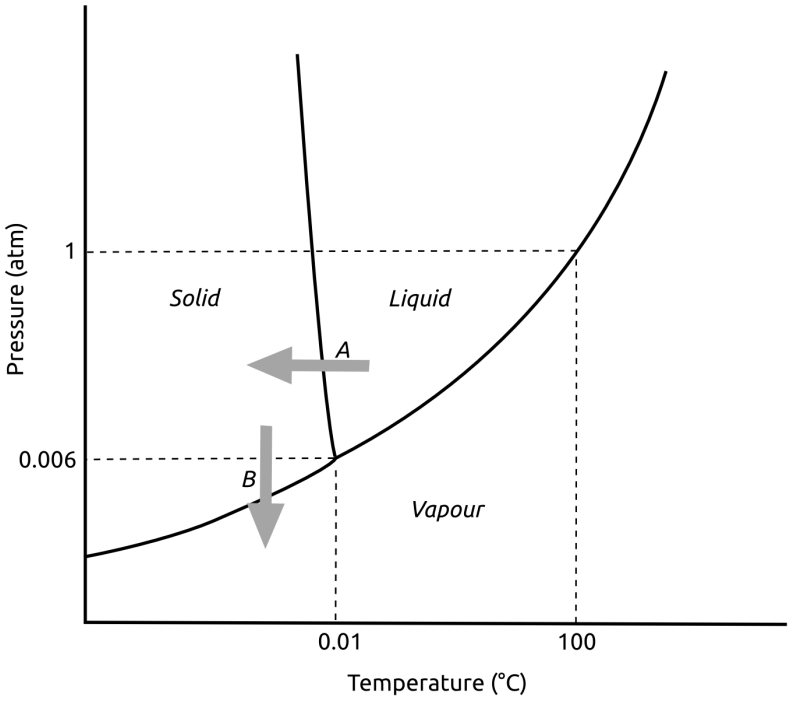


Figure 1.1. The phase diagram of water. During lyophilisation, the temperature is initially reduced to freeze water (arrow A) after which pressure is decreased below the triple point of water to cause sublimation (arrow B). The pressure unit used in the remainder of this thesis for lyophilisation is Torr, please note that 1 atm = 760 Torr (mmHg).

Modern lyophilisation processes at an industrial scale often involve more

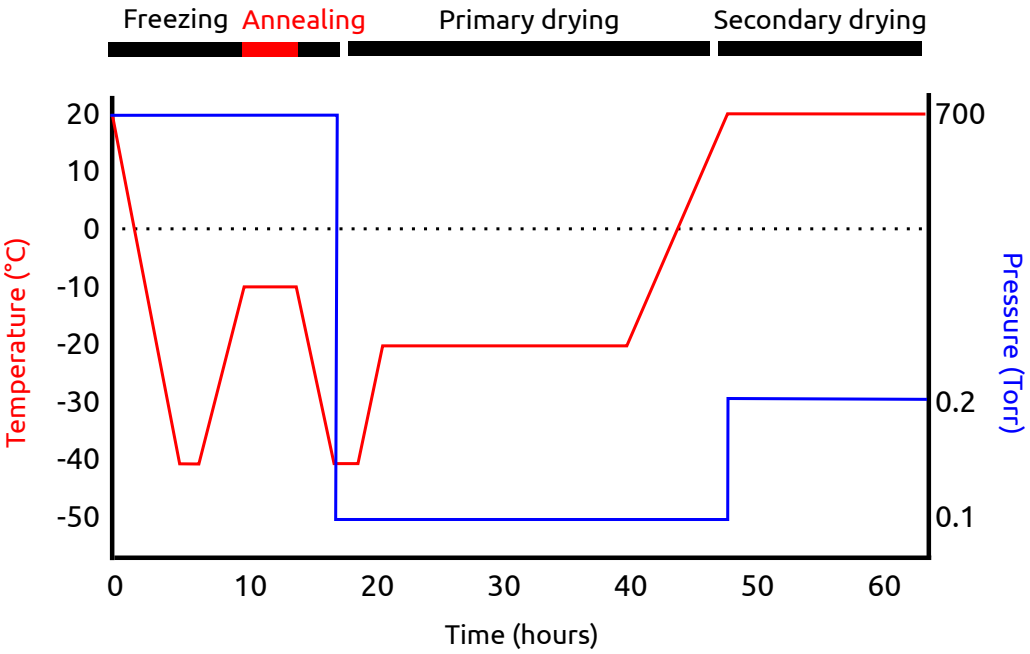


Figure 1.2. A typical lyophilisation cycle which can be used to dry proteins. The cycle is separated into three stages: freezing (including an annealing step in which the temperature is raised), primary drying, and secondary drying.

complicated regimes. A typical lyophilisation cycle can be seen in Figure 1.2 and consists of three stages: freezing, primary drying and secondary drying. Modifications of the freezing stage often involve the addition of an annealing step, in which the temperature may be raised for a fixed amount of time. For the lyophilisation of proteins drying is often considered in two stages, firstly with low temperature and pressure to remove ice and secondly with higher pressure and higher temperatures to facilitate the desorption of water from the protein.

1.1.1 Instrumentation

An illustration for a typical bench-top freeze dryer can be seen in Figure 1.3, and is of similar design to those used throughout this work. The first step of the lyophilisation process is cooling, which can be carried out externally from the freeze dryer, for example by placing the vials in liquid

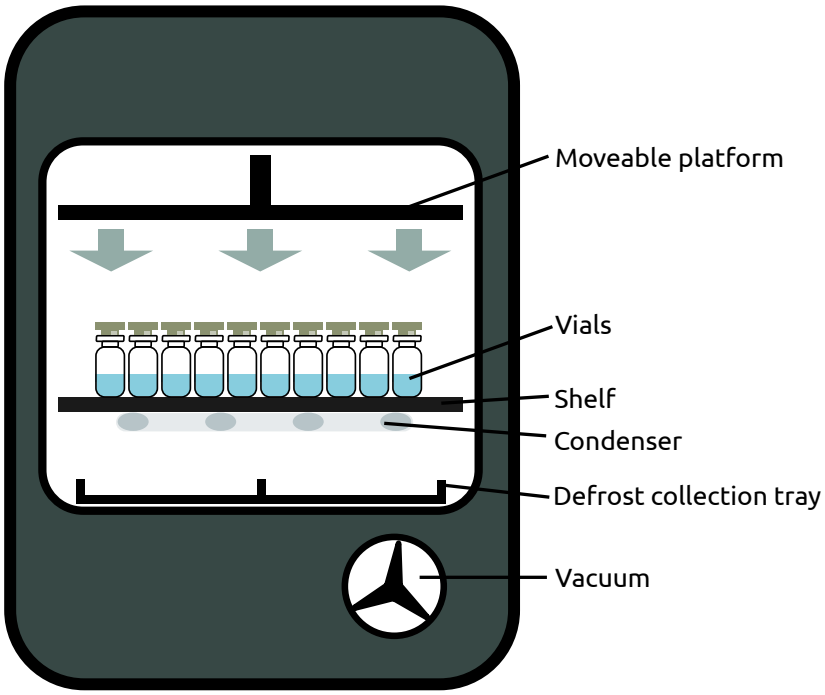


Figure 1.3. An illustration of a bench-top freeze dryer, similar to the one used in this thesis, in which vials are placed on the shelves within a sealed chamber. The freeze dryer consists of a vacuum pump, a condenser, a temperature-controlled shelf and a moveable platform which allows automatic stoppering of the vials.

nitrogen, or internally where the vials are placed onto shelves which are cooled *in situ*, such as in Figure 1.3. Internal cooling using shelves allows the cooling rate and temperature to be carefully controlled.

After freezing of the solution, a vacuum is applied to reduce the pressure of the chamber, typically to below 10 mTorr (Trappler, 2004). A condenser, which is often placed between the product and the valve to the vacuum pump (Kobayashi, 1985), is able to remove large quantities of ice leading to lower achievable chamber pressures (Trappler, 2004). After sufficient drying the pressure can be raised using an inert gas, such as nitrogen and the vials are stoppered automatically, under slight vacuum (e.g. 500 Torr), by compressing the semi-inserted stoppers into the vials using a moveable platform.

1.1.2 The freezing step

The importance of the freezing step in lyophilisation is widely known in the literature. It is the major dehydration step in lyophilisation (Pikal and Rambhatla, 2002), and the final ice morphology can influence both drying times and the resulting lyophilised structure (Searles *et al.*, 2001a,b). As mentioned in the previous section, freezing can take place externally to the freeze dryer, or internally. The latter is commonly used in industrial and pilot scale applications where reproducible batches are required (Cameron, 1997).

During cooling, ice does not always form at its equilibium freezing point (0 °C) and can lead to supercooling of the liquid. The number, growth rate and size of ice crystals depend on the degree of supercooling (Kasper and Friess, 2011). Often with shelf ramped cooling, the contents of the vial achieve a similar level of supercooling (global supercooling) which allows the formation of many ice nuclei throughout the vial. Growth occurs rapidly and leads to the formation of numerous small ice crystals in the vial. When only a small volume of the solution undergoes supercooling, which can occur at rapid cooling rates, the nucleation and ice front grows into a non-nucleated volume and results in directional solidification (Kasper and Friess, 2011).

In solution, three patterns of ice crystal habits are thought to occur (Petzold and Aguilera, 2009): (1) If growth occurs slowly, ice forms stable, hexagonal stellar dendrites. (2) If ice is incorporated at a fast rate then irregular dendrites grow from the centre of crystallisation. (3) At very high freezing rates many ice spears originate from the centre without side branches and are known as spherulites (Petzold and Aguilera, 2009). Whereas it is thought that hexagonal stellar dendrites form from global

supercooling (Kasper and Friess, 2011), and after annealing (Felix Franks, 2007), directional solidification leads to spherulites, which can ultimately result in a lyophilised product with cylindrical pores and a lamellar structure (Searles *et al.*, 2001a).

The temperature at which ice nucleates is difficult to predict (Liu, 2006, Pikal and Rambhatla, 2002), despite a well controlled lyophilisation cycle. The ice nucleation temperature, and consequently its resulting ice size distribution, can vary from one vial to the next within the same batch (Kasper and Friess, 2011). Due to this, modifications to the freezing step may be required and are discussed in the following section.

Crystallisable excipients may crystallise at the eutectic melting temperature as the temperature of the vial is lowered during the freezing step. For non-crystallisable excipients, the high concentration and viscosity of the remaining solution can lead to the formation of an amorphous supercooled liquid, known as the freeze-concentrate. The changes in enthalpy and volume, which are indicative of the material's heat capacity and thermal expansion coefficient (Hancock and Zografi, 1997), for an amorphous compared to the crystalline material is shown in Figure 1.4.

On cooling, if the liquid is able to form long-range molecular order a crystal can result, in which only a small increase in volume and enthalpy are observed as the temperature is increased. For an amorphous material, cooling does not lead to long-range molecular order but instead results in a supercooled liquid. On further cooling, a change in volume and enthalpy occurs at the glass transition temperature (denoted as Tg' for the freeze-concentrate and Tg for the dried state), in which the amorphous material transitions from a rubbery to a glassy state. Below this temperature, the

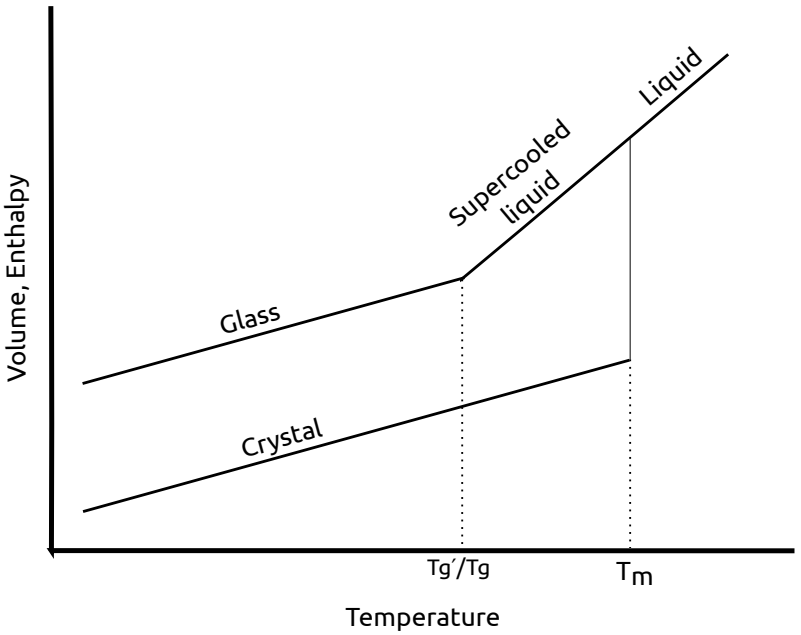


Figure 1.4. The variation in volume and enthalpy as a function of temperature for crystalline and amorphous states, adapted from reference (Hancock and Zografi, 1997). The Tg′ and Tg are the glass transition temperatures of the freeze concentrate and dried material, respectively, and Tm is the melting temperature.

material is "kinetically frozen" into a thermodynamically unstable glass with slower molecular mobility (i.e. it has longer relaxation times) and higher viscosities than the supercooled liquid above Tg (Hancock and Zografi, 1997). In the lyophilisation process, the Tg′ of the freeze concentrate has important implications during the drying stages.

1.1.3 Modifications to the freezing step

Annealing

The annealing step involves holding the temperature of the frozen solution at a temperature higher than its Tg′ for a fixed duration. It is often used to allow efficient crystallisation of excipients, such as mannitol or glycine when used as bulking agents[1]. Where the annealing temperature is raised

[1] A bulking agent is often incorporated into a formulation to prevent product collapse, to improve reconstitution times or to provide mechanical strength (Wang, 2000).

to between 10 and 20 °C above the Tg′ but below the eutectic melting temperature and held for several hours (Tang and Pikal, 2004). With increasing protein concentration, longer annealing durations are often needed to achieve crystallisation of the bulking agent (Liao *et al.*, 2005, Sundaramurthi and Suryanarayanan, 2010).

Including an annealing step for formulations with non-crystallisable excipients has several advantages: (1) a greater molecular mobility above Tg′ allows unfrozen water to crystallise which can further increase the Tg′ of the formulation (Zuo *et al.*, 2005); (2) a reduction in inter-vial heterogeneity; (3) larger ice crystals grow at the expense of smaller ice crystals, which can decrease the resistance to sublimation, leading to shorter drying times (Searles *et al.*, 2001a); (4) the smaller ice interface which results from larger ice crystals can have important consequences for protein stability. With its multiple benefits, an annealing step is therefore often added to an industrial lyophilisation process.

During annealing, the recrystallisation processes of Ostwald ripening, accretion and isomass rounding can occur leading to a change in the ice crystal structure. Ice begins to dissolve at the onset of Tg′ (Ablett *et al.*, 1992), and annealing above this temperature leads to an increase in the mobility of the amorphous freeze-concentrated phase. The increased mobility allows the system to progress towards an equilibrium state of minimal free energy. According to the radius of curvature (or Kelvin) effect, smaller ice crystals have more surface energy per volume than larger ice crystals, which depresses their melting point (Cook and Hartel, 2010). Smaller ice crystals will therefore melt at a faster rate than larger ones. As melting is endothermic and will take energy out of the system, this provides the heat sink for the latent heat of crystallisation of larger crystals (Cook and Hartel,

2010). This process, which is known as Ostwald ripening and can be seen in Figure 1.5 (a), allows larger ice crystals to grow at the expense of smaller ones.

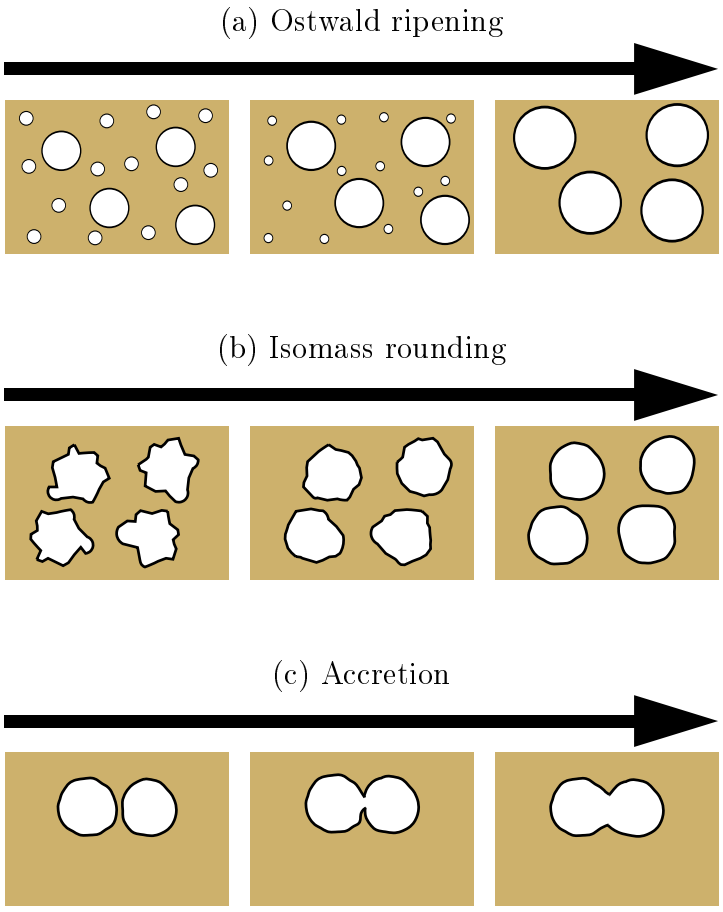


Figure 1.5. Three mechanisms of ice recrystallisation which can occur during annealing, adapted from reference by Goff and Hartel (2006). The arrow illustrates the direction of time.

The conventionally accepted theory for Ostwald ripening (or 'coarsening') was established by Lifshitz, Slyozov, and Wagner (LSW) (Lifshitz and Slyozov, 1961, Wagner, 1961). Although it is beyond the scope of this thesis to describe the formulae of LSW theory in detail, three aspects appear important for the discussion of ice crystal growth during annealing. Firstly, there is a critical radius, above which larger crystals will grow at the expense of smaller crystals. Secondly, a steady-state regime is attained during Ostwald ripening and, finally, a limiting distribution will be obtained when

the average crystal radius is equivalent to the critical radius (De Smet *et al.*, 1997). It has been reported in the lyophilisation literature that the steady-state regime of Ostwald ripening will be diffusion-limited (Searles *et al.*, 2001a), in which the average crystal radius will increase with time to the power of 1/3 during annealing.

Isomass rounding and accretion (Figure 1.5 (b) and (c), respectively) are also recrystallisation events that can occur during annealing. Again, both mechanisms are driven by the tendency to reduce surface energy. During isomass rounding, localised regions on a crystal (such as the tips of ice crystals) have high curvature radii. The solubility of these areas are therefore also increased, leading to recrystallisation and a more regular, spherical ice crystal structure (Goff and Hartel, 2006). With accretion, two adjacent ice crystals join together to form one, larger crystal. This occurs as the junction between two spherical crystals will be concave and consequently have a lower chemical potential then the surrounding surface (Searles *et al.*, 2001a). The chemical potential difference creates a driving force for the formation of a neck between the crystals and eventually the two crystals become indistinguishable from each other (Blond *et al.*, 2006).

Controlled ice nucleation (CIN) techniques

A number of methods have been developed to allow spontaneous ice nucleation at a desired temperature, such as through vacuum-induced surface freezing (Kramer *et al.*, 2002), ultra-sound controlled ice nucleation (Nakagawa *et al.*, 2006), electrofreezing (Petersen *et al.*, 2006) and the use of ice nucleating agents in the formulation (Petzold and Aguilera, 2009). By far, the most applicable techniques for the scale up to industrial freeze dryers are the ice fog and depressurisation techniques (Kasper *et al.*, 2013b, Patel

et al., 2013).

During the ice fog technique, vials are cooled through the shelf so that the solution becomes supercooled. Nitrogen gas is then pumped into the chamber which freezes the water vapor surrounding the vials which then serve as seeds for ice nucleation (Geidobler and Winter, 2013). Numerous modifications have been made to this technique to reduce the variability between vials and improve its scalability (Chakravarty *et al.*, 2012, Rambhatla *et al.*, 2004). Recently, it has been found that if a batch is large enough, depressurisation to ∼2.8 mTorr will generate enough water vapor to be collected by the ice condenser and, on repressurisation, ice nucleation can be achieved almost instantaneously (Geidobler *et al.*, 2012, Patel *et al.*, 2009).

For the depressurisation (also known as high-pressure shift freezing) technique, the pressure in the chamber is initially increased using an inert gas to approximately 1500 Torr overpressure (Geidobler *et al.*, 2012, Konstantinidis *et al.*, 2011). The temperature is then lowered to less than 0 °C and the chamber is rapidly evacuated to allow uniform supercooling and ice nucleation of the solution (Fernandez *et al.*, 2006). However, the mode of ice nucleation in this technique is not completely understood and may involve the formation of bubbles that act as nucleants and liquid product surface expansion (Geidobler and Winter, 2013, Konstantinidis *et al.*, 2011).

1.1.4 Primary and secondary drying

Drying of the product occurs through sublimation of ice and desorption of amorphous water. Sublimation is essentially a heat and mass transfer process whereby heat is required to transfer ice from the sublimation front

of the product to the ice condenser. The heat needed for sublimation is provided through three mechanisms: conduction, radiation and convection. Summation of their individual contributions provides the vial heat transfer coefficient, K_v. An illustration of the sublimation front and the various heat transfer mechanisms are shown in Figure 1.6. Conduction provides the greatest amount of heat transfer and occurs between the shelf and bottom of the vial. Radiation occurs between two surfaces, such as from the warmer sides or door of the freeze dryer to the colder vial. Although radiation is not a dominant mechanism for heat transfer, due to the low temperatures within the freeze dryer, it can have a significant impact when warm surfaces are present and can lead to drying heterogeneity within the batch (Rambhatla and Pikal, 2003). Convection can also transfer heat through gas molecules to the product vial. However, the low pressures used during lyophilisation make the contribution of convection to the heat transfer process negligible (Boylan and Nail, 2002).

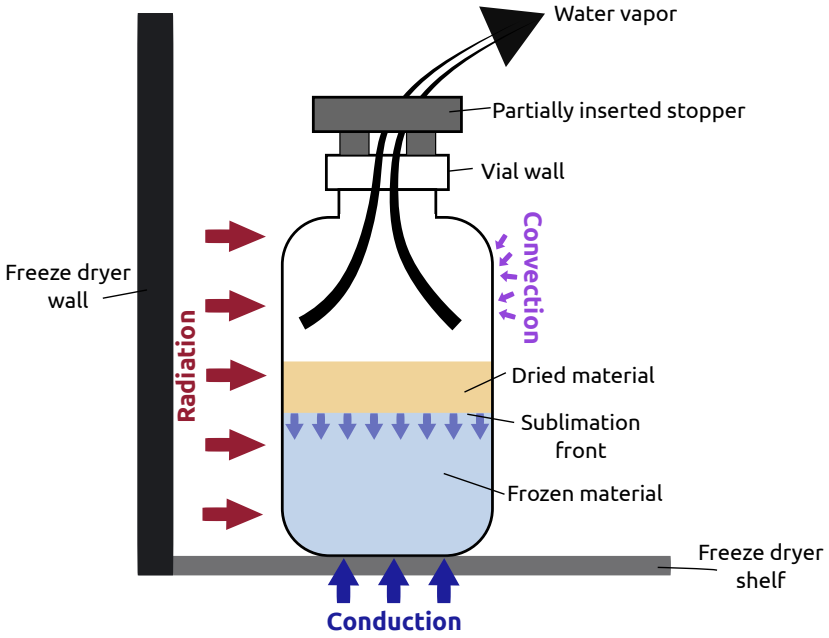


Figure 1.6. An illustration of the three heat transfer mechanisms which provide the energy required for sublimation: radiation, convection and conduction. The sublimation front moves from the top of the product towards the bottom of the vial while the water vapour sublimed must exit the vial and solidify on the ice condenser.

Lyophilisation is an expensive process with long processing times, high energy requirements[2] and a substantial capital investment (Banga, 2005). Primary drying is the longest stage in the lyophilisation process and, therefore, reducing the length of this step is often key for designing an economical process (Tang and Pikal, 2004). Primary drying begins after freezing when the pressure in the chamber is reduced to below the triple point of water (often to approximately 100 mTorr). The sublimation of ice during primary drying is generally assumed to be pseudo steady-state and can be expressed by the following equation:

$$\Delta H_s \left(\frac{(P_0 - P_c)}{(R_s + R_p)} \right) - A_v K_v (T_s - T_p) = 0 \tag{1.1}$$

[2]The latent heat of sublimation is approximately 2838 kJ/kg (Sivasankar, 2005).

Where A_v is the heat transfer area of the vial, T_s and T_p are the shelf and product temperatures, respectively, P_0 is the vapour pressure of ice at the product temperature and P_c is the chamber pressure. R_s and R_p are the stopper and product resistances, respectively, and ΔH_s is the sublimation rate (Rambhatla and Pikal, 2004). This equation assumes a perfect balance between the energy provided for sublimation and the energy removed by sublimation. As such, there is no change in the product temperature. A pressure difference between the chamber and the vapour pressure of ice (at the product temperature) is necessary for maintaining rapid sublimation rates, whilst the energy for the process is provided by the shelf temperature. As the vapour pressure of ice also increases logarithmically with increasing temperature (Franks, 1998), raising the shelf temperature can lead to faster sublimation rates. It has been reported that increasing the shelf temperature by 1 °C can reduce the primary drying time by 13 % (Tang and Pikal, 2004).

Although it is important to maximise the product temperature in order to provide a more economical lyophilisation cycle, raising the temperature too high can affect the structural integrity of the final lyophilised material (also known as a cake). Large scale (macro) collapse can occur when an increase in molecular mobility during drying leads to viscous flow of the amorphous freeze concentrate which results in an increase in density and blockage of the cake pores (Schersch *et al.*, 2010). Consequently, the temperature at which the cake collapses (Tc) is closely related to its Tg′. Large scale collapse of the cake can lead to an increase in product resistance which can increase drying times and result in products with high moisture content (Adams and Irons, 1993).

Product resistance, which can greatly reduce sublimation rates, is also

highly dependent on the product formulation (Kuu *et al.*, 2011). Product resistance does not remain constant during lyophilisation and will increase as the dried layer becomes thicker as it provides a more tortuous pathway for the water vapour to exit from the cake. However, small scale (micro) collapse, which is often demonstrated post lyophilisation by the presence of small holes (∼2-20 μm) in the pore walls of the lyophilised material, can reduce product resistance by improving vapour flow (Overcashier *et al.*, 1999).

The temperature of the product increases as ice is sublimed from the vial. Often, the end of primary drying is determined when the product temperature equals the shelf temperature (Tang and Pikal, 2004). Caution should be used with this approach as the product temperature, which is measured using a thermocouple placed within a vial, is not always representative of the whole batch (Patel *et al.*, 2010). By the end of primary drying, the product may still contain between 15-20 % unfrozen water (Kasper and Friess, 2011).

Secondary drying is a desorption process and is used to remove amorphous water, in which higher temperatures (∼20 °C) and pressures (∼200 mTorr) are used. Shrinkage of the lyophilised cake is thought to be due to the removal of water volume during secondary drying. Despite efforts to minimise shrinkage, such as by maintaining the product temperature below the Tg, volumetric shrinkage has been found to occur no matter what the product thermal history (Rambhatla *et al.*, 2005). Secondary drying may also occur simultaneously to primary drying, however, if the shelf temperature is increased without complete ice sublimation this may lead to an extreme type of cake collapse known as 'meltback'. Two-dimensional non-steady state models have therefore been developed to help predict both the

primary and secondary drying behaviour of formulations. For more details on these models, and their assumptions, the reader is advised to read the reference by Rambhatla and Pikal (2004).

Determining the length of the secondary drying stage often requires an element of trial and error as it can be strongly influenced by the solid state of the product, its surface area and the total solid content (Tang and Pikal, 2004). In general, secondary drying will be stopped when enough water has been desorbed to provide the product with a desired residual moisture content, which for protein formulations, is often less than 2 % (Wang, 2000).

1.2 Protein structure and stability

Therapeutic proteins are highly successful in the clinical setting with over 100 approved products in the US and European Union in 2010 (Dimitrov, 2012). The current clinical uses of therapeutic proteins are both large and varied, and as such an interested reader is directed towards the review article by Leader *et al.* (2008) for a thorough understanding.

1.2.1 The three-dimensional structure of proteins

The biological function of a protein is dictated by its three-dimensional structure in a physiological environment. The foundation of the structure begins with a sequence of amino acids, which is unique to a particular protein, forming the polypeptide chain (for proteins these generally contain more than 50 amino acids (Banga, 2005)). This is also known as the primary structure and its folding into higher order structures is illustrated in Figure 1.7. Hydrogen bonding is able to form between various amino acids in the primary structure and the resulting spatial orientation of the protein backbone provides the protein's secondary structure. Within the secondary structure, characteristic motifs can be established through the repetition of amino acid planes at specific angles (Whitford, 2005). The motifs include α-*helices*, which resemble coiled springs; β-*sheets* which occur as the extended polypeptide chain runs parallel or anti-parallel next to each other forming pleated structures. *Turns*, which allow the protein to fold back on itself, and *unordered* structures which are generally defined as a conformation that is not α-helix, β-sheet or turn (Pelton and McLean, 2000).

The global conformation of a protein is determined by the spatial arrangement of the secondary structure motifs. This provides the tertiary

structure of the protein and is maintained though ionic, hydrophobic, hydrogen and van der Waals interactions (Buxbaum, 2007). Disulphide bridges can also stabilise the tertiary structure through oxidation of the thiol groups on cysteine amino acid residues. For the biological function of some proteins, such as haemoglobin, the assembly of more than one polypeptide chain is required. The organisation of these units forms the quaternary structure and it is generally stabilised, but more weakly, by the non-covalent interactions that contribute to the tertiary structure (Stoker, 2009).

Figure 1.7. The three dimensional structure of proteins in which the sequence of amino acids (the polypeptide chain) forms the primary structure of the protein. Intra-molecular hydrogen bonding between the amino acids leads to the formation of the protein secondary structure (for example α-helices), which then arrange to form the tertiary structure. The quaternary structure applies to multimeric proteins, in which the organisation of more than one polypeptide chain leads to larger assemblies.

Maintaining the structure and consequently the biological function of therapeutic proteins is a critical issue. Degradation of the protein can occur chemically, through hydrolysis, oxidation, deamidation and disulphide bond exchange and physically, through the formation of aggregates (Arakawa *et al.*, 2001, Wang, 1999, 2005). Protein aggregation has been implicated in numerous disease states including Alzeimers, Parkinsons and systemic amyloidosis (Koo *et al.*, 1999, Ross and Poirier, 2004), and it is of key concern to the pharmaceutical industry where it poses a considerable immunogenicity risk to patients (Mehta *et al.*, 2014).

Protein denaturation can occur when the secondary, tertiary and quaternary structures of the protein are disrupted leading to changes in its three-dimensional shape (Stoker, 2009). Often protein aggregates contain a high amount of non-native, intermolecular β-sheet (Dong *et al.*, 1995). In solution, the native protein is folded to minimise exposure of hydrophobic portions. However, on denaturation the protein can unfold. In order to reduce the free energy associated with unfavourable interactions between hydrophobic portions of the protein and the solvent, the unfolded intermediates may interact together to form larger aggregates. The formation of protein aggregates is described in greater detail in Chapter 6. Denaturation can occur through numerous mechanisms, for which the reader is advised to read the reference by Chi *et al.* (2003), and can occur throughout all stages of processing and manufacture (Mehta *et al.*, 2014). In the solution state, agitation or shaking during storage and handling is one of the most common physical stresses that can cause protein aggregation (Chang and Yeung, 2010).

1.2.2 Stresses created during lyophilisation

Water mediates both chemical and physical instability mechanisms in protein solutions. Therefore, in order to improve the stability of a protein water can be removed. Although lyophilisation is the most commonly used method to dry proteins (Wang, 2000), the process inherently causes stresses which can denature the protein.

Low temperature stresses

Low temperature stresses occur prior to freezing as the shelf temperature is being lowered. Before ice nucleates the physical properties of water begin to alter such as diffusion rates, dielectric constant, mobility and hydrogen bonding energies (Franks and Hatley, 1991). With decreasing temperatures, the solubility of non-polar groups increases causing a weakening of the hydrophobic interaction (Dill *et al.*, 1989, Wang, 2000). The result is often a reversible unfolding of the protein which returns to the folded state with increasing temperature, however, this may predispose the protein to irreversible unfolding during freezing (Singh *et al.*, 2009).

Stresses during freezing

As ice crystals nucleate and grow, proteins may become adsorbed to the ice interface leading to unfolding and denaturation. The mechanism of protein adsorption is still disputed, in which hydrophobic, hydrophilic and direct interactions through hydrogen bonding have all been implicated (Gray, 2004, Harding *et al.*, 1999, Wierzbicki *et al.*, 2007). The extent of the ice interface has been proposed as the mechanism of protein denaturation in numerous studies (Costantino *et al.*, 2002, Devineni *et al.*, 2014, Hsu *et al.*, 1995, Webb *et al.*, 2003, 2002b, Xu *et al.*, 2014). As well as ad-

sorption, freezing may also cause physical distortion of the protein through anisotropic compression (Haas *et al.*, 1995), when the space between ice crystals becomes less than the molecular volume of the protein (Strambini and Gabellieri, 1996).

As the water progressively freezes, solutes in the unfrozen solution begin to concentrate and can increase by 20–50 times their initial concentrations (Hatley and Mant, 1993, Heller *et al.*, 1999). The increase in concentration can lead to an increase in degradative reactions (Wang, 2000) and the formulation may separate into distinct phases, causing the protein to be removed from its intended stabiliser. This phase separation process, which can be reduced at low temperatures by slow molecular mobility, may become both thermodynamically and kinetically favoured at the higher temperatures used in the annealing step. Several studies have proposed that phase separation during annealing can be detrimental to protein stability (Bhatnagar *et al.*, 2010, 2011, Heller *et al.*, 1997, 1999b, Izutsu *et al.*, 2013).

Crystallisation of formulation components can also occur at low temperatures. The pH of the protein solution is often tightly regulated to stabilise the protein in its native state and prevent unfolding from repulsion between charged residues. However, during the freezing stage, crystallisation of buffer salts can occur. A well known example is with that of sodium phosphate buffers, in which the dibasic sodium salt (which has a eutectic temperature of -2 °C (Chang and Randall, 1992)) can cause a shift in solution pH ($\sim$3.6) due to the monobasic sodium salt remaining present in the solution (Randolph, 1997).

Stresses during drying

Removal of water and disruption of the protein hydration shell can lead to either reversible or irreversible denaturation of the native state (Prestrelski *et al.*, 1993). Water may also form part of the active site of the protein and may be necessary for protein function, removal of this water may consequently lead to inactivation of the protein (Nagendra *et al.*, 1998).

1.2.3 Maintaining protein stability

In the final lyophilised protein product the formulation may contain a number of excipients such as preservatives, bulking agents and tonicity agents which do not directly affect protein stability (Wang, 2000). The formulation will also contain excipients which can be lyoprotectants, if they protect the protein during lyophilisation, or cryoprotectants, if they protect the protein during the freezing step. Three theories have been proposed to account for the protective behaviour of excipients: preferential exclusion, the water replacement hypothesis and vitrification (Wang, 2000).

During freezing

At the start of lyophilisation, the protein is surrounded in an aqueous environment containing excipients. It is reasonably well accepted that, due to the various interactions between the excipient and protein, the excipient may become preferentially excluded from the vicinity surrounding the protein (Arakawa and Timasheff, 1982). This creates an environment where it would be unfavourable for the protein to unfold from its native state (Figure 1.8).

Excipients that stabilise through this mechanism often include certain salts, sugars and polyols. In general, excipients which preferentially interact

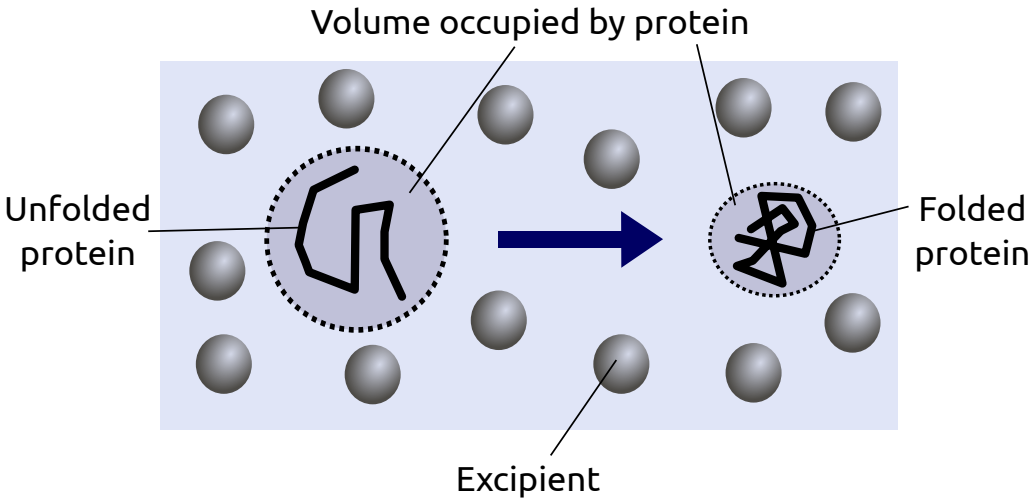


Figure 1.8. The preferential exclusion theory, in which an excipient is excluded from the immediate vicinity surrounding the protein creating an environment in which it would be thermodynamically unfavourable for the protein to unfold. Adapted from the review article by Ohtake *et al.* (2011).

with the protein surface, i.e. salting in additives, are destabilising whereas those that are preferentially excluded from the surface, salting-out, are stabilising (Arakawa *et al.*, 2007). The surface tension increment of salts is often considered a major contributor to its preferential interaction ability, with those that increase the surface tension allowing preferential hydration of the protein (Arakawa and Timasheff, 1984). The volume occupied by an excipient molecule can also lead to preferential hydration of the protein surface through its exclusion from the vicinity surrounding the protein (Ohtake *et al.*, 2011).

During freezing, the protein becomes exposed to the ice interface. The addition of surfactants, which are thought to compete with the protein for the interface, has been found to effectively prevent denaturation of the protein (Chang *et al.*, 1996). For proteins which are sensitive to the ice interface, the process may also be adapted to reduce the size of the interface, for example by avoiding fast cooling rates and replacing the annealing step (which initially has a large interface) with controlled ice nucleation

techniques (Geidobler and Winter, 2013).

During drying

In a formulation without lyoprotectants, dehydration can remove approximately 10 % of the protein's hydration shell (Prestrelski *et al.*, 1993). To compensate for the loss of water, the protein can change conformation to maximise both intra- and inter-molecular hydrogen bonds. In particular, an increase in β-sheet content is thought to occur during drying as it allows for the highest amount of hydrogen bonding within the protein (Avis and Wu, 1996).

Direct interaction of an excipient with the protein through hydrogen bonding can replace the water deficit during drying (Carpenter and Crowe, 1988, 1989, Carpenter *et al.*, 1991, Griebenow and Klibanov, 1995, Lippert and Galinski, 1992), Figure 1.9.

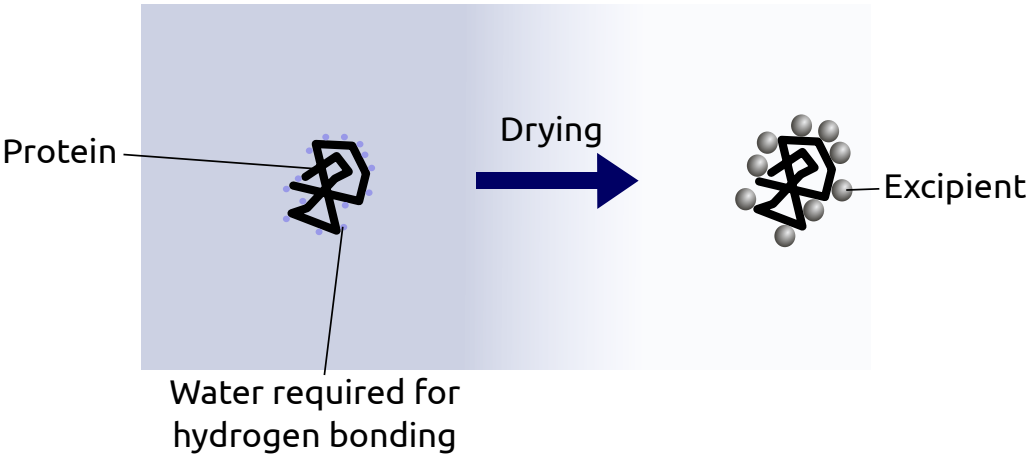


Figure 1.9. The water replacement hypothesis, in which excipients are able to replace the hydrogen bonding with the protein that is lost through the removal of water during lyophilisation.

Excipients such as sugars have been found to be particularly successful in stabilising proteins during drying (Carpenter and Crowe, 1988, 1989, Carpenter *et al.*, 1987a,b). This effect is believed to be due to their flexi-

ble structure, relatively small size (compared to e.g. the polymer dextran (Allison *et al.*, 1999)), and high hydrogen bonding capacity (Kayser and Varzecha, 2012).

Over-drying of a protein can also occur during lyophilisation. Often a bell-shaped curve is observed between protein stability and residual moisture content, in which too much or not enough drying can be detrimental to the product (Wang, 2000). Therefore care should be taken to determine the optimal residual moisture content for the protein formulation.

In the dried state

During lyophilisation, an amorphous glass may form and was described in this chapter in Section 1.1.2. Within the glassy matrix the protein can become immobilised and has been depicted in Figure 1.10.

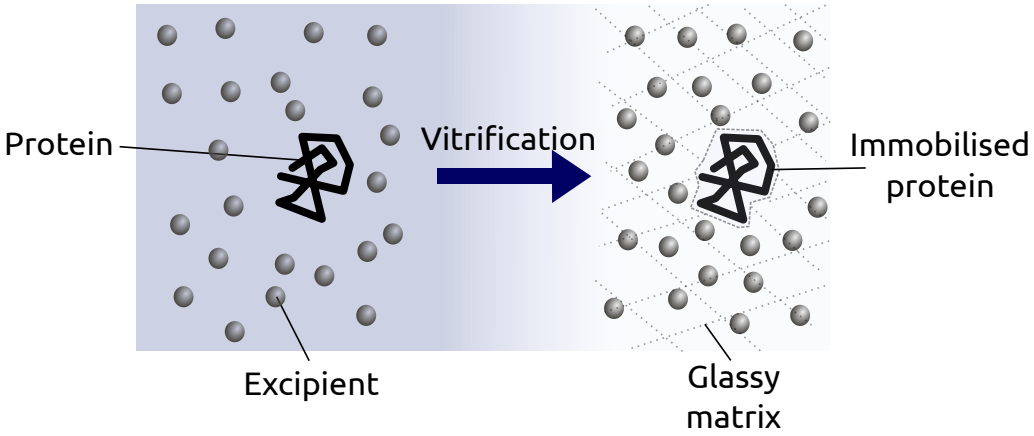


Figure 1.10. During lyophilisation, the freezing and dehydration of water can allow non-crystallising excipients to form an amorphous glass. Through this vitrification process, the protein can become immobilised preventing protein-protein interactions.

Whereas the water replacement mechanism provides stability through a thermodynamic process, vitrification provides stability through a kinetic mechanism. It is greatly debated whether one mechanism contributes more to protein stability than the other (Cicerone and Douglas, 2012, Grasmeijer

et al., 2013), although neither can fully explain stabilisation in the glassy state (Chang *et al.*, 2005a, Pikal *et al.*, 2008, Wang *et al.*, 2009).

Most degradation reactions, including aggregation through protein-protein interactions, require a degree of molecular mobility (Yoshioka and Aso, 2007). The relationship between diffusion (e.g. of a protein molecule) and viscosity, η, can be described using the Stokes-Einstein equation:

$$D = \frac{k_b T}{6\pi\eta R} \tag{1.2}$$

Where, D is the diffusion coefficient, k_b is the Boltzmann constant, T is the temperature, η is viscosity and R is the radius of the diffusing particle. Consequently, the decrease in viscosity that occurs at the Tg can result in an increase in diffusion and molecular mobility. As a rule of thumb, amorphous pharmaceutical glasses are often stored at least 50 °C lower than their Tg (D. Lechuga-Ballesteros, 2002). As higher Tg's are associated with slower molecular mobility during storage (Xu *et al.*, 2013), excipients that increase the Tg of the final product are often extremely advantageous.

The global mobility that occurs at the Tg is due to α-relaxations. These are often described as co-operative and occurring with a non-Arrhenius relationship and are linked with viscous flow (Yu, 2001). Several studies have found an excellent correlation between the Tg and physical/chemical stability (Duddu and DalMonte, 1997, Pikal *et al.*, 2008, Yoshioka and Aso, 2005). However, poor correlations have also been observed (Cicerone and Douglas, 2012). Secondary relaxation processes, such as β- relaxations, have also been considered as important to protein stability (Abdul-Fattah *et al.*, 2007a, Chang *et al.*, 2005b, Cicerone and Douglas, 2012, Cicerone and Soles, 2004, Pikal *et al.*, 2008, Wang *et al.*, 2009). These are much weaker than

α-relaxations and exhibit Arrhenius behaviour. Importantly, β-relaxations occur locally due to intra-molecular orientations of the protein (Sixou *et al.*, 2001).

1.3 A Quality by design approach

The concept of designing quality into a product, rather than testing for it after manufacture, was pioneered by the quality expert J. M. Juran (1992). In 2002, the Food and Drug Administration (FDA) adopted this approach after concerns were raised regarding high product waste (up to 50 % in some cases) and the quality review process for biopharmaceuticals (Rathore and Winkle, 2009). Quality by Design (QbD) can be described as *"a systematic, scientific, risk-based, holistic and proactive approach to pharmaceutical development"* (M. Nasr, 2006). Later, between 2009 and 2012, international guidelines were introduced and a pilot programme between the FDA and the European Medicines Agency (EMA) was initiated, allowing the parallel evaluation of QbD aspects of marketing-authorisation applications (EMA, 2014).

Guidance on how to implement QbD has been published in 'PAT [Process Analytical Tools] - A Framework for Innovative Pharmaceutical Development, Manufacturing, and Quality Assurance' (FDA, 2004), and by the International Conference on Harmonisation of Technical Requirements for Registration of Pharmaceuticals for Human Use (ICH) in the topics of Pharmaceutical Development (ICHQ8, 2009), Quality Risk Management (ICHQ9, 2005) and Pharmaceutical Quality System (ICHQ10, 2008).

The approach involves the following principles: identification of the critical quality attributes that are deemed important to product safety and/or efficacy; design of the formulation and process to deliver these attributes; implementation of a control strategy to ensure consistent quality; monitoring of the process to identify improvement opportunities (Rathore, 2009).

However, this approach requires an understanding of how process and formulation parameters affect the final product quality. To define the 'design space', i.e. the relationship between the process and formulation inputs and the critical quality attributes (Patel and Pikal, 2013), QbD principles recommend the use of prior-knowledge and past experience to identify the initial parameters. This is thought to not only help build quality into the product but also prevent excessive costs arising from repeating work (Jameel and Khan, 2009). As such, the implementation of QbD by the FDA has led to the publication of numerous case studies (Awotwe-Otoo *et al.*, 2012, Mockus *et al.*, 2011a,b, Sundaram *et al.*, 2010, Zidan *et al.*, 2007) and theoretical models (Nakagawa *et al.*, 2007, Pikal *et al.*, 2005, Velardi and Barresi, 2008) regarding the impact of formulation and lyophilisation processing parameters on critical quality attributes. The use of multivariate analysis techniques is also encouraged through PAT, in which they can offer a powerful and robust method for identifying whether relationships exist between variables and quality attributes (Huang *et al.*, 2009).

For a lyophilised biopharmaceutical, the quality attributes of the cake have been described in Table 1.1, and have been separated into those that are desirable and those that are critical to the final product (Sane and Hsu, 2010). Despite the significant progression made in the last ten years to discern which lyophilisation process and formulation parameters affect quality attributes, a comprehensive understanding at a mechanistic level remains elusive. In the following experimental chapters, a review of literature has been carried out to identify these gaps in our current understanding and provides new insights for designing quality into biopharmaceuticals.

Table 1.1. The quality attributes of a lyophilised biopharmaceutical product.

Desirable quality attributes	Critical quality attributes
Elegant cake appearance	Sterility
Low moisture content	Stability
Quick reconstitution time	Batch uniformity
Fast and cost effective process	

2 | Thesis Aims and Objectives

The aim of this thesis is to provide a better understanding of how process and formulation factors affect the quality of lyophilised biopharmaceuticals. To provide insights into this broad topic, three quality attributes are characterised: reconstitution time, the structure of the lyophilised cake and protein stability. To achieve this, the work will be detailed in the following manner:

Chapter 4 | **Insights into the Influence of the Cooling Profile on the Reconstitution Times of Lyophilised Protein Formulations**

Recent research suggests that surface area is not the predominant factor for determining the reconstitution times of lyophilised biopharmaceuticals (Awotwe-Otoo *et al.*, 2013, Cao *et al.*, 2013, Geidobler *et al.*, 2013), however it is often an important parameter in the reconstitution of low molecular weight drug formulations. In order to explore this further Chapter 4 investigates how the reconstitution times of three sucrose based formulations containing BSA (50 mg/mL and 200 mg/mL) or a monoclonal antibody (40 mg/mL) are affected by both the lyophilisation cooling profile and the structure of the resulting lyophilised cake.

Chapter 5 | **Insights into the Influence of Annealing Duration and Formulation on Lyophilised Protein Cake Structural Properties**

The lyophilised product should have an elegant appearance without collapse and an open network of pores to allow shorter primary drying times. However, the previous chapter highlighted that the addition of an annealing step may alter the lyophilised cake structure through a more complex process than previously understood within the literature. Chapter 5 investigates this further by altering the lyophilisation process to include annealing steps of different durations. Furthermore, this chapter also investigates the impact of four dicarboxylic acid salts of arginine on cake structure and compares to a conventional sucrose formulation. To the author's knowledge this is the first comprehensive study investigating the behaviour of arginine-dicarboxylic acid salts as excipients in lyophilised protein formulations.

Chapter 6 | **Insights into the Influence of the Annealing Duration and Formulation on Lyophilised Protein Stability**

Protein stability is regarded as a critical quality attribute of a lyophilised biopharmaceutical. Therefore, Chapter 6 evaluates the effect on protein stability of the formulations and processing conditions described in the previous chapter. The impact on protein conformation through changes in secondary structure is investigated, in which a multivariate analysis approach is used to analyse Raman spectra. In addition, both soluble and insoluble aggregation are monitored over a three month period during which the lyophilised cakes are stored at an elevated temperature of 40 °C.

3 | Instrumental Methods

The purpose of this chapter is to provide the reader with a theoretical background for the main experimental techniques employed within this thesis. The technical details of these techniques are then provided within each chapter.

The most important instrumental method in this thesis is that of lyophilisation. However, as this has been described in great detail in Chapter 1 it will not be covered in this chapter. The techniques described herein are broadly divided into four categories: those that are used to determine properties of the formulations prior to lyophilisation; those that provide information on the solid state of the material (including its moisture content); those that provide information on the physical and structural properties of the lyophilised cakes; and those that are used to provide details about protein aggregation and conformational changes.

3.1 Determining formulation properties

3.1.1 Differential Scanning Calorimetry (DSC)

When a protein solution is cooled, ice can form with the remaining unfrozen solution increasing in viscosity, ultimately leading to the formation of an amorphous phase. The glass transition temperature of this freeze concentrated phase (Tg′) can be determined using DSC. A schematic drawing of the inside of a DSC can be seen in Figure 3.1.

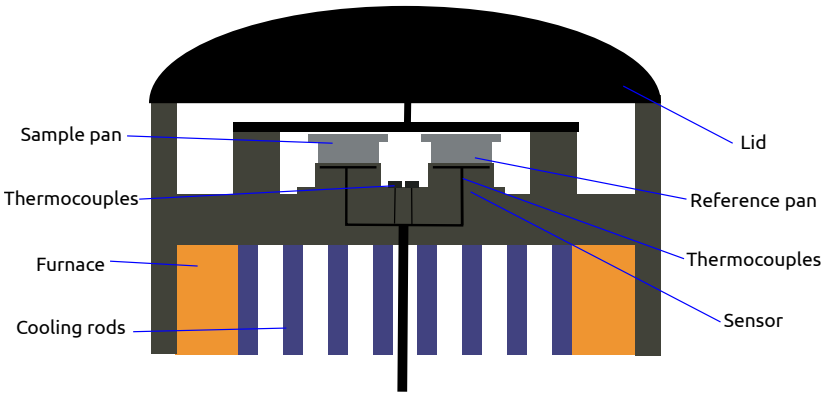


Figure 3.1. A schematic illustration of a DSC, adapted from reference (TA Instruments, 2014). During a standard DSC experiment, the sample and reference pans are heated/cooled at the same rate whilst the thermocouples are used to measure the temperature of pans.

During a DSC experiment, two pans are placed into the DSC with one containing the sample and the other as an empty reference. Under the pans are thermocouples which can accurately measure their temperature. As the pans are heated/cooled by the surrounding furnace or cooling equipment the sample may go through various thermodynamic events such as crystallisation (exothermic) or melting (endothermic).

Overall, the DSC experiment measures the heat required to maintain the pans at the same temperature. The heat flow in a DSC experiment

consists of:

$$\frac{\delta H}{\delta t} = Cp\frac{\delta T}{\delta t} + f(T,t) \tag{3.1}$$

Where $\delta H/\delta t$ is the heat flow, Cp is the sample's specific heat capacity, $\delta T/\delta t$ is the heating rate and $f(T,t)$ is the kinetic component in which heat flow is a function of time at an absolute temperature (Thomas, 2005). It is possible to determine the Tg′ of a formulation when heat flow is plotted against temperature, an example of which is shown in Figure 3.2, as materials have a higher heat capacity above the Tg′ rather than below it.

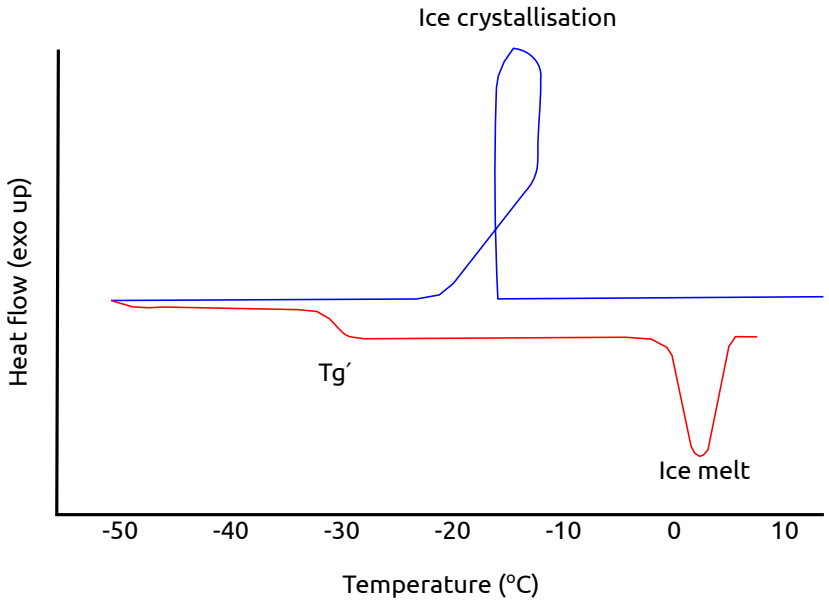


Figure 3.2. An illustrated DSC trace of a protein solution which is cooled (blue line) allowing the ice to form and then heated (red). On heating, the heat flow baseline changes due to an increase in the sample's heat capacity (Tg′) which is then followed by an endothermic event due to ice melting.

DSC was used in Chapters 4 and 5 in this thesis to measure the Tg′ of mAb1 and BSA formulations prior to lyophilisation. A 10 °C/min heating rate was used for all DSC experiments.

3.1.2 Freeze drying microscopy

The set up for determining the collapse temperature (Tc) of formulations can be seen in Figure 3.3, in which the sample is placed onto the cryostage which is temperature controlled. After freezing the sample, a vacuum is applied (generally 100 mTorr) and the temperature is gradually raised. The Tc is determined from the point of appearance of translucent dots behind the ice sublimation front (Izutsu *et al.*, 2010, Yamaki *et al.*, 2012). Images can also be collected allowing the data to be reviewed. An example of a typical Tc determination experiment can be seen in Figure 3.4. The sublimation front is approximately in line with the -18 °C mark and the edge of the sample can be seen at -25 °C. Although it is best to review the data as a series of images at each temperature, this example does highlight the appearance of translucent dots which start at approximately -20 °C.

This work has used freeze drying microscopy in Chapters 4 and 5 to determine the Tc of protein formulations. Identical ramp rates were used for all samples and the incremental increases in temperature can be found in Appendix Table A.1.

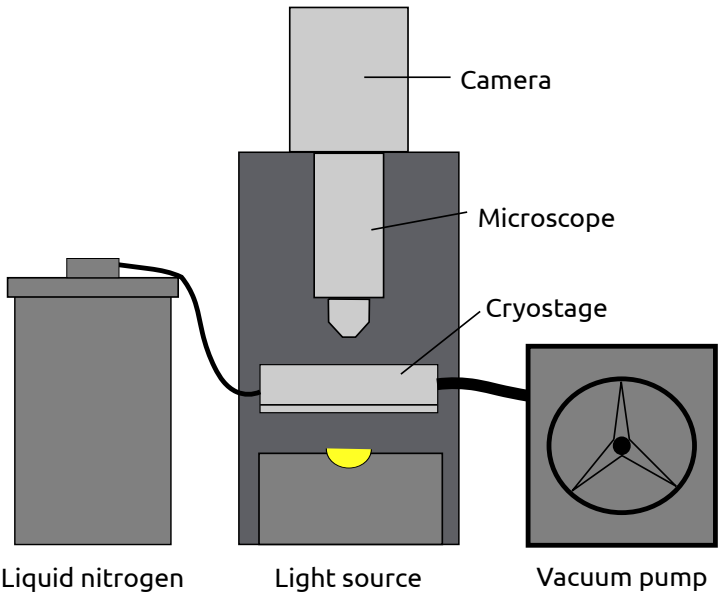


Figure 3.3. The set up employed for the freeze drying microscope stage in which the sample is placed onto the cryostage. After reducing the temperature the stage is depressurised to approximately 100 mTorr using a vacuum pump.

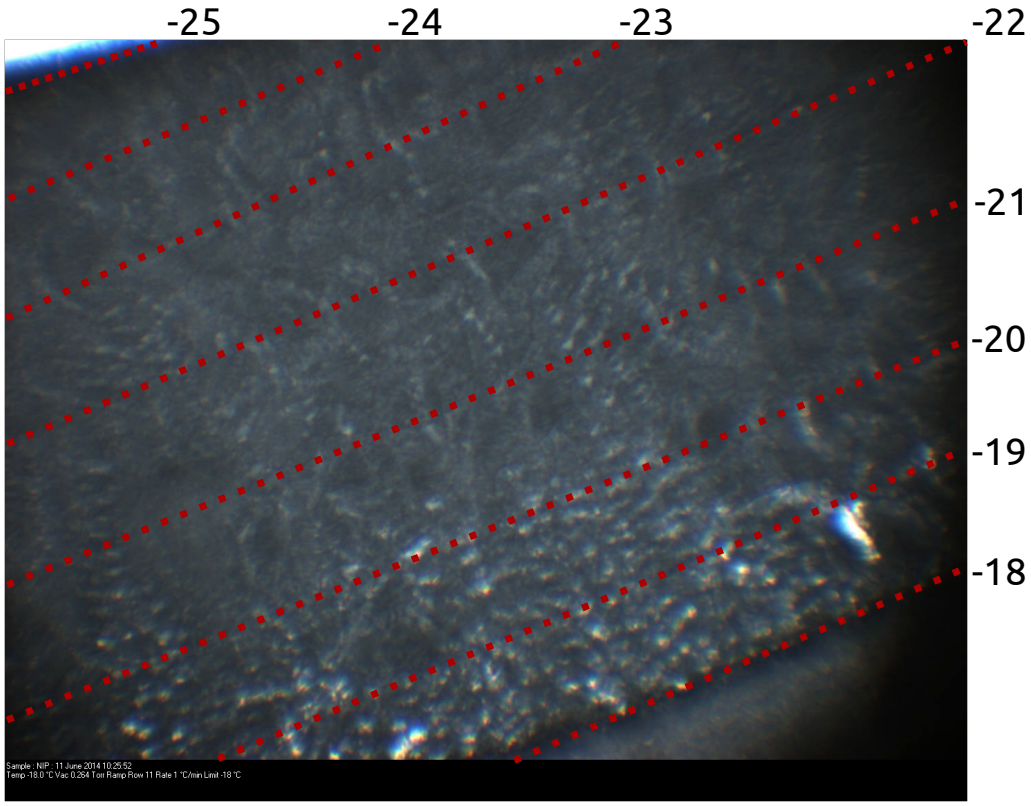


Figure 3.4. An image obtained through the freeze drying microscope. The dashed lines and temperature (°C) have been added for illustration only. The Tc is determined by the appearance of translucence through the cake, in this case it appears to start at approximately -20 °C.

3.2 Solid state characterisation

3.2.1 Karl Fisher titration

Karl Fisher titration can be either volumetric or coulometric, the primary difference being the way in which iodine is generated; it can be included with the reagents or generated at the electrochemically at the electrode, respectively. The level of detection for volumetric titration is generally in the range of 0.01–100 % compared to coulometric which is 0.0001–5 % (Mettler Toledo, 2011). Coulometric titration, which has been used in this work, measures the amount of charge required to reduce (or oxidise) an analyte.

The Karl Fisher reagents are typically: iodide salts, sulphur dioxide, anhydrous methanol and pyridine, although the use of pyridine has been largely replaced by imidazole or diethanolamine (Watson, 2012). The method proposed by Karl Fisher is regarded as being relatively specific to water (Kar, 2005), and is therefore useful in determining the moisture content of solids. The reduction of iodine by sulphur dioxide in the presence of water consists of a two step process through an alkylsulfite intermediate (Mettler Toledo, 2011):

1. $ROH + SO_2 + RN \longrightarrow (RNH) \cdot SO_3\,R$

2. $(RNH) \cdot SO_3R + 2\,RN + I_2 + H_2O \longrightarrow (RNH) \cdot SO_4R + 2(RNH)I$

A typical set up for a Karl Fisher coulometric titrator can be seen in Figure 3.5. The solutions used for the anolyte and catholyte are the Karl Fisher reagents, which are separated by a diaphragm. Iodine is formed from the anode of the generator electrode and causes the release of electrons which

then react with water. At the cathode, positive hydrogen ions are reduced to hydrogen in a process promoted by the presence of the ammonium salt (Mettler Toledo, 2011). Consequently, the amount of water in a sample can be determined by calculating the number of coloumbs required to generate iodine, as 2 coulombs are equivalent to 1 mole of water (Watson, 2012).

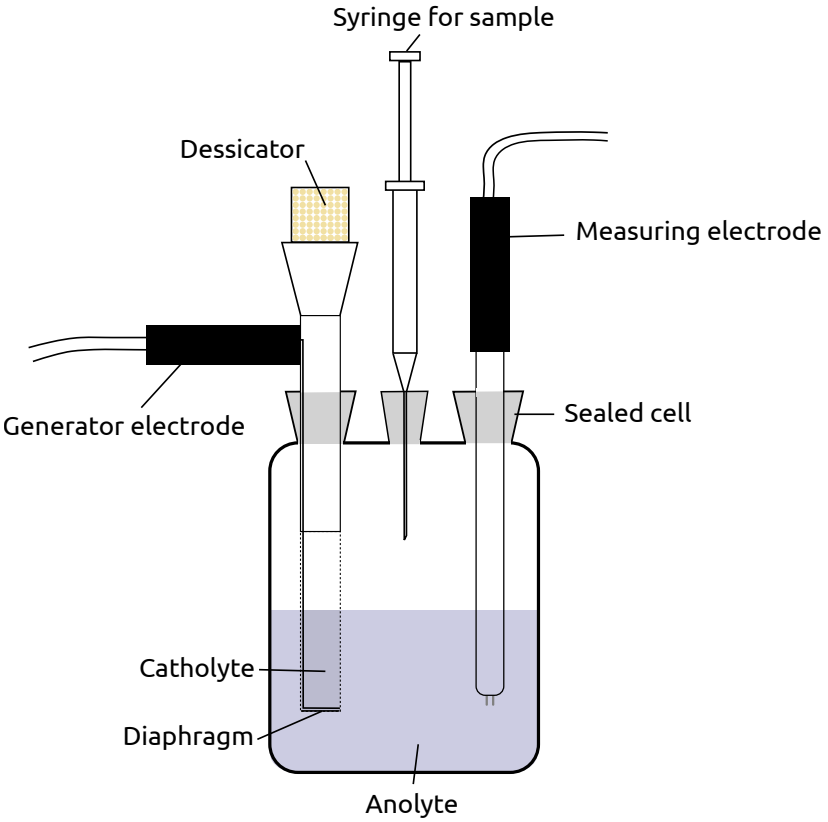


Figure 3.5. The set up for a Karl Fisher coulometric titration cell, adapted from reference (Mettler Toledo, 2011), in which the cell itself is sealed and the sample (methanol containing residual moisture from the lyophilised cake) is injected into the anolyte.

In this thesis coulometric Karl Fisher titration has been used in Chapters 4 and 5 to determine the residual moisture contents of lyophilised protein cakes. The set-up for the titration is especially beneficial for lyophilised products as it does not require the sample to be removed from the vial (which could add moisture to the sample) but instead methanol can be injected directly into the vial. The performance of the titration cell was monitored using HYDRANAL® water standards containing 1 mg/mL of

water which was measured prior to analysis and between every 10 samples. The moisture content of methanol was also determined at these intervals.

3.2.2 X-ray powder diffraction (XRPD)

Diffraction occurs when radiation interacts with electrons surrounding an atom. Within a crystal, molecules are orientated with long range order and the distances between atoms effectively behave as 'planes' (Troy *et al.*, 2006). If the rays reflecting off the plane interfere constructively with each other then a diffraction peak is produced, and Bragg's Law is satisfied:

$$n\lambda = 2d\sin\theta \tag{3.2}$$

Where n is the order of the diffraction, λ is the wavelength of radiation, d is the distance between atoms and θ is the angle of incidence. Consequently, a diffraction pattern provides information on the translational symmetry within a crystalline material.

Amorphous materials have no long range molecular and, rather than producing a diffraction pattern with characteristic peaks, result in a broad halo which represents the average spacing between molecules (Williams and Bause, 1996). It is also possible to detect partial crystallinity in an amorphous material, in which low intensity diffraction patterns may be produced. However, it has been reported that a sample would need to contain at least 10 % crystalline material in order for a diffraction pattern to be detected (Varlashkin, 2011).

A schematic diagram of the set up for a typical X-ray powder diffractometer can be seen in Figure 3.6. In general, the wavelength of radiation

is usually kept constant in an XRPD experiment. X-rays are emitted from an X-ray source and then pass through several filters prior to interaction with the sample. The XRPD model used in this study employed a Bragg-Brentano geometry between the X-ray source, sample and detector, which results in the sample being scanned through an angle of θ while the detector is at 2θ.

XRPD was used in Chapters 4 and 5 to determine the presence of amorphous or crystalline material in the as received excipients and also lyophilised cakes. Furthermore, XRPD was used in Chapter 5 to detect whether any material crystallised in lyophilised cakes after 12 weeks of storage at 40 °C.

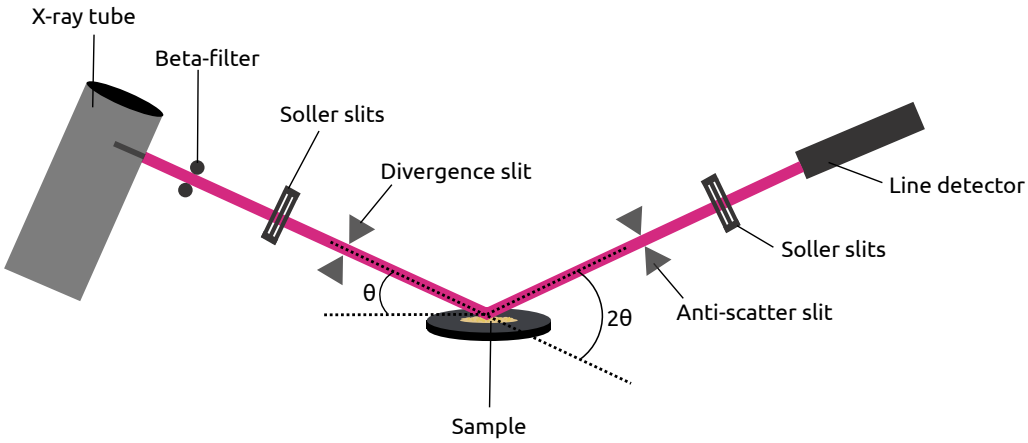


Figure 3.6. A schematic illustration showing the set up for an X-ray powder diffractometer, similar to the one used in this study. Adapted from reference (PANalytical B.V., 2014).

3.2.3 Dynamic mechanical analysis (DMA)

During a DMA experiment an oscillating force is applied to a material and the energy absorbed and material stiffness (modulus) are measured (Menard, 2008). A material's modulus is complex and consists of the storage modulus (G′) which indicates a material's elastic response and the loss modulus (G″) which relates to the viscous component of the matieral (Roy-

all *et al.*, 2005). The ratio of these effects gives the dampening parameter, tan δ.

A number of accessories exist for measuring different deformation modes such as shear, compression and tension and also for different solids depending on whether they are intact or in a powder (Mahlin *et al.*, 2009). In this work, a compression clamp was used to find the Tg of lyophilised cakes and is illustrated in Figure 3.7. The sample is placed onto a fixed stage with an oscillating plate above it. As a material's Tg is dependent on the oscillation frequency, a frequency of 1 Hz is often used as a standard to allow comparisons between materials (Foreman *et al.*, 2014). The stage and sample are enclosed inside a furnace which can control the heating rate. Following this, the storage and loss modulus and tan δ are determined and can be plotted against temperature (Figure 3.8). Due to difficulties in determining the onset of the Tg by monitoring the storage modulus, the peak in the loss modulus is often used to determine the Tg of a material and indicates the maximum change in molecular mobility (Foreman *et al.*, 2014).

In this thesis, DMA was used in Chapter 5 to find the glass transition temperature (Tg) of lyophilised cakes. A compression clamp was used in the experimental set up. In order to calibrate the DMA indium was placed on the clamp and heated at 3 °C/min under controlled force. The melting temperature of indium was then measured as function of clamp displacement. The Tg of the lyophilised cakes were determined as the peak maximum of the sample loss modulus as a function of temperature.

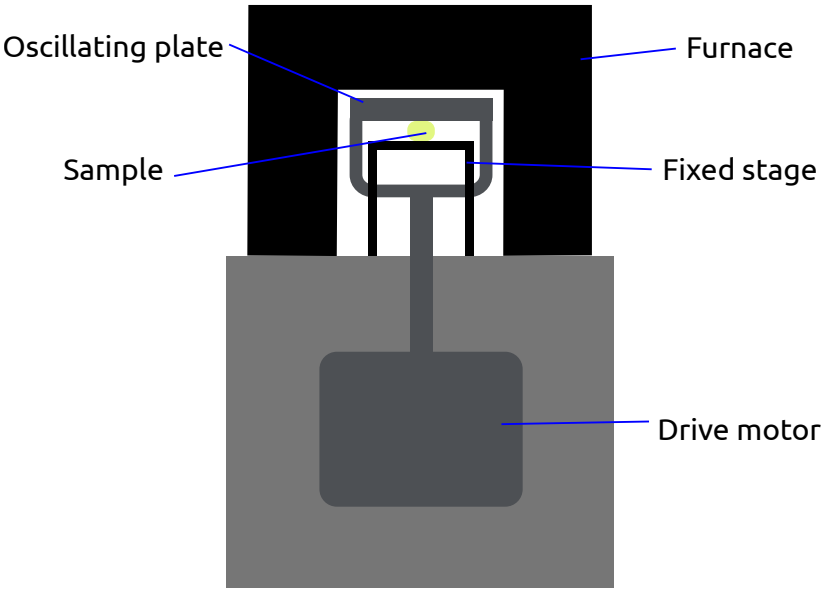


Figure 3.7. A schematic illustration showing the set up for a DMA with a compression clamp in which the lyophilised cake is placed onto a fixed stage and heated whilst the plate above oscillates at a particular frequency (1 Hz).

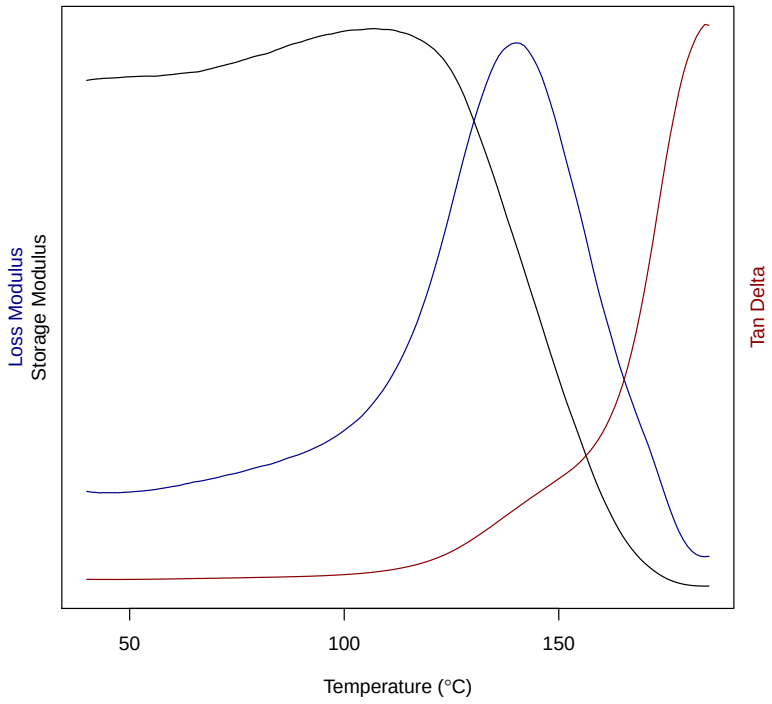


Figure 3.8. An example trace of the DMA of a sample from this thesis. The Tg was determined using the peak maximum of the loss modulus.

3.3 Physical characterisation

3.3.1 Inspection of lyophilised cakes

After lyophilisation, all cakes were visually inspected for differences in colour, the presence of particles or visible contamination and the overall elegance of the cake appearance. In general, there are five types of structural features that can occur with lyophilised cakes, which were described in Chapter 1 Section 1.1.4 and can be seen in Figure 3.9. The most desirable cake appearance is one with no collapse and a uniform distribution of material in the vial. However, unless a bulking agent has been added to the formulation often some cracking and volumetric shrinkage is observed with the lyophilised cake. An increased molecular mobility during lyophilisation may lead to the blockage of pores (Schersch *et al.*, 2010). This can result in large scale (macro) collapse, at its most extreme this may lead to complete meltback of the formulation.

The physical appearance of all lyophilised protein cakes were inspected immediately after lyophilisation, have been described in Chapters 4 and 5.



No collapse | Volumetric shrinkage | Cracking | (Macro-) Collapse | Meltback

Figure 3.9. The physical appearance of lyophilised cakes which can range from an elegant structure with no collapse to complete meltback of the product.

3.3.2 Scanning electron microscopy (SEM)

SEM is a powerful technique for characterising the surfaces, structures and morphologies of a wide range of organic and inorganic samples. Consequently, SEM often plays an important role in characterising the surface and structural features of pharmaceutical products.

A schematic drawing of a conventional SEM can be seen in Figure 3.10. Under vacuum, an electron beam is accelerated and then refined through a lens and series of apertures. The beam is then rastered across the sample using deflection scanning coils (Carlton, 2011). Interaction of the electron beam with the sample causes the production of various types of electrons from the material. Most commonly, secondary electrons are produced but also back scattered electrons can be detected. These electrons are then able to modify the signals which form the final image (Reimer, 1998).

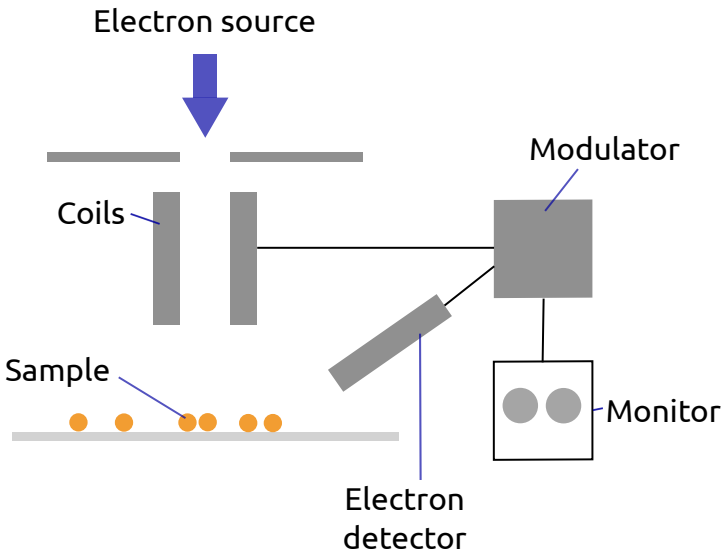


Figure 3.10. A schematic of an SEM in which an electron beam is rastered across the sample using deflection scanning coils. Electrons from the surface are produced and detected, leading to modifications in the signal which form the final image (Carlton, 2011).

Prior to SEM analysis, samples usually require coating with a thin car-

bon or metal film to prevent the accumulation of static charge ('charging') on the surface of the sample by the electron beam (Haefele and Paulus, 2010, Kim *et al.*, 2010).

SEM has been used extensively for characterising lyophilised cakes, most notably for inspecting microcollapse (Overcashier *et al.*, 1999) and phase separation (Heller *et al.*, 1999a,b). In this thesis, SEM has been used in Chapters 4 and 5 to characterise the pore structure and determine the presence of microcollapse in the lyophilised protein material.

3.3.3 Gas adsorption isotherms

Adsorption is a physical process which, in this case, a gas molecule interacts with a solid surface through weak van der Waals interactions. The process is exothermic with a large enthalpy of adsorption to overcome the loss of entropy of the gas molecule (Barnes and Gentle, 2011). The adsorption of a gas onto a solid increases with increasing pressure. Consequently, if the temperature is kept constant but the pressure is increased it is possible to measure the amount of gas molecules adsorbed onto the surface of the solid, as described in Figure 3.11.

Figure 3.11. The solid sample is placed within a controlled environment, usually with the temperature at 77.3 K (the boiling point of nitrogen at 1 atm). As the pressure (P) is increased a fraction relative to the vapour pressure of the gas (P_0) adsorbs onto the surface. After the formation of a monolayer of gas molecules on the surface, multiple layers may form.

Prior to analysis, a sample is degassed by heating and then purged with an inert gas to remove moisture and other weakly adsorbed molecules which may affect any adsorption measurements. The temperature of the sample is then lowered to the boiling point of the adsorbing gas (77.3 K for nitrogen) and placed under high vacuum (<10 mmHg). The gas is dosed onto the sample at pre-defined points and allowed to equilibrate forming an isotherm. As the gas is adsorbed to the surface of the solid it begins to form a monolayer and subsequently multiple layers may form. The volume of gas adsorbed onto the sample can then be expressed as a function of pressure, or more specifically the pressure resulting from the nitrogen dose (P) relative to the vapour pressure of the gas (P_0). By plotting the volume of adsorbed gas against relative pressure it is possible to characterise the curve by the shape of the isotherm. After pressurising the sample, the pressure is reduced (the gas is desorped) back to vacuum pressure. There are six known types of adsorption isotherms and these have been illustrated in Figure 3.12.

The Type 1 (or Langmuir) isotherm occurs when volume rather than surface area limit the uptake of gas, this commonly occurs with microporous (<2 nm) samples in which the adsorbing gas forms a monolayer on the surface (Sing *et al.*, 1985). Type 2 isotherms are often found with mesoporous (2–50 nm) and macroporous (>50 nm) samples in which the gas is able to form multiple layers on the surface. Type 3 isotherms result from solids which have only a weak interaction with the gas (Sing *et al.*, 1985). Types 4 and 5 isotherms are similar to Type 2 and 3, respectively however hysteresis occurs on desorption which is the result of capillary condensation and can provide information on pore uniformity and shape (Balbuena and Gubbins, 1993). A type 6 isotherm is only found with non-porous solids

with a uniform surface.

Numerous models have been applied to adsorption isotherms in order to calculate a sample's surface area. By far the most popular models are those by Langmuir in 1918 for monolayer adsorption (Langmuir, 1918) and (through extension of this) Brunauer, Emmett and Teller in 1938 for multilayer adsorption (Brunauer *et al.*, 1938). The BET multipoint model, which is used in this thesis, can be seen in Equation 3.3.

$$\frac{P}{V_a(P_0 - P)} = \frac{C-1}{V_m C} \times \frac{P}{P_0} + \frac{1}{V_m C} \tag{3.3}$$

Where P is the partial pressure of the adsorbed gas in equilibrium and P_0 is its vapour pressure. V_a is the volume of gas adsorbed, V_m the volume of gas adsorbed to produce a monolayer and C is the BET constant. To determine the surface area of a sample with a Type 2 or 4 adsorption isotherm the values V_m and C must be calculated and can be found by plotting $P/[V_a(P_0 - P)]$ against P/P_0. Regression of a straight line should then provide an intercept of $1/V_m C$ and a slope of $(C-1)/V_m C$ (Webb and Orr, 1997). The BET specific surface area (i.e. the surface area divided by the dry mass of the sample after degassing) can be determined by multiplying V_m by the area occupied by each molecule of gas[1].

The BET constant C must be a positive value and relates to the enthalpy of adsorption of the adsorbed gas. It is not however a quantitative measure of the enthalpy of adsorption and a conversion is required (Sing *et al.*, 1985). Instead, the BET constant can provide an indication of the strength of an interaction energy. In general, values of C less than 1 are due to Type 3

[1]For Nitrogen gas, the volume occupied by one molecule is 0.162 nm^2 at 77.3 K (Barnes and Gentle, 2011).

isotherms whereas values greater than 1 relate to type 2 isotherms (Barnes and Gentle, 2011). If the interaction energy is weak, such as in a Type 3 isotherm, the BET model can not be applied (Sing *et al.*, 1985).

Lyophilised protein cakes are typically macroporous and can have low surface areas (Webb *et al.*, 2003). However, at low surface areas, the number of gas molecules in the free space (i.e. not adsorbed) can become large and may lead to a higher level of uncertainty in the results. To overcome this, longer equilibration times or greater sample masses can be used. Using a gas with a lower vapour pressure, for example by replacing nitrogen with krypton gas, can also improve the results of low surface area samples. This is because krypton (at 77.3 K) has a saturation pressure approximately 1/300 lower than nitrogen, consequently, the free space above the sample contains 1/300 less gas molecules than nitrogen at the same relative pressure (Webb and Orr, 1997).

In this work, nitrogen adsorption isotherms have been used to calculate the BET SSA of lyophilised protein cakes in Chapters 4 and 5. The BET constant and error associated with the BET fit for the samples in each experimental chapter can be found in Appendix A and B, respectively. Nitrogen gas was used as it is relatively inexpensive and is often used to calculate surface areas down to 0.5–1 m^2/g. To verify the accuracy of the equipment, nitrogen adsorption isotherms were collected on reference material including low surface area Alumina (nitrogen multipoint BET: 0.28 ± 0.03 m^2/g) and high surface area Silica-alumina (nitrogen multipoint BET: 213 ± 6 m^2/g), which were found to have BET SSA within the recommended range.

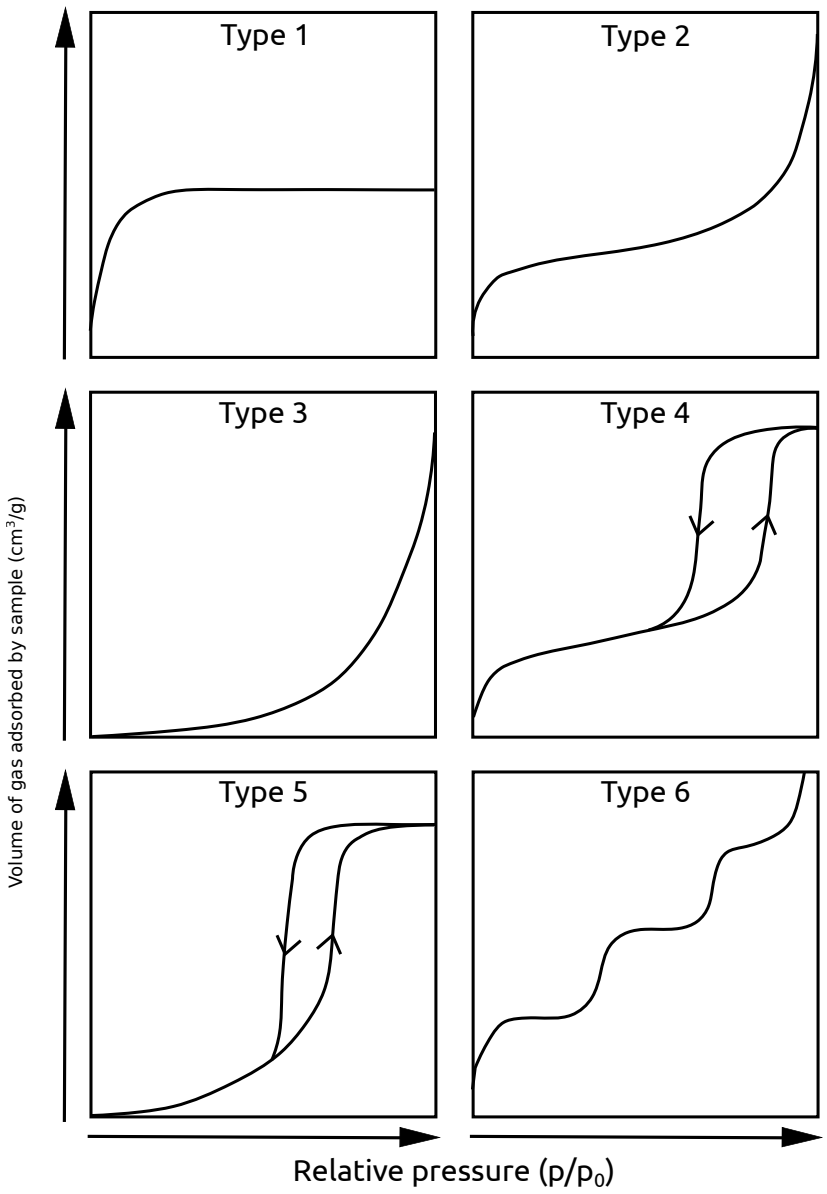


Figure 3.12. The six basic types of adsorption isotherms, adapted from reference by Sing *et al.* (1985).

3.3.4 Mercury intrusion porosimetry (MIP)

Mercury can be used to provide information on the pore size, pore distribution and porosity of a sample. Mercury acts as a non-wetting probe and will not enter the pores of a sample unless pressure is applied. The relationship between pressure (P) and pore diameter (D) can be found using the Washburn equation (Washburn, 1921b):

$$D = \frac{-4\gamma \cos\theta}{P} \tag{3.4}$$

Where γ is the surface tension and θ is the contact angle. In a typical experiment found in this thesis, the lyophilised cake is broken into pieces and placed inside a powder penetrometer, which has been illustrated in Figure 3.13. The penetrometer is glass with the exception of a metal plating and a metal cap. After a vacuum has been applied (70 μmHg for ten minutes) the penetrometer is filled with mercury through the stem which forms an electrical contact between the metal cap and plating. Consequently, the penetrometer acts as a capacitor in which it is able to provide sensitive measurements about the volume of mercury within the stem (Webb and Orr, 1997). As the pressure is applied to the stem, either by air or hydraulic fluid for high pressure analysis, the mercury will only intrude into pores of a specific pore diameter (determined by the Washburn equation).

MIP has several important disadvantages which can limit its use and can affect the interpretation of results. For instance, intrusion of mercury will only occur into open pores. Areas in the sample which have closed pores (Figure 3.14a), or pores smaller than the highest equivalent pressure used are not accessible and will therefore not be analysed.

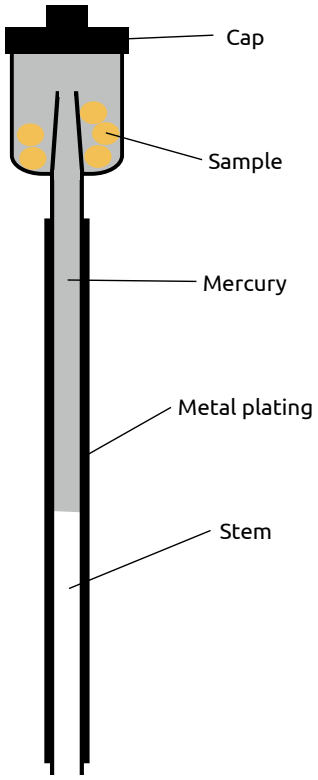


Figure 3.13. A diagram of a powder penetrometer which can be used for mercury intrusion experiments. As the pressure is increased mercury can only move up the stem if it intrudes into sample pores.

It is assumed in MIP that the pores are cylindrical and the pore size diameter is a reflection of the cylinder width. However, with spherical pores the throat of the pore is smaller than the pore body (Figure 3.14b) resulting in hysteresis on extrusion and higher pressures required to intrude the mercury. This can skew the data to smaller pore diameters. A comparison of pore size obtained by MIP and SEM will therefore often reveal larger pores in the SEM analysis.

When increasing pressure is applied, mercury will intrude larger pores before smaller pores. An ideal sample therefore consists of larger pores on the outside of the sample with pores becoming consecutively smaller internally (Figure 3.14c), which is not always the case. Finally, during intrusion mercury may crush the sample. This can often be observed visually by the

presence of a linear slope when cumulative pore volume is plotted against increasing pressure (Alie *et al.*, 2001).

Despite these limitations, mercury porosimetry is a useful technique for examining the physical structure of samples. It is widely used for the determination of pore size and porosity for a number of materials such as soil and cement samples (Galle, 2001, Romero and Simms, 2008), and lyophilised tissue scaffolds and hydrogels (Ferreira *et al.*, 2005, Gao *et al.*, 2011, Levesque *et al.*, 2005). The bulk density of a sample can also be calculated using MIP in which a pressure is applied (0.51 psi in this work) to allow mercury to surround the sample but not penetrate into pores. The bulk density is then calculated as the weight divided by the volume of the sample, which will include open and closed pores (Webb and Orr, 1997).

Mercury intrusion porosimetry has been used in Chapters 4 and 5 to assess the pore size and pore size distributions of lyophilised protein cakes. The bulk density and total intrusion volume (which represents the total pore volume) was also determined. The surface tension and contact angle of mercury were kept constant at 0.485 N/m and 130°, respectively, which are the most widely accepted values (Goworek, 2006).

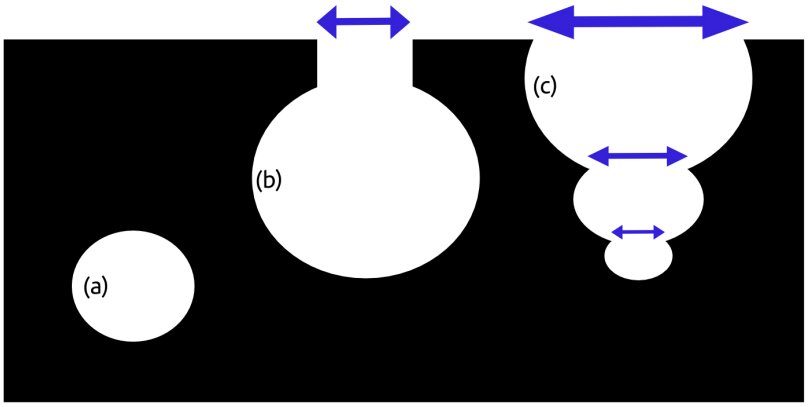


Figure 3.14. The different types of pore structure including (a) a closed pore, (b) an open pore, the width of which is defined by the pore throat in MIP and (c) an ideal pore structure for MIP, in which pores become consecutively smaller further into the sample.

3.3.5 X-ray microtomography (Micro-CT)

X-ray computerised tomography (CT) was first introduced in 1973 (Hounsfield, 1973) and, with technological advances in detector resolution, 3D imaging and reconstruction algorithms in the 1980's (Weissleder and Gambhir, 2010), it is now possible to non-invasively determine the interior structure of objects to less than a micrometre scale. For a structure to be visible in an X-ray image, it must have physical contrast to its surrounding. This contrast is often provided by the material's thickness, its density or its atomic number. For instance, the difference in density between the solid muscle of the heart and the air space in the lungs can lead to contrast in an X-ray image, whereas bones can be distinguished from surrounding tissue as they are richer in calcium (Patil, 2008).

A simple set up for a micro-CT can be seen in Figure 3.15. A cone-beam configuration was used in this work, in which the beam expands in both x and y directions, requiring the sample to be rotated (Yin, 2012). As the transmission of an X-ray will follow a straight line, the beam configuration

can be altered to allow magnification of the projection depending on the distance between the X-ray source, sample and detector. After rotating the sample by 180°, the projections can be reconstructed, providing the user with a series of 2D images. Stacking of these images can then be used to generate 3D models of the sample.

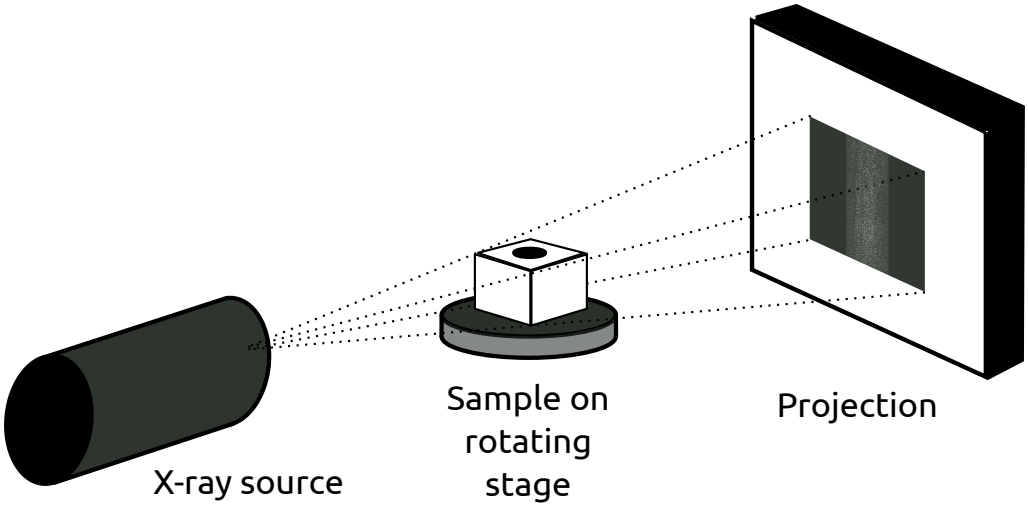


Figure 3.15. A simple set up for a micro-CT system with a cone-beam configuration in which X-rays are taken as the sample rotates 180° on a moveable stage, adapted from (Weissleder and Gambhir, 2010).

The disadvantages of micro-CT often involve its spatial resolution, field of view and contrast in the images. In general, to increase the spatial resolution of an image the field of view must be reduced, as the final volume of the 3D data is proportional to the third order of the voxel size (Yin, 2012). Smaller features also absorb less energy, which can lead to images with poor contrast and can be observed as a loss in the fine detail or transparency in the reconstructed image.

Application of micro-CT to pharmaceutical dosage forms is a relatively new area but uses include: determining the spatial distribution of phases (i.e. the different densities of material such as in a capsule), investigating the pore structure in granules and controlled release matrix tablets and uptake studies for drug delivery (Laity *et al.*, 2010, Liu *et al.*, 2013b, Noguchi *et al.*,

2013, Stock, 2008).

Few published studies exist for the use of micro-CT with lyophilised protein cakes (Ekenlebie and Ingham, 2011, Izutsu *et al.*, 2014, Parker *et al.*, 2010, Peters *et al.*, 2014). However, micro-CT requires minimal sample preparation, provides high resolution 3D imaging and is non-destructive, therefore making it an ideal technique to examine various cake structures. Micro-CT was used in Chapter 5 of this work to investigate the lyophilised cake structure of BSA arginine-C4 (succinic acid) formulations which were annealed for different annealing durations (0, 2 and 4 hours).

3.4 Characterising protein aggregates

3.4.1 IR and Raman spectroscopy

Vibrational spectroscopy methods such as IR and Raman spectroscopy are often used to assess changes in chemical composition and protein secondary structure. Furthermore, experiments can be carried out in the solid and solution states requiring minimal sample preparation. Although IR and Raman spectroscopy techniques are considered complementary to each other, the basis of how the monochromatic light interacts with matter is fundamentally different. Consequently, they provide different chemical information.

A Jablonski diagram of the energy transitions observed with IR absorption, Rayleigh and Raman scattering can be seen in Figure 3.16. Molecular vibrations depend on the masses of atoms, their geometric arrangement and the strength of the chemical bonds (Larkin, 1997). For a molecule to be IR active, the incident light must match the resonance frequency of a normal mode of bond vibration, causing a change in dipole moment. This results in a change in vibrational energy level.

Light scattering results from the electromagnetic fields of incident light causing a deformation in the electron cloud of the molecule, leading to an induced dipole moment (Larkin, 1997). Therefore, for a molecule to be Raman active there must be a change in molecular polarisability. Raman scattering is an inelastic process and results in the scattered photon having less (Stokes) or greater (anti-Stokes) energy than the incident photon. Rayleigh scattering is elastic and the scattered photon has no change in energy.

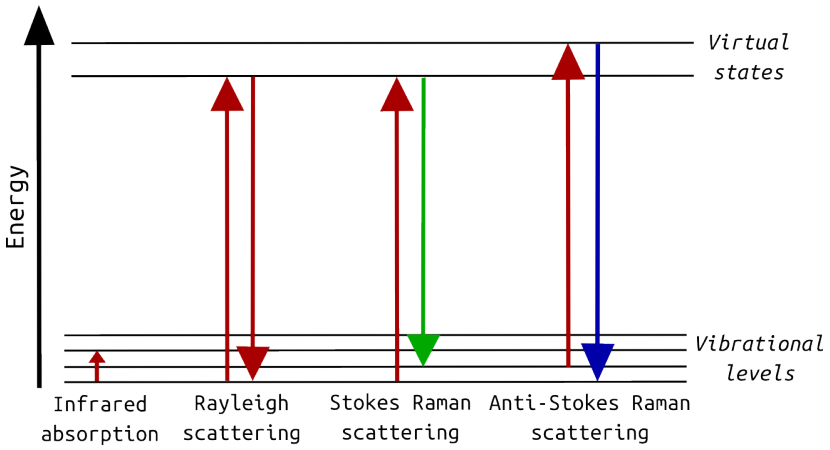


Figure 3.16. Jablonski diagram of the energy transitions observed with IR absorption, Rayleigh and Raman scattering (adapted from reference (Gamry Instruments, 2014).

IR and Raman spectroscopy have a high sensitivity to interactions such as hydrogen bonding (Hovgaard *et al.*, 2013). By using these techniques, it is therefore possible to observe changes in protein secondary structure such as α-helix to unordered or β-sheet transitions (Avis and Wu, 1996, Pelton and McLean, 2000). Proteins exhibit several characteristic vibrational bands. The most sensitive to hydrogen bonding is the amide I band (1700–1600 cm^{-1}), which relates to the protein secondary structure, and is due to carbonyl stretching vibrations within the peptide backbone (Kong and Yu, 2007).

However, protein secondary structure components are often extensively overlapped within the amide I region and may require mathematical algorithms to resolve the components, such as through second derivative analysis (Dong *et al.*, 1990, Jackson and Mantsch, 1995). Assignments of secondary structures to resolved components have been reported previously by other authors and were used in this thesis to inform the interpretation of changes in secondary structures in the lyophilised and solution (before lyophilisation and after reconstitution) states. The work by Jackson and Mantsch

(1995), Matheus *et al.* (2006), Pelton and McLean (2000) was used as references for IR spectral analysis. The peak positions and secondary structure components are summarised in Table 3.1.

Table 3.1. Peak positions within the amide I band and corresponding secondary structure components. Adapted from references (Jackson and Mantsch, 1995, Matheus *et al.*, 2006, Pelton and McLean, 2000).

Peak position (cm^{-1})	Secondary structure
1675 - 1700	Intramolecular β-sheet (Antiparallel)
1680 - 1696	Turns
1655 - 1675	Turns
1650 - 1660	α-helix
1640 - 1650	Unordered
1615 - 1625	Intermolecular β-sheet (Extended strand)
1612 - 1640	Intramolecular β-sheet (Antiparallel)

In both IR and Raman spectra, α-helices occur at approximately the same frequency (Lippert *et al.*, 1976). Whereas anti-parallel β-sheets can be observed at approximately 1630 and 1685 cm^{-1} in IR spectroscopy, a strong band at 1670 cm^{-1} occurs in Raman spectroscopy (Parker, 1983). Due to this, and the absence of β-sheets in the X-ray crystal structures of serum albumins, the band at 1630 cm^{-1} in the Raman spectrum is often assigned to short-segment chains connecting the α-helical segments in BSA (Murayama and Tomida, 2004). Distinctive bands can also occur in the Raman spectrum of proteins between 1550–1620 cm^{-1} , and are due to the ring vibration modes that are assigned to aromatic amino acids, which are either very weak or not observed in the IR spectrum (Gremlich and Yan, 2001).

IR spectroscopy has been employed in Chapters 4 and 6 to determine the secondary structure of lyophilised and reconstituted BSA and mAb1 formulations with sucrose. Absorption of arginine-dicarboxylic acids in the

amide I region prevented the use of IR spectroscopy for the analysis of arginine formulations. A transmission cell was used for IR experiments in which solids were prepared as a mull which, in a method comparison study by Luthra *et al.* (2007), was found to be the best alternative to KBr pelletization for hydrated and lyophilised proteins. Furthermore, the transmission cell provides a suitable alternative to an FTIR attenuated total reflectance accessory for proteins in solution, which could lead to overestimations of conformational changes due to protein adsorption onto the crystal surface.

Raman spectroscopy was used in Chapter 6 in combination with principal component analysis (PCA) to explore whether relationships exist between formulation and processing parameters, and the protein secondary structure. To minimise interference in the Raman spectrum by fluorescence from the protein, the highest wavelength laser available was used, which in this research was 785 nm.

PCA provides a multivariate analysis approach for transforming a large number of independent observations (i.e. spectra) into a smaller set of observations, known as principal components (PCs). It is beyond the scope of this thesis to detail the operation of PCA and an interested reader is therefore advised to read the references by Jolliffe (2002) or Dunteman (1989). In brief, the PCs are linear combinations of the original observations. The first PC accounts for the greatest amount of variance within the dataset. The second PC is orthogonal to the first PC and maximises the variance within the residuals provided by the first PC (Dunteman, 1989). This process continues and if all possible PCs are used, all variance will be accounted for within the original dataset, and the number of PCs will equal the number of original observations (Dunteman, 1989). However, as a general rule, it is often sensible to have a cut-off range for the number of PCs in the region

of 70–90 % total variation depending on the number of initial observations (i.e. in this case, the number of spectra) (Jolliffe, 2002).

In Chapter 6, PCA has been used to analyse the Raman spectra of BSA formulations. PC loadings, which are the linear composites of the data and effectively 'capture' the variability information, are used to discriminate trends in the data between formulation composition and changes in the protein secondary structure. PC scores are used to provide a measure of distance indicating how closely each spectrum follows the the PC loading (Chester and Kuruganti, 2009).

3.4.2 Size exclusion chromatography (SEC)

SEC has been used for over 50 years for estimating the molecular weight of proteins and separating protein fractions (Irvine, 1997). It is widely used to assess and quantify protein aggregation, largely due to its ease of use, wide molecular weight range (5–1000 kDa), and high performance (approximately 30 minutes per sample) (Sharma and Kalonia, 2010).

The separation of components by SEC is based on their molecular hydrodynamic volume or size (Mori and Barth, 1999), the process of which is illustrated in Figure 3.17. The sample, which is generally diluted to approximately 1 to 10 mg/mL, is injected into the SEC column. The column is filled with gel beads containing pores. Polymers such as dextran are often used to create the beads, the degree of cross-linking they undergo during development enables control of the pore size (Walsh, 2007). By flowing a buffer through the column, solutes become separated as small solutes can diffuse into the pores and become hindered whereas larger solutes are less hindered and able to flow quickly through the column. Consequently, larger

solutes elute first. Detection of solutes is often through ultraviolet-visible absorption, in which photodiode array detectors are able to simultaneously measure the intensity of transmitted light at multiple wavelengths (Mori and Barth, 1999).

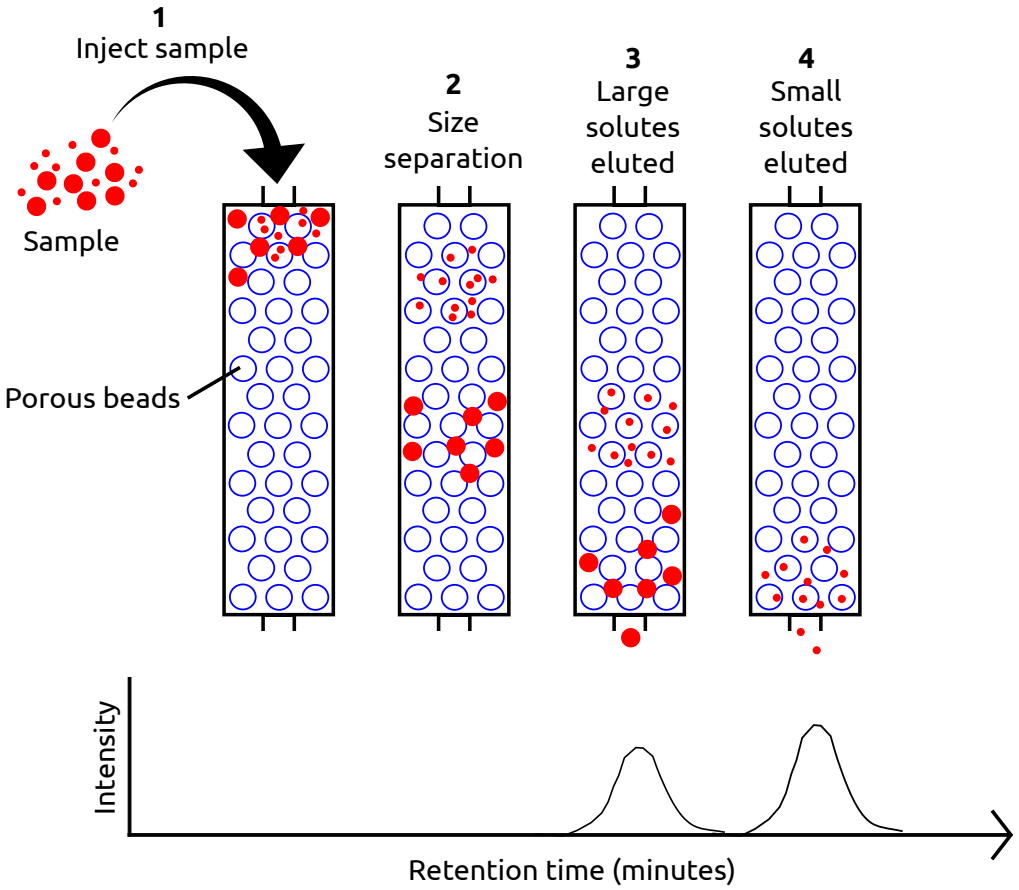


Figure 3.17. Elution of a sample (e.g. a protein solution with monomer and dimer) through an SEC column. After injection of the sample, smaller particles become trapped within gel beads in the SEC column. Consequently, larger solutes are eluted first followed by smaller solutes which have a longer retention time.

The main disadvantages of SEC include: interactions between the protein and column, the filtering out of larger aggregates (e.g. they do not flow through the column) and often dilution of the sample is required prior to injection (Sharma and Kalonia, 2010).

In this thesis, SEC was used in Chapter 6 to calculate the monomer

content of BSA and mAb1 formulations, in which the monomer is expressed as a percentage of the total soluble protein content (monomer, dimer and trimer *etc.*). The storage stability of lyophilised BSA formulations were also assessed at 0, 6 and 12 weeks when stored at 40 °C. The degradation rate of amorphous glasses have often be described by global α-relaxation processes and 'square root of time kinetics' (Abdul-Fattah *et al.*, 2008, Chang *et al.*, 2005b, Pikal and Rigsbee, 1997, Yoshioka *et al.*, 2001). In which the change in monomer content of a formulation over time can often be fitted to the following linear equation, in which a value of $n = 0.5$ would show square root of time kinetcis:

$$\%P = P_0 + kt^n \tag{3.5}$$

Where $\%P$ is the percent purity (% monomer), P_0 is the initial amount of monomer in the product, t is time and k is the rate constant (Chang *et al.*, 2005b). To determine whether the soluble aggregation rate of BSA formulations followed square root of time kinetics, the data were fitted to t^n using values of n between 0.1 and 1. The 'goodness of fit' was then measured using the F-value, as described by Abdul-Fattah *et al.* (2008), and the soluble aggregation rate (k) was determined.

3.4.3 Micro-Flow Imaging (MFI)

MFI can be used for the detection of subvisible particles in the size range of 1 to 70 μm (Sharma *et al.*, 2010). A schematic diagram of an MFI system can be seen in Figure 3.18. The theory behind MFI is relatively simple: a sample is pumped through a narrow capillary and a series of bright field images are captured of the particles contained within.

Standardised methods for determining particulate matter in parenteral injections are described in US, Japanese and European Pharmacopoeias

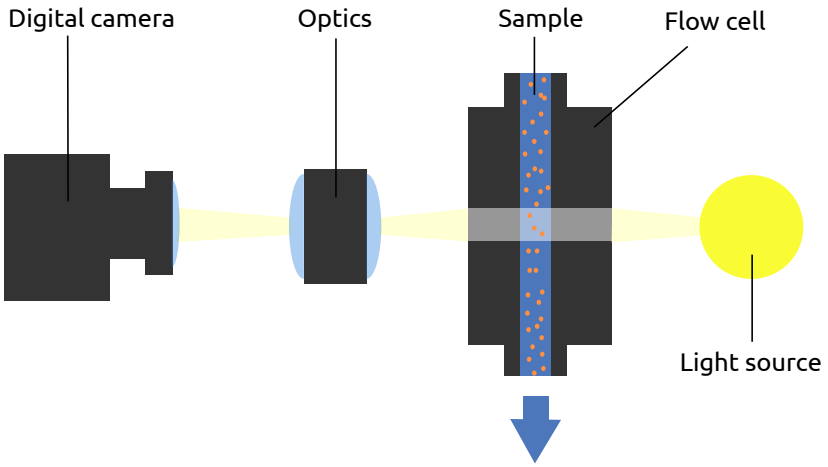


Figure 3.18. A schematic diagram of an MFI instrument, adapted from reference (ProteinSimple, 2014). The sample is drawn through a narrow capillary in the flow cell during which bright field images are taken of any subvisible particles present.

(Ph. Eur. method 2.9.19, 2013). Two methods are included for determining particulate size and are described in USP 787 and USP 788. These are: the light obscuration particle count test and microscopic particle count test. However, due to technical limitations, such as the detection of translucent particles and the small volume analysed in the microscopy method, orthogonal characterisation methods have been recently proposed in reference (USP <1787>, 2013) and include the use of flow imaging analysis (e.g. MFI).

Studies investigating the use of MFI as a technique for sub-visible particle detection have found several advantages over the light obscuration and microscopy techniques. Firstly, analysis and filtering of images allows discrimination of particles by morphology and translucency, making it possible to count protein aggregates rather than air bubbles or silicone oil droplets (Strehl *et al.*, 2012). Secondly, the sizing and accuracy of MFI has not been found to be affected by the opalescence of certain protein solutions (Sharma *et al.*, 2010). The large volume (>1 mL) of sample that can be analysed and the relatively quick analysis time (minutes) also make MFI a useful technique in the analysis of particulate contamination. Limitations of MFI

include: its destructive behaviour (i.e. the sample cannot be retrieved), alterations of the algorithm used to classify particles may also be subjective and there may be difficulty in visualising particles with a refractive index matching the solution (Zölls *et al.*, 2013a). However, it may be possible to minimise these errors based on the selection of MFI equipment used (Zölls *et al.*, 2013b).

MFI was used in Chapter 6 to determine the extent of subvisible particles in reconstituted solutions. Prior to analysis, lyophilised cakes were stored at 40 °C and reconstituted at 0, 6 and 12 weeks. To reduce the presence of air bubbles in the sample, which can form after reconstitution, MFI was carried out 24 hours after reconstitution and all samples were allowed to equilibrate to room temperature for approximately one hour prior to analysis.

4 Insights into the Influence of the Cooling Profile on the Reconstitution Times of Lyophilised Protein Formulations

Lyophilisation is a relatively expensive process with high energy requirements and long processing times (Shire *et al.*, 2010). It is essential that whilst optimising the process a high quality biopharmaceutical product is maintained. One approach which has been found to significantly alter product quality is by modifying the lyophilisation cooling profile (Kasper and Friess, 2011).

A quick reconstitution time is a desirable quality attribute of a lyophilised biopharmaceutical and, motivated by the production of low volume, high concentration protein formulations, there has been a recent research interest into the factors that govern reconstitution time (Awotwe-Otoo *et al.*, 2013, Cao *et al.*, 2013, Geidobler *et al.*, 2013). However, considerable disagreement in the literature exists on how this is affected by the lyophilisation cooling profile (AlHusban *et al.*, 2010, Blue and Yoder, 2009, Searles *et al.*, 2001a, Webb *et al.*, 2002a).

The motivation of this study was therefore to provide a greater understanding of how the lyophilisation cooling profile and formulation influence reconstitution time. Based on these findings, this chapter provides new experimental data and proposes a mechanism of how the lyophilised cake structure may prolong reconstitution times.

4.1 Introduction

To improve the shelf-life and stability of a protein formulation, water can be removed to slow the chemical and physical degradation pathways. The most common method of drying is by lyophilisation (Allison *et al.*, 1998). Prior to administration the lyophilised product must be reconstituted back into solution, however for some protein formulations this can be time consuming. For example, the humanised $IgG_{1\kappa}$ monoclonal antibody Omalizumab (Xolair ®), can take 20 minutes to dissolve (Genentech, Inc. and Novartis Pharmaceuticals Corporation, 2014). A short reconstitution time is especially important for concentrated protein formulations which are required in the management of chronic diseases, where patients may wish to self-administer by subcutaneous injection. Long reconstitution times increase the complexity of the administration process and can be problematic for emergency therapeutics. For instance, two lyophilised anti-venom products for pit viper snake bites were found to take 40 minutes (polyclonal antibodies) and $>$ 90 minutes (monospecific antibody fragments) to reconstitute (Hill *et al.*, 2001).

At present there are 38 therapeutic monoclonal antibodies approved for use by the FDA (FDA, 2014a), 11 of which are formulated as lyophilised products. Table 4.1 summarises the different reconstitution guidelines, as described by their respective prescribing information leaflets. This table highlights several important aspects of reconstituting biopharmaceuticals. Firstly, reconstitution procedures can be complex depending on the protein and the formulation. Secondly, it illustrates that some reconstitution times can be very lengthy, and thirdly there are no harmonised guidelines for reconstitution procedures.

Table 4.1. A summary of the reconstitution guidelines provided in the prescribing information of currently FDA approved lyophilised monoclonal antibodies.

mAb	Reconstitution procedure summary
Benlysta® (Belimumab[c])	Aim diluent stream towards side of vial. Swirl gently for 60 seconds every five minutes. Do not shake, Dissolution normally takes 10-15 minutes but may take up to 30 minutes.
Kadcyla® (Ado-trastuzumab emtansine[a])	Swirl gently to dissolve. Do not shake.
Ilaris® (Canakinumab[a])	Swirl vial gently at 45° for approximately one minute then leave to stand for five minutes. Do not shake. Turn up and down ten times. Leave to stand for 15 minutes at room temperature.
Adcentis® (Brentuximab vedotin[b])	Direct diluent stream to side of vial (not directly on to cake). Swirl gently to dissolve. Do not shake.
Cimzia® (Fab fragment[d])	Gently swirl without shaking, leave undisturbed for 30 minutes.
Xolair® (Omalizumab[a])	Inject diluent directly onto the cake, keep upright, gently swirl upright for one minute until evenly wet. Do not shake. Then swirl vial for 5-10 seconds every five minutes. Should take 15-20 minutes to dissolve.
Simulect® (Basiliximab[b])	Shake vial gently.
Herceptin® (Trastuzumab[a])	Aim diluent stream at cake, swirl gently, do not shake. Leave undisturbed for five minutes.
Remicade® (Infliximab[b])	Direct diluent stream to side of glass vial, swirl by rotating vial. Avoid prolonged or vigorous agitation. Do not shake. Leave to stand for five minutes.
Sylvant® (Siltuximab [b])	Gently swirl, do not shake or swirl vigorously. Should dissolve in less than 60 minutes.
Entyvio® (Vedolizumab[a])	Direct diluent stream at side of vial. Do not vigorously shake or invert. Gently swirl the vial for at least 15 seconds to dissolve then allow the solution to sit for up to 20 minutes. Do not use the vial if the drug product is not dissolved within 30 minutes.

[a] humanised $IgG_{1\kappa}$; [b] chimeric $IgG_{1\kappa}$; [c] humanised $IgG_{1\lambda}$; [d] Derived from murine IgG_2 with κ light chain and γ_1 heavy chain constant regions (European Medicines Agency, 2008).

4.1.1 The influence of the cooling profile on reconstitution time

Cooling rate, nucleation temperature, degree of supercooling and heat treatment within a lyophilisation cycle can all affect the ice crystal morphology during the initial stages of lyophilisation (Chang and Patro, 2004). As the ice provides a template for the pores in the cake, it is therefore of considerable interest to understand how the cooling profile affects reconstitution.

Lyophilisation of poorly soluble low molecular weight drugs has been used to improve the dissolution time of rapidly disintegrating oral tablets (Fu *et al.*, 2004). It is thought that the highly porous structure of the lyophilised cake can promote greater water absorption and wetting. Another commonly used approach for increasing dissolution time is by increasing the surface area of the product, for example, by formulating in a solid dispersion (Leuner and Dressman, 2000), or through size reduction techniques (Merisko-Liversidge *et al.*, 2003). However, the following recent research has suggested that surface area is not a predominant factor in reducing the reconstitution times of lyophilised protein formulations. In the studies conducted by Geidobler *et al.* (2013) and Awotwe-Otoo *et al.* (2013), the impact of controlled ice nucleation (CIN) techniques, which were described in greater detail in Chapter 1 Section 1.1.3, on process performance and quality attributes of lyophilised monoclonal antibodies were investigated. Both studies found that CIN led to smaller surface areas, larger pore sizes and shorter reconstitution times compared to uncontrolled ice nucleation cycles. Another study, conducted by Cao *et al.* (2013), investigated multiple formulation parameters, such as protein concentration and excipient choice on

reconstitution time and found that surface area —which is related to pore size —was not found to be a critical factor for improving reconstitution time with an Fc-fusion protein formulation.

The impact of the addition of an annealing step to the cooling profile also remains elusive with studies showing either an increase (Webb *et al.*, 2002a), or a decrease (AlHusban *et al.*, 2010, Blue and Yoder, 2009, Searles *et al.*, 2001a) in reconstitution time compared to non-annealed samples. The influence of cooling rate on reconstitution time has also yet to be described in detail. However, a study conducted by Dawson and Hockley (1992) found that a cooling rate of 150 °C/min gave better reconstitution times than those cooled at 1 °C/min.

4.1.2 Sucrose as a lyoprotectant

In nature, sugars have been found to preserve living cells and proteins during freezing (Ohtake and Wang, 2011), although this is often only at low efficiency (Fuller, 2004). Furthermore, anhydrobiotic organisms which undergo drying into a state of suspended animation, are believed to survive due to the formation of an intracellular sugar glass (Green and Angell, 1989, Sun *et al.*, 1998). The ability of sugars to protect during both freezing and drying stresses make them desirable formulation excipients for lyophilised proteins (Cicerone and Douglas, 2012).

Sucrose is often used as an excipient in lyophilised products and has numerous uses in low molecule weight drug products including as a granulation agent and in tablet coatings (RSC, 2014). Sucrose is a non-reducing, low molecular weight disaccharide, the chemical structure of which can be seen in Figure 4.1.

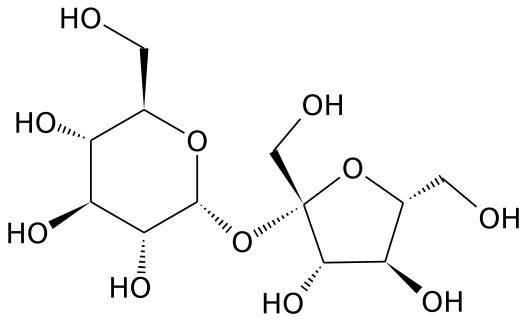


Figure 4.1. The chemical structure of sucrose.

4.1.3 Model proteins

Bovine serum albumin (BSA)

Albumins are the most abundant protein in human plasma at a concentration of approximately 50 mg/mL and a molecular weight of 66.5 kDa (Peters Jr., 1985). The function of albumins are conserved between species where it is used for maintaining blood pH and osmotic pressure. There is 76 % sequence homology between human and bovine serum albumin, with the former containing 585 amino acids and 69 % alpha-helix (Wang *et al.*, 2013) and the latter containing 583 amino acids and 63 % alpha-helix, determined by X-ray crystallographic studies (Bujacz, 2012). BSA is used in a number of molecular and biological techniques where it can be used as a blocking reagent, in which it non-specifically binds to solid phases, and as a supplement to cell culture growth media (Sigma-Aldrich, 2014). Conjugation of BSA to biopharmaceuticals also provides a strategy for prolonging their therapeutic half-life (Dennis *et al.*, 2002). BSA is separated and purified from whole blood using a multi-step fractionation process (Sigma-Aldrich, 2014). As it is a by-product from the cattle industry, the large quantities produced make BSA an attractive, low cost globular protein model for research and development studies, especially when high protein concentrations are required.

Immunoglobulin G (IgG)

IgG has a number of subtypes, however they all share a similar function and structure (Divan and Royds, 2013). As IgG_1 was used in this work, this subtype will be described in greater detail. IgG_1 is a Y-shaped antibody with a molecular weight of approximately 150 kDa. The protein consists of two identical halves connected by two disulfide bonds and is illustrated in Figure 4.2. The constant (Fc) region of the protein can bind to receptors on immunomodulatory cells, whereas the ability to bind specifically to epitopes on antigens is due to the variable (Fv) region of the molecule. Each half of the molecule consists of one light chain (25 kDa) of which there are two types: λ or κ; and one heavy chain (50 kDa) (Murphy, 2011). The ability to produce IgG from a single clone results in the antibodies binding to the same eptitope, and are therefore known as 'monoclonal antibodies' (mAbs). Since the 1980's mAbs have been studied as treatments for cancer and immunological disorders (Reichert, 2008). Recent technological advances in the production of 'human' mAbs can reduce their immuogencity and, with a current trend towards targeted therapeutics, could intensify their use in the future (Nelson *et al.*, 2010). Therefore, mAbs represent an important class of therapeutic proteins and their use as model proteins is key in formulation development studies.

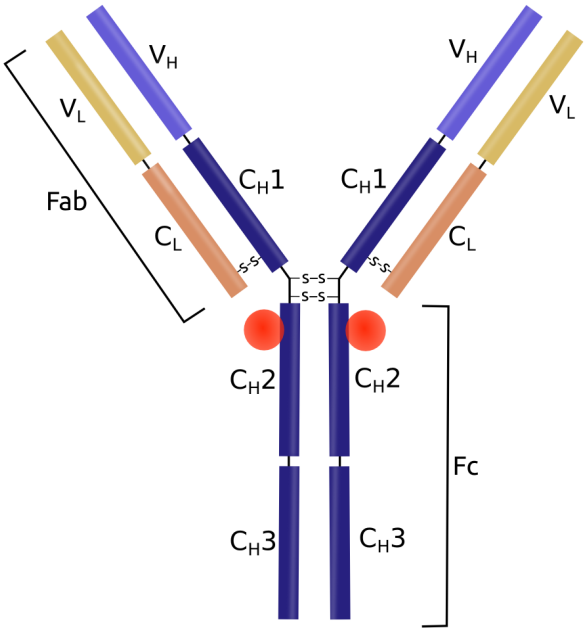


Figure 4.2. Structural features of human IgG, where H is the heavy chain, L is the light chain, V is the variable region, C is a constant region and carbohydrate chains are shown in red (adapted from reference (Grewal, 2009).

4.1.4 Chapter motivation

Despite the increasing therapeutic importance of biopharmaceuticals, there have been limited studies on the factors influencing reconstitution time of lyophilised formulations, and those that have been published show considerable disagreement between their conclusions. Therefore, the motivation of this chapter was to provide a greater understanding of how the lyophilisation cooling profile and formulation affect reconstitution time. Furthermore, other quality attributes such as cake elegance and protein stability were investigated.

BSA (50 and 200 mg/mL) and an IgG_1 (40 mg/mL) were used as model proteins in a sucrose based formulation. To alter the cooling profile two ramp rates were used: 0.5 °C/min and quench cooling through liquid nitrogen immersion. The addition of an annealing step into the cooling profile

was also investigated.

To gain a greater understanding of how reconstitution time is influenced by cake structure, this study explored physical properties of the cake such as pore size, bulk density and surface area measurements. This chapter provides new insights into the relationship between cooling profile and reconstitution time. It is hoped that this study will encourage further research into the factors that govern the reconstitution process.

4.2 Materials and Methods

4.2.1 Materials

BSA and sucrose were purchased from Sigma-Aldrich (>98 % and >99.5 % purity, respectively). Histidine buffer salts were purchased from J.T. Baker (FCC grade). BSA was prepared in a 25 mM histidine buffer solution, pH 6.0, with 7 % w/v sucrose to give final concentrations of 50 mg/mL and 200 mg/mL. Monoclonal IgG_1 (molecular weight 144.754 kDa, pI 8.44), hereafter referred to as 'mAb1', was kindly provided by MedImmune Ltd. at 40 mg/mL in a 25 mM histidine solution, pH 6.0, with 7 % sucrose. The three formulations were filtered (0.22 μm) and the protein concentrations were confirmed by UV absorbance at 280 nm (NanoDrop®, Thermo Fisher Scientific).

4.2.2 Methods

Differential scanning calorimetry (DSC)

The Tg′ of the formulation was determined using a TA Q1000 DSC (TA Instruments) in which 10 μL of sample was hermetically sealed and equilibrated at -70 °C for five minutes and then ramped at 10 °C/min in standard mode to 20 °C. The temperature of the DSC was calibrated prior to use with indium as a reference material.

Freeze drying microscopy

To determine the collapse temperature (Tc) of BSA containing formulations, an FDCS196 freeze drying cryostage (Linkam Scientific Instruments Ltd.) was used in combination with a Lyostat2 imaging station (BioPharma

Process Systems Ltd.) and QICAM Fast 1394 camera (QImaging). A 10× objective was used for magnification. A small amount of silicone oil was used to improve the thermal conductivity between the stage and a quartz slide, on top of which 3 μL of sample was placed and sandwiched between a glass coverslip (separated by a metal spacer). The stage was cooled and heated, the rates and hold times of which are described in Appendix Table A.1. A vacuum (100 mTorr) was applied from -25 °C onwards and images were taken every 10 seconds. The collapse temperature (Tc) was determined by the appearance of translucent areas in the cake structure (as shown in greater detail in Chapter 3 Section 3.1.2).

Lyophilisation

The three formulations were lyophilised using a 1 mL fill volume in 13 mm Schott Type I clear tubular glass injection vials (West Pharmaceutical Services) with Daikyo D777-1 13 mm single vent lyo stopper (West Pharmaceutical Services). Vials were placed within a custom made stainless steel fence which was used to keep vials in the centre of the freeze dryer. Two freeze dryers were used: a Virtis Advantage Plus two shelf freeze dryer (SP Scientific) for cooling profiles without an annealing step and a Virtis Advantage Plus one shelf freeze dryer (SP Scientific) for cooling profiles with an annealing step. Thermocouples, calibrated before use, were placed into one BSA 200 mg/mL formulation in the centre of the freeze dryer for each cycle. The four cooling profiles used in this study can be seen in Table 4.2. At the end of each profile, the pressure was reduced to 100 mTorr and the temperature was raised to -20 °C and held for 41.5 hours to allow primary drying. The shelf temperature was then ramped at 0.1 °C/min to 20 °C for secondary drying and then held at this temperature for 12 hours at 200 mTorr.

Table 4.2. A description of the protocol utilised for each lyophilisation cooling profile.

	Cooling profile
0.5 °C/min	Samples were cooled at 0.5 °C/minute to -40 °C and held for two hours.
0.5 °C/min + annealed	Samples were cooled at 0.5 °C/minute to -40 °C and held for two hours. The temperature was then ramped over 30 minutes to -5 °C and held for four hours after which the shelf temperature was lowered over 30 minutes to -40 °C and held for a further 30 minutes.
Quench cooled	Samples were immersed for approximately 2 minutes in liquid nitrogen and then placed onto the freeze dryer shelf which was pre-cooled to -40 °C. This shelf temperature was then maintained for two hours.
Quench cooled + annealed	Samples were immersed for approximately 2 minutes in liquid nitrogen and then placed onto the freeze dryer shelf which was precooled to -40 °C. This shelf temperature was then maintained for two hours after which it was ramped over 30 minutes to -5 °C and held for four hours before lowering it over 30 minutes to -40 °C and holding for a further 30 minutes.

Karl Fisher Moisture Determination

After each lyophilisation cycle, three vials of each BSA formulation were removed. The residual water content was determined by injecting 2 mL of methanol into sealed vials which was then mixed in a vortex for 15 minutes to extract the moisture and analysed by a Mettler Toledo C30 Coulometric Karl Fischer Titrator. MAb1 samples were not used for this analysis due to the limited number of samples available for this formulation.

X-ray Powder Diffraction (XRPD)

To characterise the solid state of the lyophilised powders XRPD was performed using a PANalytical X'Pert Pro diffractometer (PANalytical B.V.) with an angular range (2θ) of 2–40° and a resolution of 0.05° 2θ. Samples were broken into smaller fragments and loaded into a brass sample holder with a 10mm diameter. Samples were spun at 1 revolution/second dur-

ing data collection. The radiation source was monochromated Copper Kα_1 radiation (40 kV/40 mA) and a total scan time of 4.5 minutes was used.

Reconstitution Time

The volume of water required for reconstitution was calculated based on the amount of water removed from each formulation (i.e. total weight less the amount of solids). This value was then rounded to the nearest 0.1 mL, based on the graduation of syringes found in a hospital setting. For BSA (50 mg/mL) and mAb1 (40 mg/mL) formulations, 0.9 mL of water was used for reconstitution and for BSA (200 mg/mL) 0.8 mL of water was used. Prior to reconstitution, the samples requiring different reconstitution volumes were separated and the formulation labels blinded to randomise the cooling profiles and maintain a level of objectivity. Samples were then reconstituted using a syringe with the water flow aimed at the inside wall of the vial. The vial was then swirled for approximately five seconds to ensure the sides and bottom of the lyophilised cake were wetted. The vial was then left upright on a counter without further agitation until fully dissolved. The reconstitution time was defined as the time needed to dissolve all visible solids in the vial from the point of water injection. Six vials of each formulation were reconstituted. Statistical analyses were performed using a one-way analysis of variance with Bonferroni post test.

Scanning Electron Microscopy (SEM)

To alleviate compression of the cake during preparation for SEM, a sharp scalpel was used to cut the lyophilised material to expose an internal cross-section. Samples were placed onto stubs and a Leica EM SCD005 sputter coater (Leica Microsystems) was used to coat samples in gold for 120 seconds at 26 mAmp. A JEOL JSM 6060LV SEM (JEOL Ltd.) was used with an

acceleration voltage of 16 kV.

Brunauer, Emmett & Teller (BET) Specific Surface Area Measurements

Nitrogen adsorption isotherms were acquired using an Automated Surface Area Porosity Analyser (ASAP2420, Micromeritics Instrument Corporation) at 77.3 K using a relative pressure range of 0.01–0.99. Prior to analysis samples (weight 100 to 150 mg) were gently broken using a spatula and were then degassed under vacuum for 3 hours at ambient temperature. Helium gas was used to calculate warm (ambient) and cold free space. BET specific surface area (SSA) was calculated using the adsorption range of 0.1 to 0.4 relative pressure providing positive BET constants.

Mercury intrusion Porosimetry (MIP)

Mercury intrusion porosimetry was performed using an AutoPore IV Mercury Porosimeter (Micromeritics Instrument Corporation) on lyophilised protein formulations with measurements taken between 1 and 3600 psi, the pressure range and equivalent pore size diameters can be seen in Appendix Table A.2. A contact angle of 130° was used with the density of mercury adjusted according to room temperature. Again, due to the limited number of mAb1 samples, only the BSA formulations were used for this analysis. Bulk density was calculated using a pressure of 0.51 psi.

Clarity of reconstituted solutions

The presence of visible particles was determined by assessing the clarity of solutions. After reconstitution, samples were left to stand for approximately 1 hour at room temperature. Using a black and white panel with

fluorescent light, samples were swirled for approximatively 15 seconds and compared to opalescent standards (Appendix Figure A.1). The standards, outlined by Ph. Eur. method 2.2.1 (2013), are based on dilutions of formazin with nephelometric turbidity units (NTU) of 0 (water) to 1000.

Fourier Transform Infrared Spectroscopy (FTIR)

FTIR was used to determine the secondary structure of proteins in the lyophilised and reconstituted states and also in solution prior to lyophilisation. A liquid transmission cell with demountable calcium fluoride windows was used to collect the spectra of BSA and mAb1 samples using an FTS 6000 Spectrometer (Bio-Rad Laboratories). Lyophilised cakes were prepared as a mull for analysis in which approximately 5 mg of sample was gently mixed with approximately 100 mg of Fluorolube® (Thermo Scientific) using a spatula and then spread thinly between the windows. For each spectrum, 256 scans were co-added with a 2 cm^{-1} resolution. The sample spectra for cakes from three separate vials were measured for each formulation, after which vapour and water (for liquid samples) were subtracted (an example of this process can be found in the Appendix Figure A.2). The second derivative of the protein spectra was calculated using a 9-point window, after which a flat baseline was obtained and the area of the second derivative was normalised to one as described by Dong *et al.* (1995) and Kendrick *et al.* (1996).

4.3 Results

4.3.1 Tg′, Tc and product collapse

The Tg′ and Tc values of the formulations investigated can be seen in Table 4.3. Both BSA 50 mg/mL and the mAb1 formulations were found to have similar Tg′ and Tc values. The Tc of -20 °C for the BSA 50 mg/mL formulation (equivalent to approximately a 40:60 protein to sugar ratio) appears comparable to other studies investigating protein-sugar mixtures, in which a 35:65 BSA to sucrose formulation was found to have a Tc of approximately -22 °C (Meister and Gieseler, 2009). Typically, the difference between Tg′ and Tc values is 2–5 °C (Pikal and Shah, 1990, Tang and Pikal, 2004), although greater differences can be observed with increasing protein concentration (Patel *et al.*, 2013). In this study, the difference between Tg′ and Tc of the BSA 200 mg/mL formulation is less than the difference observed with the 50 mg/mL formulation. This is likely due to difficulties in the accurate determination of the Tg′ from the DSC trace, which is partially obscured by the ice melting endotherm (Appendix Figure A.3), and the interpretation of Tc from freeze drying microscopy images with high solid contents. Overall, the primary drying temperature of -20 °C used in this study did not exceed the Tc values of the formulations.

Table 4.3. The Tg′ and Tc values of BSA and mAb1 formulations.

Formulation	Tg′ (°C)	Tc (°C)
BSA 50 mg/mL	-28	-20
BSA 200 mg/mL	-23[†]	-17
mAb1 40 mg/mL	-28	-19

[†] Tg′ is partially obscured by ice melting endotherm (Appendix Figure A.3).

The shelf and product temperatures for the four different lyophilisation cycles can be seen in Figure 4.3.

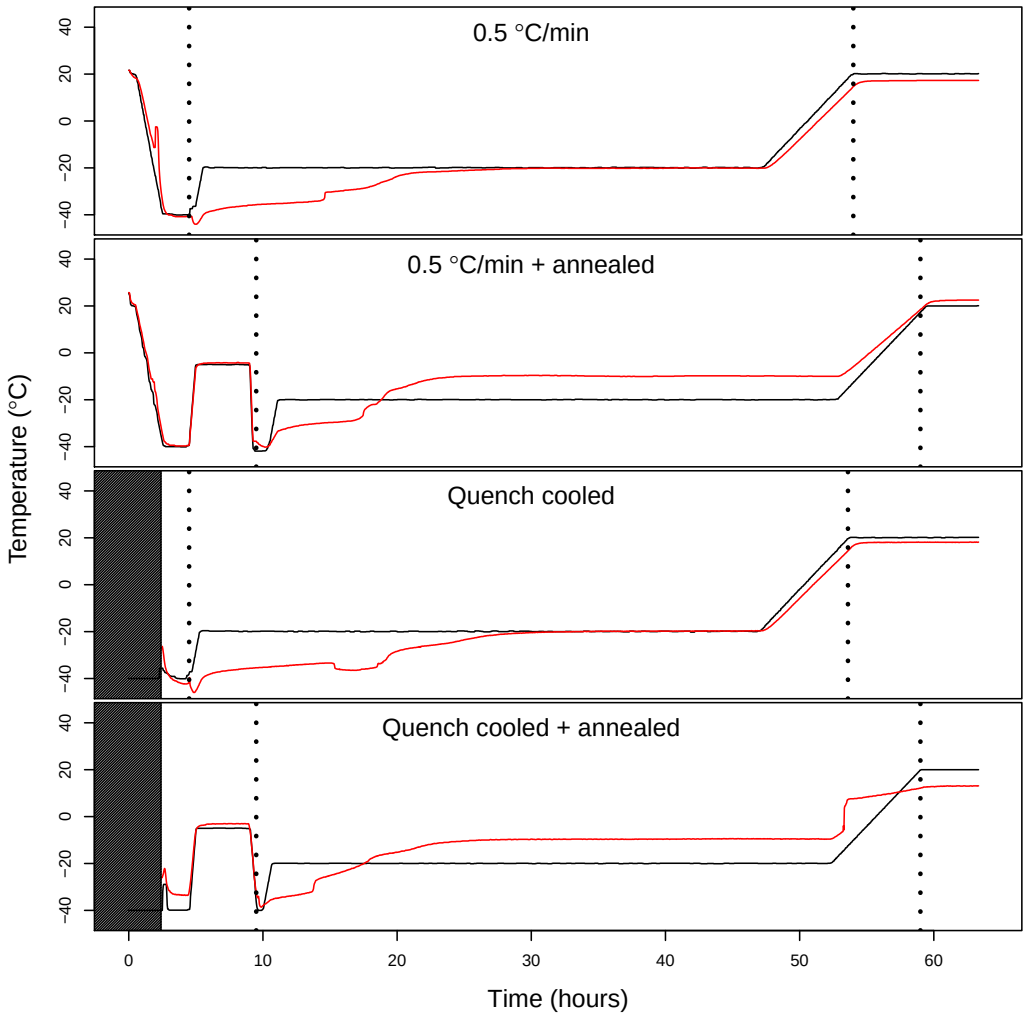


Figure 4.3. The shelf (solid black line) and product (solid red line) temperature profiles during lyophilisation. The data for the product temperature was from a thermocouple placed into one vial containing BSA with sucrose (200 mg/mL) in the centre of the freeze dryer. The vertical dotted lines represents changes in pressure, firstly from atmospheric to 100 mTorr and then to 200 mTorr. Quench cooling of samples took place externally from the freeze dryer (shaded out) and were then placed on pre-cooled shelves.

The approach of product temperature to shelf temperature can be used as an indicator of the end of primary drying. However, this method is subject to bias as the vial with the thermocouple may not be representative of the whole batch (Patel *et al.*, 2010). The product temperature of samples produced from cooling profiles with an annealing step were found to equal the shelf temperature within five to ten hours compared to non-annealed samples, which took 20 to 25 hours. The observation of faster primary drying times with annealed compared to non-annealed samples is consistent with other literature (Searles *et al.*, 2001a).

After lyophilisation, all BSA cakes were found to be amorphous by XRPD (Appendix Figure A.4). The lyophilised cakes from each cooling profile were also visually inspected and can be seen in Figure 4.4. Small scale uniform cake shrinkage and cracking were observed for all samples and, to a greater extent, with quench cooled only samples in which the cakes were no longer in contact with the sides of the vial. This was likely due to a high amount of unfrozen amorphous water remaining in the formulation prior to secondary drying. Macrocollapse, in which there is significant shrinkage and loss of structural integrity of the cake, was not evident in the samples. This is rather unsurprising as, in general, amorphous lyophilised cakes with greater than 20 mg/mL protein are not prone to collapse (Johnson and Lewis, 2011).

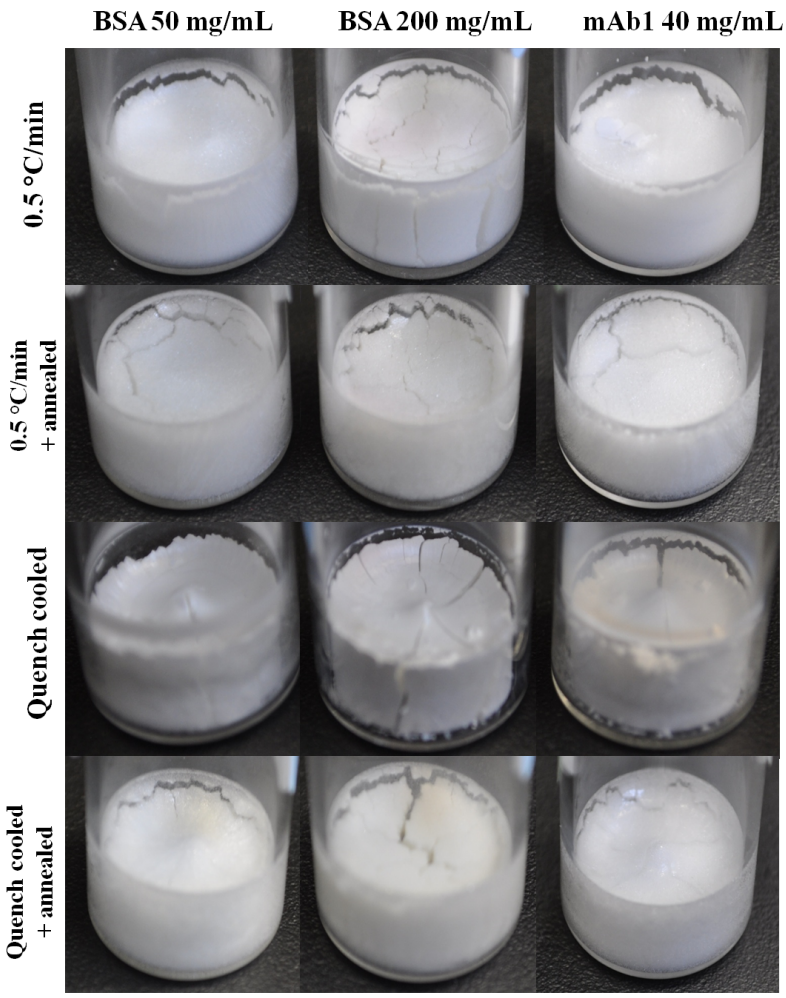


Figure 4.4. The appearance of the different protein formulations after lyophilisation.

4.3.2 Reconstitution time

The reconstitution times of the three lyophilised formulations are shown in Figure 4.5. The reconstitution times of BSA 50 mg/mL and mAb1 formulations were found to be significantly longer in samples lyophilised by quench cooling. Increasing the BSA concentration from 50 mg/mL to 200 mg/mL led to longer reconstitution times of up to approximately 40 minutes, although no statistically significant differences were observed between the different cooling profiles.

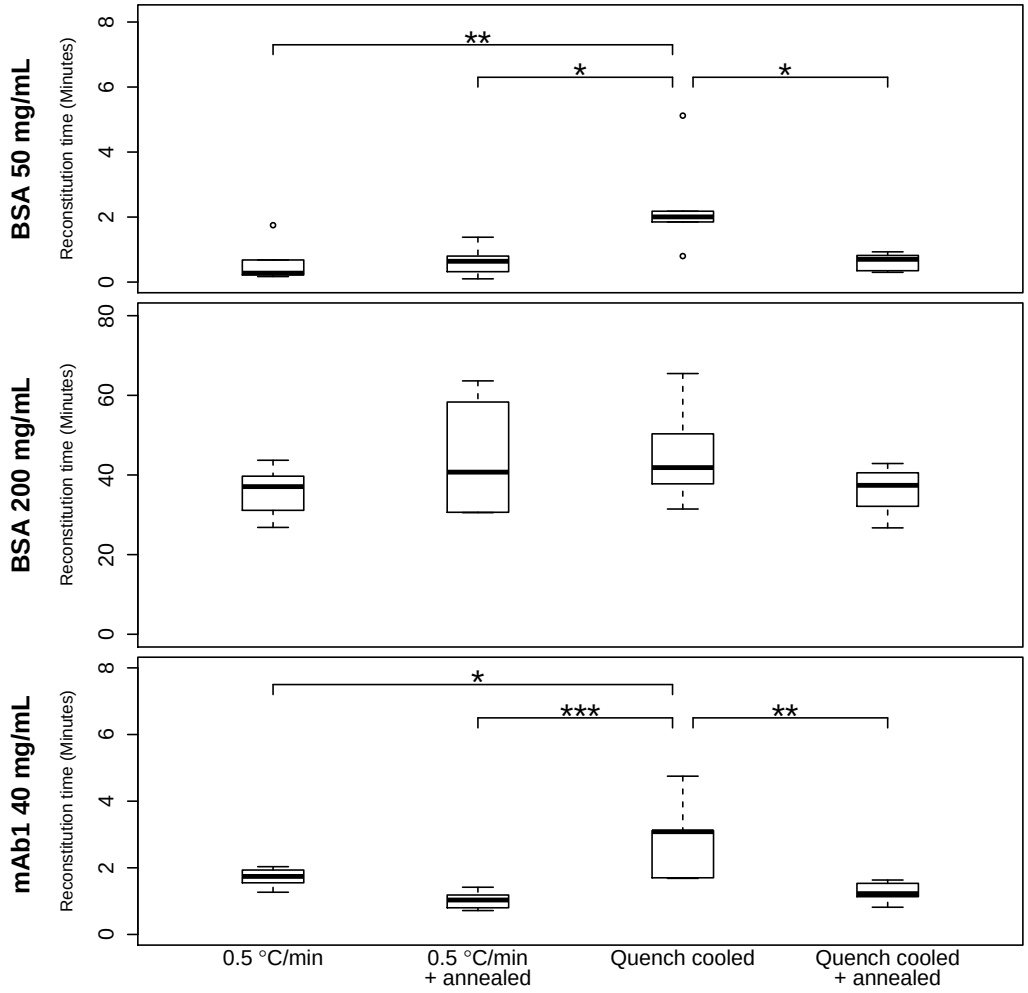


Figure 4.5. The reconstitution times of the three lyophilised formulations using four different cooling profiles, (n = 6). Statistically significant differences are denoted by *($p < 0.05$), **($p < 0.01$) and ***($p < 0.001$). Please note the difference in y-axis scale. Each box plot represents the interquartile range with the median as the thick horizontal line. Dashed lines show the minimum and maximum reconstitution times. Outliers, defined as being greater than 1.5 times the distance from the lower and upper quartiles, are shown as circles.

4.3.3 Cake structure

Pore appearance by SEM

Two distinct pore morphologies were created by the different cooling profiles: interconnected, spherical shaped pores (for samples lyophilised using a 0.5 °C/min cooling rate or annealing profile) and cylindrical pores for the quench cooled samples with no annealing step (Figure 4.6). The alterations in pore shape most likely reflect the different ice morphologies created by the different freezing mechanisms. Firstly, slow cooling rates, such as the shelf ramped 0.5 °C/min cooling rate, can allow a high degree of supercooling and, once the ice nucleation temperature has been reached, small ice crystals will grow throughout the solution, resulting in spherical pores. Faster cooling rates, as experienced by quench cooling in liquid nitrogen, will allow a small amount of supercooling in localised regions, from which ice crystals can grow without branching, leading to cylindrical pores between plate (lamellar) structures (Claus *et al.*, 2013, Searles *et al.*, 2001a).

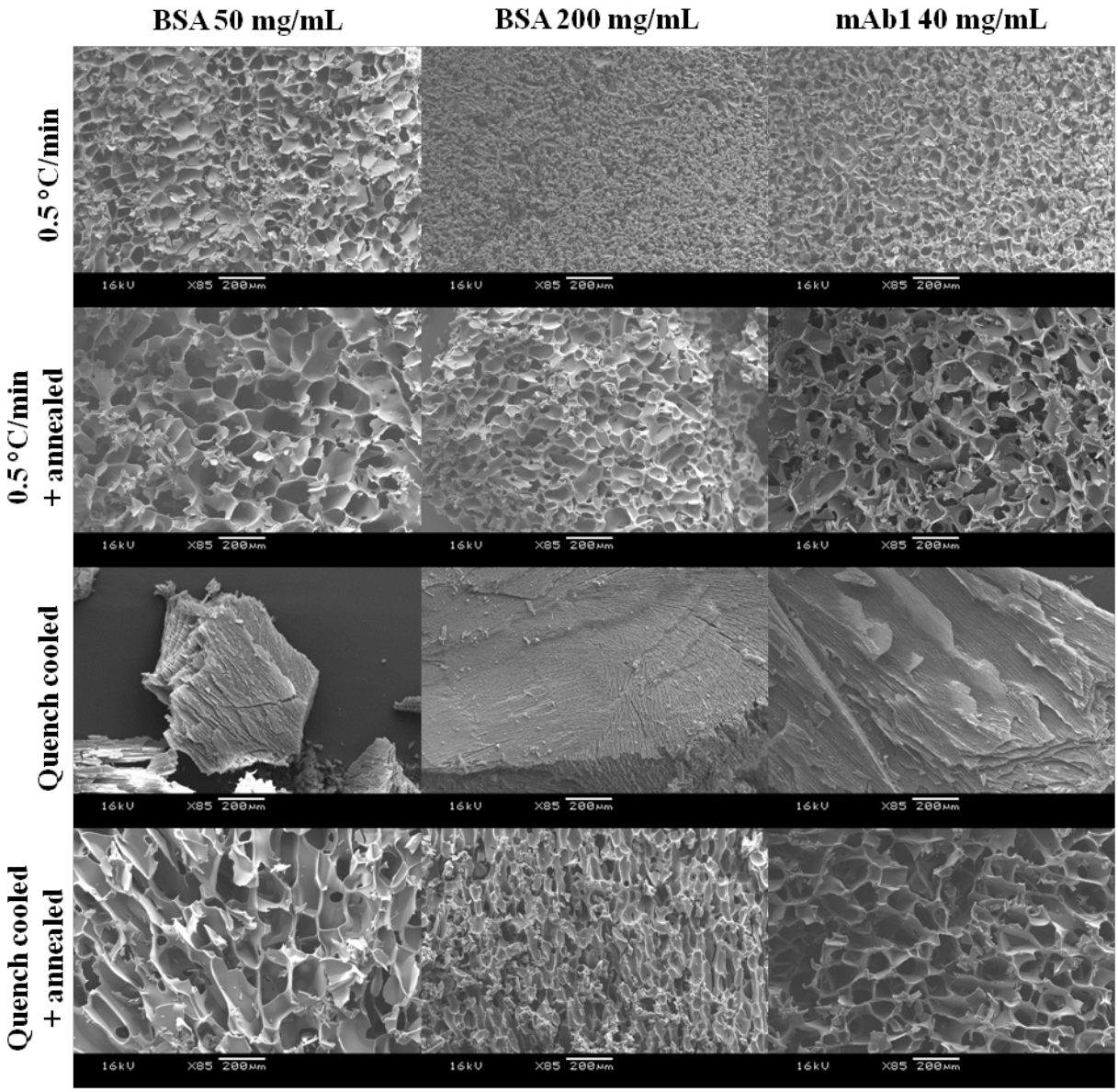


Figure 4.6. The appearance of protein formulations after lyophilisation using the different cooling profiles. The scale bar for each image is 200 μm.

It is clear from Figure 4.6, that the addition of an annealing step to the cooling profiles resulted in larger pores. This is most likely due to the process of Ostwald ripening in which larger ice crystals grow at the expense of smaller crystals (and was described in greater detail in Chapter 1 Section 1.1.3), the increased molecular mobility for the process is provided by the higher temperatures during annealing. The mechanism of morphology change from cylindrical pores to spherical pores through annealing has been described previously by Searles *et al.* (2001a) and is based on observations from metallic alloy systems. In brief, sphericalisation of ice crystals involves retraction of the plate edges (which have large positive radii of curvature) and isomass rounding, which was described in detail in Chapter 1 Section 1.1.3).

BET SSA and residual moisture content

The BET specific surface area (SSA) and residual moisture content of the lyophilised cakes can be seen in Figure 4.7. Type 2 isotherms were observed for the lyophilised cake, an example of which can be seen in Appendix Figure A.5. The BET constant and error associated with fit for each sample can also be seen in Appendix Tables A.3 and A.4, respectively.

Quench cooled samples were found to have the largest BET SSA at approximately 3 m^2/g. The increased surface area of samples prepared by quench cooling compared to those frozen slowly is consistent with other literature (Sarciaux *et al.*, 1999). Samples that were lyophilised with an annealing step in the cooling profile were found to have the lowest BET SSA, which is comparable with SEM images that showed the appearance of larger pores in the annealed samples. The residual moisture contents, measured by Karl Fisher titration, were all found to be less than 1 % which

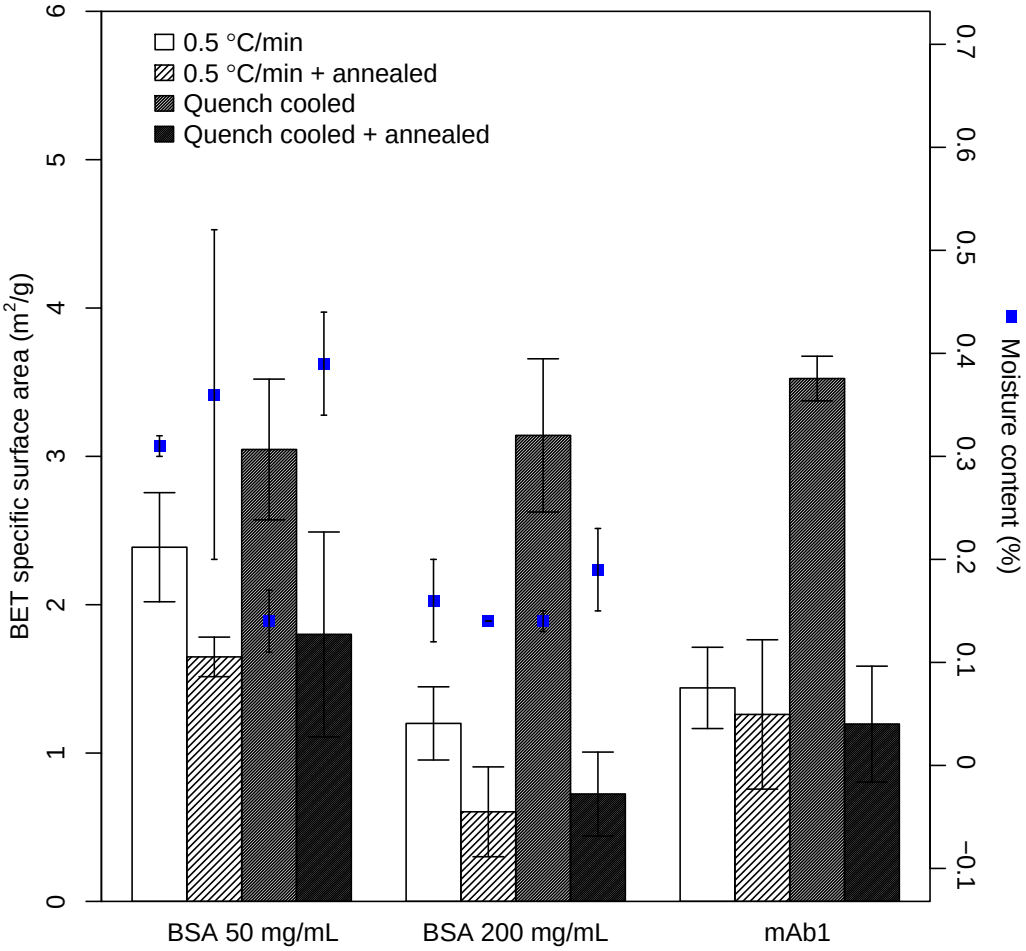


Figure 4.7. The BET specific surface area of lyophilised formulations and the corresponding residual moisture content, determined by Karl Fisher titration (n = 3, mean ± s.d.). Statistically significant differences for the BET SSA include: for BSA 50 mg/mL annealed and quench cooled ($p < 0.05$); BSA 200 mg/mL all cooling profiles and quench cooled ($p < 0.001$); for mAb1 all cooling profiles and quench cooled ($p < 0.01$).

is a suitable level for a lyophilised protein formulation (Wang, 2000). The residual moisture content for the BSA 50 mg/mL formulation was found to be lower after quench cooling compared to the other cooling profiles. This is likely due to the larger SSA which allows faster water desorption rates resulting in less residual moisture within the lyophilised cake (Pikal *et al.*, 1990).

MIP measurements

The pressure which allows mercury, a non-wetting probe, to intrude into a porous sample can be used to determine the pore size through a relationship described by the Washburn equation (Washburn, 1921a). The distribution of pore sizes obtained by MIP can be seen in Figure 4.8. For each BSA formulation and cooling profile, three samples were analysed. The pore size and pore size distributions of these three samples appear in good agreement with each other suggesting that the cake structure is reproducible in the batch, depending on the initial formulation and processing parameters.

One broad pore size distribution was observed between 10 and 50 μm for the BSA 50 mg/mL formulation lyophilised at a 0.5 °C/min cooling rate. With the addition of an annealing step, a trimodal pore size distribution was observed after both 0.5 °C/min and quench cooling rates. The observation of discrete pore size distributions after annealing has not previously been reported in the lyophilisation literature. A bimodal pore distribution was observed with BSA 50 mg/mL after quench cooling: the first between 1 and 8 μm and the second between 8 and 50 μm (with the majority of pores between 10 and 20 μm). The smaller pore sizes appear consistent with the width of cylindrical pores from SEM images. It is possible that the larger pore sizes are a result of the breakage or rupture of pore walls between two

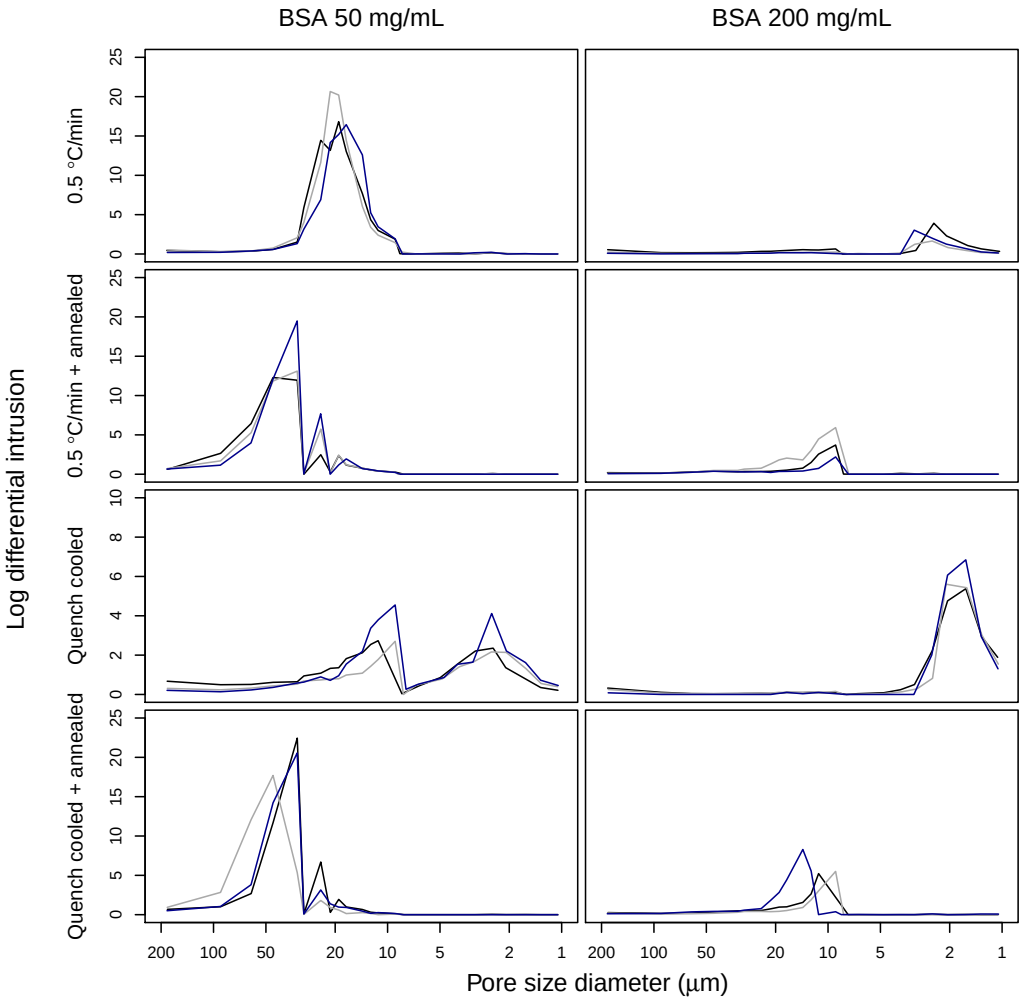


Figure 4.8. The pore size distributions of the two BSA formulations. Three vials of each formulation were analysed and are shown separately. Please note the different y-axis scale for quench cooled samples.

or more cylindrical pores, an example of which has been shown in the SEM image in Appendix Fig. A.6.

In Figure 4.9 and Figure 4.10 the bulk density and total pore volume, derived from MIP experiments, have been shown, respectively. The bulk density of samples were measured by applying a pressure that allowed mercury to surround the sample without penetrating into the pores (0.51 psi). The resulting sample volume therefore includes both solid material and pore spaces. The total pore volume of the samples were determined using the volume of mercury intruded into the sample (up to a pressure of 3600 psi).

Although bulk density and total pore volume have been shown separately, their multiplication can be used to describe the porosity of the sample.

No significant differences were observed in bulk density between the different cooling profiles of the lyophilised BSA 200 mg/mL formulation. For the BSA 50 mg/mL cakes, a significantly higher bulk density ($\sim$0.16 g/cm^3) was observed after quench cooling compared to the annealed samples ($\sim$0.13 g/cm^3). As quench cooled samples were also observed to have the greatest degree of volumetric shrinkage (Figure 4.4), these results correspond well with reports that collapse of the cake structure can lead to an increase in bulk density (Krokida *et al.*, 1998).

The total pore volume for the BSA 50 mg/mL formulation was found to be significantly lower after quench cooling ($\sim$2.5 cm^3/g) compared to the other cooling profiles ($\sim$6 cm^3/g). It is possible that this was due to the denser structure that results after volumetric shrinkage. Closed pores may also be present in the cake which would prevent the intrusion of mercury into the sample.

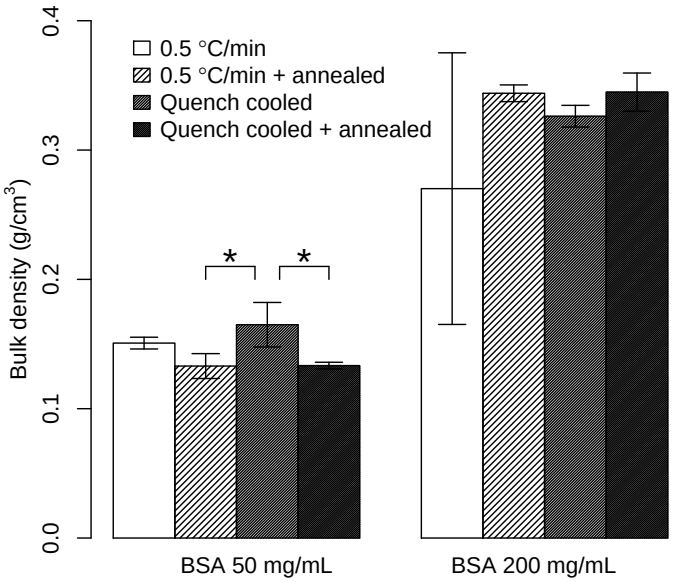


Figure 4.9. The bulk density of lyophilised BSA formulations (n = 3, mean ± s.d.). Statistically significant differences are denoted by *($p < 0.05$).

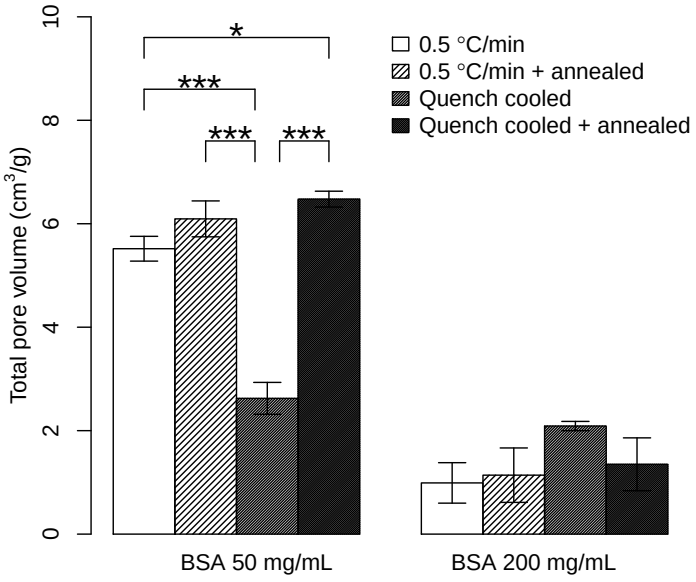


Figure 4.10. The total pore volume of BSA formulations (n = 3, mean ± s.d.). Statistically significant differences are denoted by *($p < 0.05$) and ***($p < 0.001$).

4.3.4 Secondary structure analysis by FTIR

In a study by Webb *et al.* (2002a), protein secondary structure changes were observed by FTIR spectroscopy with recombinant human interferon-γ after lyophilisation. After reconstitution, better refolding and reduced soluble aggregation levels were observed in samples with longer reconstitution times (in which reconstitution was slowed by the addition of a surfactant). It was therefore proposed that longer reconstitution times could allow more time for protein refolding. To explore whether a correlation exists between long reconstitution times and reduced protein denaturation, this chapter has used FTIR spectroscopy to identify changes in the protein secondary structure in the lyophilised and reconstituted states.

The second derivative FTIR spectra between the proteins in solution, prior to lyophilisation, and then in the lyophilised states can be seen in Figure 4.11. The most dominant secondary structure component in BSA solution is the α-helix which can be seen in both BSA formulations at approximately 1657 cm^{-1}. This component is reduced in the BSA 50 mg/mL lyophilised formulation where there is a shift towards unordered content at 1645 cm^{-1} and, more predominantly, there is an increase in β-sheet and turn structures. Lyophilisation of the BSA 200 mg/mL formulation showed a better conservation of secondary structure than 50 mg/mL samples. Similarly to the 50 mg/mL formulation there is a decrease in α-helical content, however, there is only an increase in turn structures rather than β-sheet content. Quench cooling gave the best retention of protein secondary structure, whereas annealed samples gave the worst retention, in the lyophilised state for the BSA 200 mg/mL formulation.

MAb1 is a predominantly β-sheet protein, which corresponds to the

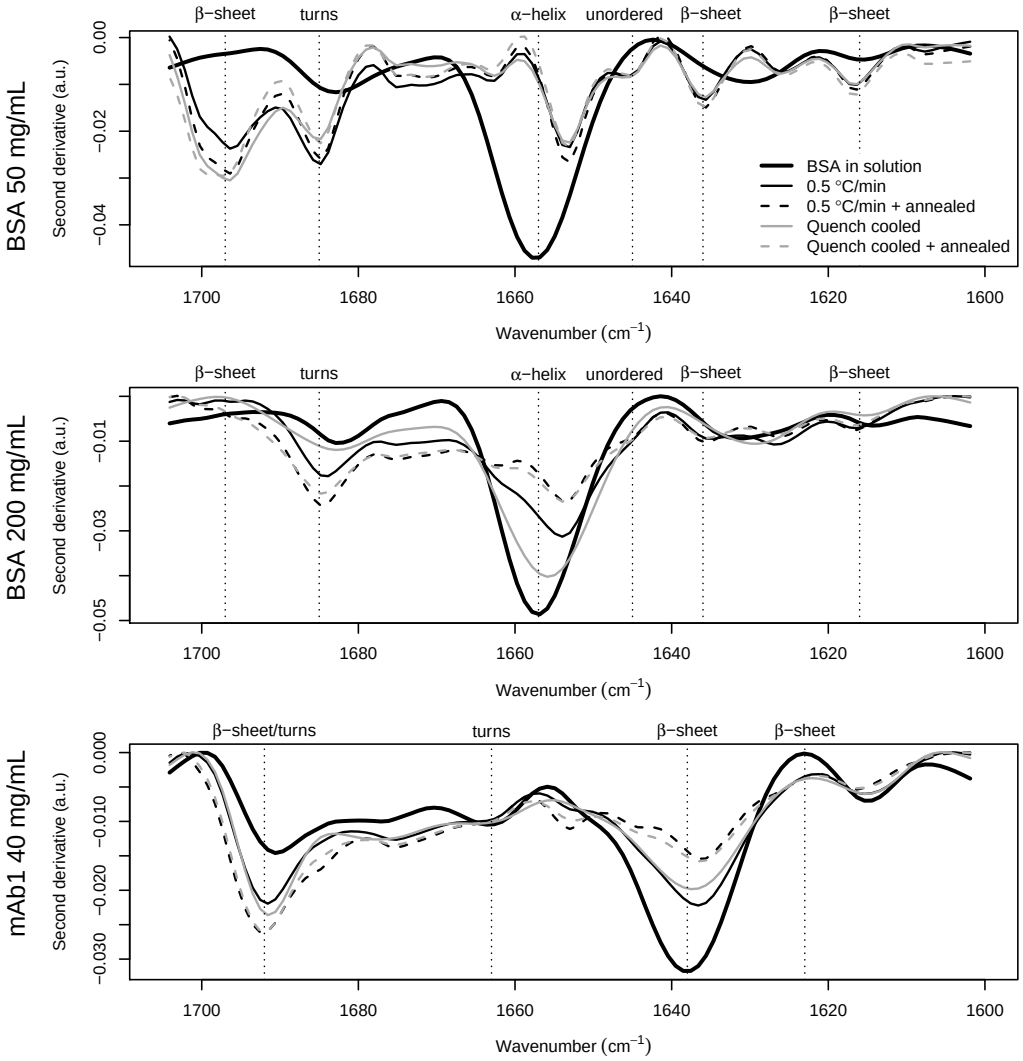


Figure 4.11. The second derivative IR spectra of the protein formulations, lyophilised using different cooling profiles and compared to the protein in solution (prior to lyophilisation). The results shown represent the mean spectra for three separate samples.

large peak at 1638 cm^{-1} in Figure 4.11. After lyophilisation, this secondary structure component is reduced and there is an increase in non-native β-sheet and turn structures at $\sim$1692 cm^{-1}. Again, as seen with the BSA 200 mg/mL formulation, lyophilisation with an annealing step resulted in the worst retention of protein secondary structure.

To provide a quantitative measure of the difference between protein secondary structure in the solution (pre-lyophilised state), lyophilised and re-

constituted states a correlation coefficient (r) can be used and has been employed previously by Kendrick *et al.* (1996), Prestrelski *et al.* (1993). The correlation coefficient can be calculated as follows:

$$r = \frac{\Sigma(x_i y_i)}{\sqrt{\Sigma x_i^2 \Sigma x_y^2}} \tag{4.1}$$

Where x_i and y_i are the intensity of second derivative spectra at reference (prior to lyophilisation) and comparison (lyophilised or reconstituted) spectra, respectively, at wavenumber i. A correlation coefficient value of 1 corresponds to a sample spectrum which is identical to the reference spectrum, whereas a value of 0 shows that there is no similarity between the two spectra. The correlation coefficients for the lyophilised and reconstituted protein formulations studied can be seen in Table 4.4. The correlation coefficients for the lyophilised cakes are in agreement to the spectral changes observed in Figure 4.11, which is as expected. On reconstitution, no visible particles were observed in any of the reconstituted solutions (NTU 0) and the secondary structure of both proteins returned to the pre-lyophilised state, despite varying degrees of denaturation in the dried cake.

Table 4.4. The correlation coefficients for second derivative spectra of lyophilised and reconstituted samples, compared to the protein in solution prior to lyophilisation. The correlation coefficients were calculated using the mean second derivative spectra of three samples.

		Lyophilised	Reconstituted
BSA	0.5 °C/min	0.17	0.97
50	0.5 °C/min then annealed	0.14	0.96
mg/mL	Quench cooled	0.10	0.98
	Quench cooled then annealed	0.10	0.98
BSA	0.5 °C/min	0.82	0.98
200	0.5 °C/min then annealed	0.53	1.00
mg/mL	Quench cooled	0.94	0.99
	Quench cooled then annealed	0.59	0.98
mAb1	0.5 °C/min	0.85	0.99
40	0.5 °C/min then annealed	0.54	1.00
mg/mL	Quench cooled	0.81	0.97
	Quench cooled then annealed	0.60	0.99

4.4 Discussion

The key result from this chapter is that significantly longer reconstitution times were observed with (1) the high concentration BSA formulation and (2) after quench cooling with the lower BSA concentration and mAb1 formulations. A further result which is of considerable interest is that discrete pore size distributions were observed, using MIP, after the addition of the annealing step. The high reproducibility between the samples suggests that this is a genuine result and not an artefact of the technique. To the author's knowledge, the formation of discrete pore size distributions after annealing has not previously been reported in this research field and raises questions regarding the mechanism of ice growth during annealing. Current opinion is that annealing will to lead larger pore sizes with a narrower distribution (Kasper and Friess, 2011). In order to elucidate the effect of annealing on the ice crystal structure, further investigational studies have been conducted in Chapter 5 of this thesis.

Despite the quench cooled BSA 50 mg/mL and mAb1 formulations having the largest surface area out of the cooling profiles investigated, longer reconstitution times were observed. These findings are in agreement with other recent research (Awotwe-Otoo *et al.*, 2013, Cao *et al.*, 2013, Geidobler *et al.*, 2013) in which surface area was not found to be a predominant factor in determining lyophilised cake reconstitution time.

This chapter has also explored whether a correlation exists between reconstitution time and protein stability, as proposed by Webb *et al.* (2002a). However, despite the changes in secondary structure in the lyophilised state, few differences were observed in the reconstituted solutions compared to the protein in solution (pre-lyophilisation). Consequently, these results do not

provide additional evidence to corroborate the theory that slower reconstitution times allow better refolding of the protein. Nevertheless, choice of protein is likely to be a key mechanistic factor and a wider selection may provide a more detailed picture of protein refolding during reconstitution in the future.

Changes in protein secondary structure were observed in the lyophilised state for both BSA and mAb1 proteins. BSA is well known to be susceptible to solid state aggregation (Costantino *et al.*, 1997) and drying induced structural alterations (Fu *et al.*, 1999). The better retention of BSA structure at 200 rather than 50 mg/mL may be due to the smaller proportion of total protein at the ice interface (Sarciaux *et al.*, 1999). It is perhaps not surprising that BSA can be denatured by ice interfaces as it has strong surface activity, which has led to research exploring its use as an emulsifying agent (Burgess and Sahin, 1998). Quench cooling provided the best conservation of secondary structure for the BSA 200 mg/mL formulation. This is perhaps rather contradictory as these samples also had the largest BET SSA (and were therefore likely to have been exposed to the largest ice interface). A possible explanation is that faster cooling rates may quickly prevent the molecular mobility required for physical and chemical degradation (Miller *et al.*, 2013). The loss of secondary structure in both mAb1 and BSA 200 mg/mL formulations after annealing may be the result of phase separation. It has been proposed in several studies that the addition of an annealing step may kinetically and thermodynamically favour the separation of protein from its intended stabiliser (Heller *et al.*, 1997, 1999). This may then lead to denaturation of the protein during lyophilisation and has been investigated further in Chapter 6.

4.4.1 Influence of protein concentration on reconstitution time

Altering the lyophilisation cooling profile was not found to affect the reconstitution time of BSA 200 mg/mL. However, the reconstitution times of this formulation were much longer (∼40 minutes) than those of the BSA 50 mg/mL formulation (<5 minutes). The long reconstitution times observed with this formulation are likely to be related to the dissolution rate of the cake, which can be described by the Nernst-Brunner equation:

$$\frac{dC}{dt} = \frac{DS}{Vh}(C_s - C) \tag{4.2}$$

Where dC/dt is the rate of dissolution, D is the diffusion coefficient, S is the surface area, V is the volume of dissolution medium, h is the thickness of the diffusion layer, C_s is the saturation solubility and C is the concentration at time, t (Dokoumetzidis and Macheras, 2006). The difference between the saturation solubility and the protein concentration in solution is the driving force for faster dissolution. Accordingly, formulations with higher protein concentrations will approach C_s more closely leading to a reduction in the dissolution rate and an increase in reconstitution time.

The dissolution of highly concentrated lyophilised proteins is further complicated by the effects of increasing viscosity, which can lead to a decrease in the diffusion coefficient (D). The relationship between diffusion and viscosity has already been described by the Stokes-Einstein equation in Chapter 1 Section 1.2.3 of this thesis. At high protein concentrations macromolecular crowding can also occur (and is illustrated in Figure 4.12) in which the free volume available to the protein is reduced, leading to an

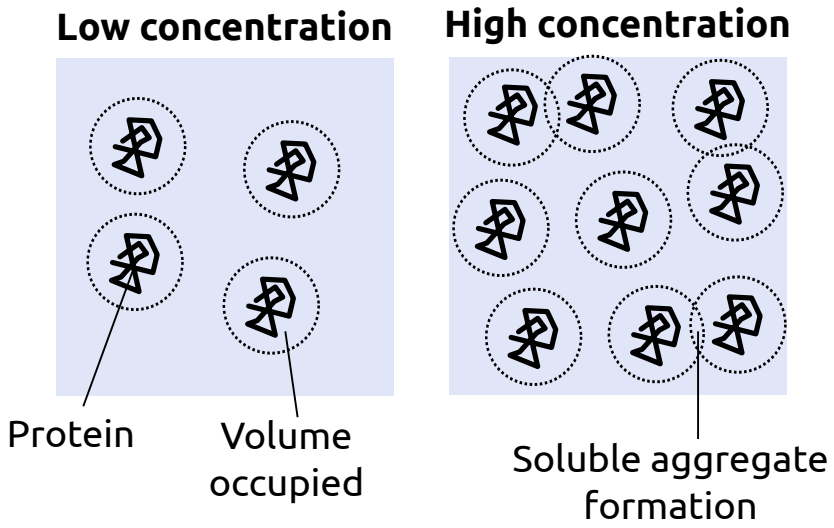


Figure 4.12. Macromolecular crowding occurs at high protein concentrations when the effective free volume available to the protein is reduced, this can lead to self-association of the protein and the formation of soluble aggregates.

effective increase in the protein concentration which can then favour self-association and the formation of soluble aggregates (Shire *et al.*, 2004). This non-ideal behaviour can lead to large increases in viscosity with increasing protein concentration, which may result in long reconstitution times. It is also possible that water penetration into the solid may become impeded by the establishment of high concentration and viscosity regions within the lyophilised cake, further slowing the reconstitution process.

4.4.2 Influence of cake structure on reconstitution time

Two structural features are believed to have led to the reconstitution times observed for the low concentration protein formulations: the presence of closed pores and the size of pores after quench cooling. In other studies (Johnson *et al.*, 2010, Overcashier *et al.*, 1999), the openness and connectivity of pores has been found to be important for decreasing vapour transit resistance during lyophilisation. Conversely, a more open network of pores could also allow better penetration of water into the lyophilised

cake. Here, BSA 50 mg/mL cakes were found to have the smallest total pore volume after quench cooling compared to the other cooling profiles, an effect which was attributed to volumetric shrinkage and the presence of closed pores. Difficulties in penetrating mercury into the sample may also correspond to poor water penetration into the cake, which may result in slower reconstitution times.

Narrow cylindrical pores were evident in SEM images of quench cooled samples compared to the large spherical pores of the other cooling rates (Figure 4.11). Both Darcy's Law, which describes the permeability of a fluid through a porous material (Brown, 2002), and the Hagen-Poiseuille equation, which relates flow rate through a cylinder, (Eq. 4.3), describe permeability/flow rate as being directly proportional to the pore size in a power-law relationship.

$$Q = \frac{\pi R^4 \Delta P}{8\eta L} \tag{4.3}$$

Where Q is the volumetric flow rate, R is the radius of the cylinder which has a length of L, ΔP is the change in pressure across the cylinder and η is the viscosity of the medium. The relationship between flow rate and pore size described by the Hagen-Poiseuille equation can have important consequences when comparing samples with different pore diameters of, for example: 2, 20 and 50 μm (which are similar to those observed in Figure 4.8 for BSA 50 mg/mL quench cooled, cooled at 0.5 °C and annealed samples, respectively). Through simple calculation, a 10,000-fold increase in flow rate may be observed by increasing the pore diameter from 2 to 20 μm. However, only a 40-fold increase occurs between pores that are 20 and 50 μm in diameter. The longer reconstitution times that were observed with

the BSA 50 mg/mL quench cooled samples may be explained by this theory, as approximately half of the pore volume was associated with pores that were approximately 2 μm in diameter. It is interesting to consider that if a power-law relationship does exist between pore size and reconstitution time, then there may also be a critical pore size below which reconstitution time will be prolonged by slow water penetration into the lyophilised cake.

The morphology of pores in the quench cooled samples, which appeared cylindrical in SEM images whereas the other cooling profiles appeared spherical, may have also influenced the reconstitution time. However, it is likely that faster flow rates would be favourable through cylindrical pores rather than spherical pores, in which the narrower pore throats would provide resistance to the flow. Consequently, this study proposes that small or closed pores, rather than pore morphology, are likely to be the cause of long reconstitution times in quench cooled samples.

To confirm whether smaller pore sizes lead to longer reconstitution times it would be prudent to systematically test lyophilised cakes with various pore sizes. However, it is difficult to assess the impact of pore size on reconstitution time without altering other cake parameters. Adjusting the fill volume, whereby a greater volume of a diluted formulation is lyophilised and then reconstituted with less water to provide the correct final concentration, may offer the best approach as no changes to the lyophilisation cycle would be needed. The published work by Shire *et al.* (2004) and Cao *et al.* (2013) have already investigated various fill volumes on the reconstitution time of lyophilised proteins and, indeed, both observed improvements in reconstitution time, however details on pore size was lacking. Fluid flow modelling may also provide some insight into effect of pore size, morphology and connectivity on reconstitution times but as George E. P. Box said *"essentially,*

all models are wrong, but some are useful" (1987), and this is likely to be true for a dynamic process such as reconstitution, even without considering the chemical nature of the formulation.

4.5 Conclusions

This chapter has investigated the effect of altering both formulation and the lyophilisation cooling profile on the reconstitution times of lyophilised protein cakes. The key result was that significantly longer reconstitution times were observed with the high concentration BSA formulation and after quench cooling with the lower concentration BSA 50 mg/mL and mAb1 formulations. The presence of discrete pore size distributions was also observed in this study after annealing and has not previously been reported in the lyophilisation literature.

The mechanism which governs the reconstitution time of lyophilised, highly concentrated protein formulations appear complex. However, it is likely that the reconstitution time is dominated by factors that affect the dissolution rate of the cake. These factors include the difference between protein concentration and its saturation solubility, and the viscosity of the solution. As the viscosity behaviour can be significantly different across proteins of the same class (Galush *et al.*, 2012), predicting the reconstitution time based on formulation alone remains elusive.

A cause of long reconstitution times in low protein concentration formulations has also been presented, in which small and closed pores are likely to be the predominant cause of prolonging reconstitution times. It has also been proposed that the reconstitution time may follow a power-law relationship with pore size. Further consideration should therefore be given to a possible "cut-off" in pore size below which the increase in reconstitution time becomes impractical to lyophilised formulations.

5 Insights into the Influence of Annealing Duration and Formulation on Lyophilised Protein Cake Structural Properties

The structure of the lyophilised cake is important, not only to provide an elegant product, but as physical collapse has been implicated in a number of quality issues, such as: long reconstitution and primary drying times and an increase in moisture content (Johnson and Lewis, 2011, Searles *et al.*, 2001a). Furthermore, collapse may indirectly lead to protein instability issues (Chamow *et al.*, 2013).

As the previous chapter highlighted that the addition of an annealing step may alter the lyophilised cake structure through a more complex process than previously understood within the literature, this chapter investigates this further by altering the lyophilisation process to include annealing steps of different durations. Furthermore, as arginine has recently received interest as a lyophilisation excipient, due to its numerous beneficial properties, this chapter also investigates the impact of four dicarboxylic acid salts of arginine on cake structure and compares to a conventional sucrose formulation.

This chapter describes previously unreported data regarding pore size distributions in lyophilised protein cakes and leads to a discussion on ice crystal growth during the annealing step.

5.1 Introduction

5.1.1 Properties of the cake structure

It is important that lyophilised cakes have an elegant appearance and, perhaps rather superficially, no collapsed product will be released on the market (Schersch *et al.*, 2010). However, large scale (macro) collapse can also have important consequences for other cake quality attributes. Collapse can lead to a loss in lyophilised cake surface area, a reduction in porosity and an increase in cake density which may result in poor rehydration properties and an increase in reconstitution time (Johnson and Lewis, 2011, Schersch *et al.*, 2010). Maintaining an open network of pores is also considered to be important for reducing vapour transit times during drying (Johnson *et al.*, 2010, Overcashier *et al.*, 1999). The increased product resistance caused by large scale collapse can therefore lead to long drying times and high moisture contents (Adams and Irons, 1993).

In general, the collapse of lyophilised cakes do not directly influence protein stability and difficulties in this regard have only been reported in a couple of studies (Lueckel *et al.*, 1998, Passot *et al.*, 2007). However, an increase in residual moisture content resulting from collapse may increase degradation rates and reduce protein stability (Chamow *et al.*, 2013).

Strategies to prevent collapse include the addition of a bulking agent, such as mannitol or glycine, and maintaining the product temperature below the collapse temperature of the product (Tang and Pikal, 2004).

5.1.2 Improving excipient diversity through arginine salts

Sucrose is often used as a lyoprotectant in formultions, however, its effects on long term storage stability and lyophilisation-induced protein unfolding can be difficult to predict (Carpenter *et al.*, 2002, Yu *et al.*, 2008). To allow a greater choice in the formulation design of biopharmceuticals there is an increasing research interest in the use of alternative stabilising excipients. Amino acids offer a wide range of chemical and physical properties and have recently been used in lyophilised orally disintegrating tablets due to their good wettability and high disintegration times (AlHusban *et al.*, 2010).

The amino acid arginine has multiple uses throughout different stages in the manufacture of biopharmaceuticals. It is used to facilitate the refolding process of recombinant proteins from inclusion bodies (Arakawa and Tsumoto, 2003, Tsumoto *et al.*, 2004). It can enhance the solubility of proteins (Golovanov *et al.*, 2004, Reddy K. *et al.*, 2005, Shukla and Trout, 2011) and has been found to be effective at increasing the recovery of antibodies during protein-A and protein-G affinity chromatography (Arakawa *et al.*, 2004, 2014, Ejima *et al.*, 2005, Shukla *et al.*, 2011b). Furthermore, arginine can decrease the viscosity of antibody solutions (Inoue *et al.*, 2014a), an effect which is thought to be predominantly due to weakening of protein-protein interactions (Inoue *et al.*, 2014b).

At physiological pH, arginine has two positively charged (from the guanidyl group) and one negatively charged (carboxylic acid) groups (Figure 5.1). Part of the arginine structure resembles guanidinium hydrochloride which is often used for protein unfolding, in which it exposes hydrophobic regions

of the protein by interacting strongly with polar peptide linkages, anionic sites and hydrogen bonding sites (Xie *et al.*, 2004). The guanidinium cation is very stable in water due to its resonance structure. However, arginine itself does not have any strong influence on the structural stability of proteins (Arakawa and Tsumoto, 2003).

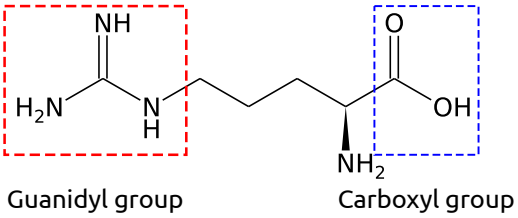


Figure 5.1. The chemical structure of arginine.

As the free arginine base is alkaline, it is of often formulated with a salt (most commonly arginine HCl) to balance the pH of the solution (Lange and Rudolph, 2009). However, the effect on protein aggregation behaviour can be significantly different from one salt to the next. For example, arginine sulphate, but not the chloride salt, was found to suppress the association of monomeric β-galactosidase into its biologically active tetrameric unit (Fujimoto *et al.*, 2010). Based on an investigation into the Hofmeister series as arginine counterions (Schneider *et al.*, 2011), it was proposed that anions which are able to form strong attractive interactions with the guanidinium group (for example: phosphate, sulfate, and citrate) are able to enhance the protein aggregation suppression effects of arginine by bridging multiple arginine molecules into clusters.

5.1.3 Dicarboxylic acids as arginine counterions

Dicarboxylic acid solutions have been found to improve the thermal stability of proteins (Kaushik and Bhat, 1999). However, their use as arginine counterions has not received a great deal of interest for several reasons. Re-

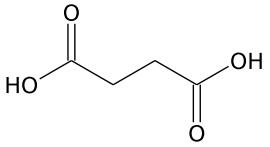
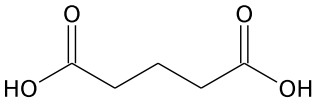
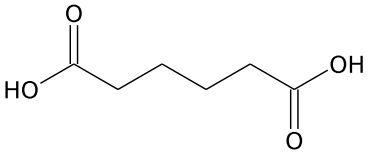
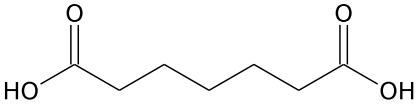
cently, the dicarboxylic acids oxalic acid (C2) and succinic acid (C4) were investigated as counterions to determine if they increased the Tg′ of arginine formulations (Izutsu *et al.*, 2009a). Although some improvements were observed they were not as successful as the tricarboxylic acid, citric acid (Kadoya *et al.*, 2008, Yamaki *et al.*, 2012). Succinic acid has also been used in pharmaceutical applications, however it has been reported to crystallise on freezing (Lin *et al.*, 2007, Sundaramurthi and Suryanarayanan, 2012) which would generally make it unsuitable for lyophilisation. Furthermore when the sodium salt of succinic acid was formulated with 10 mg/mL BSA, despite being amorphous, it failed to prevent the loss of α-helical structure when lyophilised (Izutsu *et al.*, 2009b). Nonetheless, increasing the alkyl chain length of dicarboxylic acids here offers a systematic way of investigating how arginine interacts with a series of functionally similar counterions but with different chemical properties.

Dicarboxylic acids are frequently used in the manufacture of polymers; most notably adipic acid is used in the production of nylon. Both succinic acid and adipic acid also have use in the food industry and are both listed as 'Generally Recognised as Safe' (FDA, 2014b). As well as being used to regulate acidity in food (Zeikus *et al.*, 1999), adipic acid is often used in baking powder due to its low hygroscopicity (RSC, 2014). In general, dicarboxylic acids are less toxic and more soluble than monocarboxylic acids and therefore make them suitable candidates for pharmaceutical purposes.

Based on the dissociation constants of dicarboxylic acids, four are able to form solutions with arginine free base[1] to give similar pH solutions ($\sim$7). Therefore, the four dicarboxylic acids that are of interest to this research study were: succinic acid, glutaric acid, adipic acid and pimelic acid, which

[1] In a 1:2 molar ratio of dicarboxylic acid to arginine.

Table 5.1. The chemical structures and dissociation constants of the dicarboxylic acids of interest in formulation studies.

Name	Chemical structure	pKa†
Succinic acid (C4) (butanedioic acid)		1 = 4.19 2 = 5.48
Glutaric acid (C5) (pentanedioic acid)		1 = 4.34 2 = 5.42
Adipic acid (C6) (hexanedioic acid)		1 = 4.42 2 = 5.41
Pimelic acid (C7) (heptanedioic acid)		1 = 4.48 2 = 5.42

†Dissociation constants taken from the reference by Brown *et al.* (1955).

have alkyl chain lengths of 4, 5, 6 and 7 carbon atoms, respectively (as indicated henceforth by the notation of C4, C5, C6 and C7). The chemical structure and dissociation constants for each of the dicarboxylic acids of interest can be found in Table 5.1.

The crystalline structures of arginine dicarboxylic acid salts have been resolved in references (Prasad and Vijayan, 1990, Roy *et al.*, 2005, Saraswathi and Vijayan, 2001, Saraswathi *et al.*, 2003) in which two arginine molecules are associated with a dicarboxylic acid through specific guanidinium – carboxylate interactions. In general, a pKa difference of 3 between acid and base is required to make a salt (Gaisford and Saunders, 2013). Although, the succinic acid salt of doxylamine is able to form with a pKa difference of just 0.2 (Wells, 1988). The dissociation constants for arginine are 2.17, 9.04, 12.5 (RSC, 2014). Based on this, and the strong interaction that occurs be-

tween coplanar guanidinium and carboxylate groups (Shah *et al.*, 2012), it is likely that the argininine-dicarboxylic acid combinations will form a salt in solution.

Both succinic and adipic acid have been used as inactive ingredients in FDA approved pharmaceuticals. A list of the dosage forms that they have been incorporated into can be seen in Table 5.2. It is clear to see from this table that, whereas sucrose has been widely used in a variety of dosage forms, arginine is listed in only 9 products. No formulations containing arginine with the dicarboxylic acids of interest in this study are currently listed in any of the FDA approved drugs and, to the best of the author's knowledge, there is no literature regarding their combined use in any protein formulation, whether solution or lyophilised.

Arginine and dicarboxylic acids have been studied separately in the formulation development of small drug molecules but to opposite effects. That is, amino acids have been used to enhance the amorphous character of drugs, such as through ball milling of indomethacin with arginine (Lobmann *et al.*, 2013), whereas dicarboxylic acids have been used to enhance the crystalline character of drugs, such as through ball milling of sulfadimidine and salbutamol (Curtin *et al.*, 2013a,b). Therefore, the use of dicarboxylic acids as arginine counterions presents an interesting data study to conduct.

Table 5.2. A list of FDA approved drug products that contain the excipients of interest in this study as an inactive ingredient. Data collected from (FDA, 2013), which is updated quarterly.

Name	Present in FDA approved drug products?	Number of products	Dosage forms
Sucrose	Yes	78	Oral tablet (buccal, sublingual, extended release, immediate release, enteric coated, film coated), lyophilised powder for injection solution, solution for injection, powder for injection solution, oral capsule (immediate release, extended release, enteric coated pellets), granule for oral suspension (immediate and extended release), oral syrup, oral suspension (immediate release extended release), rectal solution, topical ointment
Arginine	Yes	9	Oral tablet, powder for injection solution
Succinic acid	Yes	10	Oral concentrate, oral powder for suspension, oral tablet (immediate release, controlled release, chewable)
Glutaric acid	No		
Adipic acid	Yes	2	Solution for injection, vaginal insert
Pimelic acid	No		

5.1.4 Chapter motivation

It is thought that by using longer annealing durations during lyophilisation, inter-vial heterogeneity and pore size distribution can be reduced (Kasper and Friess, 2011). However, it was observed in Chapter 4 of this thesis that discrete pore size distributions were present in the lyophilised cake after annealing with the lower concentration BSA formulation. To the author's knowledge this has not previously been reported in this research field and highlights that the annealing process may be more complex than previously thought.

In order to investigate this further, this chapter has characterised the cake structural properties of BSA (100 mg/mL) and mAb1 formulations when lyophilised with and without an annealing step. In order to provide greater mechanistic detail of the annealing process, annealing durations of 2, 4, 8 and 16 hours were used and an annealing temperature, lower than the previous chapter (-10 °C compared to -5 °C), was used in order to 'slowdown' the process.

To explore the impact of formulation on cake structural properties, BSA was formulated with either 7 % sucrose or an arginine-counterion combination, the counterions of which were a series of dicarboxylic acids increasing in alkyl chain length (C4 to C7).

5.2 Materials and Methods

5.2.1 Materials

BSA, sucrose and histidine buffer salts were described in Chapter 4 Section 4.2.1. Succinic acid, adipic acid and pimelic acid were all purchased from Sigma-Aldrich with purities of >99 %. Glutaric acid was purchased from Alfa Aesar with purity of 99 %. BSA was prepared in a 25 mM histidine buffer solution, pH 6.0, with 7 % w/v sucrose to give a final protein concentration of 100 mg/mL. The mAb1 formulation was kindly provided by MedImmune Ltd and was described in Chapter 4 Section 4.2.1. For BSA with arginine-dicarboxylic acid formulations, BSA was prepared (100 mg/mL) in a solution containing a 2:1 molar ratio of arginine to dicarboxylic acid, to a total weight of 7 % w/v excipient. No additional buffer was used. Prior to lyophilisation all formulations were filtered (0.22 μm), the pH was confirmed using a PHM220 pH meter (Radiometer analytical), and the protein concentrations were determined by UV absorbance at 280 nm (NanoDrop®, Thermo Fisher Scientific).

5.2.2 Methods

Differential scanning calorimetry, freeze drying microscopy, Karl Fisher moisture determination, X-ray powder diffraction, Brunauer, Emmett & Teller (BET) specific surface area measurements and mercury intrusion porosimetry were all carried out as described in Chapter 4 Section 4.2.2.

Lyophilisation

The formulations were lyophilised using a 1 mL fill volume in 13 mm Schott Type I clear tubular glass injection vials (West Pharmaceutical Ser-

vices) with Daikyo D777-1 13 mm single vent lyo stopper (West Pharmaceutical Services). Vials were placed within a custom made stainless steel fence which was used to keep vials in the centre of the freeze dryer. Two freeze dryers were used: a Virtis Advantage Plus two shelf freeze dryer (SP Scientific) for cycles with annealing durations of 4, 8 and 16 hours and a Virtis Advantage Plus one shelf freeze dryer (SP Scientific) for cycles with 0 and 2 hours annealing duration. Thermocouples, calibrated before use, were placed into two BSA sucrose formulations with one in the centre and one at the front of the freeze dryer for each cycle.

Samples were cooled at 0.5 °C/minute to -40 °C and held for two hours. Five annealing durations were selected for investigation: 0, 2, 4, 8 and 16 hours. Following cooling for the 0 hour duration (i.e. no annealing) the cycle commenced into primary drying, as described below. For the cycles including an annealing step the temperature was ramped at 1 °C/min to -10 °C and then held for the desired annealing duration, after which the temperature was reduced by 1 °C/min to -40 °C and held for 30 minutes prior to primary drying.

To allow primary drying, the pressure in the chamber was reduced to 100 mTorr at -40 °C for 20 minutes followed by a temperature ramp of 1 °C/min to -20 °C which was then held for 24 hours. Following this, the temperature was ramped at 0.1 °C/min to 20 °C and held for 12 hours at 200 mTorr to allow secondary drying.

Dynamic mechanical analysis (DMA)

A Q800 DMA (TA Instruments) with a liquid nitrogen cooling system was used to determine the Tg of BSA containing lyophilised cakes. After opening of the vial, a spactula was used to remove a piece of lyophilised

cake approximately 3 to 4 mm in size. The sample was placed into the DMA and held using a compression clamp. A constant amplitude of 5 μm and frequency of 1 Hz was used throughout the study. The temperature was ramped at a heating rate of 3 °C/minute from 50 °C to 180 °C. The Tg of the material was determined as the peak maximum of the sample loss modulus as a function of temperature.

Scanning electron microscopy (SEM)

To alleviate compression of the cake during preparation for SEM, a sharp scalpel was used to cut the lyophilised material to expose an internal cross-section. Samples were placed onto stubs and a Leica EM SCD005 sputter coater (Leica Microsystems) was used to coat samples in gold for 300 seconds at 26 mAmp. A JEOL JSM 6060LV SEM (JEOL Ltd.) was used with an acceleration voltage of 16 kV.

Reconstitution Time

The volume of water required for reconstitution was calculated based on the amount of water removed from each formulation (i.e. total weight less the amount of solids). This value was then rounded to the nearest 0.1 mL, based on the graduation of syringes found in a hospital setting. For BSA 100 mg/mL and mAb1 40 mg/mL formulations, 0.9 mL of water was used for reconstitution. Prior to reconstitution, the samples requiring different reconstitution volumes were separated and the formulation labels blinded to randomise the cooling profiles and maintain a level of objectivity. Samples were then reconstituted using a syringe with the water flow aimed at the inside wall of the vial. The vial was then swirled for approximately five seconds to ensure the sides and bottom of the lyophilised cake were wetted and then placed onto an orbital shaker at 140 rpm until fully dissolved. The re-

constitution time was defined as the time needed to dissolve all visible solids in the vial from the point of water injection. Five vials of mAb1 and seven vials of each BSA formulation (per annealing duration) were reconstituted. Statistical analyses were performed using a two-way analysis of variance (ANOVA) with Bonferroni post test for BSA containing formulations and a one-way ANOVA with Bonferroni post test for mAb1 formulations.

X-ray microtomography (Micro-CT)

The pore structure of lyophilised BSA with arginine-C4 cakes (annealed for 0, 2 and 4 hours) were examined using an XRADIA Versa XRM-500 micro-CT system (Carl Zeiss X-ray Microscopy, Inc.). After opening each vial the central section of each cake was removed using a corer (approximately 5 mm in diameter). The sample was then mounted on to a rotary stage and scanned through a 3 mm diameter central portion of the cake, which was rotated 180° in 2034 equiangular steps. The images consist of 1994 slices with a voxel size of 1.5 μm in all three axes. The porosity of each image slice was calculated using the software Fiji (Schindelin *et al.*, 2012), in which a macro was written to process each slice and can be found in the Appendix (Figure B.1). Processing of each slice consisted of binarising the image and applying a despeckling filter. Porosity was calculated as the percentage of white (free space) pixels to white and black (material) pixels within the 3 mm region of interest.

5.3 Results

5.3.1 Notes on manufacture

As this is the first report on arginine-dicarboxylic acid combinations as formulation excipients for a lyophilised protein it is worth describing in some detail issues with their manufacture. Firstly, as discussed in the introduction only four dicarboxylic acids were taken forward as formulation excipients. As the effect of extremes of pH on protein stability is well known (Talley and Alexov, 2010), it was considered important that the counterions chosen should all result in similar pH solutions. The pH of the solutions, prior to lyophilisation, can be seen in Table 5.3. However, it should be noted that the BSA sucrose formulation was maintained at pH 6 to allow comparisons with the previous chapter. As the isoelectric point of BSA has previously been reported as 4.7 (Peng *et al.*, 2004), the lower pH of the sucrose formulation may allow more protein-protein interactions.

Table 5.3. The pH of BSA containing formulations.

Formulation	pH
BSA + sucrose	5.97
BSA + arginine-C4	6.85
BSA + arginine-C5	6.83
BSA + arginine-C6	6.83
BSA + arginine-C7	6.90

The solubilities of the dicarboxylic acids in water at 20 °C have been reported to be C4=80, C5=430, C6=15 and C7=50 g/L (FisherScientific, 2014a,b,c,d). Due to the low solubility limits of succinic, adipic and pimelic acid it was not possible to lyophilise any of the dicarboxylic acids alone. Although glutaric acid (C4) was soluble in solution, the lyophilisate was determined to be crystalline by XRPD.

The Tg′ and Tc of BSA formulations can be seen in Table 5.4. Both with and without BSA, the Tg′ of sucrose formulations were found to be approximately 3 °C higher than the arginine based formulations. Without BSA, the Tg′ for all formulations were reduced by 10 °C. The collapse temperatures of the sucrose and arginine-dicarboxylic acid formulations were found to be comparable.

Table 5.4. The Tg′, both with and without protein, and Tc of BSA (100 mg/mL) formulations.

Formulation	Tg′ (°C) - BSA	Tg′ (°C) + BSA	Tc (°C) + BSA
Sucrose	-34	-24	-16
Arginine-C4	-37	-27	-17
Arginine-C5	-38	-28	-15
Arginine-C6	-38	-28	-17
Arginine-C7	-37	-27	-15

5.3.2 Primary drying time and moisture content

The length of primary drying (determined by the approach of product to shelf temperature) for each annealing cycle can be seen in Table 5.5, the thermocouple data can also be found in Appendix Figure B.2. Unfortunately, due to a computer error which occurred during the 4 hour annealing duration cycle, no corresponding thermocouple data was recovered. However, it should be stressed that the freeze dryer operates separately from the computer and correct running of the cycle could be confirmed. Two findings can be observed from the results of primary drying times, firstly, that the product temperature at the front of the freeze dryer was higher than vials in the centre and secondly, much longer primary drying times resulted from 8 and 16 hour annealing duration cycles. It is well known that vial position in a freeze dryer can affect the product drying times, and often there are ways to minimise the heterogeneity through the use of use of thermal shields

(Tang *et al.*, 2006). At its extreme, the primary drying time was found to have doubled between front and middle of the freeze dryer, although this is not an isolated case and doubling of the sublimation rate has also been reported elsewhere (Rambhatla and Pikal, 2003).

The primary drying times of these cycles were found to be less than those in Chapter 4 of this thesis. Likely this is due to the higher concentration of BSA (200 mg/mL in the previous chapter) compared to this chapter, which would increase product resistance and impede ice sublimation rates through the dried layer (Rambhatla and Pikal, 2004).

In Chapter 4 Section 4.3.1, a reduction in primary drying time was observed with the addition of an annealing step, which is consistent with other literature (Searles *et al.*, 2001a, Webb *et al.*, 2003). However, in this chapter, only a slight decrease in primary drying time was observed after the 2 hour annealing duration. It is possible that the four hour annealing duration may have resulted in a further reduction of primary drying time. With the 8 and 16 hour annealing durations the primary drying time was found to have doubled compared to the 0 and 2 hour annealing durations. An increase in primary drying times with increasing annealing duration was also observed by Searles *et al.* (2001a), who reported a significant reduction in the primary drying times of excipients in the first 30 minutes of annealing, followed by a plateau and then a slight increase in primary drying time after approximately 10 hours of annealing.

One of the most commonly used methods for determining batch heterogeneity in a lyophilisation cycle is through monitoring the variation in product residual moisture content (Sane and Hsu, 2010). The moisture content, determined by Karl Fisher titration, can be seen in Figure 5.2. All sam-

Table 5.5. The primary drying times for the lyophilisation cycles with different annealing durations. TC 1 and 2 represent the data from thermocouples placed in vials in either the centre or the front of the freeze dryer, respectively.

Annealing duration (hours)	Length of primary drying (hours)	
	TC1 (centre)	TC2 (front)
0	10	6
2	9	6
4	†	†
8	22	11
16	23	10

†No thermocouple data recovered.

ples were found to have moisture contents below 1 % (w/w) which is highly desirable for a lyophilised protein formulation (Wang, 2000). For almost all formulations, a significant increase in residual moisture content was observed for the 8 hour annealing duration. However, an increase in standard deviation of the residual moisture content was also observed with increasing annealing duration. This appears to correlate well with the results of primary drying time, in which a greater difference in product temperature was observed between the front and centre of the freeze dryer for the longer annealing durations, which suggests variable sublimation rates.

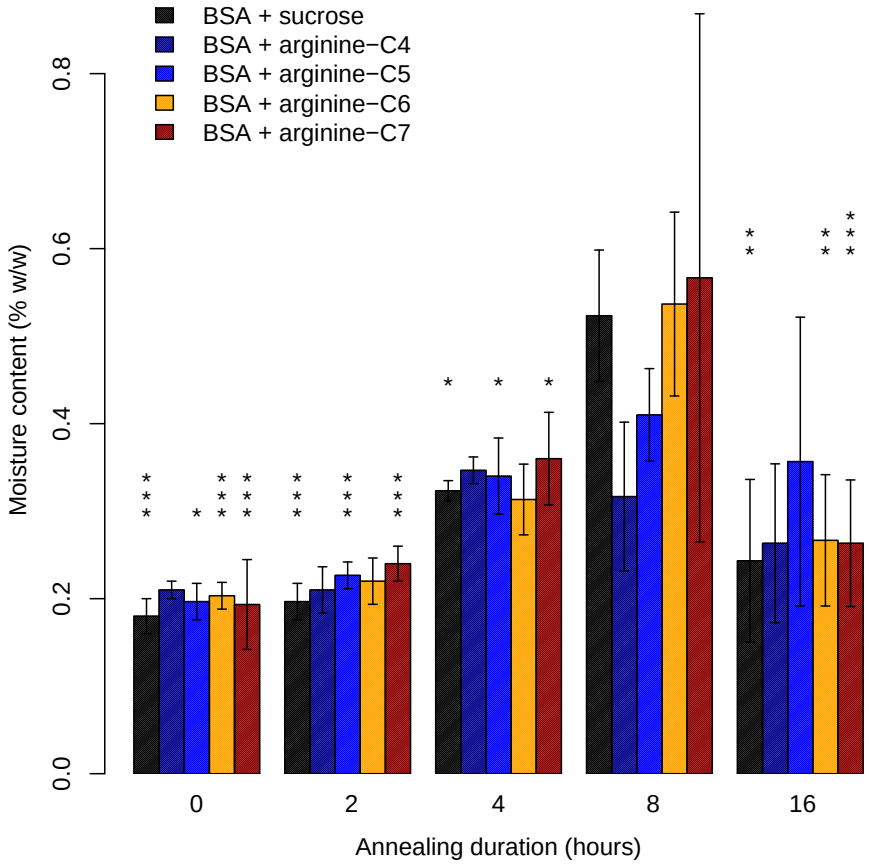


Figure 5.2. The residual moisture content of BSA formulations, lyophilised for different annealing durations. For statistical analysis a two-way ANOVA was used with Bonferroni post-test in which *all* annealing durations were compared. Statistical significance was only found between the 8 hour and the other annealing durations. For simplicity, the levels of significance are shown above only the columns found significantly different from the 8 hour duration. Statistically significant differences are denoted by $^{*}(p < 0.05)$, $^{**}(p < 0.01)$ and $^{***}(p < 0.001)$.

5.3.3 Cake appearance and solid state characterisation

The appearance of BSA cakes after lyophilisation can be seen in Figure 5.3. Some volumetric shrinkage was observed with all BSA formulations and some cracks were visible in the cakes. However, no large scale collapse was observed and, overall, lyophilisation using the different annealing durations and formulations resulted in cakes with an elegant appearance.

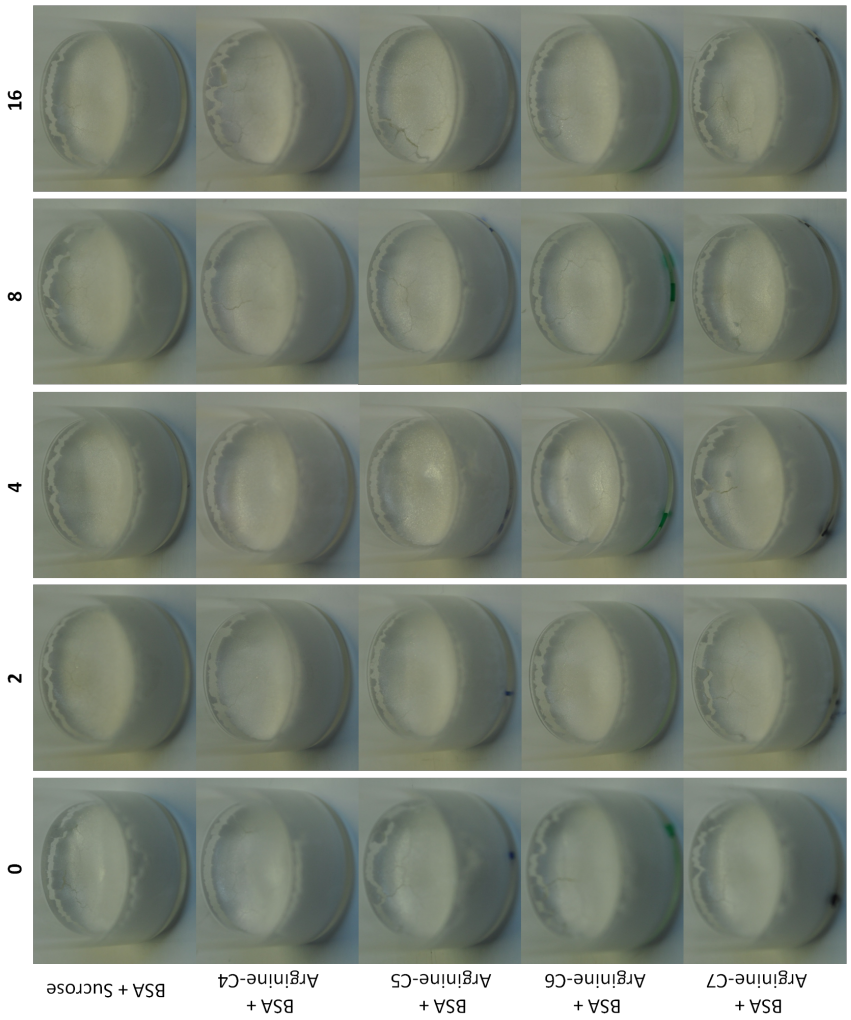


Figure 5.3. The appearance of BSA formulations after lyophilisation using different annealing durations (in hours).

SEM images of the lyophilised cakes can be seen in Figures 5.4 and 5.5 for the BSA sucrose and BSA arginine-C4 formulations, respectively, and Appendix Figures B.3, B.4 and B.5 for the BSA arginine-C5 to C7 formulations. For simplicity, only the annealing durations of 0, 2 and 16 hours have been shown.

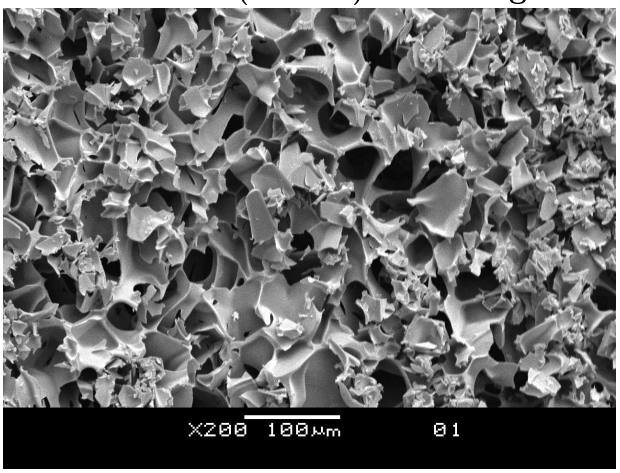
All samples appeared to have an interconnected spherical pore morphology. A more open pore structure can be observed with increasing annealing duration. However, changes in pore structure, resulting from the inclusion of an annealing step, were much more evident in the SEM images of Chapter 4 Section 4.3.3, in which larger pores were observed. It is likely that this is due to the lower annealing temperature used in this chapter (-10 °C).

All lyophilised formulations, both with protein and without, were confirmed amorphous by XRPD, the diffraction patterns of which (along with the crystalline as received excipients) can be found in the Appendix (Figures B.6, B.7, B.8). Furthermore, excipients were confirmed as amorphous by XRPD after storage for 12 weeks at 40 °C (Appendix Figure B.9). To the author's knowledge, this is the first report of an amorphous arginine-dicarboxylic acid glass.

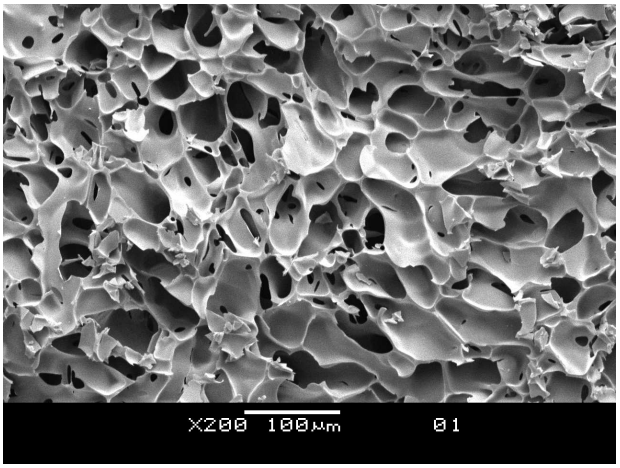
DSC is commonly used to find the glass transition temperature of amorphous pharmaceuticals by detecting a change in the heat capacity of the material. However, amorphous proteins behave as strong glasses and often only exhibit a small change in heat capacity over a broad temperature range, making detection of the Tg difficult (Pikal *et al.*, 2007). Rather than measuring changes in heat capacity, DMA has been used to measure changes in the viscoelastic properties of a material (Saunders and Gabbott, 2011).

Although few studies have been published in which DMA has been

Without (0 hour) annealing



2 hour annealing duration



16 hour annealing duration

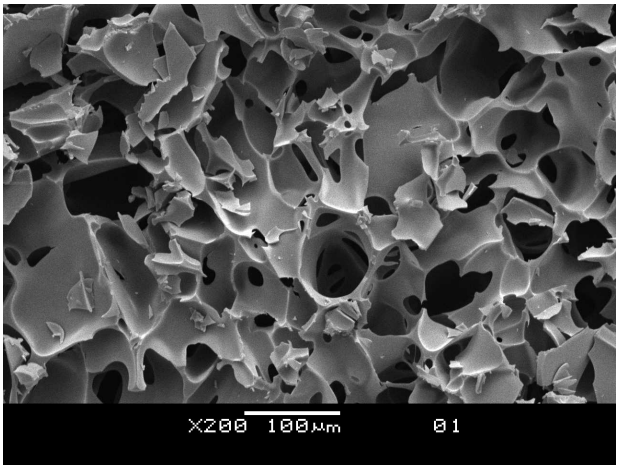
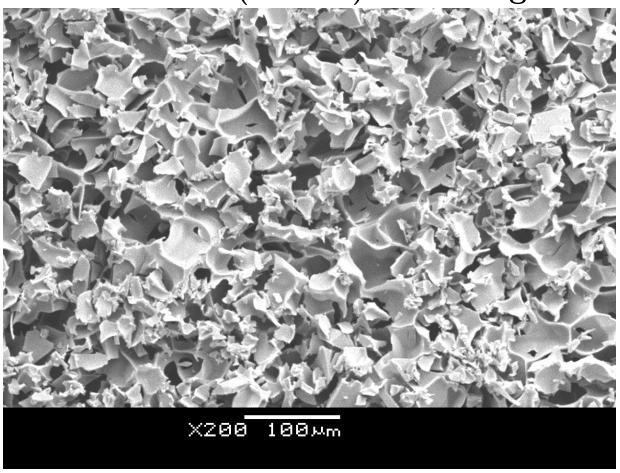
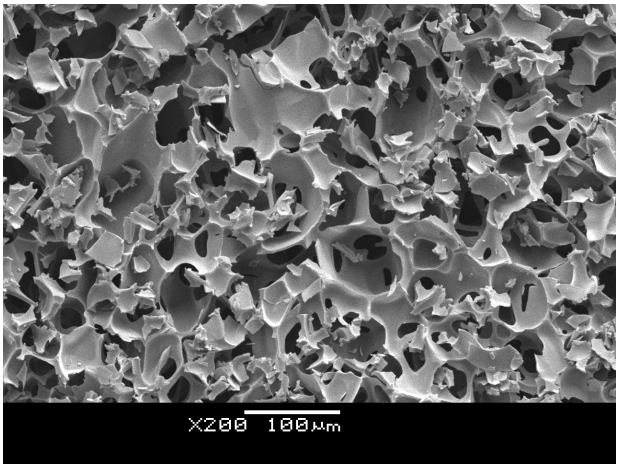


Figure 5.4. SEM images of BSA sucrose cakes lyophilised using 0, 2 and 16 hour annealing durations.

Without (0 hour) annealing



2 hour annealing duration



16 hour annealing duration

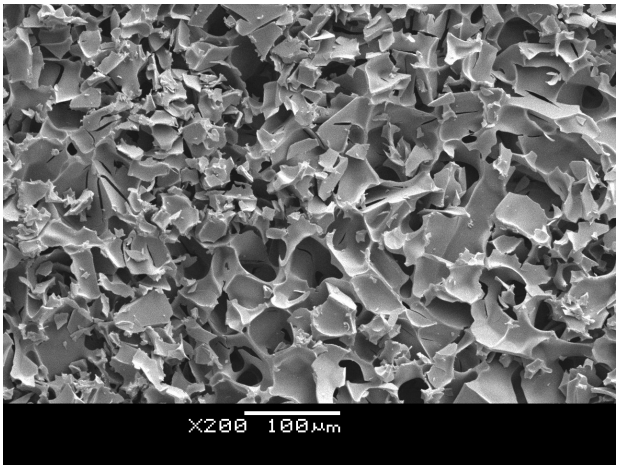


Figure 5.5. SEM images of BSA arginine-C4 cakes lyophilised using 0, 2 and 16 hour annealing durations.

Table 5.6. The Tg of lyophilised BSA formulations, annealed for different durations. The Tg was determined by DMA using the loss modulus (n=3, mean ± s.d where investigated, for all other samples n=1).

	Tg (°C)				
	Annealing duration (hours)				
	0	2	4	8	16
BSA + sucrose	108 ± 1.8	110	116	116	111
BSA + arginine-C4	136 ± 3.7	138	141	136	144
BSA + arginine-C5	141	139	140	145	137
BSA + arginine-C6	133	137	137	138	138
BSA + arginine-C7	133	137	134	139	135

utilised in determining the Tg of lyophilised proteins, one study has found it to be a viable alternative to DSC (Carpenter *et al.*, 2009a). The Tg of lyophilised BSA cakes can be found in Table 5.6. Due to a limited number of samples available, only BSA with arginine-C4 and BSA with sucrose were repeated three times, the standard deviations of which were found to be ± 1.8 and ± 3.7 °C, respectively. No trends were apparent between increasing annealing duration and Tg. Based on the deviations from the two samples studied, it is not possible to confidently determine whether differences also exist between formulations of different dicarboxylic acids. However, it is clear from these results that the arginine formulations have a Tg approximately 20 °C higher than the BSA sucrose formulation.

5.3.4 Cake surface area and bulk density measurements

The BET SSA of the lyophilised BSA formulations can be seen in Figure 5.6, the BET constants and error associated with the fit can be seen in Appendix Tables B.1 and B.2, respectively. The surface area for BSA 100 mg/mL with sucrose was found to be in the region of 1.7 m^2/g, which corresponds well with the previous chapter (Section 4.3.3) in which the SSA for BSA 100 mg/ml and 200 mg/mL with sucrose were found to be ∼2 and ∼0.7 m^2/g, respectively (excluding the values from quench cooled cycles).

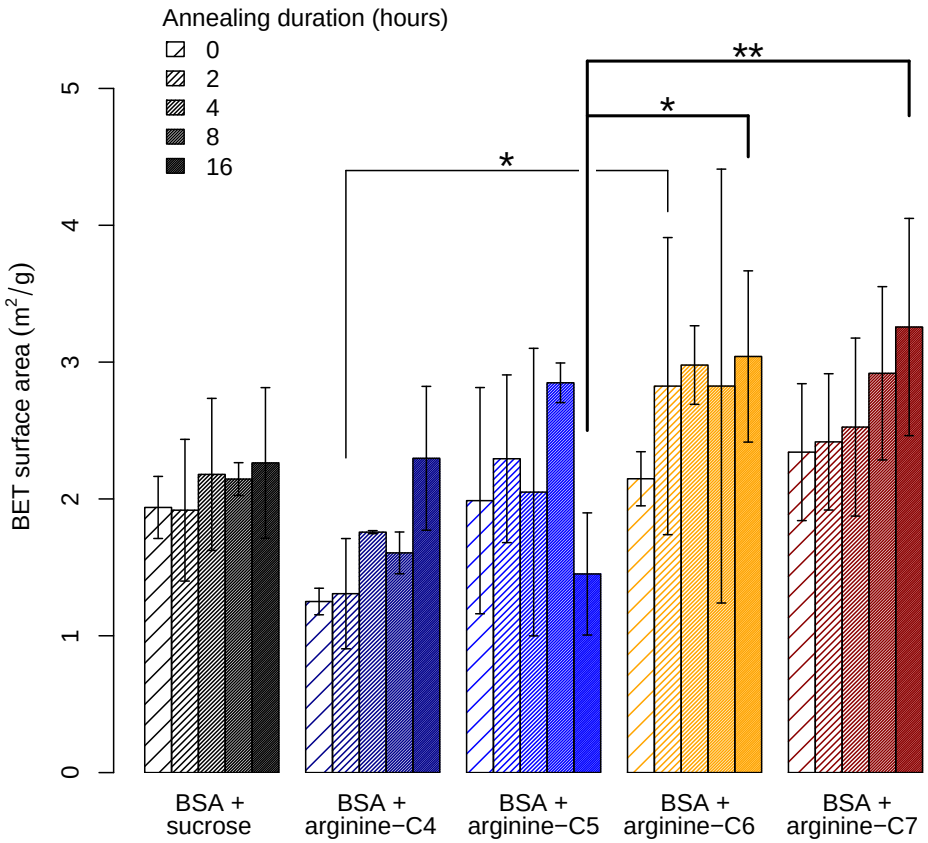


Figure 5.6. The BET specific surface area of lyophilised BSA formulations (n=3, mean ± s.d.). A two-way ANOVA with Bonferroni post test was used to compare all formulations. Statistically significant differences are denoted by *($p < 0.05$) and **($p < 0.01$).

The BET SSA for arginine formulations were found to be in the region of 1 and 3 m^2/g. No significant differences were observed between the different annealing durations for each formulation. Between formulations, there are several significant differences between the shorter (C4 and C5) and longer (C6 and C7) dicarboxylic acids. However, the error associated with fitting the BET equation (Appendix Table B.2) was found to be 2–3 fold higher with the BSA arginine-C4 lyophilised cakes. This may be the result of low surface areas affecting the sensitivity of the measurements and may

affect the statistical significance of these results. As there was no significant effect of including annealing duration or its interaction with formulation in the two-way ANOVA ($p<0.05$), annealing duration was removed from the analysis and a one-way ANOVA was performed. The BET SSA for each formulation can be seen in Figure 5.7. These results show that the formulations with C6 and C7 dicarboxylic acids are significantly higher than the shorter C4 dicarboxylic acid.

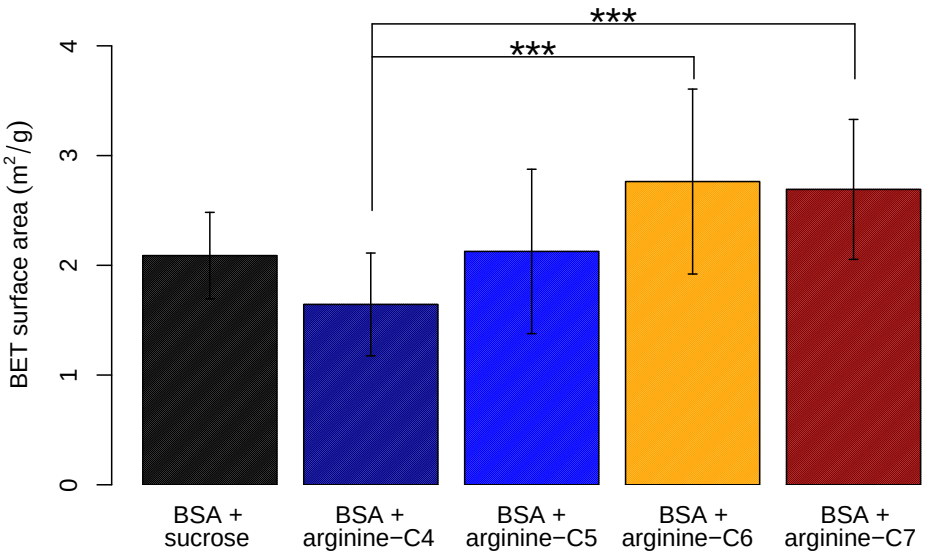


Figure 5.7. The BET specific surface area of lyophilised BSA formulations, in which the effect of the various annealing durations are not considered (n=15, mean ± s.d.). A one-way ANOVA with Bonferroni post test was used to compare the formulations. The statistically significant difference is denoted by ***(p <0.001).

The bulk density was measured for the BSA formulations using MIP and can be seen in Table 5.7. In general, the BSA sucrose formulation was found to have a slightly higher density (∼0.2 g/cm^3) than the arginine formulations (∼0.18 g/cm^3). No clear trends were observed between bulk density and increasing annealing duration or dicarboxylic acid alkyl chain

Table 5.7. The bulk density (determined using MIP at a pressure of 0.51 psi) of BSA formulations lyophilised for different annealing durations (n=1).

	Annealing duration (hours)				
Formulation	0	2	4	8	16
BSA + sucrose	0.2034	0.2153	0.2108	0.2098	0.2078
BSA + arginine-C4	0.1807	0.1864	0.1845	0.1792	0.1749
BSA + arginine-C5	0.1787	0.1773	0.1796	0.1782	0.1817
BSA + arginine-C6	0.1629	0.1832	0.1806	0.1831	0.1830
BSA + arginine-C7	0.1820	0.1827	0.2089	0.1939	0.1888

length. In the previous chapter, Section 4.3.3, an increase in bulk density of approximately 0.03 g/cm^3 was observed between annealed and quench cooled BSA 50 mg/mL samples and was attributed to a greater degree of volumetric shrinkage between cakes. In this chapter, the difference between arginine and sucrose formulations was approximately 0.02 g/cm^3, it is likely that this is, in part, due to the additional mass of histidine buffer in the sucrose formulation ($\sim$4 mg/mL). A greater degree of volumetric shrinkage may also be present in sucrose compared to arginine formulations, although this was not discernible by visual inspection.

5.3.5 Pore size and distribution

The pore size distributions obtained by MIP of the lyophilised BSA cakes can be seen in Figure 5.8. The arginine formulations appear to be mainly unimodal with a pore size distribution greater than 5 μm. However, a second, low volume, small diameter ($<$5 μm) distribution can also be observed with arginine formulations at most of the annealing durations, and can be seen in greater detail in Appendix Figure B.10, although no clear trend is evident between this pore size distribution and annealing duration.

For 0, 4, 8 and 16 hour annealing durations, the pore size distribution for arginine formulations is centred at approximately 10 μm although the long

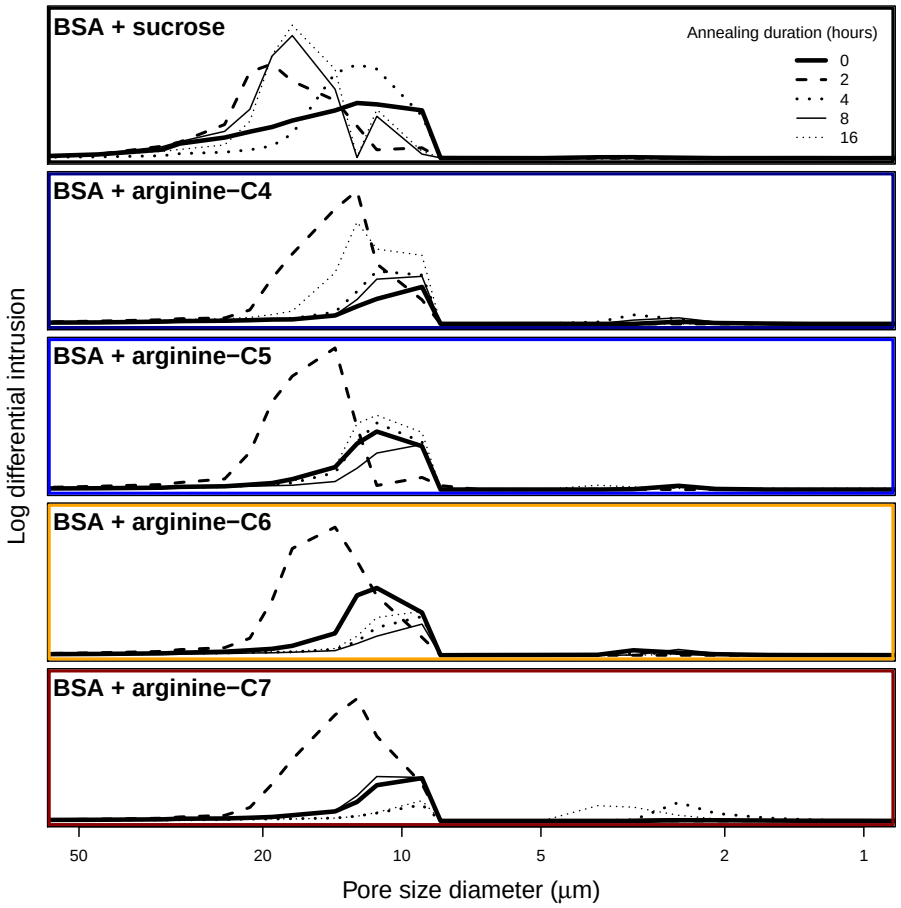


Figure 5.8. Representative pore size distributions of lyophilised BSA formulations by mercury intrusion porosimetry (n=1). The y-axis, which is not shown, is the same for all formulations.

tail to the left indicates a broad distribution of larger pores. Interestingly, an increase in pore size and intruded volume occur after the 2 hour annealing duration.

For the sucrose formulation without an annealing step, there is a unimodal distribution at approximately 10 μm and, again, a tail is evident showing a broad distribution of larger pores. At 2 hour annealing duration the pore size increases and a unimodal distribution centred at $\sim$20 μm can be observed. After a 4 hour annealing duration the average pore size is

decreased to approximately 13 μm. The pore size distribution for both 8 and 16 hour annealing durations appear similar for the sucrose formulation, which has a bimodal distribution with the majority of pore volume at $\sim$18 μm and the minority at $\sim$11 μm.

The total pore volume for the lyophilised BSA cakes can be seen in Figure 5.9. A larger pore volume is clearly evident for the 2 hour compared to the other annealing durations for arginine formulations, although an increase does also appear to occur at 16 hours for C4 and C5 dicarboxylic acids formulations. For the sucrose formulation, the pore volume appears largely unaffected by annealing duration.

One possible explanation for the reduced pore volume observed with arginine formulations, with the exception of those from the 2 hour annealing duration, is cake collapse. However, collapse was not observed on visual inspection and the bulk density, which can often indicate cake collapse (Krokida *et al.*, 1998), appeared similar across all annealing durations. To investigate this further, micro-CT was used to provide cross-sectional images of arginine-C4 cakes annealed for 0, 2 and 4 hours. From the top to the bottom of the cake, the horizontal 2D images (or 'slices') can be seen in Movie A (0, 2 and 4 for their respective annealing durations) which has been presented on the CD attached to this thesis. Through visual inspection, it appears that the cake annealed for 2 hours has pores that are elongated whereas at 4 hours the pores appear more spherical.

To illustrate more detail of the pore walls within the cake, the images were processed and binarised to show material as black pixels and free space as white pixels (as described in Section 5.2.2 of this chapter). An example horizontal cross-section through the central portion of each cake can be seen

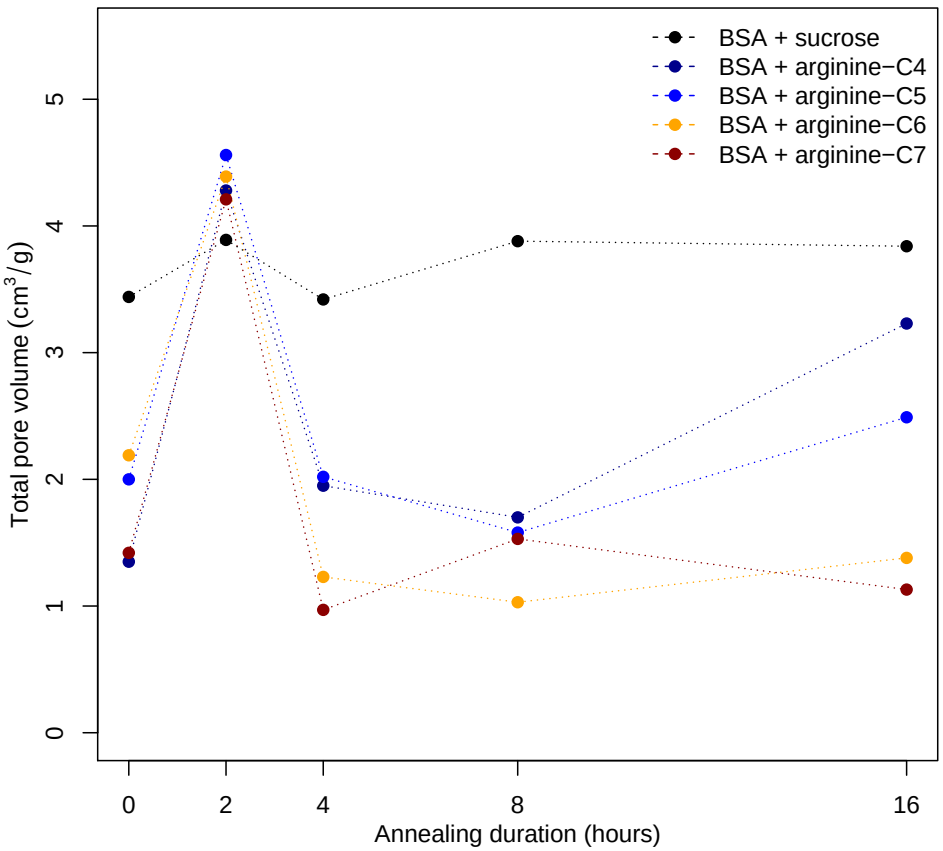


Figure 5.9. The total pore volume of lyophilised BSA formulations (determined by MIP). Please note the lines are used as guides and do not represent a line of best fit.

in Figures 5.10, 5.11 and 5.12 before and after image processing. Possibly the most notable difference between the different annealing durations is that for the sample without an annealing step there appears to be a greater amount of material per area compared to the pore space. After 2 hours, pores appear larger and less spherical than those of the 4 hour annealing duration.

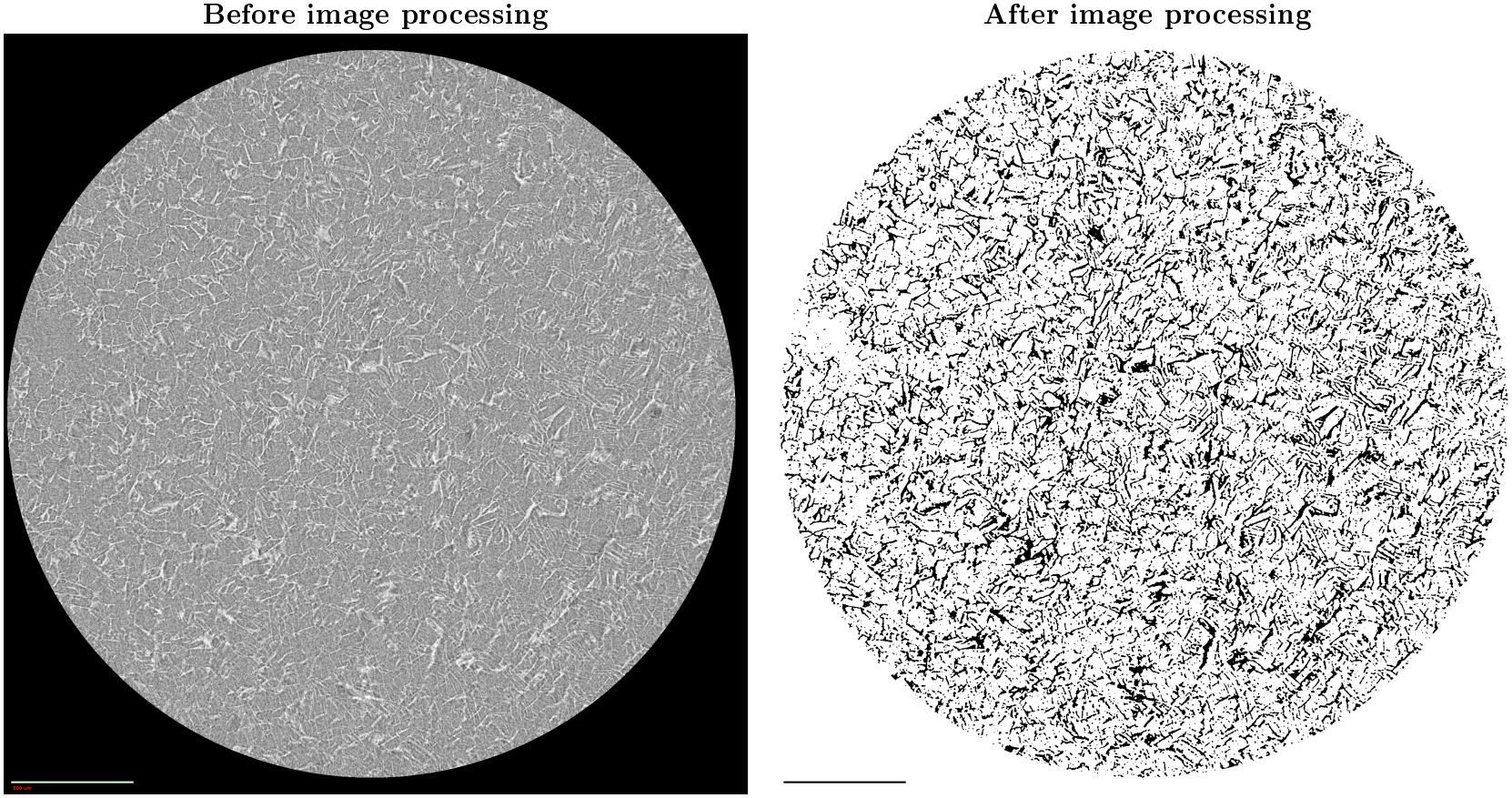


Figure 5.10. Before and after image processing of 2D slices, taken from the centre (horizontal cross-section) of a BSA arginine-C4 cake which was lyophilised without an annealing step. The scale bar in the left hand corner is 500 μm.

Figure 5.11. Before and after image processing of 2D slices, taken from the centre (horizontal cross-section) of a BSA arginine-C4 cake which was lyophilised with an annealing duration of two hours. The scale bar in the left hand corner is 500 μm.

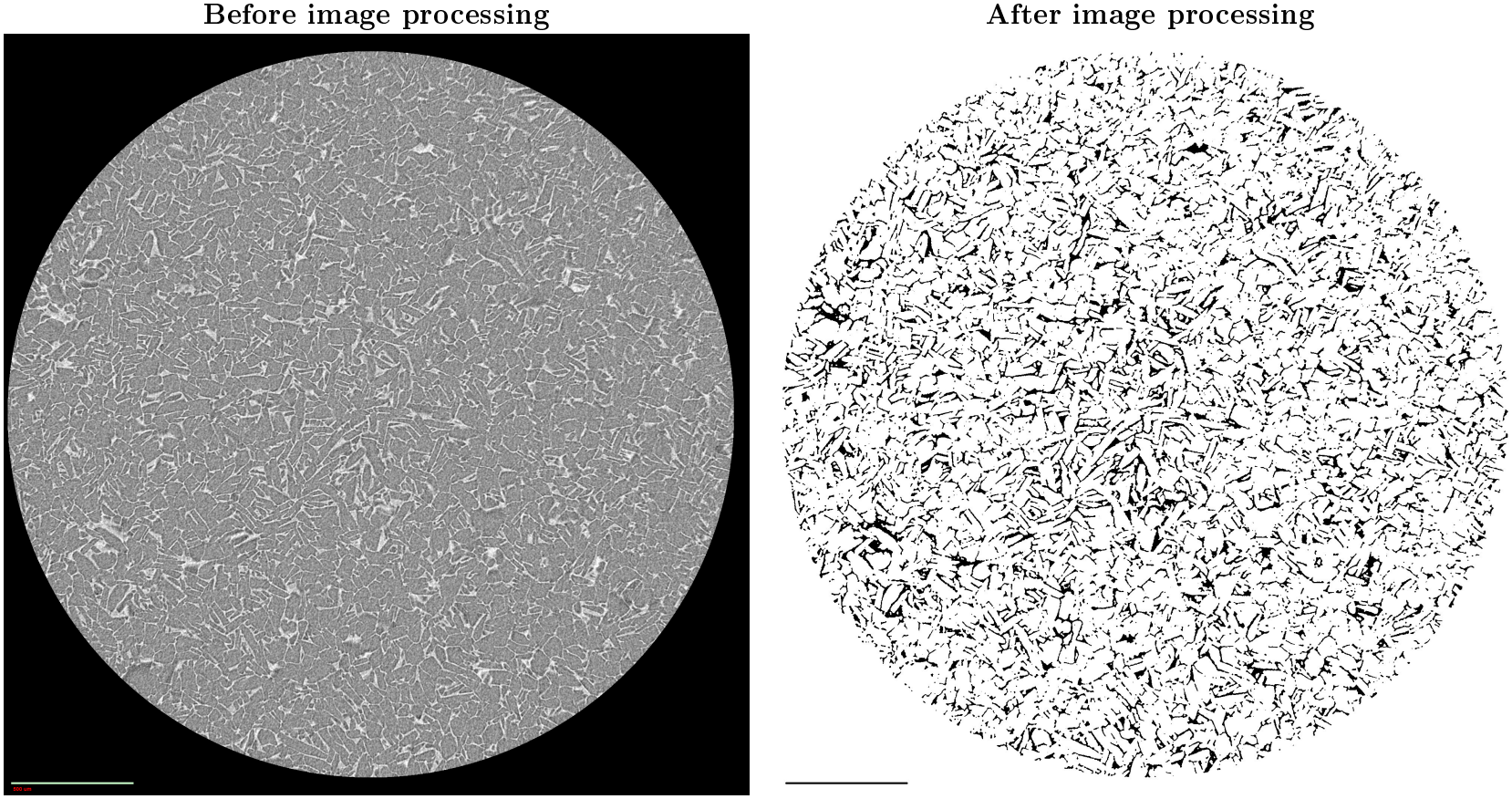


Figure 5.12. Before and after image processing of 2D slices, taken from the centre (horizontal cross-section) of a BSA arginine-C4 cake which was lyophilised with an annealing duration of four hours. The scale bar in the left hand corner is 500 μm.

By using the processed images, the porosity of each horizontal slice was calculated and is shown in Figure 5.13. It is clear to see in this figure that the porosity is lower at the top and bottom of the lyophilised cake, however, this again could be partly due to the resolution of the micro-CT. Through the central portion of the cake, porosity is lower when no annealing step is used. A crack is present in the 2 hour annealed lyophilised cake and is the likely cause of higher porosity in the the top 1200 slices of the cake. After taking cracks into consideration, porosity between the 2 and 4 hour annealed cakes appear similar which provides further evidence that there is no large scale collapse in cake structure between these annealing durations.

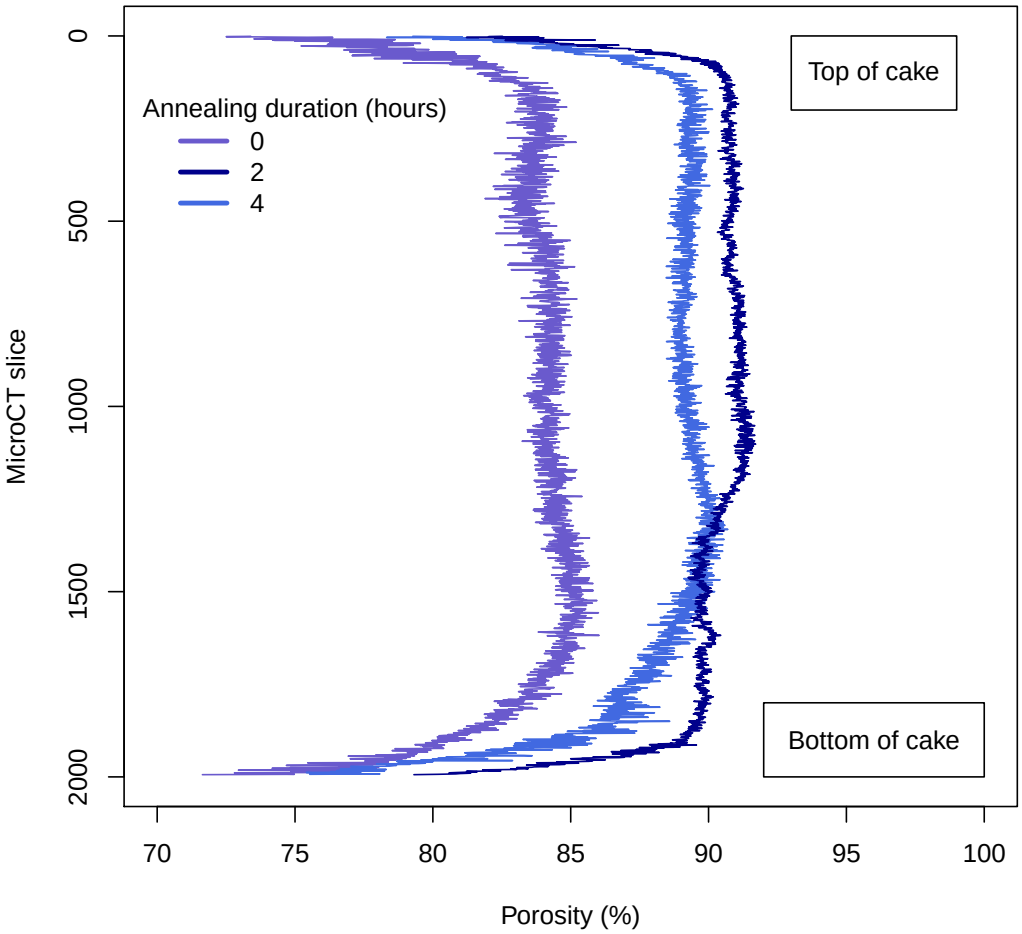


Figure 5.13. The porosity of 2D Micro-CT slices (after image processing) through BSA arginine-C4 cakes, which were lyophilised using different annealing durations.

A 3D rendering of the combined cake slice images can be seen in Figure 5.14 and have been included as Movie B (0, 2 and 4 for their respective annealing durations) on the CD provided. For all three annealing durations, pores appear smaller at the top and bottom of the lyophilised cakes. A higher material density was also observed in the top of lyophilised cakes in the micro-CT study by Izutsu *et al.* (2014). Here, pores appear less well defined in the cake with no annealing step, although this is could be a resolution issue in which pore walls are not adequately defined by the voxel size. Larger pores appear at 2 and 4 hour annealing durations, with pores appearing elongated after two hours but more spherical after the four hour annealing duration.

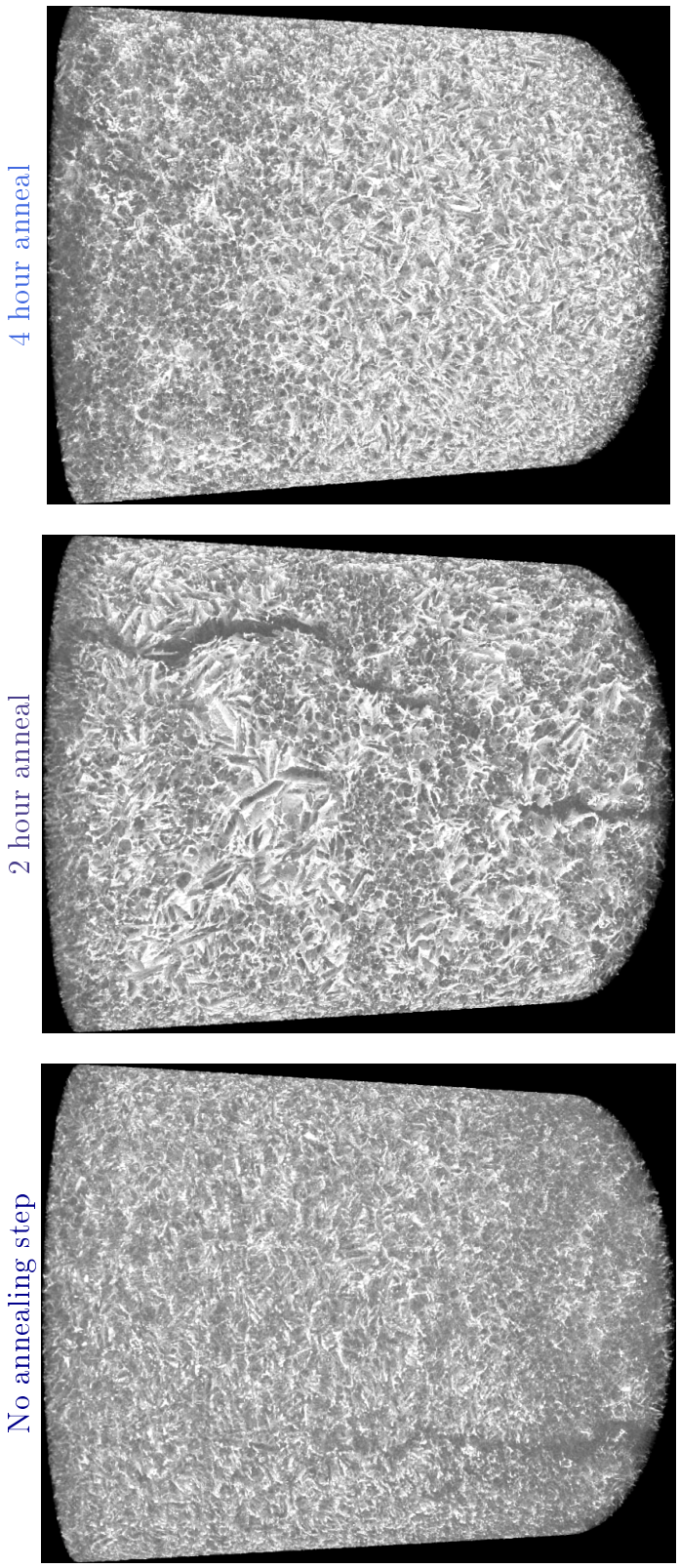


Figure 5.14. A 3D rendering of micro-CT images for BSA arginine-C4 cakes, lyophilised using different annealing durations.

5.3.6 Reconstitution time

The reconstitution times of the BSA 100 mg/mL formulations can be seen in Figure 5.15. A two-way ANOVA was used to determine whether there were statistically significant differences between the results. Overall, the reconstitution times between formulations with sucrose and arginine appear comparable (∼7 to 8 minutes), with the only significant difference found with the arginine-C7 formulation which had been annealed for four hours (∼12 minutes).

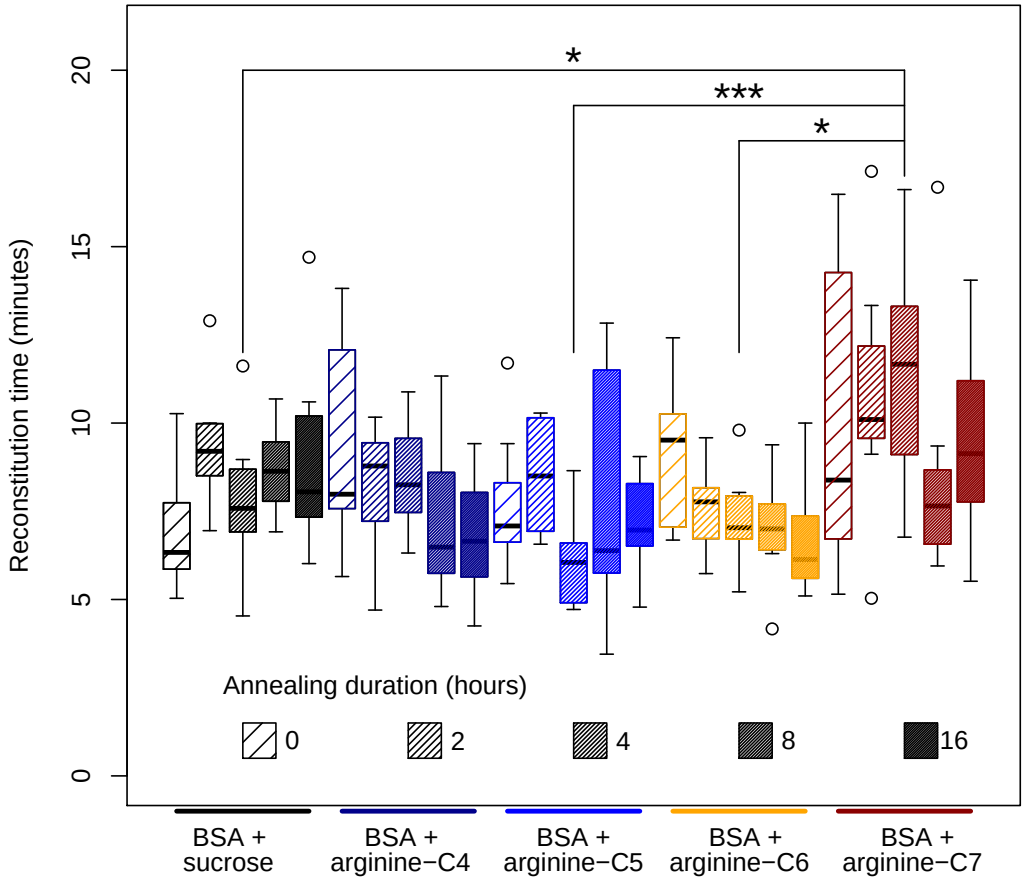
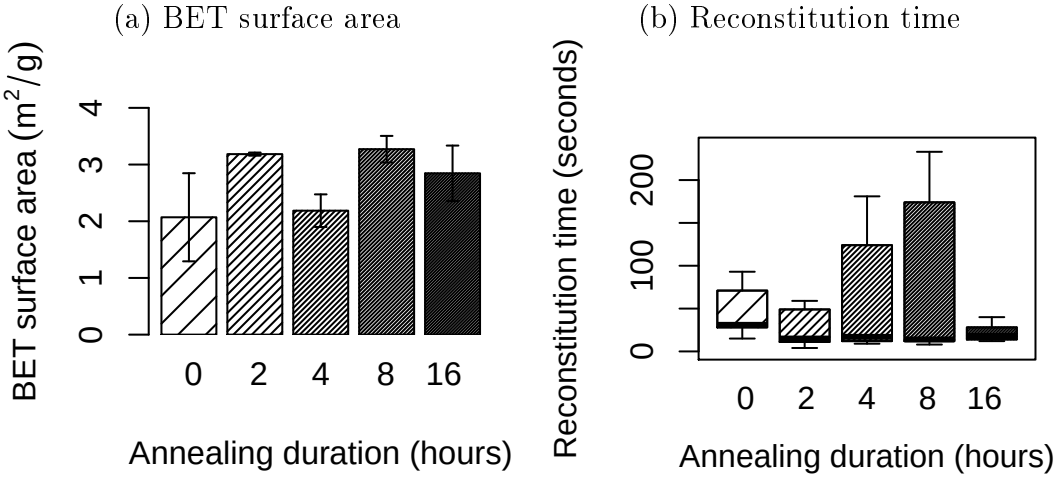


Figure 5.15. The reconstitution times of BSA formulations (n = 7). Statistically significant differences are denoted by *(p <0.05) and ***(p <0.001). Each box plot represents the interquartile range with the median as the thick horizontal line. Dashed lines show the minimum and maximum reconstitution times. Outliers, defined as being greater than 1.5 times the distance from the lower and upper quartiles are shown as circles.

5.3.7 Cake properties of mAb1

The mAb1 formulation was found to form elegant lyophilised cakes for all annealing durations (Appendix Figure B.11), which were all confirmed amorphous by XRPD (Appendix Figure B.7). An interconnected spherical pore morphology was also observed by SEM (Appendix Figure B.12) similar to the images in Chapter 4 Section 4.3.3.

No significant differences were observed with the BET SSA between annealing durations (Figure 5.16a) nor with the reconstitution times (Figure 5.16b). The distribution of pore sizes by MIP can be observed in Figure 5.16c. A unimodal pore distribution was observed at approximately 20 μm, which increased to $\sim$23 μm after the two hour annealing duration. Similarly to the arginine and sucrose formulations in Figure 5.8, a reduction in pore size was observed for the 4 hour annealing duration. After 8 hours, the pore size appears to become trimodal with discrete distributions at $\sim$19, 25 and 35 μm. At the 16 hour annealing duration only one pore size distribution is evident and is centred at approximately 25 μm. The bulk density and total pore volume measurements (obtained using MIP) for the mAb1 formulations can be see in Appendix Table B.3. Similarly to the BSA sucrose formulation, the bulk density and total pore volume remained consistent across all annealing durations at approximately 1.3 g/cm^3 and 6.4 cm^3/g, respectively.



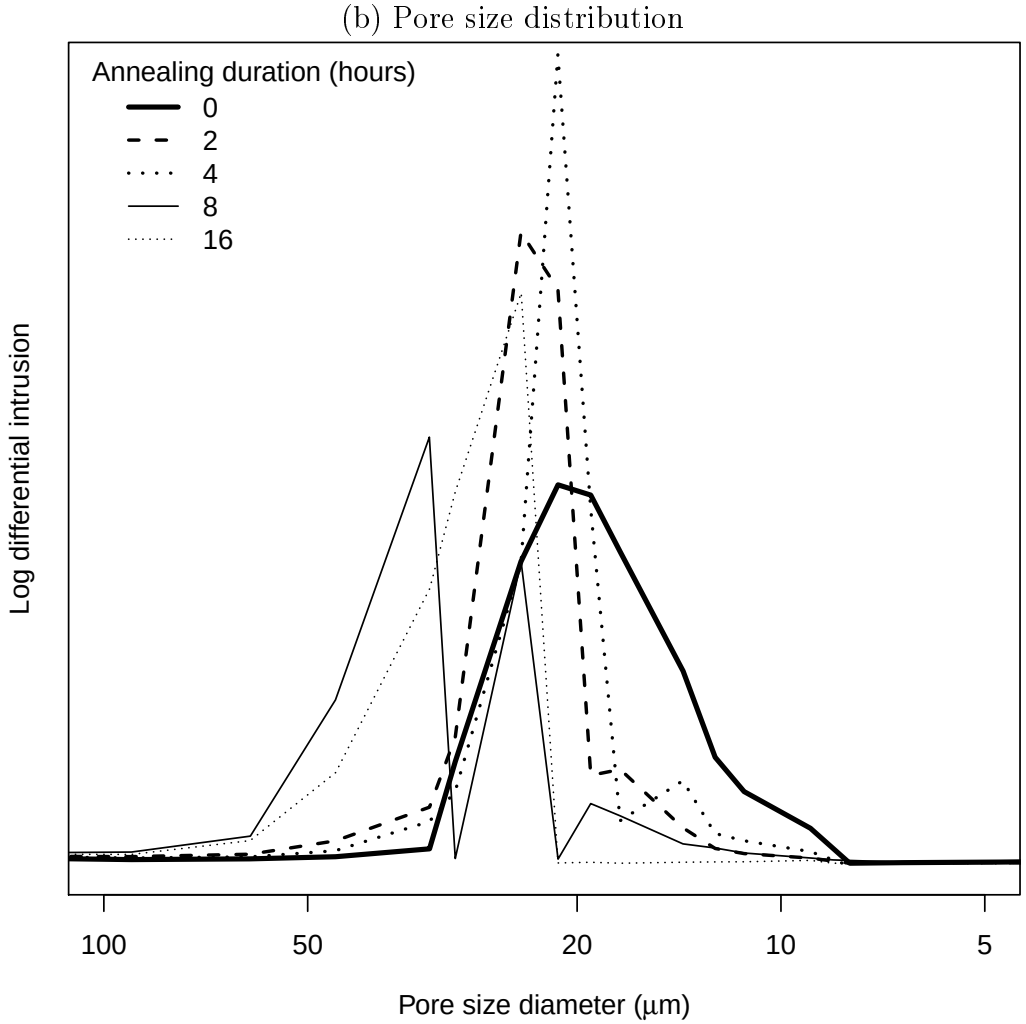


Figure 5.16. Cake structural characteristics of mAb1 including (a) the BET specific surface area (n=3, mean ± s.d); (b) the reconstitution times of the lyophilised cakes; (c) the pore size distribution by MIP (n=1)

5.4 Discussion

5.4.1 Arginine-dicarboxylic acids as excipients

The BSA arginine-dicarboxylic acid formulations were found to have slightly lower Tg′ values than the sucrose formulation, although the Tc values appear comparable. Furthermore, all formulations were found to form elegant cakes with no large scale collapse and only minor volumetric shrinkage. The glass transition temperature of the lyophilised BSA arginine formulations were found to be approximately 20 °C higher than the sucrose formulation. It would be prudent to increase the number of samples in order to confirm reproducibility and allow statistical testing in the future. As high Tg formulations are often associated with slower molecular mobility (Xu *et al.*, 2013), the arginine-dicarboxylic acids may provide better storage stability than the sucrose formulations, which will be assessed in the following chapter.

The BET SSA of lyophilised formulations were not found to be significantly affected by annealing duration. Analysis between formulations only (i.e. by not considering the effect of annealing duration), showed a statistically significant difference between the shorter (C4) and longer (C6 and C7) dicarboxylic acid formulations. It is possible that a trend exists between increasing dicarboxylic acid chain length and SSA, although this requires further experimental verification. Reducing the high error values from the fit of the multipoint BET should enable more accurate results and may be accomplished in the future by increasing the sample mass, using longer equilibration times, or, by replacing the adsorption gas from nitrogen to krypton, which was discussed in more detail in Chapter 3 Section 3.3.3.

If a trend between dicarboxylic acid alkyl chain length and SSA does exist, this may be the result of surface tension effects. Dicarboxylic acids are known to increase the surface tension of water in an effect that diminishes with increasing alkyl chain length (Shulman *et al.*, 1996). Increased cohesive forces with the shorter dicarboxylic acids may minimise the surface area. This could have important implications in protein stability as numerous studies have reported a correlation between surface area and protein denaturation (Costantino *et al.*, 2002, Devineni *et al.*, 2014, Hsu *et al.*, 1995, Webb *et al.*, 2003, 2002b, Xu *et al.*, 2014). It is thought that this is due to the larger ice interface which can denature the protein (as described in Chapter 1 Section 1.2.2). Characterisation of low molecular weight amorphous pharmaceuticals have also found that a greater molecular mobility exists at the surface than the bulk of amorphous material (Wu and Yu, 2006, Zhu *et al.*, 2008, 2010), and is therefore also a possible mechanism of protein denaturation at the surface. The effect of formulation of protein stability will be assessed in the following chapter.

5.4.2 Proposed mechanism for ice crystal growth during annealing

The influence of annealing duration on pore size, pore size distribution and pore connectivity presented the most unexpected results in this chapter. To summarise, the following results were observed:

- 1. The BET SSA was not found to be significantly different between annealing durations.

- 2. The total pore volume from MIP of arginine formulations was low, with the exception of the two hour annealing duration. Whereas the

total pore volume for the sucrose and mAb1 formulations remained consistently high.

- 3. The porosity of the arginine-C4 formulation by micro-CT appears to be similar between two and four hour annealing durations.

- 4. For all formulations investigated, a unimodal pore size distrubtution was observed for 0, 2 and 4 hour annealing durations, in which the pore size increased between 0 and 2 hour annealing durations and then decreased for the 4 hour annealing duration, where it remained for the 8 and 16 hour arginine formulations. For the sucrose formulation, the distribution becomes bimodal after 8 and 16 hour annealing durations (peaks at ∼11 and 17 μm), and for mAb1 it becomes trimodal after 8 hours (with peaks at ∼19, 25, and 35 μm) and after 16 hours one peak dominates at ∼24 μm.

To account for the similarities in BET SSA and porosity across the annealing durations[2] but large difference in total pore volume (by MIP). It is likely that closed pores, or pores with throats less than the minimum pore size investigated (0.05 μm), were present in the arginine formulations, with the exception of those lyophilised for a two hour annealing duration.

Ice recrystallisation processes are thought to occur during annealing and were described in greater detail in Chapter 1 Section 1.1.3. A large body of literature exists in the food science research field on ice recrystallisation processes, most notably with ice cream, as this can be detrimental to the overall texture and quality of the final product (Cook and Hartel, 2010, Kaale and Eikevik, 2014, Miller-Livney and Hartel, 1997, Petzold and Aguilera, 2009).

[2]The similar porosity was observed between 2 and 4 hour annealing durations using micro-CT.

For an excellent review on ice cream recrystallisation the reader is referred to the reference by Cook and Hartel (2010). In addition, the annealing process has been well characterised in metal alloy systems (Flemings, 2005, Kammer and Voorhees, 2006).

To account for the effects of annealing duration on pore size, pore size distribution and pore connectivity, the following mechanism of ice crystal growth has been proposed.

Without annealing, shelf-ramped freezing generates a large number of small ice crystals due to the process of global supercooling (Kasper and Friess, 2011). Outside of the ice volume, the remaining freeze concentrate may contain amorphous water. At the start of annealing, the higher temperatures allow a greater molecular mobility in the freeze concentrate which can lead to devitrification (Goff and Hartel, 2013), in which amorphous water is able to crystallise and cause an increase of the Tg' of the freeze concentrate (Zuo *et al.*, 2005). Between the tip and base of ice dendrites is an area surrounding the ice, known rather nicely as the 'mushy zone', with a low freezing point which can lead to thickening (Huang and Glicksman, 1981) and accretion (joining together) of the ice dendrite branches (Cook and Hartel, 2010). It is proposed here that at the start of the annealing process amorphous ice may freeze in the mushy zones and increase the width of the dendrites. On sublimation this would lead to wider pore throats, and would explain the increase in pore size for all formulations after two hours of annealing, which was observed by MIP in this chapter. The increase in porosity by micro-CT between 0 and 2 hour annealing durations is the likely result of an increased ice fraction creating larger pores and a reduction in the excess free volume of the glass which can relax during annealing (Webb *et al.*, 2003).

For all formulations investigated in this chapter, a decrease in pore size was observed at the four hour annealing duration. This may be caused by the recrystallisation of dendritic branches, which was described in greater detail in Chapter 1, but essentially involves the breaking off of dendrites at the points of attachment where the radius of curvature is high (Flemings, 2005). The shrinking of pore throats during this process appears to be a reasonable explanation for the decrease in pore size observed using MIP in this chapter. After the four hour annealing duration, changes in the pore size appear to be arrested for the arginine formulations.

During annealing, it is likely that isomass rounding, accretion and Ostwald ripening occur simultaneously (and were described in greater detail in Chapter 1 Section 1.1.3). The research article by Searles *et al.* (2001a) is often cited in lyophilisation literature when discussing the annealing process (Abdelwahed *et al.*, 2006, Abdul-Fattah *et al.*, 2007b, Kasper and Friess, 2011, Rambhatla *et al.*, 2004, Webb *et al.*, 2003), in which the ice crystal size is thought to increase with annealing duration$^{1/3}$. Indeed, as discussed by Searles *et al.* (2001a), this is predicted to occur in the steady-state diffusion-limited Ostwald ripening process, as described by LSW theory (Lifshitz and Slyozov, 1961, Wagner, 1961). However, this does not explain the formation of discrete pore size distributions which were observed by MIP in the current and previous chapters.

The presence of a transient bimodal particle size distribution has been reported in coarsening studies of ceramic and metal alloy materials (Rohrer, 2005). A mechanism, called nucleation-limited coarsening theory, has been recently proposed to account for these effects and is based on the idea that a single crystal surface will only grow by the lateral motion of steps (Rohrer *et al.*, 2002, Sano and Rohrer, 2007). In the absence of these steps, an

energy barrier prevents the nucleation of new layers on the crystal surface. This results in a distribution of small crystals which are unable to grow and a distribution of large crystals which grow through the presence of steps. Over time, the smaller crystals will disappear by Ostwald ripening leaving a unimodal distribution.

This work therefore proposes that ice crystal growth during annealing may be nucleation-limited, rather than diffusion-limited which has previously been described by Searles *et al.* (2001a). However, it is likely that once the smaller ice crystal distribution is removed and a unimodal distribution is established, growth would occur though a diffusion-limited process. The practical implications of discrete pore size distributions are not fully understood. It is possible that it may influence vapour transit and, conversely, reconstitution time. Although, no significant differences were observed in reconstitution time before and after the addition of an annealing step to the 0.5 °C/min cooling rate in the previous chapter.

Three questions appear important about the proposed annealing mechanism: *What causes the process to arrest? Why are the pore throats smaller with arginine formulations? And, is there an optimal stage to the process?*

In short, the first answer would appear to be: it depends on formulation properties. The molecular mobility of a formulation has been reported to be a significant factor in Ostwald ripening rates (Ablett *et al.*, 2002), where slow mobility can reduce recrystallisation. Although the Tg′ was found to be similar between sucrose and arginine formulations with BSA, the Tg of the lyophilised solid was approximately 20 °C higher with arginine formulations, implying that it will form a glass with less molecular mobility than the sucrose formulation.

The smaller pore throats, which have been described as the cause of low total pore volume of arginine in MIP experiments, may also be explained by formulation properties. Although not fully understood, the smaller pore throat sizes could be related to surface tension or freezing point depression effects of the arginine-dicarboxylic acid salts. This could lead to a greater degree of supercooling and consequently smaller ice crystals/smaller dendritic branches may be formed, although this would need further experimental verification.

Finally, in terms of product quality characteristics, it appears that there is an optimal stage to the proposed mechanism. Based on the primary drying times, batch heterogeneity and variable residual moisture contents that were observed in this chapter, annealing for 2 hours provided the best quality attributes. The detrimental effects caused by long annealing durations may be due to the loss of dendrite branches, which was thought to occur at the four hour annealing duration, which may reduce the connectivity of pores. Ostwald ripening and isomass rounding, unlike accretion, are also not likely to improve pore connectivity and could therefore lead to a decrease in pore connectivity.

5.5 Conclusion

In this chapter, the influence of formulation and annealing duration on the resulting lyophilised cake structure was analysed. The formulations investigated included a conventional sucrose formulation and a series of arginine-dicarboxylic acid combinations, which have not previously been investigated. Arginine-dicarboxylic acids were found to have a number of desirable characteristics in common with sucrose formulations, such as similar collapse temperatures and elegant cake appearances. Furthermore, the Tg of the lyophilised arginine cakes were found to be approximately 20 °C higher than the sucrose formulation. The longer alkyl chain dicarboxylic acid formulations were found to have a significantly larger BET SSA than the shorter (C4) dicarboxylic acid formulation. It is possible that a trend exists between increasing dicarboxylic acid alkyl chain length and increasing surface area, which is likely to be related to surface tension effects, although this needs further experimental verification.

Increasing the annealing duration led to longer primary drying times and a greater variation in cake residual moisture contents. Increasing the annealing duration was not found to significantly affect the BET SSA of lyophilised cakes despite the differences observed with total pore volume. It was concluded that arginine formulations may have smaller pore throat diameters. Based on these findings, the following mechanism of ice crystal growth during annealing was proposed. Initially, devitrification allows amorphous water to crystallise, leading to thickening of dendrites. Due to recrystallisation, the dendrite branches break off at their points of attachment. It is suggested here that this loss of dendrite connectivity may be the cause of the long primary drying times and variable residual moisture con-

tents observed with samples from the 8 and 16 hour annealing duration. If the molecular mobility in the glass permits it, recrystallisation events such as Ostwald ripening continue during annealing. The formation of discrete pore size distributions observed in this study are proposed to be caused by nucleation-limited Ostwald ripening. After recrystallisation of the smaller ice crystal distribution, growth of ice is likely to proceed through diffusion-limited Ostwald ripening and accretion processes.

6 Insights into the Influence of Annealing Duration and Formulation on Lyophilised Protein Stability

In order to produce a high quality lyophilised biopharmaceutical, it is vital to understand the mechanisms by which formulation excipients interact with proteins. To date, most formulation development relies on empirical results and previous experience and, in this respect, current approaches lack scientific robustness (Chan and Rogueda, 2011).

The amino acid arginine has received increasing interest as a formulation excipient for lyophilised biopharmaceuticals. Despite refinement through experimental and molecular dynamic studies (Arakawa *et al.*, 2007, Shukla and Trout, 2010, Vagenende *et al.*, 2013), the molecular basis of protein stabilising effects by arginine still however remain poorly understood. For lyophilised biopharmaceuticals, protein stability is regarded as a critical quality attribute and is therefore an essential component to monitor in research and development studies.

The motivation of this chapter was to evaluate how the process and formulation variables examined in Chapter 5 impact protein stability and aims to provide a molecular rationalisation for the effects observed. This chapter provides new experimental data and presents important insights to be considered for future formulation and process development studies.

6.1 Introduction

6.1.1 The formation of protein aggregates

Protein aggregation has been increasingly recognised as an issue that may reduce the biological activity of therapeutics, increase the risk of immunogenicity and has been implicated in numerous disease states (Carpenter *et al.*, 2009b, Koo *et al.*, 1999, Mehta *et al.*, 2014). Elucidating the molecular mechanisms of protein aggregation is therefore a key focus in pharmaceutical research and development. In general protein aggregates can be described by four classifications: their conformation, the type of linkage, whether they are reversible and their size.

Changes in protein conformation have been discussed previously in Chapter 1 Section 1.2 and Chapter 4 Section 4.3.4 and describe changes in the protein secondary or tertiary structure from the native state. The type of linkage in protein aggregates can be described as either covalent (e.g. aggregates formed through disulphide bridges) or non-covalent in which forces such as hydrophobic, electrostatic, van der Waals or hydrogen bonding mediate interactions (Sharma and Kalonia, 2010). Aggregates are deemed reversible when removing the protein from a stress (or environment) leads to a return in native properties. Small, soluble protein aggregates (oligomers) typically have a diameter between 0.01 to 1 μm (Mahler *et al.*, 2009). Larger, insoluble aggregates are generally referred to as subvisible ($\sim$0.1–1 to 100 μm) or visible ($>$50–100 μm) particles (Carpenter *et al.*, 2009b, Mahler *et al.*, 2009).

Subvisible particle (SVP) formation can be influenced through a number of conditions such as mechanical stresses, e.g. agitation (Kalonia *et al.*, 2013,

Kiese *et al.*, 2010, Liu *et al.*, 2012, Nayak *et al.*, 2011, Telikepalli *et al.*, 2014), formulation effects (Kalonia *et al.*, 2013, Telikepalli *et al.*, 2014), the presence of silicone oil (Gerhardt *et al.*, 2014) and interfaces such as with ice, air and processing equipment (Barnard *et al.*, 2011, Jones *et al.*, 2001, Kerwin *et al.*, 1998, Liu *et al.*, 2013a).

One proposed scheme for SVP formation can be seen in Figure 6.1 where the protein changes from its native state to an aggregation prone state (Simler *et al.*, 2012). Association of the aggregation prone states leads to the formation of larger aggregates and further growth leads to subvisible and visible particles. However, this is a rather simplistic model and recent research suggests that the pathway for subvisible particle formation is different from soluble aggregation and depends on both protein and solution conditions (Jayaraman *et al.*, 2014). The complexity of SVP formation is further increased with reports that they may be reversible on storage (Kiese *et al.*, 2010) or dissociate depending on the solution conditions (Jayaraman *et al.*, 2014).

Historically, regulatory issues with intrinsic SVP has revolved around their risk of occluding blood vessels, as the risk of administering aggregated protein particles was not considered when defining pharmacopoeial particle size limits (Carpenter *et al.*, 2009b). Little is known about the immunogenic effect of formulations containing aggregated particles under current size acceptance criteria (10 μm) and therefore soluble as well as SVP should be diligently monitored throughout formulation development studies (Eon-Duval *et al.*, 2012, Porter, 2001, Singh, 2011).

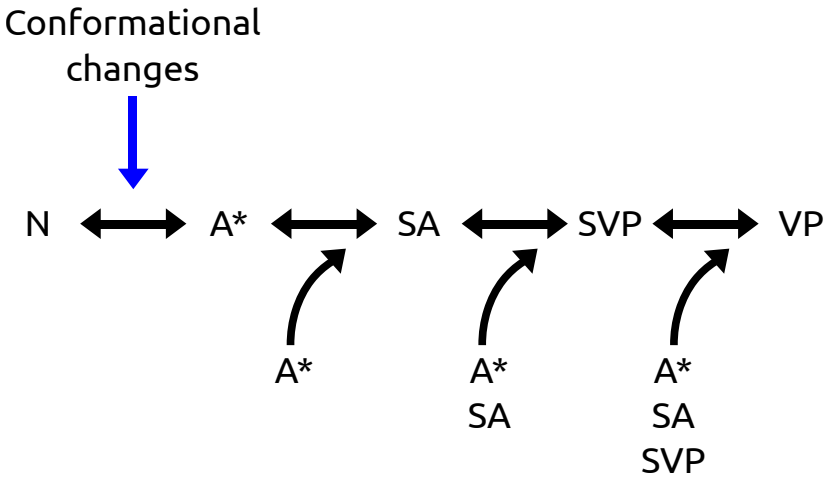


Figure 6.1. A scheme for visible particle formation, adapted from reference (Simler *et al.*, 2012). A protein in its native state (N) may undergo conformational changes when a stress, such as agitation, is applied. The protein becomes susceptible to aggregation (A*) and may form higher order soluble aggregates (SA). Association of SA and A* can lead to growth of the aggregates and may be observed as subvisible (SVP) or visible (VP) particles.

6.1.2 Protein stability in sucrose and arginine formulations

Sucrose

Lee and Timasheff (1981) first proposed that, when in a protein solution, sucrose is preferentially excluded from the vicinity surrounding the protein. A a chemical potential gradient forms between the hydrated protein and the excipient-rich solvent where unfolding of the protein would be thermodynamically unfavourable. The origin of sucrose exclusion from the protein surface is believed to be due to excluded volume effects, the chemical nature of the protein surface and the effect sucrose has on the surface tension of water (Arakawa and Timasheff, 1982).

Sugars have also been proposed to interact with proteins through hydrogen bonding. As drying removes part of the protein hydration shell, excipients that replace the hydrogen bonding are often required to stabilise

the protein. Excipients such as sugars have therefore been found to successfully stabilise proteins during drying (Carpenter and Crowe, 1988, 1989, Carpenter *et al.*, 1987a,b), an effect which is believed to be due to their flexible structure, relatively small size (compared to e.g. dextran (Allison *et al.*, 1999)), and high hydrogen bonding capacity (Kayser and Varzecha, 2012). Consolidation of the mechanisms by which sucrose can be both preferentially excluded from the protein surface yet also hydrogen bond directly with it however, remain elusive.

Arginine

At physiological pH, arginine has both positively charged and negatively charged groups (Chapter 5 Section 5.1.2). The guanidinium group is planar and neutron diffraction studies have shown that is has no recognisable hydration shell (Mason *et al.*, 2003). This allows strong interactions to occur with other molecules in solution, with less energy required for desolvation. In particular, the guanidinium group is able to form cation-π interactions and is well known to increase the solubility of aromatic amino acids (Hirano *et al.*, 2013). One mechanism of aggregation suppression by arginine is through the screening out of hydrophobic hot spots, which may be the aggregation prone sites on proteins (Das *et al.*, 2007). Through molecular dynamic simulations, the guanidinum group has been found to have a strong interaction energy with acidic residues (Shah *et al.*, 2011, 2012, Vagenende *et al.*, 2013). Arginine is also thought to interact with the protein through hydrogen-bonding and van der Waals forces (Ito *et al.*, 2011, Kamerzell *et al.*, 2011).

However, interactions between arginine and proteins appear complex. Both arginine concentration and the choice of counterion have been shown

to affect protein aggregation behaviour (Schneider *et al.*, 2011, Shukla *et al.*, 2011a). As well as participating in protein-excipient interactions, arginine can self-associate through head to tail (guanidinium-carboxylate) interactions to form larger clusters in an interaction which has been found to be more energetically favourable than the interaction with the surrounding water (Shukla and Trout, 2010).

By using molecular dynamic simulations and experimental work involving the measurement of the protein melting temperature (through microcalorimetry) and aggregate size (through SEC), Vagenende *et al.* (2013) has proposed a mechanism to account for the concentration dependent effect of arginine HCl on protein aggregation. In brief, the mechanism, which is illustrated in Figure 6.2, proposes that at low arginine concentrations ($<$0.5 M) cooperative interactions form between the guanidinium groups of arginine and carboxylate groups at specific loci on the protein surface. The long residence times of arginine at these loci allow clusters to form at the surface through head to tail bonding. The clusters are considered as extensions of the protein and are believed to be responsible for increasing the protein size by SEC (as determined by a change in elution time). As the concentration of arginine increases the interactions at specific loci become saturated leading to detachment of clusters from the protein surface. Due to their size (Shukla and Trout, 2010), the clusters become preferentially excluded from the vicinity surrounding the protein and are able to 'crowd out' protein-protein interactions.

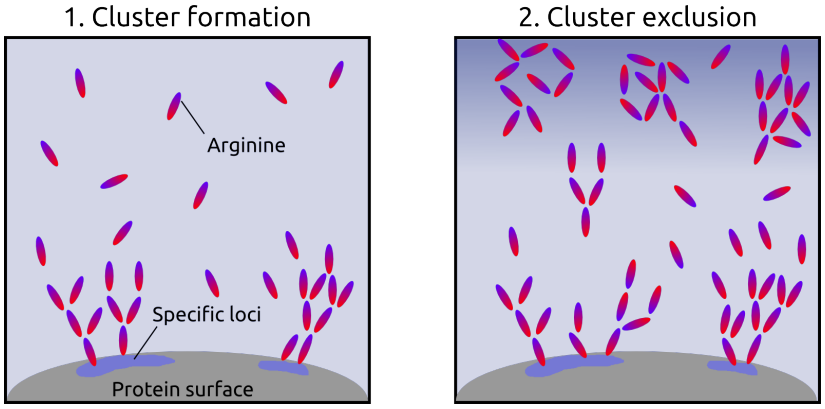


Figure 6.2. A mechanism, recently proposed by Vagenende *et al.* (2013) to account for the concentration dependent effect of arginine on protein aggregation. At low concentrations in solution (<0.5 M) arginine interacts with specific loci on the protein surface and self-associates into clusters (1). As the concentration is increased the specific loci become saturated and the clusters detach from the protein surface (2), which are then able to 'crowd-out' protein-protein interactions.

In the solid state, arginine is thought to stabilise proteins through the formation of an amorphous glass and by replacing water to maintain protein conformation (Izutsu *et al.*, 2005, 2009a, Mattern *et al.*, 1999, Tian *et al.*, 2006). By altering the acidic counterion, several studies have found it possible to alter the physical properties of the arginine glass, including its Tg′ and Tg (Izutsu *et al.*, 2005, 2009a, Yamaki *et al.*, 2012), which may have important consequences for protein stability in the lyophilised state.

6.1.3 Chapter motivation

The motivation for the current chapter was to investigate how annealing duration and arginine counterion selection affects protein stability. Aggregates were characterised by their size and conformational changes. Changes in soluble aggregates were quantified by SEC, insoluble aggregates by MFI and visual inspection and changes in protein secondary structure evaluated using IR and Raman spectroscopy. Furthermore, a multivariate analysis technique was used to identify relationships between formulation and an-

nealing duration variables and protein secondary structure by Raman spectroscopy. Phase separation, which was alluded to as a possible cause of protein denaturation, has also been assessed.

This research provides an important opportunity to advance the understanding of lyophilisation processing and formulation factors on protein stability - a critical quality attribute for a lyophilised biopharmaceutical. As this is the first report in which arginine-dicarboxylic acids have been studied as lyophilisation excipients the findings herein should also make an important contribution to the field of formulation development. It is hoped that by gaining a greater molecular level understanding of the mechanisms of protein stability by arginine-counterion combinations this will encourage the use of novel counterions for fundamental research and applied science applications in the future.

6.2 Materials and methods

6.2.1 Materials

The materials used in this study were formulated and lyophilised as described in Chapter 4 Section 5.2. In brief, this included the following formulations, both with and without 100 mg/mL of BSA:

- Sucrose with 25 mM histidine buffer, pH 6
- Arginine with succinic acid (arginine-C4)
- Arginine with glutaric acid (arginine-C5)
- Arginine with adipic acid (arginine-C6)
- Arginine with pimelic acid (arginine-C7)

Additionally, BSA 100 mg/mL with 25 mM histidine buffer was lyophilised. A total excipient content of 7 % w/v was used for each formulation with a vial fill volume of 1 mL. The formulations were lyophilised using different annealing durations of 0, 2, 4, 8 and 16 hours.

6.2.2 Methods

FTIR spectroscopy was carried out using the method described in Chapter 4 Section 4.2.2.

Stability study

After initial manufacture lyophilised samples were placed in a fridge (2–8 °C) for five months prior to the start of the stability study. Due to the

large number of samples required for this study, only duplicates of the BSA formulation were used for SEC and MFI analysis. In summary, the following times and temperatures were used for this stability study:

- **Time=0 weeks** Refrigerated samples analysed
- **Time=6 weeks** Samples incubated at 40 °C analysed
- **Time=12 weeks** Samples incubated at 40 °C analysed
- **Time=12 weeks** Refrigerated samples analysed

Size exclusion chromatography (SEC)

Lyophilised samples were reconstituted (in duplicate) and then diluted to 10 mg/mL with filtered (0.2 μm) HPLC grade deionised water. No filtering of the samples were carried out prior to analysis. SEC was performed using a TSKgel® G3000 column (30 cm × 7.8 mm, Supelco) which was connected to an HPLC system (Shimadzu Scientific Instruments) consisting of a pump (LC-20AD) and an autosampler (SIL-20A) connected to a diode array detector (SPD-M20A). The mobile phase consisted of 100 mM sodium phosphate buffer (pH 7) with 100 mM sodium chloride, and a sample volume of 25 μL was injected for analysis. The flow rate was 1 mL/min and detection was at 280 nm. The monomer content was calculated as the percentage of monomer peak area to total peak area.

Micro-Flow Imaging (MFI)

Lyophilised samples were reconstituted (in duplicate) with 900 μL of filtered (0.2 μm) HPLC grade deionised water. To reduce the presence of microbubbles, samples were reconstituted approximately 24 hours prior to analysis and placed in a refrigerator. Prior to analysis samples were al-

lowed to equilibrate to room temperature for approximately one hour. A MicroFlow Imaging™ microscope DPA4200 (Brightwell Technologies Inc.) was cleaned by purging the flow cell and inlet/outlet lines with approximately 10 mL of Decon 90 10 % (v/v) followed by approximately 15 mL of HPLC grade deionised water. Using a 2 mL pipette, 0.5 mL of sample was inserted into the inlet valve. The flow cell was purged with 0.1 mL of sample after which 0.35 mL was analysed at a flow rate of 0.22 mL/min. Between each sample, the flow cells and lines were purged with approximately 5 mL of deionised water followed by 1 mL of filtered (0.2 μm) HPLC grade deionised water. The particle counts were used as is (i.e. with no filtering of data) and baseline particle counts were not removed, as per USP guidelines.

Clarity of reconstituted solutions

The presence of visible particles was determined by assessing the clarity of solutions. After reconstitution, samples were left to stand for approximately 1 hour at room temperature. Using a black and white panel with fluorescent light samples were swirled for approximatively 15 seconds and compared to opalescent standards (Appendix Figure A.1). The standards, outlined in reference Ph. Eur. method 2.2.1 (2013) are based on dilutions of formazin with nephelometric turbidity units (NTU) of 0 to 1000.

Raman spectroscopy

Raman spectroscopy was performed using a LabRAM HR (Horiba Jobin Yvon) equipped with a 785 nm NIR laser. Raman signals were diffracted through 600 lines/mm gratings and detected by a Synapse CCD detector which was thermoelectrically cooled to -70 °C. Confocal capabilities were provided by an Olympus BX41 microscope using a 50× long working distance objective. Lyophilised samples were removed from the vial with a

spatula and then cut with a sharp scalpel to reveal an internal cross section of the cake which was used for the study. An acquisition time of 5 seconds/spectra and an average of 2 spectra were used. Single window spectra were taken between wavenumbers of 1050 and 1800 cm^{-1}. Mapping of the internal cross section of cake was carried out by rastering the laser beam at 5 μm intervals across the sample to give 121 spectra in a 50 $\times$ 50 μm x-y dimension.

Three maps were collected for each of the BSA containing cakes (BSA 100 mg/ml with either sucrose or arginine-counterions). After concatenating the data files, processing and analysis was carried out using R version 2.15.2 (R Core Team, 2012). Processing of the data can be seen in Figure 6.3 and firstly includes applying a 5-point median filter to the spectrum to remove cosmic rays. A linear baseline was fitted and removed from each spectrum using the R package 'baseline' (Liland and Mevik, 2012) to remove the impact of fluorescence from the aromatic residues of BSA. The spectra were then scaled and analysed using Principal Component Analysis (PCA) from the R package 'pcaMethods' (Stacklies *et al.*, 2007). To reduce the noise and illustrate spectral features more clearly, a 30-point($\sim$15 cm^{-1}) rolling mean was used to smooth the spectra and loadings in the figures of this chapter and appendix D. Although a slight loss in peak resolution can be observed, it should be stressed that this smoothing function was only used to ease the interpretation of figures and was not used for principal component analysis.

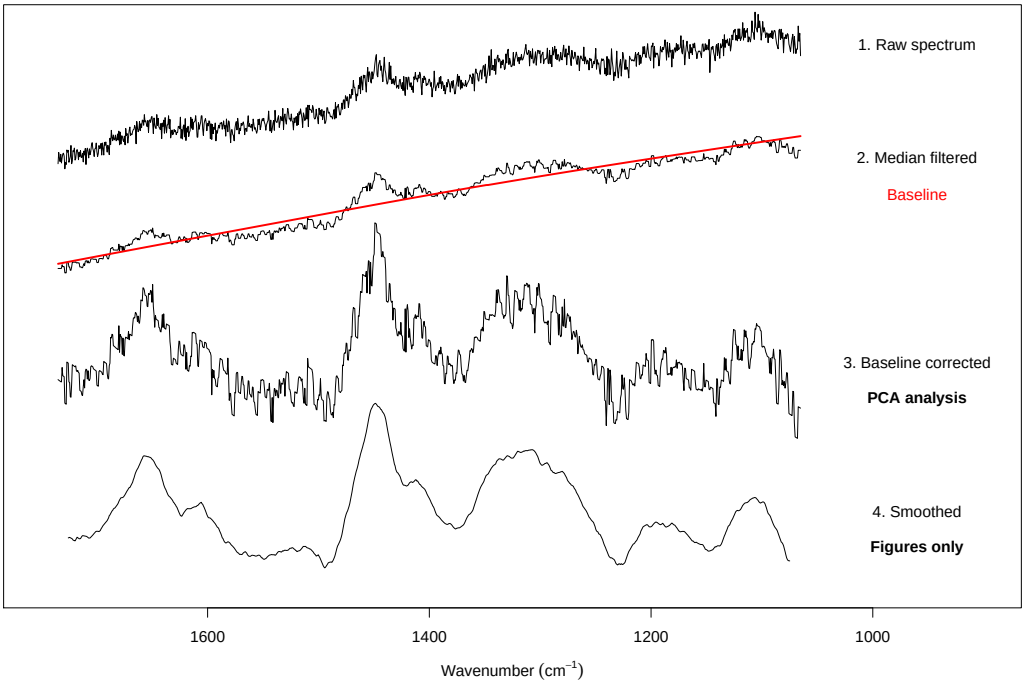


Figure 6.3. The steps involved in processing a single Raman spectrum. PCA analysis was carried out after baseline correction, although a smoothing function has been applied for illustration purposes in the Figures of this chapter.

6.3 Results

6.3.1 Soluble aggregates

The change in monomer content levels of BSA formulations, when stored at 40 °C for three months, was monitored at six week intervals using high performance SEC. An example of the monomer content observed for BSA samples lyophilised without an annealing step can be seen in Figure 6.4.

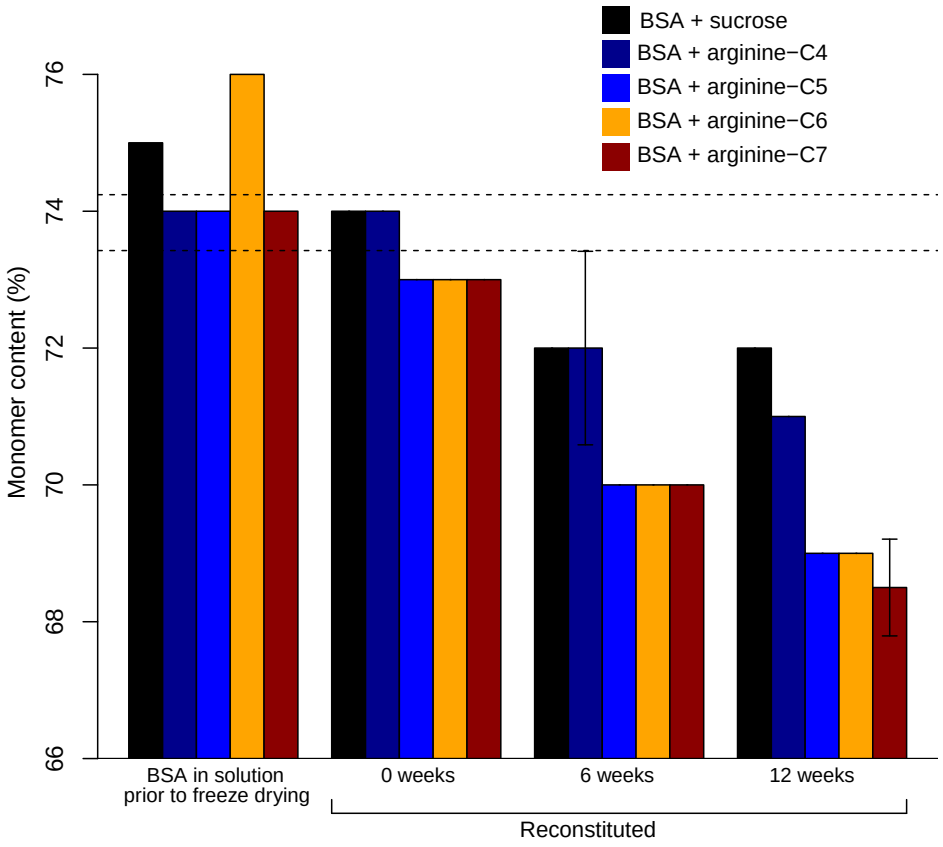


Figure 6.4. The monomer content from SEC of reconstituted BSA solutions (lyophilised without an annealing step) when stored at 40 °C for different time periods. The dashed black lines show the variation in BSA in histidine buffer (in solution prior to lyophilisation) which was used as a comparison at each time point (n=2, mean ± s.d.).

The percentage monomer content of BSA in solution, prior to lyophilisation, appears to correspond well with other studies, in which a 75 % monomer content has been observed at both pH 6 and pH 7.4 in the study by Sarangapani *et al.* (2013). A loss in monomer content was observed over 12 weeks when the lyophilised samples were stored at 40 °C. Storage of samples in a refrigerator were found to have monomer contents of approximately 72–74 % after 12 weeks, and can be found in the Appendix (Figure C.1). No change in elution time was observed for any of the BSA formulations during the storage stability study (Appendix Table C.1). This suggests that there are no arginine clusters associated with the surface of the protein, which have previously been attributed to a change in elution time (of up to a minute for BSA) in the study by Vagenende *et al.* (2013).

To determine whether the soluble aggregation rate of lyophilised formulations followed square root of time kinetics, which was described in greater detail in Chapter 3 Section 3.4.2, the data were fitted to different exponents of time. The exponent (n) giving the highest statistical F-value (which indicates the goodness of the fit) can be seen in the Table 6.1.

Table 6.1. The n (exponent of time) giving the highest F-value of the fit for SEC data, in which the F-value indicates the goodness of fit.

	n with maximum F-Value				
	Annealing duration (hours)				
	0	2	4	8	16
BSA + sucrose	0.1	0.1	0.1	0.1	1.0
BSA + arginine-SA	0.6	0.8	0.7	0.5	0.5
BSA + arginine-GA	0.4	0.5	0.4	0.8	0.5
BSA + arginine-AA	0.4	0.7	0.2	0.7	0.2
BSA + arginine-PA	0.6	0.3	0.7	0.4	0.2

For the arginine formulations, the value of n providing the best fit is generally in the range of 0.4–0.7, which suggests that the data do follow square root of time kinetics. However, a large variation of n can also be

observed in this table, most notably with the sucrose formulation which has values of either 0.1 and 1. It is likely that this is a consequence of two factors, (1) the few data points at each time point ($n = 2$) and (2) the minimal monomer loss observed with this formulation at the times investigated. In order to allow a consistent analysis of the results, the rate of monomer loss was determined by fitting data to $t^{0.5}$ for all formulations. The rate of monomer loss of the lyophilised BSA formulations in this study can be seen in Figure 6.5.

BSA formulated with sucrose was found to have a lower soluble aggregation rate than arginine formulations. No obvious trends were observed with increasing annealing duration. Increasing the length of the dicarboxylic acid does appear to affect the soluble aggregation rate, in which lower soluble aggregation rates were observed in the order of C4 >C6 >C7. The aggregation rate of the C5 formulation appeared more variable than the other dicarboxylic acids.

For the mAb1 samples, which were not included in the storage stability study, no changes in monomer content were observed after lyophilisation with different annealing durations (i.e. no higher order aggregates were detected by SEC).

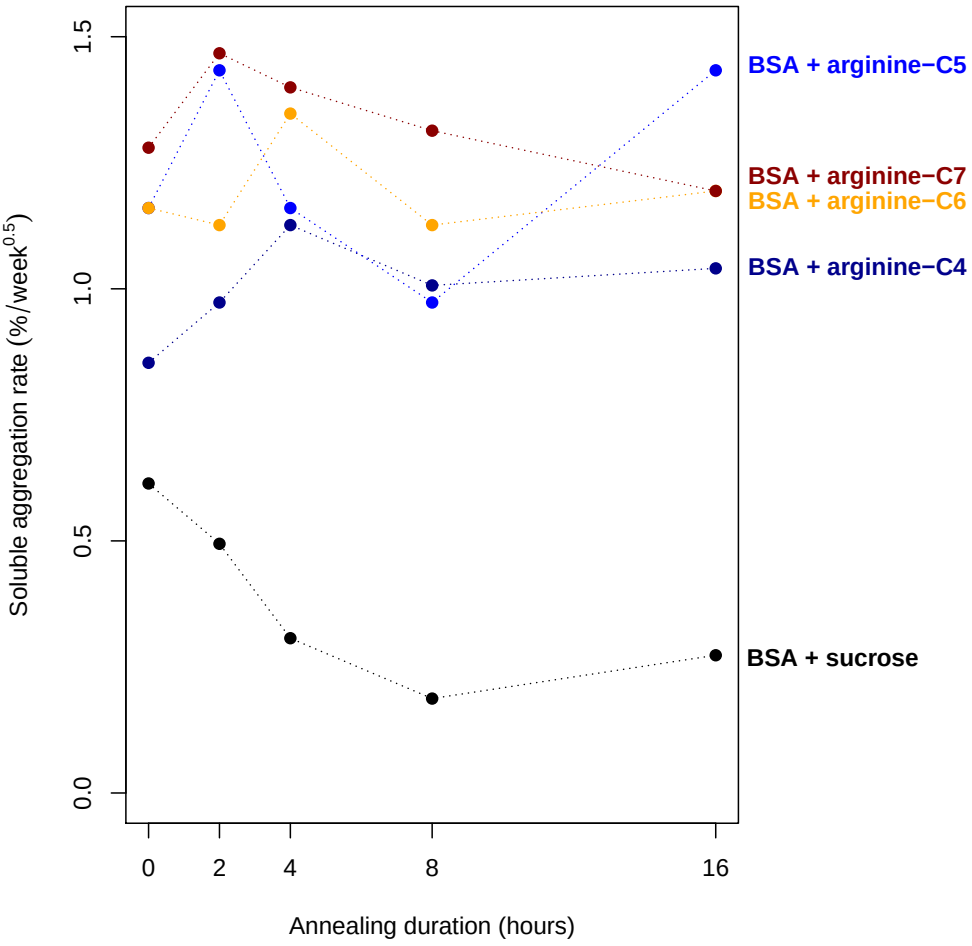


Figure 6.5. The soluble aggregation rate of the lyophilised BSA formulations. The error of the fits (which has not been plotted) were all found to be less than 0.2 and in general gave relative errors of less than 15 % for arginine samples but was much higher for sucrose samples. Please note that the dashed lines are not a lines of best fit and are included only to identify formulations.

6.3.2 Subvisible particles (SVP)

SVP in the size range of 1 to 100 μm were quantified in reconstituted solutions using MFI. Prior to lyophilisation, the solutions of all BSA and mAb1 formulations were found to have less than 1500 and 3000 particles/mL, respectively, in the range of 1–2 μm (Appendix Table C.2). After lyophilisation, BSA cakes were stored at 40 °C and were reconstituted at time points of 0, 6 and 12 weeks. The particle concentrations in the size range of 1–2 μm can be seen in Figure 6.6. After 12 weeks, lyophilised BSA cakes that had been stored in a refrigerator were also reconstituted and were found to have SVP levels comparable to samples at week 0 (Appendix Figure C.2).

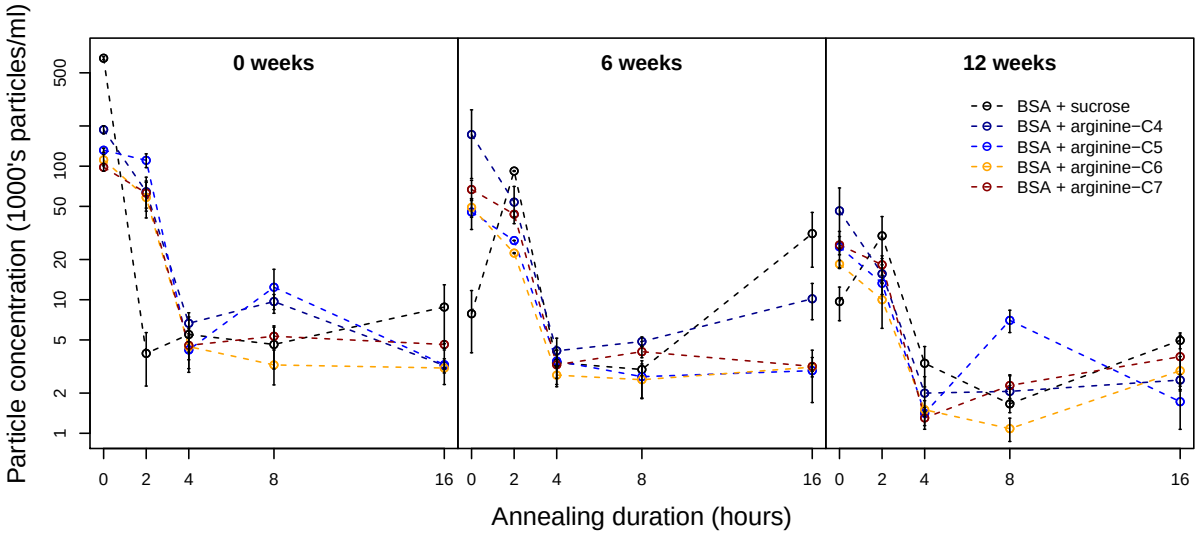


Figure 6.6. The concentration of SVP (between 1–2 μm) for BSA formulations stored at 40 °C over a 12 week period. Please note that the y-axis is a logarithmic scale and the dashed lines are not lines of best fit and are included only to help identify formulation trends (n=2, mean ± s.d.).

Two trends are clearly evident from this dataset. Firstly, increasing the annealing duration decreases the number of SVP in the reconstituted solutions, in which after a four hour annealing duration, no further reduction in SVP levels were observed. The relationship between SVP and annealing duration can also be seen with the mAb1 formulation in Figure 6.7. Secondly, unexpectedly, storage at 40 °C appeared to lead to a reduction in SVP levels.

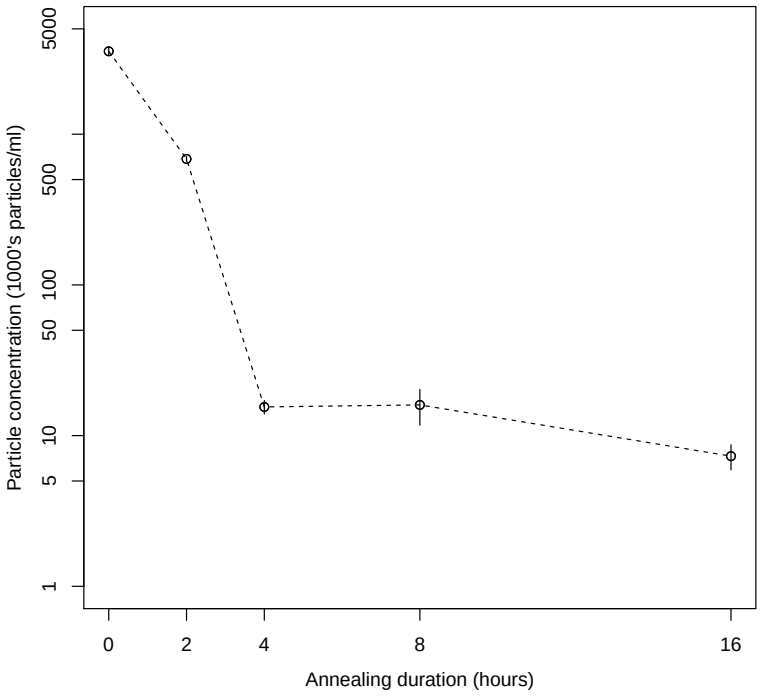


Figure 6.7. The concentration of SVP (between 1–2 μm) for the mAb1 formulation. Please note that the y-axis is a logarithmic scale and the dashed lines are not lines of best fit (n=3, mean ± s.d.).

In other studies, high levels of SVP (>1 μm) have been observed after reconstitution of lyophilised plasmid and siRNA/oligoaminoamide polyplexes (Kasper *et al.*, 2011, 2013a). The formation of these particles were attributed to impurities in excipients and the manufacturing environment. However, in the present work, impurities from excipients are unlikely to be

the cause of high SVP concentrations as the the samples of the different annealing durations were all from the same original solution. As this solution, prior to lyophilisation, had low SVP counts this data has demonstrated that the exclusion of an annealing step, or an annealing step with too short a duration, can lead to high SVP concentrations in the size range of 1–2 μm. To the author's knowledge, this is the first report of a relationship between annealing duration and SVP levels.

However, current USP guidelines only have two requirements regarding particle size limits in the subvisible range. That is, there must be no more than 6000 particles/mL over 10 μm and no more than 600 particles/mL greater than 25 μm (Ph. Eur. method 2.9.19, 2013)[1]. For all the formulations studied, the subvisible particle counts fall well within this range with BSA formulations having less than 500 for >10 μm and less than 60 for >25 μm and mAb1 formulations having less than 2000 >10 μm and up to 100 for >25 μm.

6.3.3 Visible particles

No visible particles were observed in the BSA formulations prior to lyophilisation, nor after reconstitution in this study. The mAb1 formulation was found to be a clear solution prior to lyophilisation. However, after lyophilisation visible particles were observed in the reconstituted mAb1 samples and can be seen in Figure 6.8. For this formulation, lyophilisation with no annealing step was found to be produce an opaque reconstituted solution comparable to formazin standard 6, NTU 120. Samples annealed for two hours were found to be slightly opaque and comparable to formazin standard 3, NTU 18. All other reconstituted samples appeared clear (NTU

[1]This is the requirement for parenterals in which the single unit volume is less than 100 mL (Ph. Eur. method 2.9.19, 2013).

0).



Figure 6.8. The mAb1 formulations showed some visible particles on reconstitution but solutions became clearer in samples prepared with longer annealing times (0 to 16 hour annealing durations are shown in vials from left to right).

6.3.4 Protein conformational changes

FTIR spectroscopy

The arginine-dicarboxylic acid formulations were found to absorb within the amide I region of the IR spectrum (Appendix Figure C.3, but not the Raman spectrum in Figure C.4). Therefore, only sucrose formulations were investigated using FTIR spectroscopy. The second derivative spectra of the BSA formulation, in lyophilised and reconstituted states, can be seen in Figure 6.9. A loss of α-helical content and an increase in turn structures were observed for all lyophilised samples compared to the protein in solution prior to lyophilisation, which is similar to the observations of lyophilised BSA 200 mg/mL in Chapter 4 Section 4.3.4. No trends are apparent between annealing duration and secondary structure changes in the lyophilised state. However, on reconstitution, samples lyophilised with increasing annealing duration showed fewer changes in protein secondary structure compared to the protein solution prior to lyophilisation.

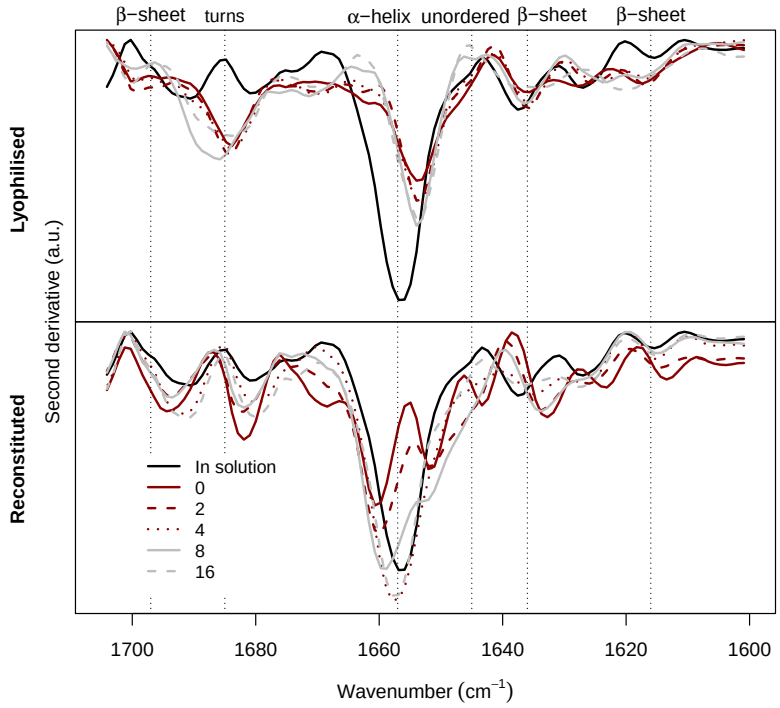


Figure 6.9. The second derivative FTIR spectra of the BSA sucrose formulation when lyophilised for different annealing durations.

The second derivative spectra for the mAb1 formulation can be seen in Figure 6.10. After lyophilisation, the β-sheet content shifts to a lower wavenumber. It is possible that this is due to the formation of inter- rather than intra-molecular β-sheets, as summarised in Chapter 3 Table 3.1. The IR spectra of the mAb1 solution used in this chapter (freeze thawed prior to lyophilisation) and Chapter 4 (not freeze thawed) are also compared. A difference in intramolecular β-sheet content was observed which suggests that freeze thawing may result in a change in the conformation of the protein. It is possible that this was also the cause of visible particles after reconstitution, which were observed in this chapter but not in the Chapter 4. On reconstitution, an increase in β-sheet and turn structures were observed at approximately 1690 and 1660 cm^{-1}, although no apparent trends were observed between annealing duration and secondary structure changes.

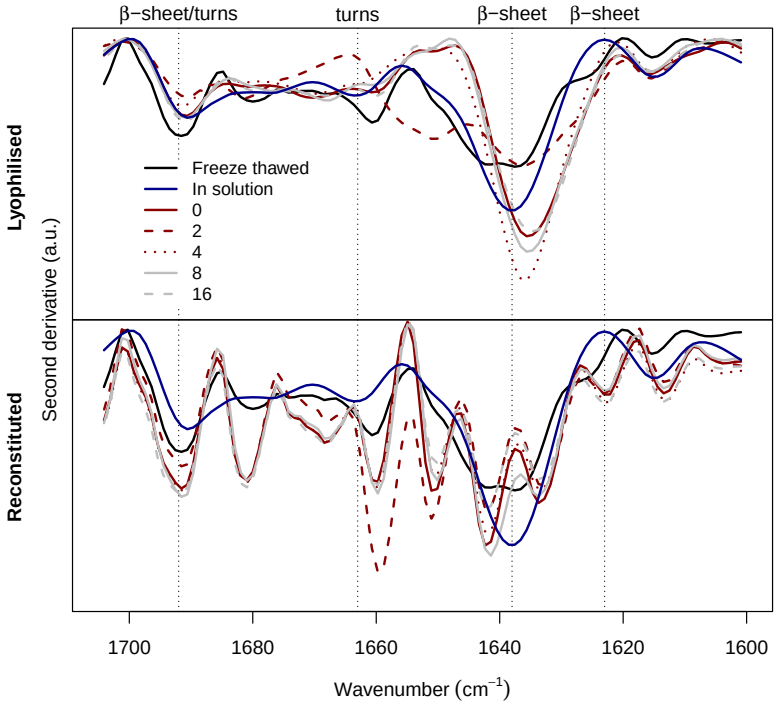


Figure 6.10. The second derivative FTIR spectra of the amide I region of the mAb1 formulation (in 7 % sucrose) lyophilised for different annealing durations.

Raman spectroscopy

Raman spectroscopy was used in this chapter to investigate changes in BSA secondary structure after lyophilisation of the arginine-dicarboxylic acid formulations, which are also compared to the sucrose formulation. Principal component analysis (PCA), which was described in greater detail in Chapter 3 Section 3.4.1, was employed to provide a multivariate analysis approach for determining relationships between variables, as recommended by QbD principals (FDA, 2004).

A large number of Raman spectra (>1800) were collected in this investigation. In order to determine which spectral features are the most important (i.e. those that provide the greatest variation within the dataset), PCA was

used to reduce the data into a smaller amount of observations, known as principal components. In total, four PCs were used for data analysis and account for 56, 16, 7 and 5 % of the variability within the dataset, respectively. The PC loadings can be seen in Figure 6.11 and, in order to provide a meaningful analysis, are compared to reference spectra of excipients and BSA, lyophilised separately.

Each spectrum within the original dataset is assigned a score which provides a measure of distance indicating how the spectrum relates to each PC. The distribution of PC scores for the BSA formulations investigated can be seen in Figure 6.12.

In the PC 1 loading, peaks at approximately 1410 and 1440 cm^{-1} relate to the presence of arginine-dicarboxylic acid. A negative peak at approximately 1460 cm^{-1} can also be observed and appears to be related to sucrose. Overall, PC 1 positively correlates to the presence of arginine-dicarboxylic acid and negatively correlates to the presence of sucrose. This is also demonstrated in the distribution of PC scores for the sucrose and arginine based formulations in Figure 6.12.

In the PC 2, 3 and 4 loadings, a peak is present between 1600 and 1700 cm^{-1} and is indicative of the amide I band of the protein. A more detailed analysis of this region can be seen in Figure 6.13. The PC 2 loading appears to have a peak at 1460 cm^{-1}, which suggests the presence of sucrose, and a narrow peak at approximately 1656 cm^{-1} in the amide I region suggesting the presence of α-helical structure. Therefore, the PC 2 loading positively correlates to spectra rich in sucrose and α-helical BSA.

Perhaps the most interesting PC loading relates to PC 3. A shift in peak positions, centred at approximately 1625 cm^{-1}, identifies the dicarboxylic

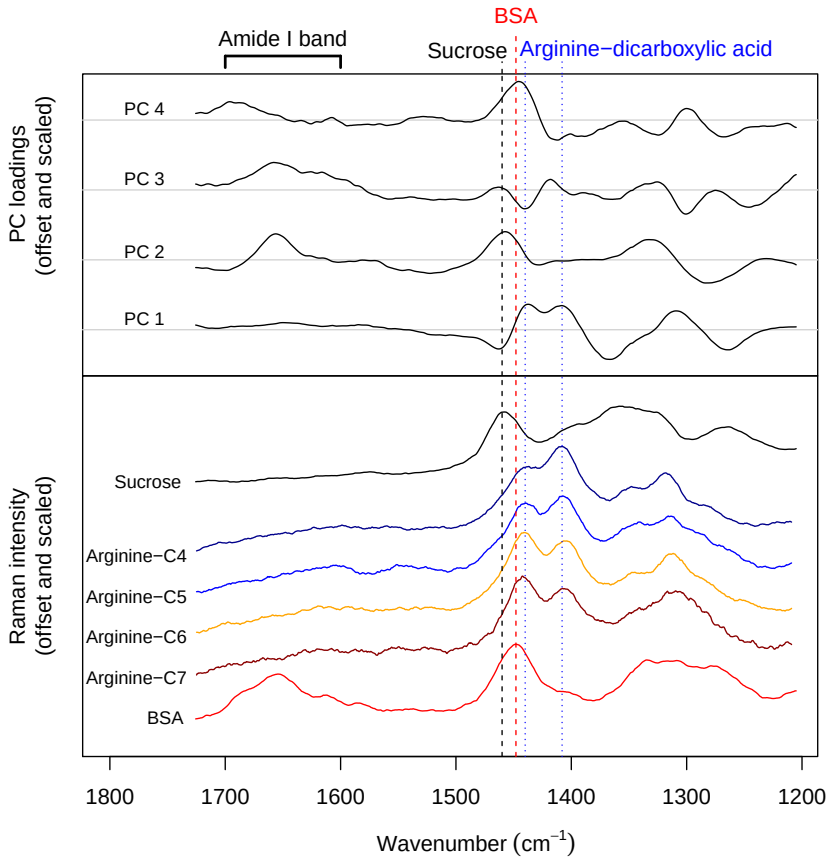


Figure 6.11. The principal component loadings and individual spectra of the lyophilised excipient only formulations. For comparison purposes, dashed vertical lines illustrate peaks of interest with sucrose (black), BSA (red) and arginine-counterion combinations (blue). No Raman spectra of amorphous arginine or dicarboxylic acids were collected separately due to issues with low solubility and crystallisation on lyophilisation.

acid in the formulation. Two peaks occur at 1410 and 1440 cm^{-1} in the reference spectra of arginine-dicarboxylic acid formulations. As the chain length of the dicarboxylic acid increases, a decrease in the ratio of the 1410 to 1440 cm^{-1} peak can be observed. The change in ratio can be discerned in the PC 3 loading which positively correlates to the arginine-C4 formulation and becomes negatively correlated as the alkyl chain length increases. This is also demonstrated in the distribution of PC scores for this loading (Figure 6.12). The PC 3 loading also has a broad peak at approximately 1656 cm^{-1} which is assigned to the presence of α-helical BSA but also some β-sheet and turn structures. Overall, the PC 3 loading positively correlates

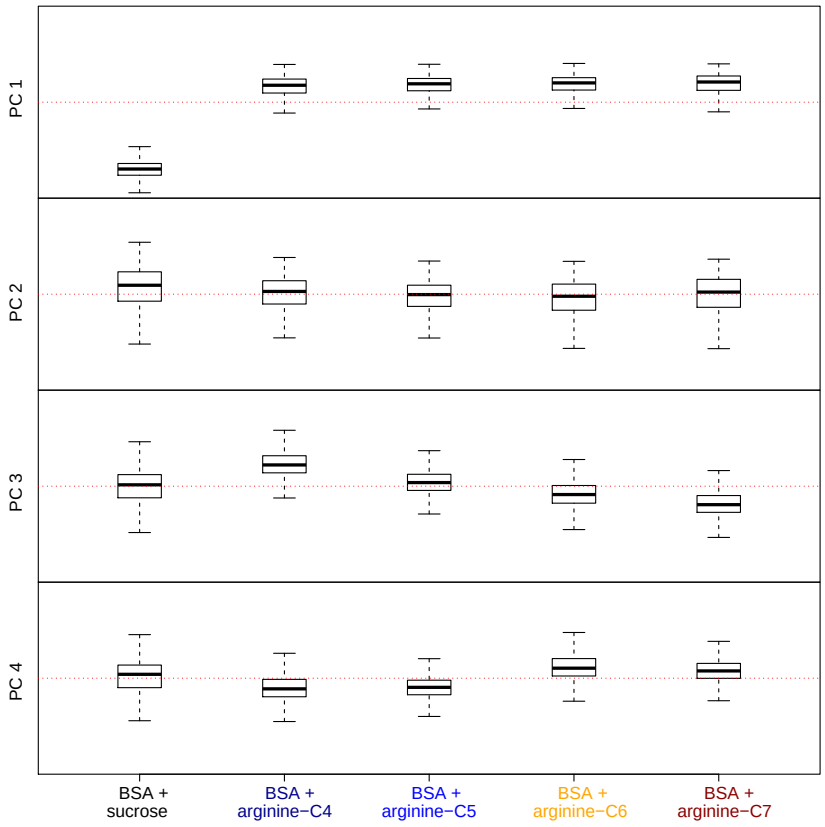


Figure 6.12. The distribution of PC scores by formulation. A score of 0 is shown by the horizontal red lines for each principal component.

to the presence of shorter alkyl chain dicarboxylic acids and α-helical BSA and negatively to the presence of longer alkyl chain dicarboxylic acids.

The PC 4 loading has a peak at approximately 1450 cm^{-1} and appears to be due to the presence of BSA. An increase in turn/β-sheet structures can also be observed in this loading and suggests that PC 4 positively correlates to spectra of BSA with poor conservation of secondary structure.

Two conclusions have been made based on the findings from the PC analysis of Raman spectra. Firstly, the formulation of BSA with sucrose led to a better retention of α-helical structure in the lyophilised state than with the arginine-dicarboxylic acids. Secondly, arginine formulations with shorter alkyl chain dicarboxylic acids led to a better retention of α-helical structure than the longer alkyl chain dicarboxylic acids.

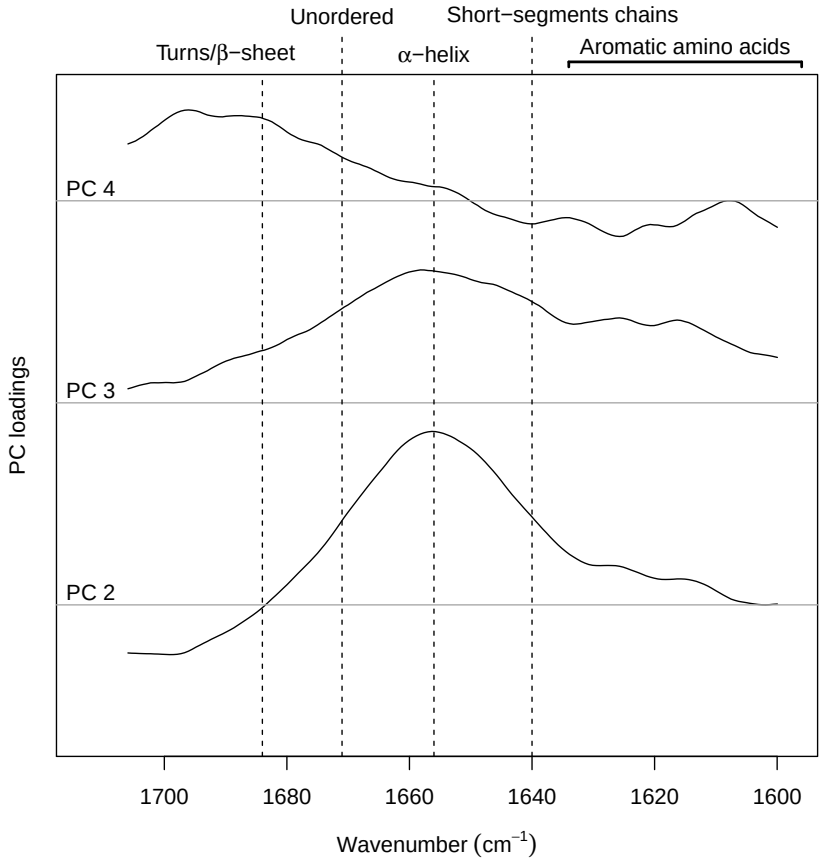


Figure 6.13. The amide I region of the PC loadings (PC 2 to 4). Secondary structure components have been assigned to particular frequencies and have been illustrated with dashed lines.

6.3.5 Phase separation using Raman spectroscopy

Long annealing durations may favour the separation of protein from its intended stabiliser (Heller *et al.*, 1997, Izutsu *et al.*, 2013). Areas in the cake which are low in stabiliser may consequently not protect the protein from drying stresses during lyophilisation. In this study, it was thought that as the PC 4 loading from the Raman spectral analysis correlated to BSA rich in β-sheet content, annealing-induced phase separation may cause more positive PC 4 scores with longer annealing durations. The distribution of PC 4 scores for each BSA formulation, and annealing duration, can be seen in Figure 6.14.

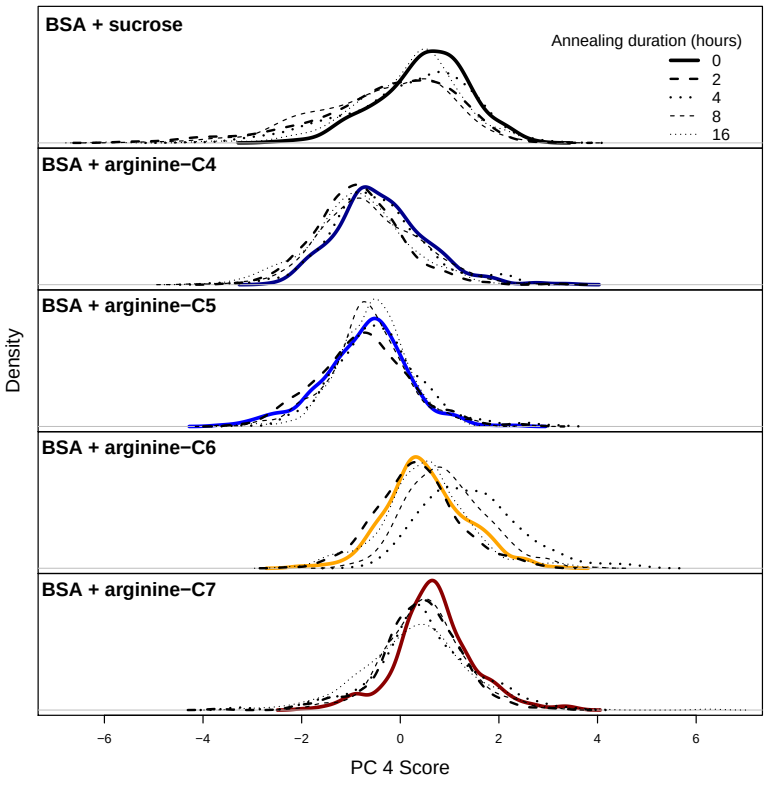


Figure 6.14. The distribution of PC 4 in the lyophilised cakes of the BSA formulations. A positive PC 4 score relates to BSA rich in β-sheets.

In general, increasing the annealing duration did not lead to more positive PC 4 scores for the arginine formulations. However, the addition of an

annealing step to the BSA sucrose formulation was found to produce more negative PC 4 scores. To investigate the cause of this further, a map containing spectra with some of the most negative PC 4 scores, was analysed and can be seen in Figure 6.15.

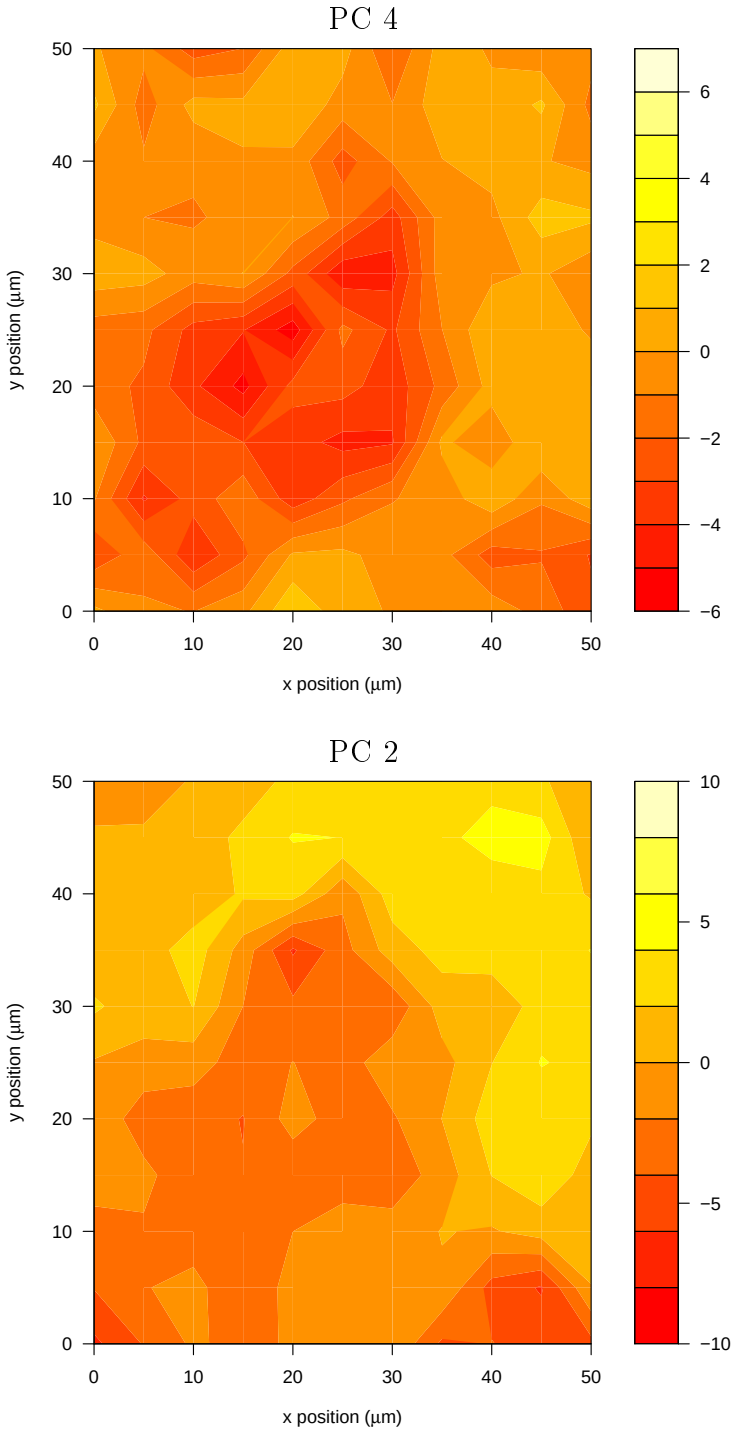


Figure 6.15. A map of an internal cross section of a BSA sucrose formulation, lyophilised using a two hour annealing duration. Although the same map is shown, the spectra are assigned colours to form heat maps showing the PC 4 scores and the PC 2 scores. Spectra were collected in 5 μm intervals across a 50 $\times$ 50 μm cross section.

The map of the BSA sucrose cake (annealed for two hours) shows a distinct region rich in negative PC 4 scores (approximately 25 μm^2) which may suggest the presence of separate phases. It is possible that PC 4 negatively correlates to areas of BSA which have a low β-sheet content, possibly due to greater protection afforded by the presence of a sucrose rich phase. An increase in α-helix content may therefore also occur in these spectra. However, the PC 2 scores, which are believed to correlate positively to α-helical BSA, are shown in Figure 6.15 and also appear negative.

To better understand whether phase separation occurs in this cross-section of sample, two spectra have been shown in Figure 6.16 from both inside and outside of the negative PC 4 region. The spectrum with both positive PC 2 and PC 4 scores is from an x-y co-ordinate of 45, 45 μm in the map in Figure 6.15. In this spectrum, the amide I band appears rich in α-helix content and the ring vibration modes can be clearly distinguished near 1600 cm^{-1}. A peak at approximately 1455 cm^{-1} can be also be observed and is attributed to a homogeneous mixture of both BSA and sucrose.

The spectrum with both negative PC 2 and 4 scores is from an x-y co-ordinate of 25, 30 μm in the map in Figure 6.15. A broad band near 1656 cm^{-1} is observed, with no clear α-helical structure or ring vibrational modes. A band centred at 1455 cm^{-1} can also be observed, however, unlike the spectrum with positive PC 2 and 4 scores, the peak maxima is broader at 1450 and 1460 cm^{-1}, suggesting an heterogeneous combination of BSA and sucrose components, respectively. Interestingly, a peak at 1410 cm^{-1} can also be observed in this spectrum (dashed green) and is absent in both the amorphous BSA and amorphous sucrose spectra. It is difficult to assign this peak to possible structural features although it may indicate that the sucrose component is beginning to crystallise. The detrimental impact on

the secondary structure of BSA in this region may therefore be due to the separation of sucrose or the presence of an impurity in the cake.

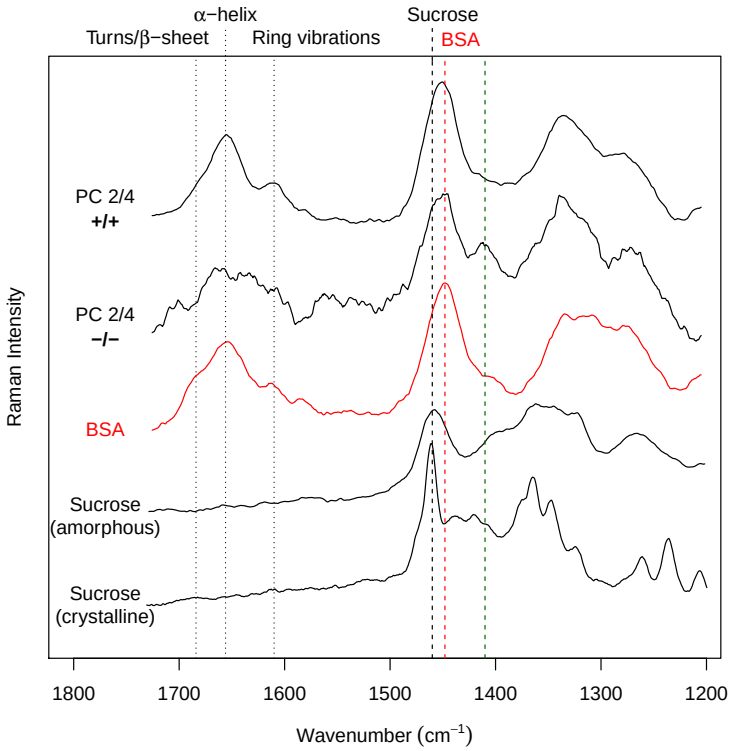


Figure 6.16. The Raman spectra a lyophilised BSA sucrose cake in which PC 2 and PC 4 are either positive, or both are negative. Three reference spectra of lyophlised BSA, lyophilised sucrose and crystalline sucrose (as received) have also been shown. For comparison purposes, dashed lines are used to illustrate peaks of interest.

6.4 Discussion

6.4.1 Proposed mechanism for arginine-dicarboxylic acid stabilising effects

Conformational changes in protein secondary structure were investigated using Raman spectroscopy. In order to evaluate the effect of formulation and processing variables, a multivariate analysis approach (PCA) was used to explore whether relationships exist between variables and responses. The sucrose formulation was found to correlate well with α-helical content, which would be expected in the native state. A relationship was also found between increased α-helical content and shorter dicarboxylic acid chain lengths.

The monomer content was monitored using SEC for lyophilised BSA samples stored at 40 °C for three months. An increase in elution time was not observed for the arginine formulations, suggesting that no clusters of arginine are associated with the surface of the protein (Vagenende *et al.*, 2013). The soluble aggregation rate, which was fitted based on square root of time kinetics, found that the BSA sucrose formulation provided the best protection against soluble aggregation during storage. A trend was also observed between increasing arginine-dicarboxylic acid chain length and soluble aggregation. However, it would be salient to complete a storage stability study, with either more storage temperatures or over a longer annealing duration, and with a greater sample number in order to verify square root of time kinetics.

Overall, this work suggests a relationship between increasing dicarboxylic acid chain length, conformational changes (a decreasing α-helical content)

and increasing soluble aggregation rate. Based on these findings, the following mechanism has been proposed to consolidate these effects in both the solid and solution state.

Both arginine and dicarboxylic acids are known to increase the surface tension of water, with shorter alkyl chains causing a greater increase in surface tension than longer alkyl chain dicarboxylic acids (Arakawa *et al.*, 2007, Kita *et al.*, 1994, Shulman *et al.*, 1996). Through a preferential exclusion mechanism (which was described in greater detail in Chapter 1 Section 1.2), the longer alkyl chain dicarboxylic acids may result in an environment which allows more unfolding of the protein than the shorter alkyl chain dicarboxylic acids.

It has been suggested in other research that arginine may form clusters in solution (Das *et al.*, 2007, Shukla and Trout, 2010), which can lead to an increase in elution time by SEC (Vagenende *et al.*, 2013). However, this was not observed in this study which suggests that arginine did not associate with the protein surface. As the interaction between guanidinium and carboxylate groups is thought to be more favourable than with the interaction between guanidinium and water (Shukla and Trout, 2010), the formation of an extended network of arginine and dicarboxylic acids may exist in solution and prevent protein-protein interactions. The interaction between shorter alkyl chain dicarboxylic acids and arginine is also likely to be stronger than with longer chain dicarboxylic acids due to stronger ionic interactions, which makes the process more enthalpically favourable, and the shorter alkyl chain lengths which reduces the unfavourable loss of entropy that occurs during the interaction.

Considering the relationship between increasing dicarboxylic acid chain

length and increased BET SSA, as discussed in Chapter 5 Section 5.4.1, it is possible that this could account for the protein stability findings. Where a larger ice interface could lead to greater protein denaturation (Costantino *et al.*, 2002, Devineni *et al.*, 2014, Hsu *et al.*, 1995, Webb *et al.*, 2003, 2002b, Xu *et al.*, 2014) and molecular mobility at the surface (Wu and Yu, 2006, Zhu *et al.*, 2008, 2010). Further research should aim to elucidate whether the solution or solid state behaviour of arginine-dicarboxylic acids is more important for protein stability. Improving the accuracy of BET SSA measurements may offer further insight into this, as described in Chapter 4 Section 5.4.1. Modification of the cooling profile, such as through the addition of a CIN technique, may also offer a method of assessing the importance of surface area on protein stability in these formulations.

The sucrose formulation was found to provide better conformational stability and lower aggregation rates than the arginine-dicarboxylic acid formulations, despite the pH being closer to the pI of the protein, which could lead to more protein-protein interactions through reduced intermolecular repulsive electrostatic interactions in solution (Kamerzell *et al.*, 2011). It has been proposed elsewhere that a specific molar ratio of stabiliser may be required to provide long term storage stability (Cleland *et al.*, 2001). However, as no optimisation studies were carried out in this thesis on the concentration of arginine-dicarboxylic acid required in the formulation, it is possible that a higher molar ratio would have been required in order to provide comparable protein stability to the sucrose formulation.

Numerous other studies have documented that sugars are able to prevent unfolding of proteins during drying by replacing water (Carpenter and Crowe, 1989, Costantino *et al.*, 1998, Prestrelski *et al.*, 1993). However, the mechanism proposed here for the protein stabilising effects of arginine-

dicarboxylic acids concludes that the excipients are excluded from the protein surface, possibly through the formation of an extended excipient network. Consequently, whereas sucrose acts as lyoprotectant, and is able to stabilise the protein from both freezing and drying stresses, the arginine-dicarboxylic acids may only act as cryoprotectants and stabilise during only the freezing stage of lyophilisation.

6.4.2 The impact of annealing duration on protein stability

IR and Raman spectroscopy were used to assess secondary structure changes in protein conformation. As the arginine-dicarboxylic acid combinations absorbed in the amide I region in the IR spectrum, only the BSA and mAb1 sucrose formulations were analysed by IR spectroscopy. On reconstitution, the secondary structure of BSA was found to be similar to the pre-lyophilised solution state with longer annealing durations. No trends were apparent for the mAb1 formulation between increasing annealing duration and changes in the protein secondary structure.

No relationship was apparent between between increasing annealing duration and soluble aggregation rates. However, SVP concentrations were found to be affected, in which longer annealing durations (and storage at 40 °C) led to a decrease in SVP levels. It is not unusual that the soluble aggregation rates and SVP concentrations do not correspond to each other and has been reported previously in other studies (Barnard *et al.*, 2011, Nayak *et al.*, 2011). This is largely attributed to filtering out of larger aggregates (typically >0.1 μm) in the SEC column.

Recently, it has been proposed that post lyophilisation annealing (in

which the lyophilised sample is heated to below its Tg and held for a fixed duration) may stabilise proteins by allowing the amorphous glass to relax towards its equilibrium (Abdul-Fattah *et al.*, 2007a). This can improve protein stability by reducing molecular mobility and free volume within the glass and by alleviating residual stress (Wang and Pikal, 2010, Webb *et al.*, 2003). It has been observed that increasing the post lyophilisation annealing duration can reduce the soluble aggregation rates of an IgG_1 fusion protein by increasing global relaxation times Wang *et al.* (2010). As elevated storage temperatures (e.g. 40 °C) are, effectively, the same as post lyophilisation annealing, it is likely that the reduction in SVP levels observed in this chapter are due to the relaxation of the amorphous glass causing an increase in global relaxation time.

Changes in local mobility (β-relaxations) have been found to be important to the storage stability of lyophilised proteins when different formulation excipients are used (Davis *et al.*, 2013, Yoshioka *et al.*, 2007). Consequently, characterising β-relaxations, which can be measured by neutron scattering (Cicerone and Douglas, 2012) or $^{1}3C$ or ^{1}H solid state NMR (Park *et al.*, 2013, Yoshioka *et al.*, 2007), may provide greater mechanistic detail on the behaviour of arginine-dicarboxylic acid formulations.

6.4.3 Phase separation in lyophilised cakes

It is widely accepted that annealing can cause amorphous phase separation (Liu, 2006) and has been observed using Raman confocal microscopy in a number of studies (Forney-Stevens *et al.*, 2014, Padilla and Pikal, 2011, Padilla *et al.*, 2011). In Chapter 4 Section 4.4, it was suggested that the changes in protein secondary structure after annealing could be due to phase separation. As long annealing durations can allow separation of protein from

its intended stabiliser (Heller *et al.*, 1997, Izutsu *et al.*, 2013), this chapter investigated this further using Raman spectroscopy.

PCA of Raman spectra found that PC 4 appeared to relate to BSA high in β-sheet. A high β-sheet content may be expected in phase separated samples where the protein was exposed to drying stresses. No obvious trends were apparent between positive PC 4 scores and annealing duration which suggests that increasing the annealing duration did not lead to a detectable increase in phase separation.

However, negative PC 4 scores were observed with the BSA sucrose formulation. On further analysis, an area was identified which appeared to be rich in sucrose and may have crystallised *in-situ*. The size of this area appears consistent with other phase separation studies which suggests the domain size of phase separation in lyophilised protein systems is in the micrometre range (Forney-Stevens *et al.*, 2014, Padilla and Pikal, 2011). Although the sample was confirmed as amorphous by XRPD, it has been reported that the mass of partially crystalline material would have to be greater than 10 % to be detected. (Varlashkin, 2011). Consequently, it was not possible to confirm whether sucrose crystallised in this study nor whether it was the result of lyophilisation, storage, or energy provided by the laser during the experiment.

6.5 Conclusion

New experimental data has been collected in this chapter regarding the effects of protein stability by arginine-dicarboxylic acids and lyophilisation with different annealing durations.

Multivariate analysis of Raman spectroscopy data identified a reduction in BSA α-helical content with increasing dicarboxylic acid alkyl chain length. An increase in soluble aggregation rates were also observed with longer alkyl chain dicarboxylic acids. To account for these effects, this chapter proposed that the formation of an extended network of arginine-dicarboxylic acids, which is stronger with shorter rather than longer alkyl chains, may act as barrier and prevent protein-protein interactions. An increase in surface tension with the shorter dicarboxylic acids is also thought to reduce protein unfolding in solution and may result in lower SSA of the lyophilised solid.

No clear relationships were found between annealing duration and changes in protein secondary structure or soluble aggregation rates. However, a strong correlation was found with SVP (1–2 μm) levels. Both mAb1 and BSA formulations lyophilised without an annealing step were found to have high SVP concentrations with moderate levels at 2 hours and low levels at longer annealing durations. As SVP levels were also reduced during the storage at 40 °C, it is likely that annealing affects the structural (α) relaxation of the amorphous glass leading to a reduction in molecular mobility and residual stress in the glass.

The arginine formulations were found to have a Tg approximately 20 °C higher than the sucrose formulations. However, the sucrose formulations

appeared to provide better conformational stability and lower soluble aggregation rates than the arginine formulations. As arginine-dicarboxylic acids were proposed to be excluded from the protein surface, it is likely that they act as cryoprotectants and do not replace hydrogen bonding during drying.

7 | Final Conclusion

The aim of this doctoral thesis was to provide a better understanding of how the lyophilisation process and formulation factors affect the quality attributes of lyophilised biopharmaceuticals. To achieve this, three quality attributes were characterised and the following insights have been generated.

Both the lyophilisation cooling profile and protein concentration were found to affect the reconstitution time of lyophilised cakes. In Chapter 4, the impact of different cooling profiles was negligible on the reconstitution time of BSA 200 mg/mL. However, the reconstitution time of the lower concentration BSA 50 mg/mL and mAb1 formulations were significantly increased after quench cooling, despite these samples having the largest surface area. The addition of an annealing step was not found to significantly alter the reconstitution time of formulations described in either Chapter 4 or Chapter 5 of this thesis. To account for these findings, we propose that small or closed pores may increase the reconstitution time of low protein concentration formulations by decreasing the flow rate of water into the cake. At high concentrations, the reconstitution process is likely to be dominated by factors that decrease the dissolution rate of the cake, such as through the increase in viscosity that is associated with macromolecular crowding effects at high concentrations.

Bimodal and trimodal pore size distributions were observed after annealing in the lyophilised cake structure of sucrose formulations in Chapters 4 and 5, respectively. Only one pore size distribution was observed with the arginine-dicarboxylic acid formulations after annealing (Chapter 5), which were found to have a lower total pore volume than the sucrose formulation with the exception of the 2 hour annealing duration. As similar porosity was observed between the 2 and 4 hour annealing durations of arginine-C4 cakes by micro-CT and no correlation with BET SSA was apparent, it was concluded that small pore throats were present in lyophilised arginine cakes, with the exception of the two hour annealing duration. Based on these findings, the following mechanism of ice crystal growth during annealing was proposed. Initially, devitrification allows amorphous water to crystallise, leading to thickening of dendrites. Due to recrystallisation, the dendrite branches break off at their points of attachment. It is suggested here that this loss of dendrite connectivity may be the cause of the long primary drying times and variable residual moisture contents observed with samples from the 8 and 16 hour annealing duration. If the molecular mobility in the glass permits it, recrystallisation events such as Ostwald ripening continue during annealing. The formation of discrete pore size distributions observed in this study are proposed to be caused by nucleation-limited Ostwald ripening. After recrystallisation of the smaller distribution, growth is likely to proceed through diffusion-limited Ostwald ripening and accretion.

Although the Tg of lyophilised arginine-dicarboxylic acid formulations were observed to be approximately 20 °C higher than the sucrose formulation, this did not directly correlate with the storage stability behaviour of BSA, which was assessed in Chapter 6. Here, the sucrose formulation

showed low soluble aggregation rates and PCA of Raman spectra showed a correlation between sucrose and high α-helical content.

Increasing the dicarboxylic acid chain length was found to increase the soluble aggregation rates of BSA and, using PCA of Raman spectra, correlated with decreasing α-helical content. It was proposed that the mechanism of protein stabilisation by arginine dicarboxylic acid salts is a preferential exclusion mechanism (which was described in greater detail in Chapter 1 Section 1.2.3), whereby the shorter dicarboxylic acids lead to an increase in the surface tension of water. Furthermore, it was suggested that arginine and dicarboxylic acids may also form an extended network of excipients in solution which are able to act as a barrier between protein-protein interactions. The BET SSA of arginine formulations (Chapter 5), were also found to be significantly larger with C6 and C7 compared to the C4 dicarboxylic acid. This could also account for the reduced protein stability observed with increasing dicarboxylic acid chain length, where the protein is likely to be exposed to a greater ice interface.

No relationships were identified between increasing annealing duration and soluble aggregation rates. However, significantly lower SVP concentrations were observed with increasing annealing duration. As a reduction in SVP levels were also observed after storage at 40 °C it is suspected that this is due to structural relaxation of the glass leading to reduced molecular mobility and residual stress.

7.1 Future outlook

This thesis has presented new insights into how the lyophilisation process and formulation parameters can affect quality attributes. The scope of future studies based on this work appears both broad and wide ranging.

With regards to reconstitution time, further consideration should be given to the power-law relationships and a possible "cut-off" in pore size below which the increase in reconstitution time becomes impractical to lyophilised formulations. Identification of such a pore size could itself be classed as a quality attribute and the lyophilisation process could be designed to achieve it.

This work has also highlighted that the addition of an annealing step may alter the lyophilised cake structure through a more complex process than previously understood within the lyophilisation literature. It has been proposed here that Ostwald ripening may be a nucleation-limited as well as a diffusion-limited process. The practical implications of this, and the formation of discrete pore sizes, is not completely understood. It seems likely that this may affect vapour transit times and, conversely, reconstitution times. To provide a better mechanistic insight as to why nucleation-limited rather than diffusion-limited growth occurs, formulations with different excipients should be characterised.

The arginine-dicarboxylic acid formulations were found to have a number of properties in common with the sucrose formulation, including similar collapse temperatures and the formation of elegant cakes with comparable residual moisture contents. It was proposed here that these salts are likely to affect protein stability only through vitrification and preferential

exclusion mechanisms, which would classify them as cryo- rather than lyo-protectants. However, this should certainly not discount them as excipients in future studies, especially as the Tg of lyophilised BSA was found to be higher with arginine-dicarboxylic acids formulations than the sucrose formulation. Optimisation of the formulations would appear to be the next reasonable step and should include simple investigations, such as determining the effect of concentration on protein stability and evaluating their potential as cryoprotectants though freeze thaw studies.

Finally, this work has suggested that there is an optimal annealing duration, beyond which there is an increase in primary drying time and batch heterogeneity. In order to avoid these complications, the addition of a CIN technique, rather than the addition of an annealing step could be used. Further investigations comparing annealing and CIN techniques are recommended and should focus on protein aggregation and, in particular, SVP levels.

Appendices

A

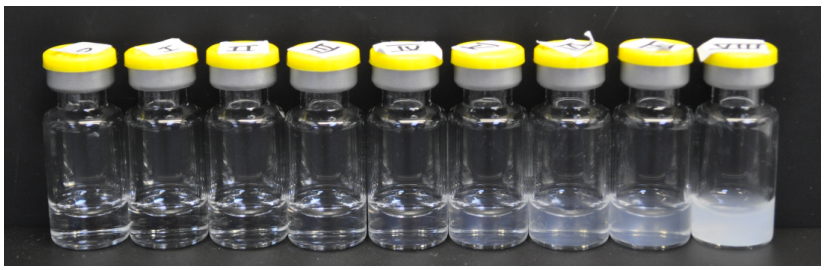


Figure A.1. Formazin standards described in reference (Ph. Eur. method 2.2.1, 2013), from left to right the vials increase in opacity from NTU 0 (a water blank) to 1000.

Table A.1. The temperature profile for determining the collapse temperature (Tc) of formulations by freeze drying microscopy.

Rate (°C/min)	Temperature (°C)	Hold time (minutes)
10	-40	2
10	-10	2
10	-40	2
10	-25	2
1	-24	2
1	-23	2
1	-22	2
1	-21	2
1	-20	2
1	-19	1
1	-18	1
1	-17	1
1	*continued*	1

Table A.2. The pressure range used for mercury intrusion porosimetry and the equivalent pore diameters.

Pressure (psia)	Pore diameter (μm)
1.0	180.0
2.0	90.0
3.0	60.0
4.0	45.5
5.5	33.0
6.0	30.0
7.5	24.0
8.5	21.0
9.5	19.0
10.5	17.0
13.0	13.8
14.5	12.4
16.0	11.3
20.0	9.0
25.0	7.2
30.0	6.0
40.0	4.5
50.0	3.6
60.0	3.0
75.0	2.4
90.0	2.0
115.0	1.6
140.0	1.3
175.0	1.0
220.0	0.8
270.0	0.7
330.0	0.5
420.0	0.4
520.0	0.3
640.0	0.25
800.0	0.23
990.0	0.18
1200.0	0.15
2350.0	0.08
2900.0	0.06
3600.0	0.05

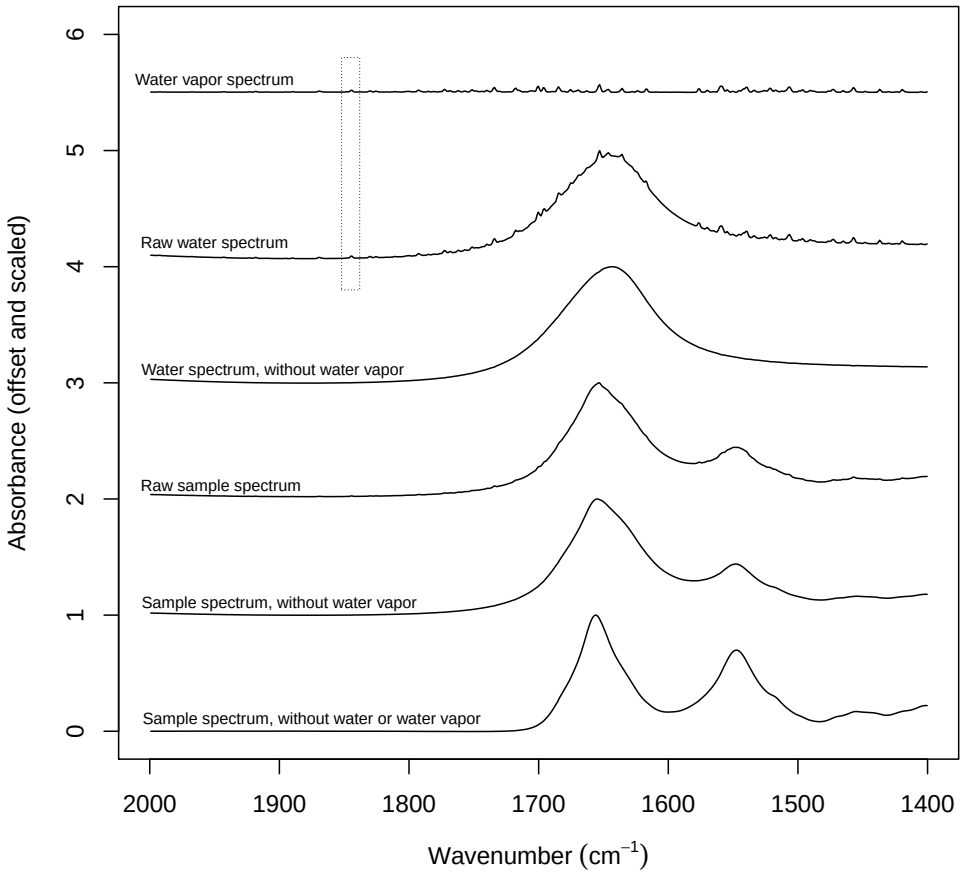


Figure A.2. The processing of an FTIR spectrum to remove water and water vapour from the protein spectrum. The dotted rectangle shows the vapour peak that was used for scaling prior to subtraction.

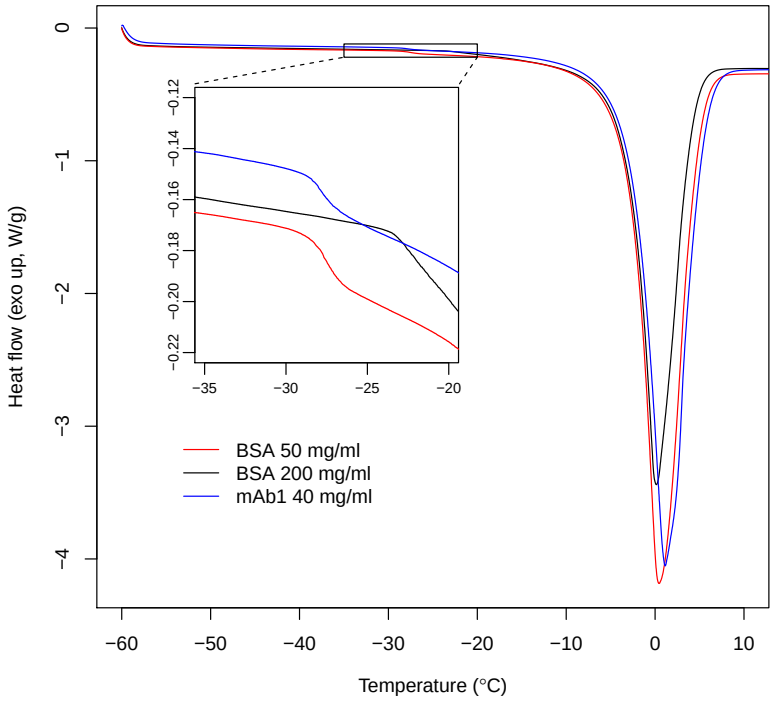


Figure A.3. The DSC traces of BSA (50 and 200 mg/mL) and mAb1 formulations illustrating the ice melting endotherm and the Tg′ which is inset within a box.

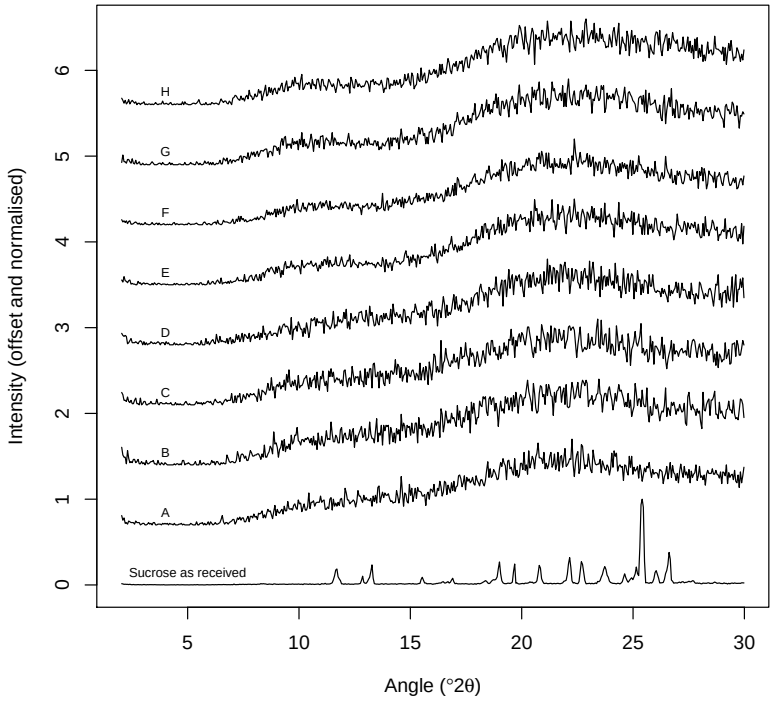


Figure A.4. The XRPD diffraction patterns of lyophilised BSA with sucrose, in which A, B, C and D are 50 mg/mL and E, F, G and H are 200 mg/mL BSA. The following cooling profiles were used: 0.5 °C/min (A and E), 0.5 °C/min then annealed (B and F), quench cooled (C and G) and quench cooled then annealed (D and H).

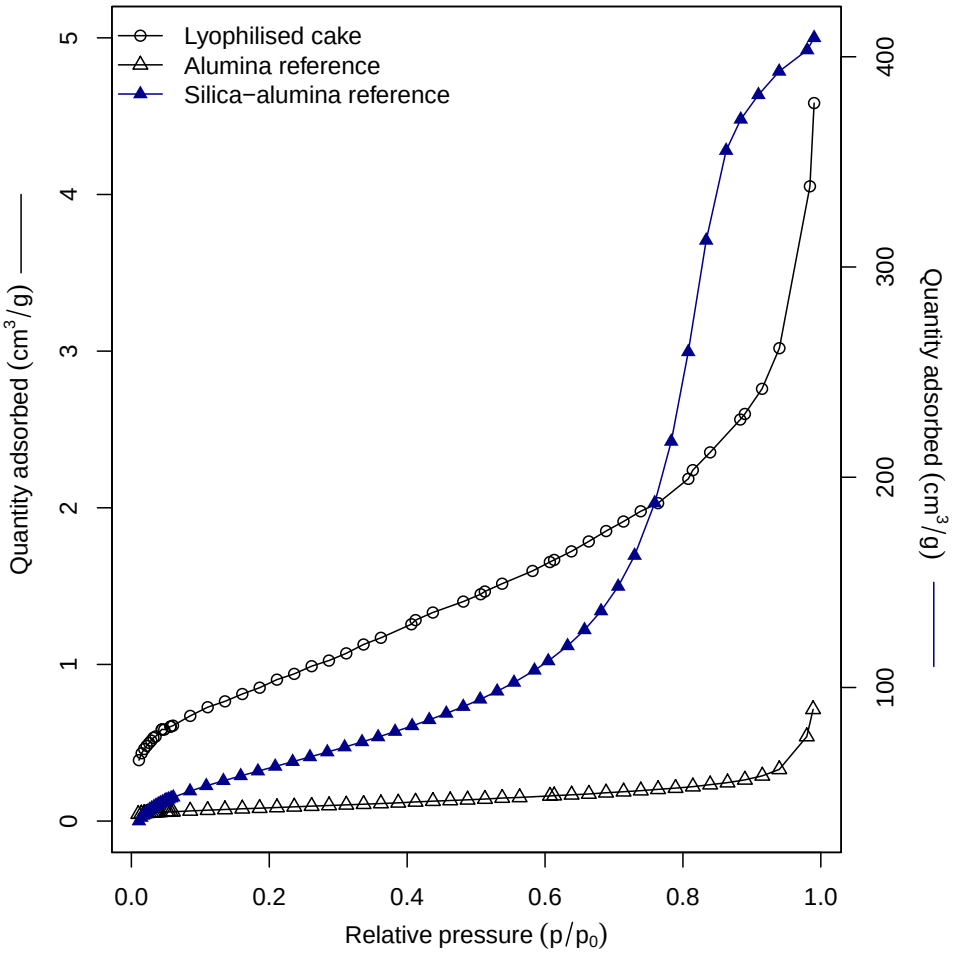


Figure A.5. A typical nitrogen adsorption isotherm that was observed with lyophilised material in this study (this example is from the quench cooled BSA 50 mg/mL cake). The two reference materials of low (alumina) and high (silica-alumina) surface area are shown. The desorption isotherms for the samples have not been included to provide a clearer illustration. Although, hysteresis was observed for the silica-alumina sample (a type 4 isotherm) whereas no hysteresis was observed for the lyophilised or low surface area reference (type 2 isotherms). However, at such low surface areas the hysteresis loop can be difficult to detect.

Table A.3. The BET constants for BSA with sucrose 50 and 200 mg/mL, and the mAb1 formulations (n=3, mean ± s.d.).

	0.5 °C/min	0.5 °C/min + annealed	Quench cooled	Quench cooled + annealed
BSA 50 mg/mL	8 ± 4	8 ± 1	39 ± 3	8 ± 2
BSA 200 mg/mL	15 ± 5	7 ± 4	39 ± 8	10 ± 5
mAb1	8 ± 4	7 ± 5	36 ± 6	11 ± 6

Table A.4. Error of the BET fit (m^2/g) for BSA with sucrose 50 and 200 mg/mL and mAb1 formulations. Calculated by performing a least-squares fit on the multipoint isotherm between the relative pressure range of 0.1 to 0.4 (n=3, mean ± s.d.).

	0.5 °C/min	0.5 °C/min + annealed	Quench cooled	Quench cooled + annealed
BSA 50 mg/mL	0.11 ± 0.06	0.08 ± 0.03	0.03 ± 0.01	0.06 ± 0.01
BSA 200 mg/mL	0.02 ± 0.00	0.05 ± 0.04	0.02 ± 0.01	0.04 ± 0.04
mAb1	0.12 ± 0.06	0.08 ± 0.04	0.03 ± 0.01	0.08 ± 0.04

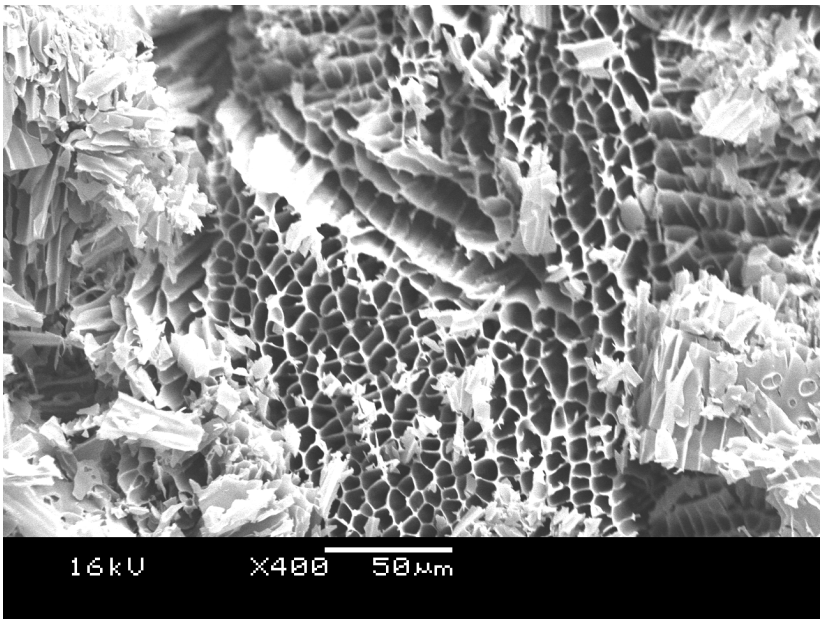


Figure A.6. An SEM image of the pores observed with the quench cooled BSA 50 mg/mL formulation. The images shows a cross-section of cylindrical pores. Breakage of the pore walls can also be observed.

B

```
function action(inputFolder,outputFolder,filename) {
open(inputFolder + filename);
// change scale
run("Set Scale...", "distance=165 known=500 pixel=1 unit=µm global");
run("Make Binary");
run("Despeckle");
//makeOval(9, 14, 977, 977);
getHistogram(0,hist,256);
ratio = hist[0]/(hist[0]+hist[255])*100;
print(filename, ratio, "%");
run("Invert");
run("Analyze Particles...", "size=0-Infinity circularity=0.00-1.00 show=[Bare Outlines] display exclude summarize");
 if (Overlay.size > 0) {
run("To ROI Manager");
close();
open(inputFolder + filename);
run("From ROI Manager");
outputPath = outputFolder + filename;
save(outputPath);
close();
}
else {
        close();
};
call("java.lang.System.gc");
};

call("java.lang.System.gc");
run("Clear Results");
inputFolder = getDirectory("Choose the input folder!");
outputFolder = getDirectory("Choose the output folder!");
setBatchMode(true);
images = getFileList(inputFolder);
run("Set Measurements...", "area centroid perimeter display add redirect=None decimal=1");
for (i=0; i<images.length; i++) {
 action(inputFolder,outputFolder,images[i]);
 showProgress(i, images.length);
};
selectWindow("Log");
saveAs("Text", "" + outputFolder + "Log.txt");
selectWindow("Results");
saveAs("Measurements", "" + outputFolder + "Results.txt");
selectWindow("Summary");
saveAs("Text", "" + outputFolder +"Summary.txt");
setBatchMode(false);
```

Figure B.1. The macro for image processing and calculation of porosity from micro-CT images.

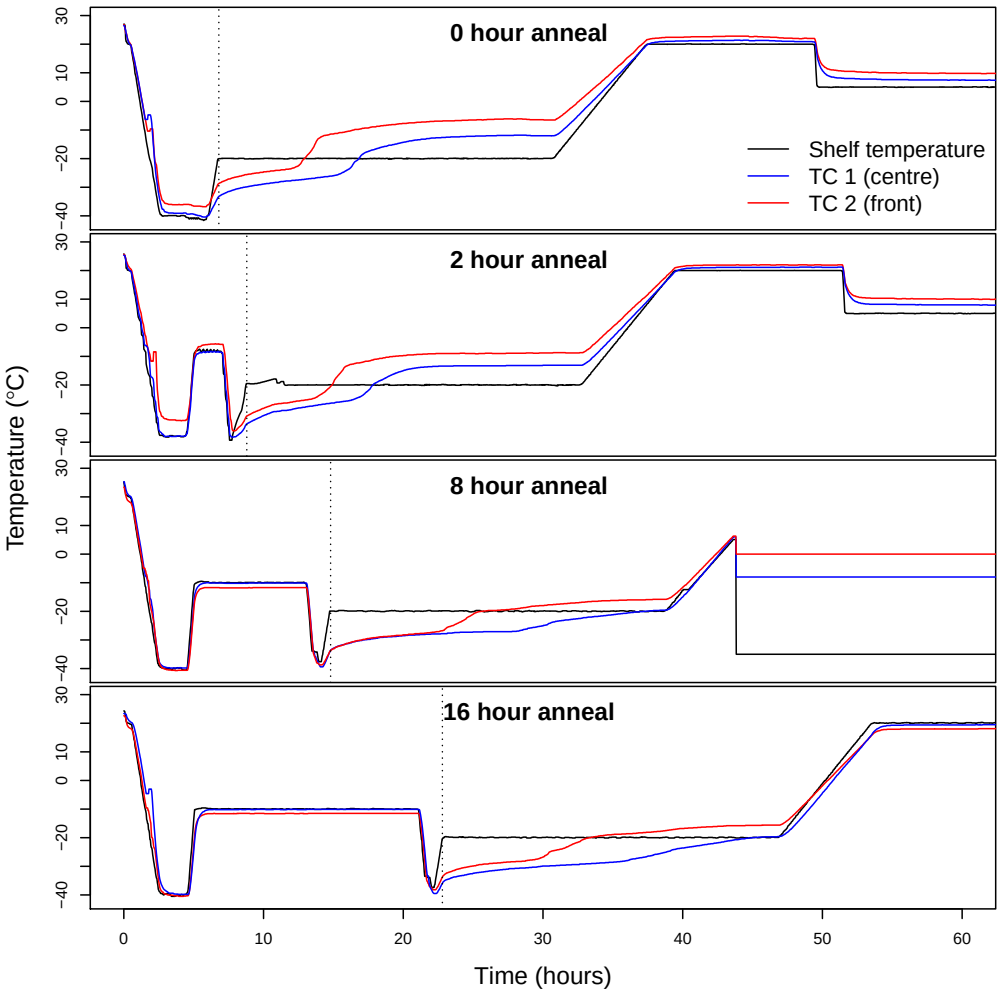
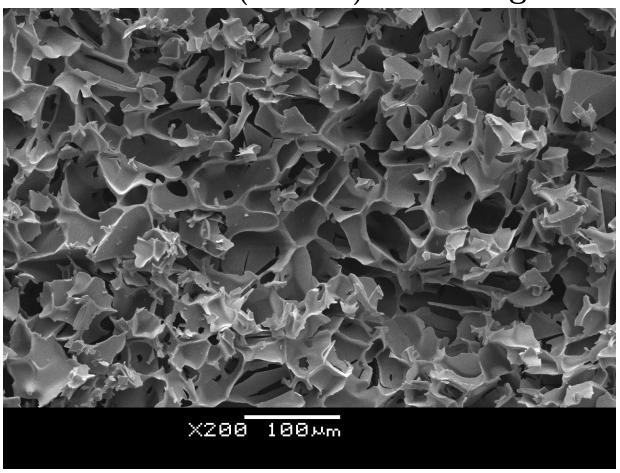
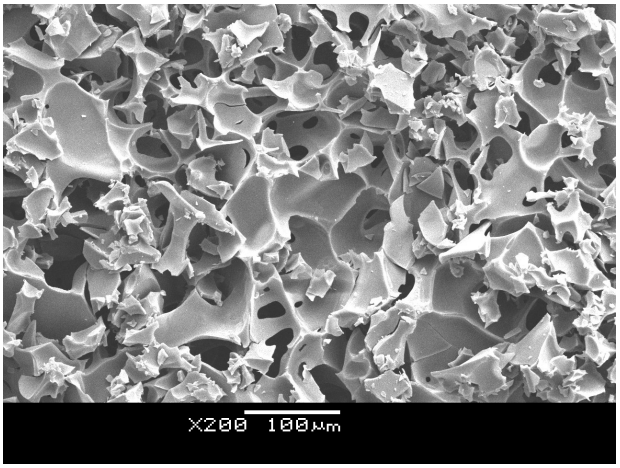


Figure B.2. The thermocouple data from lyophilisation cycles with 0, 2, 8 and 16 hour annealing durations. Unfortunately, the connection between freeze dryer and computer was lost during the 8 hour annealing cycle and at the start of the 4 hour cycle (data not shown). However, the shelf temperatures were confirmed during the cycle were confirmed by the freeze dryer display.

Without (0 hour) annealing



2 hour annealing duration



4 hour annealing duration

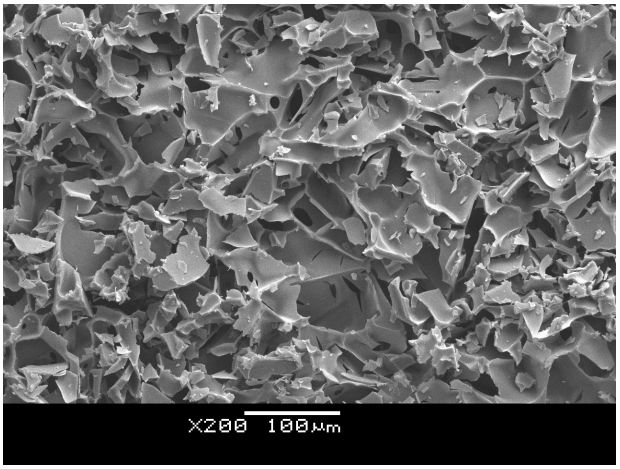
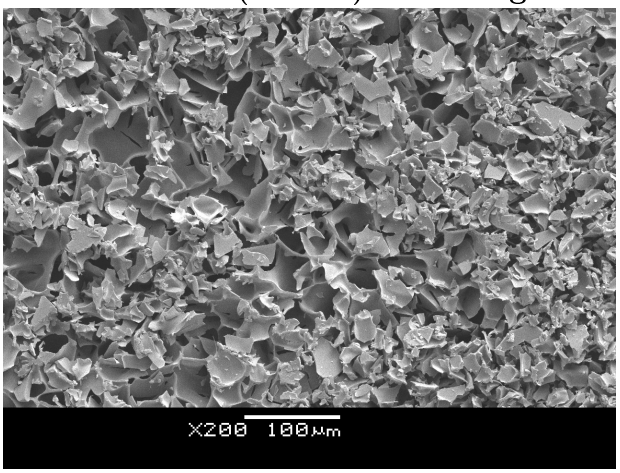
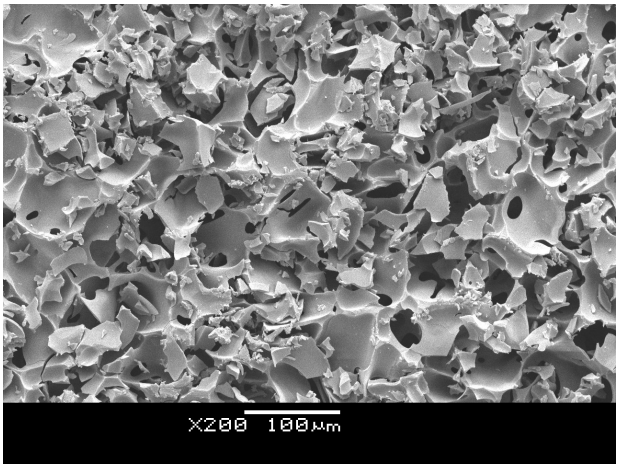


Figure B.3. SEM images of BSA arginine-C5 cakes lyophilised using 0, 2 and 16 hour annealing durations.

Without (0 hour) annealing



2 hour annealing duration



4 hour annealing duration

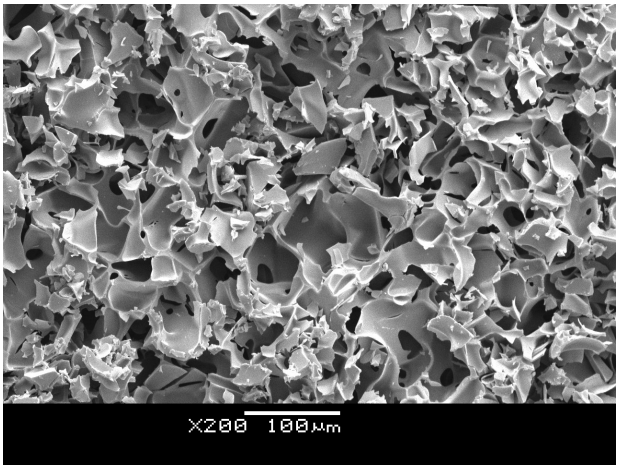
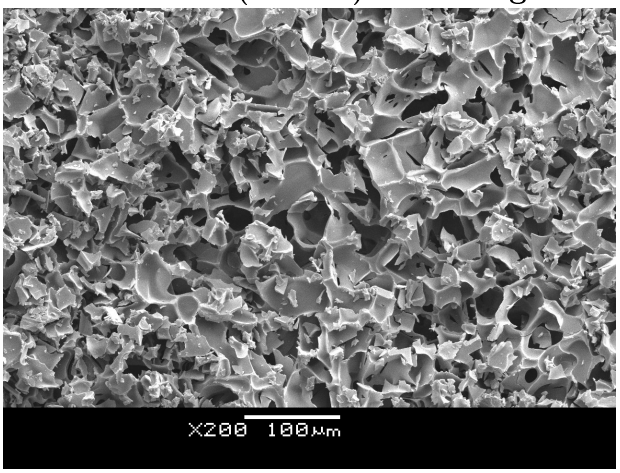
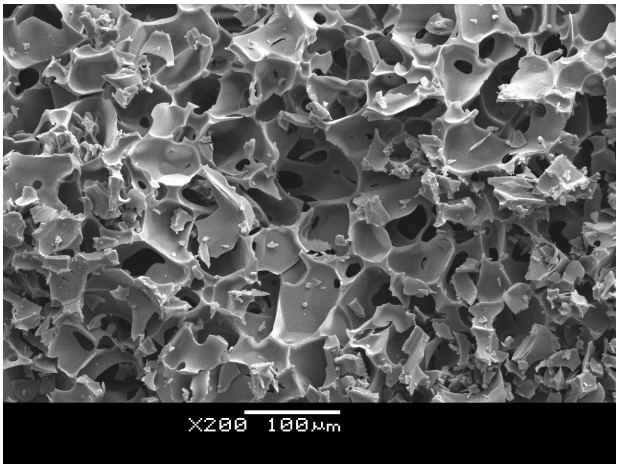


Figure B.4. SEM images of BSA arginine-C6 cakes lyophilised using 0, 2 and 16 hour annealing durations.

Without (0 hour) annealing



2 hour annealing duration



4 hour annealing duration

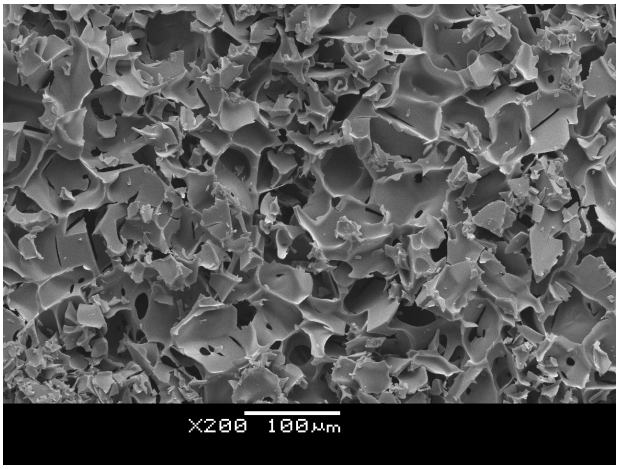


Figure B.5. SEM images of BSA arginine-C7 cakes lyophilised using 0, 2 and 16 hour annealing durations.

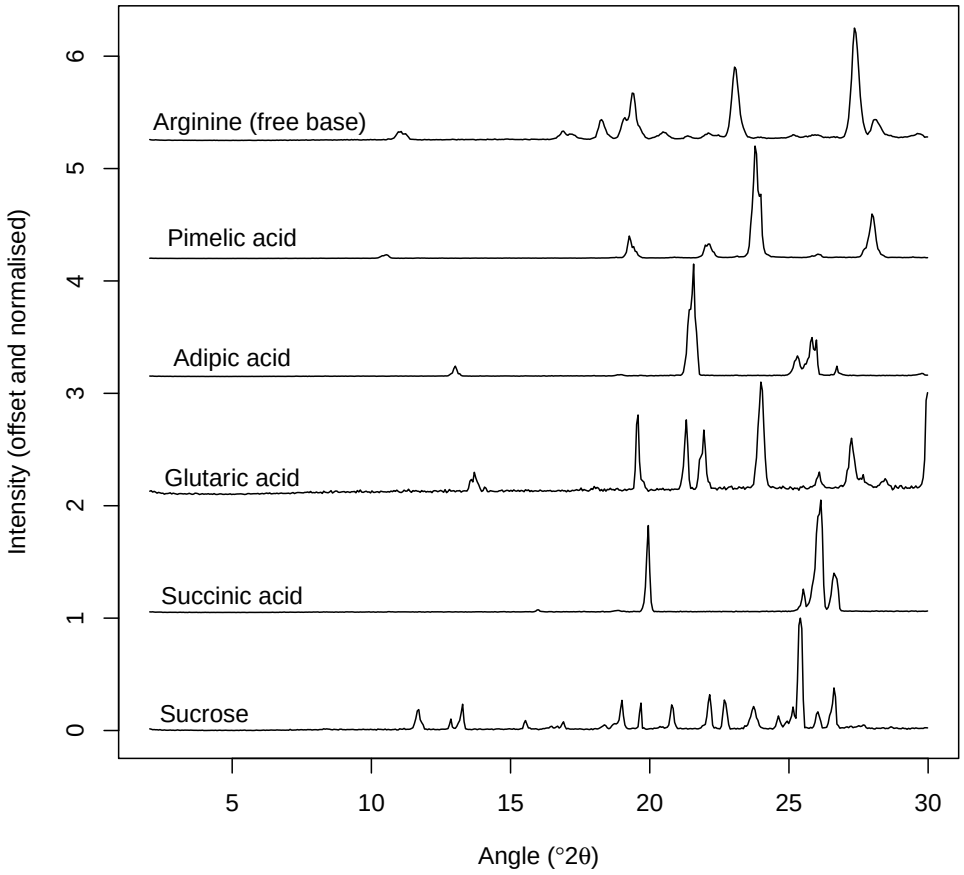


Figure B.6. The XRPD diffraction patterns for the crystalline, as received excipients.

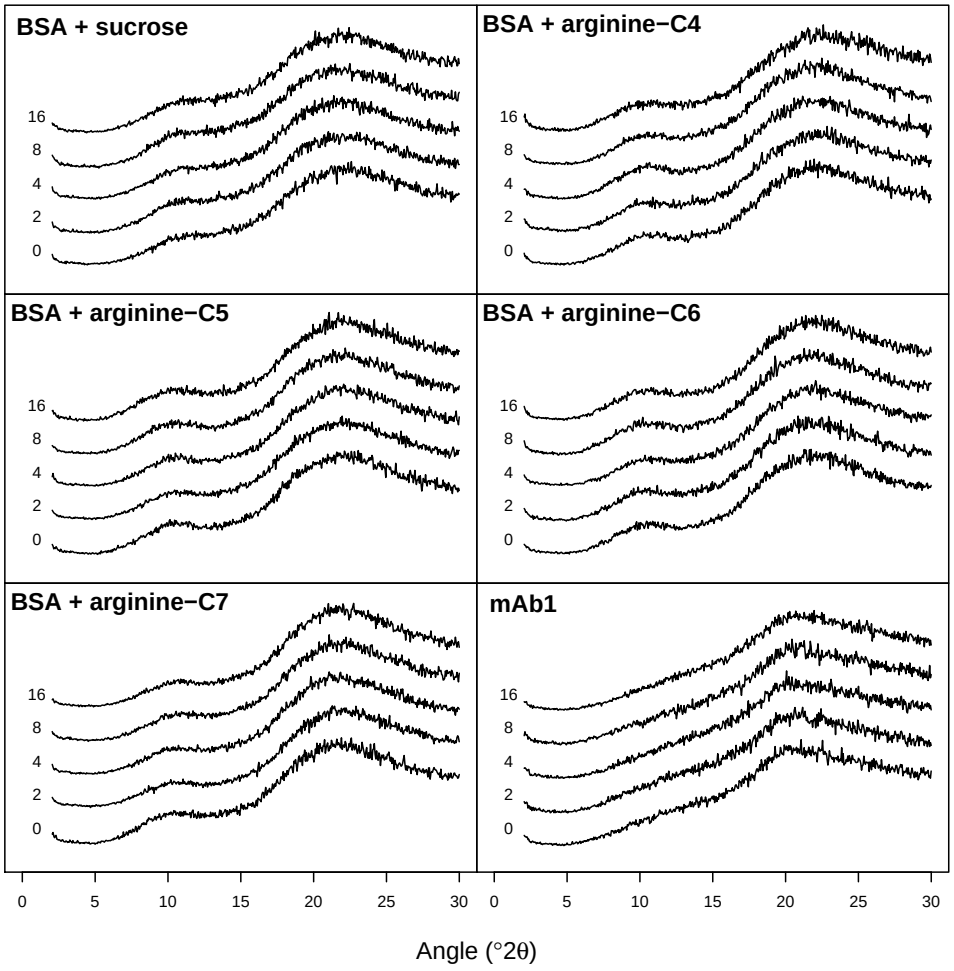


Figure B.7. The XRPD diffraction patterns of the lyophilised protein formulations. The annealing duration (in hours) is listed to the side of each trace.

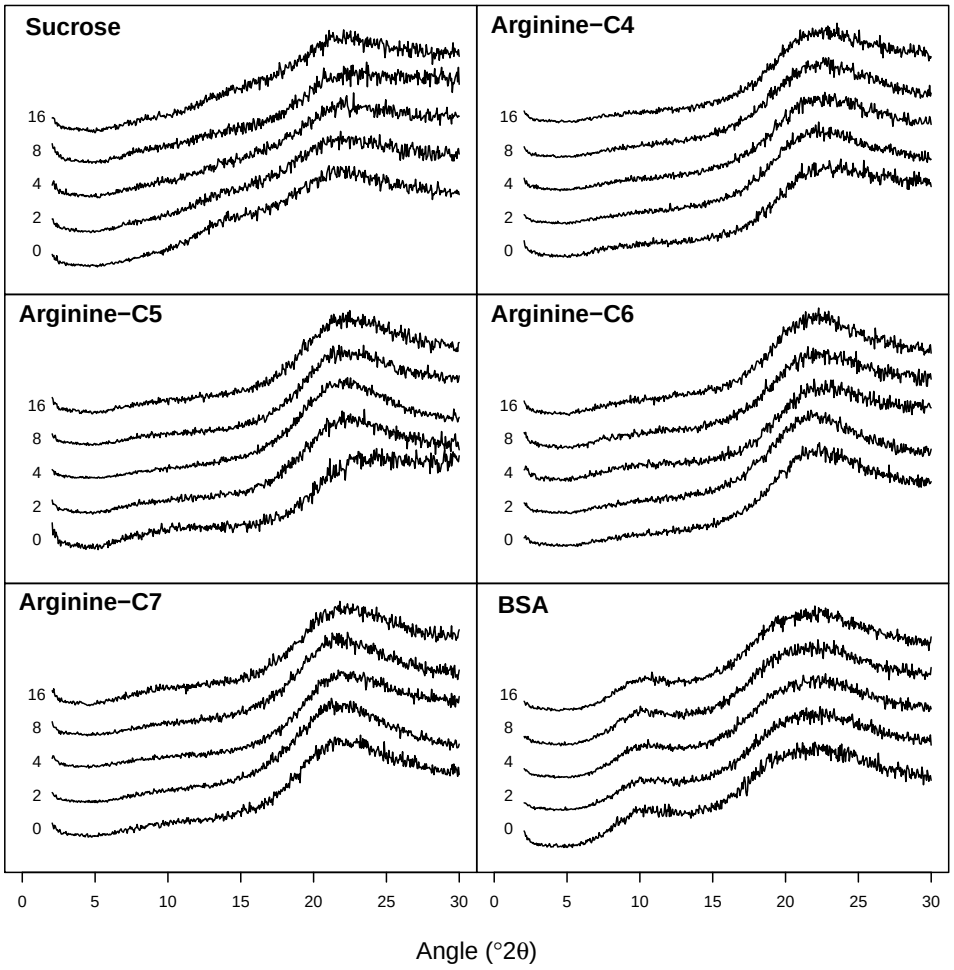


Figure B.8. The XRPD diffraction patterns of the lyophilised excipients. The annealing duration (in hours) is listed to the side of each trace.

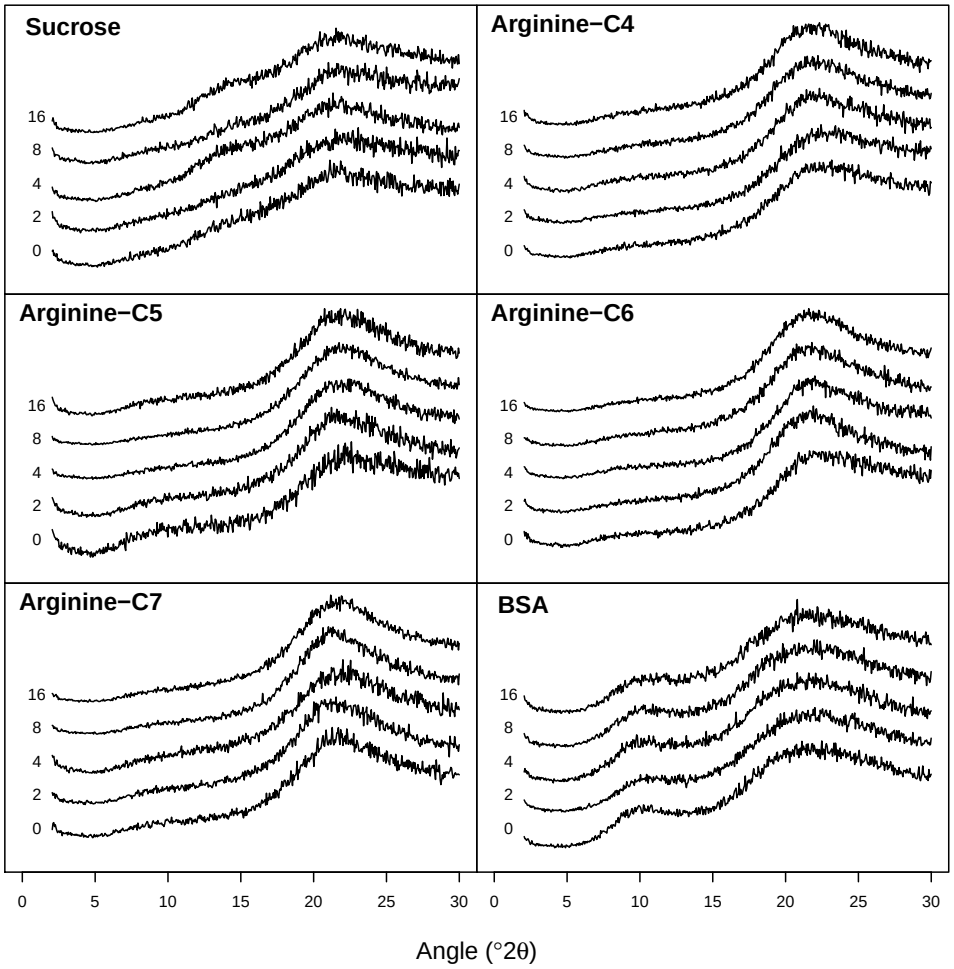


Figure B.9. The XRPD diffraction patterns of the lyophilised excipients after storage for 12 weeks at 40 °C. The annealing duration (in hours) is listed to the side of each trace.

Table B.1. The BET constants for the BSA with sucrose, arginine and mAb1 formulations (n=3, mean ± s.d.).

	0	2	4	8	16
BSA + sucrose	7 ± 1	6 ± 4	5 ± 1	6 ± 0	3 ± 1
BSA + arginine-C4	2 ± 1	2 ± 0	3 ± 1	2 ± 1	2 ± 0
BSA + arginine-C5	6 ± 2	7 ± 3	8 ± 1	8 ± 2	5 ± 3
BSA + arginine-C6	4 ± 1	5 ± 3	4 ± 1	6 ± 3	6 ± 1
BSA + arginine-C7	7 ± 0	7 ± 3	7 ± 2	6 ± 2	7 ± 2
mAb1	10 ± 3	4 ± 2	5 ± 4	5 ± 2	3 ± 1

Table B.2. Error of the BET fit (m^2/g) for BSA with sucrose, arginine and mAb1 formulations. Calculated by performing a least-squares fit on the multipoint isotherm between the relative pressure range of 0.1 to 0.4 (n=3, mean ± s.d.).

	0	2	4	8	16
BSA + sucrose	0.06 ± 0.02	0.08 ± 0.01	0.05 ± 0.01	0.06 ± 0.03	0.09 ± 0.03
BSA + arginine-C4	0.15 ± 0.05	0.33 ± 0.17	0.21 ± 0.05	0.20 ± 0.07	0.52 ± 0.07
BSA + arginine-C5	0.11 ± 0.05	0.06 ± 0.02	0.06 ± 0.02	0.11 ± 0.05	0.08 ± 0.00
BSA + arginine-C6	0.09 ± 0.01	0.13 ± 0.04	0.12 ± 0.07	0.13 ± 0.11	0.07 ± 0.02
BSA + arginine-C7	0.05 ± 0.00	0.08 ± 0.02	0.07 ± 0.04	0.08 ± 0.03	0.10 ± 0.03
mAb1	0.12 ± 0.08	0.29 ± 0.09	0.22 ± 0.15	0.15 ± 0.08	0.32 ± 0.21

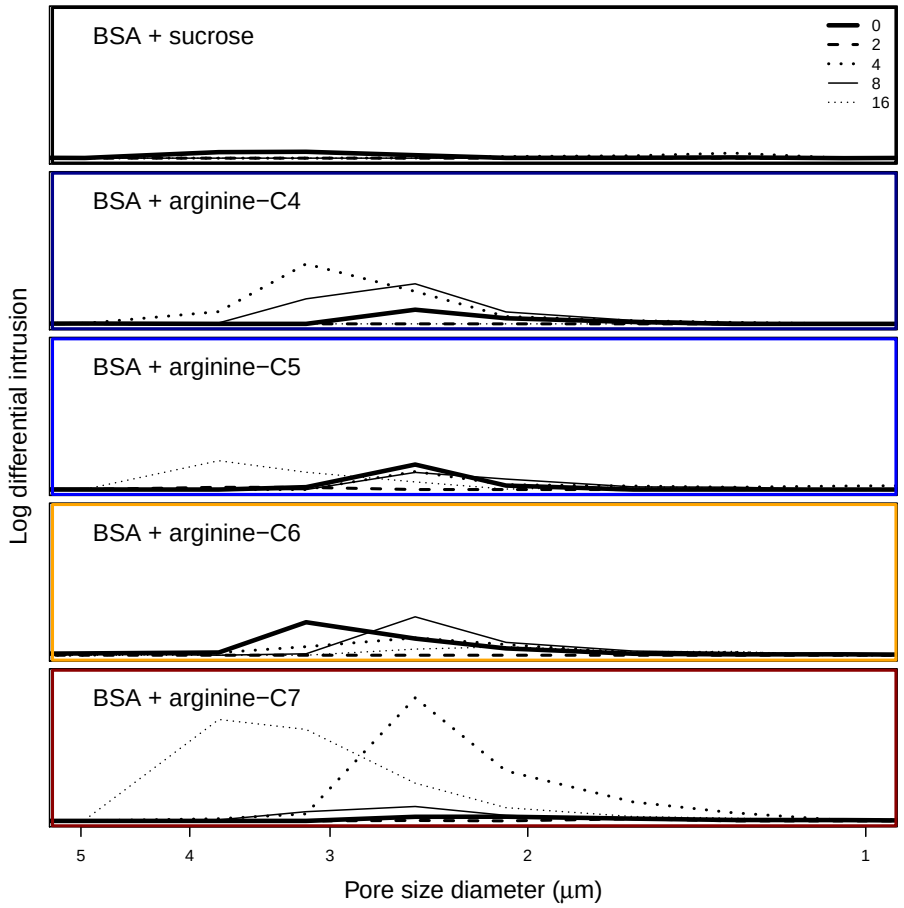


Figure B.10. Representative pore size distributions in the pore size diameter less than 5 μm for the BSA formulations, lyophilised for different annealing durations (n=1). The y-axis, which is not shown, is the same for all formulations.

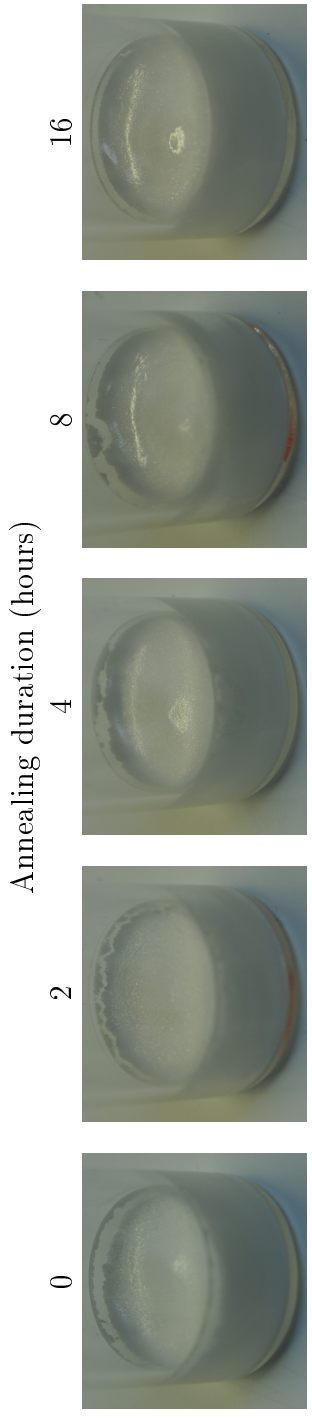


Figure B.11. Images of mAb1 cakes after lyophilisation using different annealing durations.

Table B.3. The bulk density and total pore volume measurements of mAb1, lyophilised using cycles with different annealing durations (n=1).

Annealing duration	Bulk density (g/cm^3)	Total pore volume (cm^3/g)
0	0.136	6.19
2	0.133	6.45
4	0.142	6.04
8	0.133	6.55
16	0.137	6.54

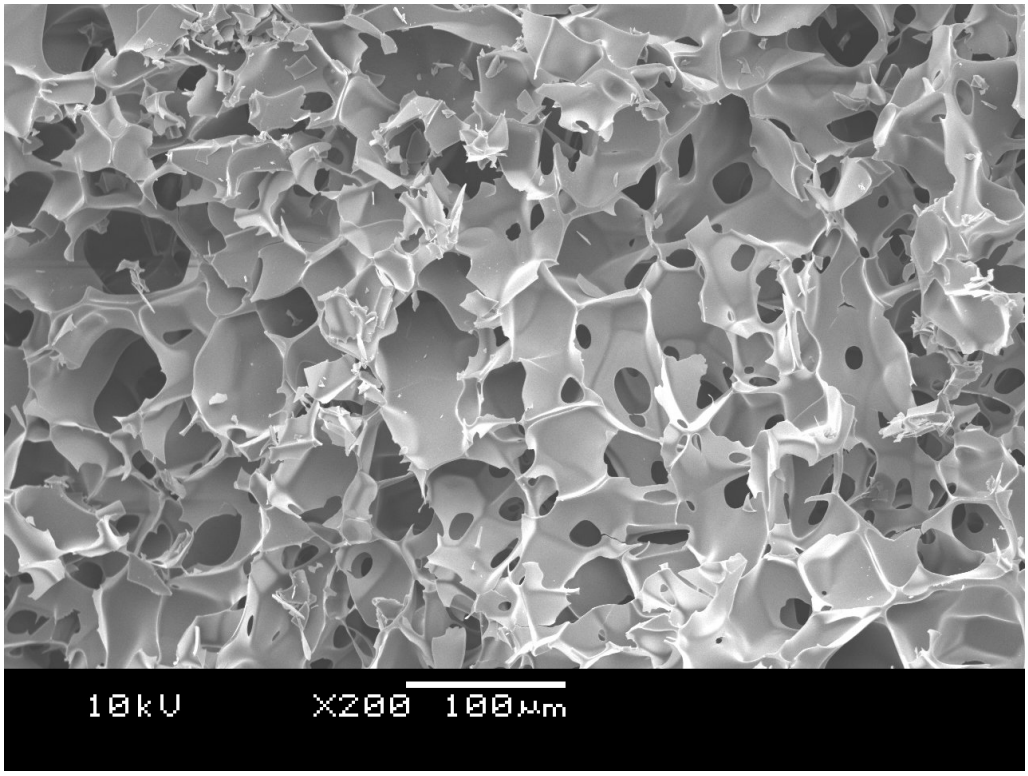


Figure B.12. An SEM image of mAb1, lyophilised without an annealing step.

C

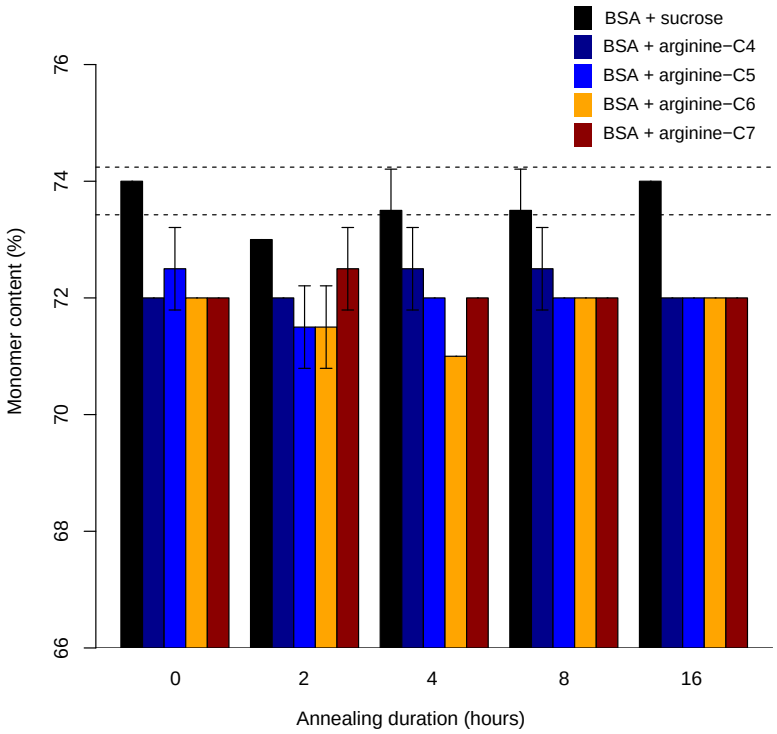


Figure C.1. The monomer content of reconstituted BSA after storage for 12 weeks in a refrigerator (n=2, mean ± s.d.). The dashed black lines show the variation in BSA in histidine buffer (in solution prior to lyophilisation) which was used as a comparison at each time point.

Table C.1. The elution times of protein formulations (in solution prior to lyophilisation). Little variation (<0.1 minutes) was observed from these values in the reconstituted state (data not shown), (n=3 ± s.d).

Formulation	Elution time (minutes)
BSA	8.92 ± 0.00
BSA + sucrose	8.92 ± 0.00
BSA + arginine-C4	8.92 ± 0.01
BSA + arginine-C5	8.91 ± 0.01
BSA + arginine-C6	8.91 ± 0.0
BSA + arginine-C7	8.92 ± 0.0
mAb1	8.17 ± 0.0

Table C.2. The subvisible particle (SVP) concentrations (in particles/mL) of protein formulations prior to lyophilisation.

	Particle size range			
Formulation	1–2μm	2–10 μm	>10 μm	>25 μm
BSA + sucrose	872	160	13	3
BSA + arginine-C4	1453	428	14	5
BSA + arginine-C5	702	237	17	3
BSA + arginine-C6	1185	248	15	6
BSA + arginine-C7	417	92	5	2
mAb1	2845	1519	164	25

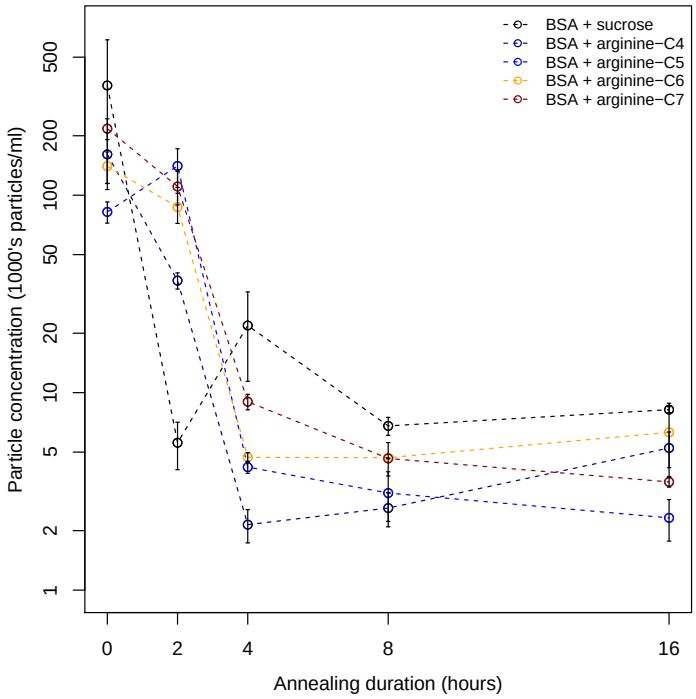


Figure C.2. The number of particles (between 1 and 2 μm) found from MFI experiments of BSA formulations after 12 weeks storage in a refrigerator. Please note that the y-axis is a logarithmic scale and the dashed lines are not lines of best fit and are included only to help identify formulation trends (n=2, mean $\pm$ s.d.).

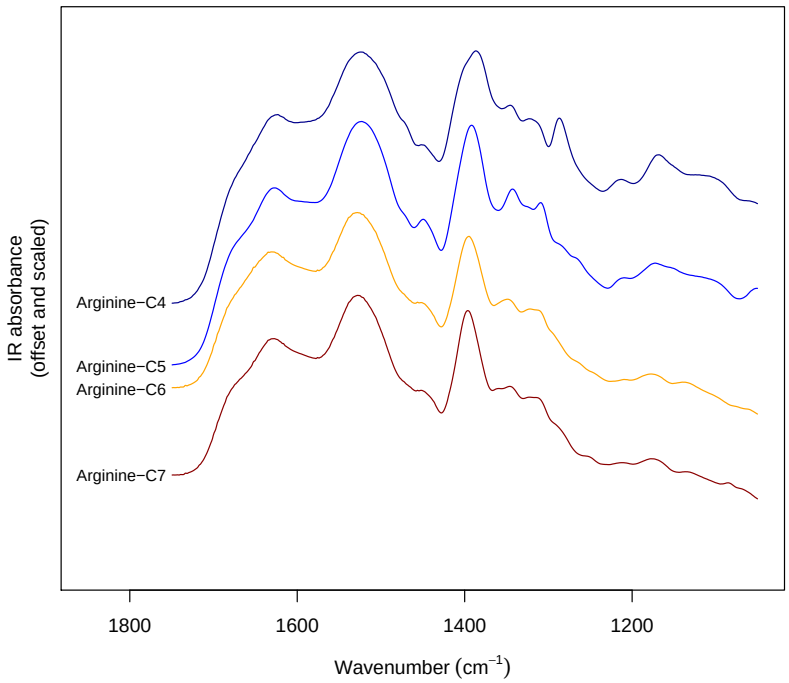


Figure C.3. The IR spectra of arginine-dicarboxylic acid formulations (without BSA) which shows absorption in the amide I region (1600 – 1700 cm^{-1}).

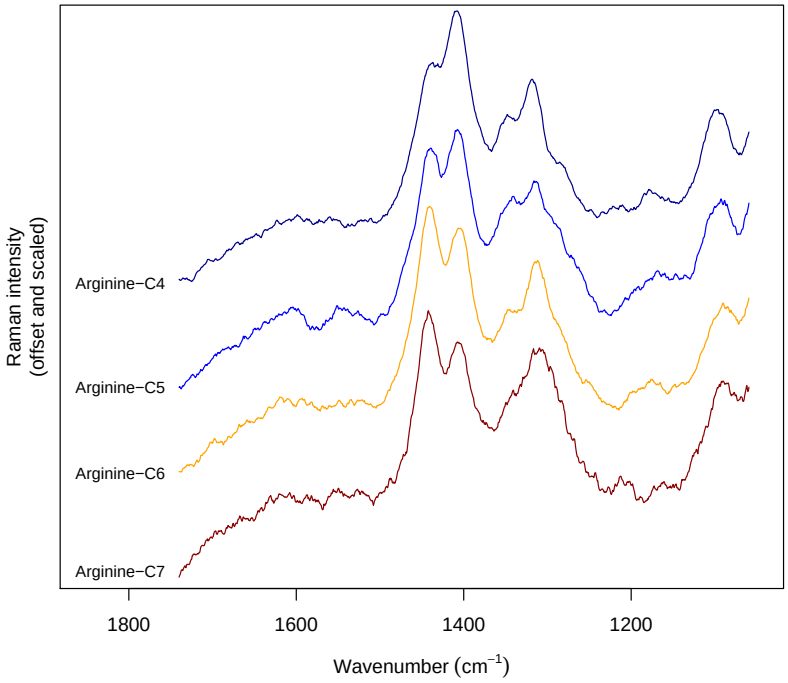


Figure C.4. The Raman spectra of arginine-dicarboxylic acid formulations (without BSA) which do not absorb in the amide I region (1600 – 1700 cm^{-1}).

Bibliography

W. Abdelwahed, G. Degobert, and H. Fessi. Freeze-drying of nanocapsules: Impact of annealing on the drying process. *International Journal of Pharmaceutics*, 324(1):74–82, 2006.

A. M. Abdul-Fattah, K. M. Dellerman, R. H. Bogner, and M. J. Pikal. The effect of annealing on the stability of amorphous solids: Chemical stability of freeze-dried moxalactam. *Journal of Pharmaceutical Sciences*, 96(5): 1237–1250, 2007a.

A. M. Abdul-Fattah, V. Truong-Le, L. Yee, L. Nguyen, D. S. Kalonia, M. T. Cicerone, and M. J. Pikal. Drying-induced variations in physico-chemical properties of amorphous pharmaceuticals and their impact on stability (I): Stability of a monoclonal antibody. *Journal of Pharmaceutical Sciences*, 96(8):1983–2008, 2007b.

A. M. Abdul-Fattah, D. Lechuga-Ballesteros, D. S. Kalonia, and M. J. Pikal. The impact of drying method and formulation on the physical properties and stability of methionyl human growth hormone in the amorphous solid state. *Journal of Pharmaceutical Sciences*, 97(1):163–184, 2008.

S. Ablett, M. J. Izzard, and P. J. Lillford. Differential scanning calorimetric study of frozen sucrose and glycerol solutions. *Journal of the Chemical Society, Faraday Transactions*, 88:789–794, 1992.

S. Ablett, C. J. Clarke, M. J. Izzard, and D. R. Martin. Relationship between ice recrystallisation rates and the glass transition in frozen sugar solutions. *Journal of the Science of Food and Agriculture*, 82(15), 2002.

G. D. J. Adams and L. I. Irons. Some implications of structural collapse during freeze-drying using erwinia caratovora L-asparaginase as a model. *Journal of Chemical Technology & Biotechnology*, 58(1):71–76, 1993.

F. AlHusban, A. M. ElShaer, J. H. Kansara, A. M. Smith, L. M. Grover, Y. Perrie, and A. R. Mohammed. Investigation of formulation and process of lyophilised orally disintegrating tablet (ODT) using novel amino acid combination. *Pharmaceutics*, 2(1):1–17, 2010.

C. Alie, R. Pirard, and J.-P. Pirard. Mercury porosimetry: applicability of the buckling-intrusion mechanism to low-density xerogels. *Journal of Non-Crystalline Solids*, 292(1-3):138–149, 2001.

S. Allison, T. W. Randolph, M. C. Manning, K. Middleton, A. Davis, and J. F. Carpenter. Effects of drying methods and additives on structure and function of actin: Mechanisms of dehydration-induced damage and its inhibition. *Archives of Biochemistry and Biophysics*, 358(1):171 – 181, 1998.

S. Allison, B. Chang, T. W. Randolph, and J. F. Carpenter. Hydrogen bonding between sugar and protein is responsible for inhibition of dehydration-induced protein unfolding. *Archives of Biochemistry and Biophysics*, 365 (2):289 – 298, 1999.

T. Arakawa and S. N. Timasheff. Stabilization of protein structure by sugars. *Biochemistry*, 21(25):6536–6544, 1982.

T. Arakawa and S. N. Timasheff. Mechanism of protein salting in and salting out by divalent cation salts: balance between hydration and salt binding. *Biochemistry*, 23(25):5912–5923, 1984.

T. Arakawa and K. Tsumoto. The effects of arginine on refolding of aggregated proteins: not facilitate refolding, but suppress aggregation. *Biochemical and Biophysical Research Communications*, 304(1):148 – 152, 2003.

T. Arakawa, S. J. Prestrelski, W. C. Kenney, and J. F. Carpenter. Factors affecting short-term and long-term stabilities of proteins. *Advanced Drug Delivery Reviews*, 46(1–3):307–326, 2001.

T. Arakawa, J. Philo, K. Tsumoto, R. Yumioka, and D. Ejima. Elution of antibodies from a protein-a column by aqueous arginine solutions. *Protein Expression and Purification*, 36(2):244–248, 2004.

T. Arakawa, D. Ejima, K. Tsumoto, N. Obeyama, Y. Tanaka, Y. Kita, and S. N. Timasheff. Suppression of protein interactions by arginine: A proposed mechanism of the arginine effects. *Biophysical Chemistry*, 127 (1-2):1–8, 2007.

T. Arakawa, K. Tsumoto, and D. Ejima. Alternative downstream processes for production of antibodies and antibody fragments. *Biochimica et Biophysica Acta (BBA) - Proteins and Proteomics*, 2014. In press. Available from http://dx.doi.org/10.1016/j.bbapap.2014.05.005.

K. Avis and V. L. Wu. *Biotechnology and biopharmaceutical manufacturing, processing and preservation*. CRC Press LLC, Boca Raton, Florida, 1996.

D. Awotwe-Otoo, C. Agarabi, G. K. Wu, E. Casey, E. Read, S. Lute, K. A. Brorson, M. A. Khan, and R. B. Shah. Quality by design: Impact of formulation variables and their interactions on quality attributes of a lyophilized monoclonal antibody. *International Journal of Pharmaceutics*, 438(1–2):167–175, 2012.

D. Awotwe-Otoo, C. Agarabi, E. K. Read, S. Lute, K. A. Brorson, M. A. Khan, and R. B. Shah. Impact of controlled ice nucleation on process performance and quality attributes of a lyophilized monoclonal antibody. *International Journal of Pharmaceutics*, 450(1-2):70–78, 2013.

P. B. Balbuena and K. E. Gubbins. Theoretical interpretation of adsorption behavior of simple fluids in slit pores. *Langmuir*, 9(7):1801–1814, 1993.

A. Banga. *Therapeutic Peptides and Proteins: Formulation, Processing, and Delivery Systems, Second Edition.* Taylor & Francis, Boca Raton, FL, 2005.

J. G. Barnard, S. Singh, T. W. Randolph, and J. F. Carpenter. Subvisible particle counting provides a sensitive method of detecting and quantifying aggregation of monoclonal antibody caused by freeze-thawing: Insights into the roles of particles in the protein aggregation pathway. *Journal of Pharmaceutical Sciences*, 100(2):492–503, 2011.

G. Barnes and I. Gentle. *Interfacial Science: An Introduction.* Oxford University Press, New York, New York, 2011.

B. S. Bhatnagar, S. M. Martin, D. L. Teagarden, E. Y. Shalaev, and R. Suryanarayanan. Investigation of PEG crystallization in frozen peg-sucrose-water solutions: II. characterization of the equilibrium behavior during freeze-thawing. *Journal of Pharmaceutical Sciences*, 99(11):4510–4524, 2010.

B. S. Bhatnagar, S. W. H. Martin, T. S. Hodge, T. K. Das, L. Joseph, D. L. Teagarden, E. Y. Shalaev, and R. Suryanarayanan. Investigation of PEG crystallization in frozen and freeze-dried pegylated recombinant human growth hormone-sucrose systems: Implications on storage stability. *Journal of Pharmaceutical Sciences*, 100(8):3062–3075, 2011.

G. Blond, D. Champion, and M. L. Meste. Principles of frozen storage. In Y. Hui, editor, *Handbook of Food Science, Technology, and Engineering*, pages 116.1–116.19. Taylor & Francis, Boca Raton, FL, 2006.

J. Blue and H. Yoder. Successful lyophilization development of protein therapeutics. *American Pharmaceutical Review*, pages 40–44, 2009.

G. E. P. Box and N. R. Draper. *Empirical Model Building and Response Surfaces.* John Wiley & Sons, New York, NY, 1987.

J. C. Boylan and S. L. Nail. Parenteral products. In G. Banker, J. Siepmann, and C. Rhodes, editors, *Modern Pharmaceutics, Fourth Edition*. Marcel Dekker, Inc, New York, NY, 2002.

G. O. Brown. Henry Darcy and the making of a law. *Water Resources Research*, 38(7):11–1–11–12, 2002.

H. Brown, H. McDaniel, and O. Hafliger. Dissociation constants. In E. Braude and F. Nachod, editors, *Determination of Organic Structures by Physical Methods*. Academic Press, New York, NY, 1955.

S. Brunauer, P. Emmett, and E. Teller. Adsorption of gases in multimolecular layers. *Journal of the American Chemical Society*, 60(2):309–319, 1938.

A. Bujacz. Structures of bovine, equine and leporine serum albumin. *Acta Crystallographica Section D*, D68(10):1278–1289, 2012.

D. J. Burgess and O. N. Sahin. Influence of protein emulsifier interfacial properties on oil-in-water emulsion stability. *Pharmaceutical Development and Technology*, 3(1):21–29, 1998.

E. Buxbaum. *Fundamentals of Protein Structure and Function*. Springer Science+Business Media, LLC, New York, NY, 2007.

P. Cameron. *Good Pharmaceutical Freeze-Drying Practice*. Taylor & Francis, Buffalo Grove, IL, 1997.

W. Cao, S. Krishnan, M. S. Ricci, L.-Y. Shih, D. Liu, J. H. Gu, and F. Jameel. Rational design of lyophilized high concentration protein formulations-mitigating the challenge of slow reconstitution with multidisciplinary strategies. *European Journal of Pharmaceutics and Biopharmaceutics*, 85(2):287 – 293, 2013.

R. A. Carlton. *Pharmaceutical Microscopy*. Springer Science+Business Media, LLC, New York, NY, 2011.

J. Carpenter, D. Katayama, L. Liu, W. Chonkaew, and K. Menard. Measurement of Tg in lyophilized protein and protein excipient mixtures by dynamic mechanical analysis. *Journal of Thermal Analysis and Calorimetry*, 95(3):881–884, 2009a.

J. F. Carpenter and J. H. Crowe. Modes of stabilization of a protein by organic solutes during desiccation. *Cryobiology*, 25(5):459 – 470, 1988.

J. F. Carpenter and J. H. Crowe. An infrared spectroscopic study of the interactions of carbohydrates with dried proteins. *Biochemistry*, 28(9): 3916–3922, 1989.

J. F. Carpenter, L. M. Crowe, and J. H. Crowe. Stabilization of phosphofructokinase with sugars during freeze-drying: characterization of enhanced protection in the presence of divalent cations. *Biochimica et Biophysica Acta (BBA) - General Subjects*, 923(1):109 – 115, 1987a.

J. F. Carpenter, B. Martin, L. M. Crowe, and J. H. Crowe. Stabilization of phosphofructokinase during air-drying with sugars and sugar/transition metal mixtures. *Cryobiology*, 24(5):455 – 464, 1987b.

J. F. Carpenter, T. Arakawa, and J. H. Crowe. Interactions of stabilizing additives with proteins during freeze-thawing and freeze-drying. *Developments in biological standardization*, 74:225–239, 1991.

J. F. Carpenter, B. S. Chang, W. Garzon-Rodriguez, and T. W. Randolph. Rational design of stable lyophilized protein formulations: Theory and practice. In J. Carpenter and M. C. Manning, editors, *Rational Design of Stable Protein Formulations*, volume 13 of *Pharmaceutical Biotechnology*, pages 109–133. Springer US, New York, New York, 2002.

J. F. Carpenter, T. W. Randolph, W. Jiskoot, D. J. Crommelin, C. R. Middaugh, G. Winter, Y.-X. Fan, S. Kirshner, D. Verthelyi, S. Kozlowski, K. A. Clouse, P. G. Swann, A. Rosenberg, and B. Cherney. Overlooking subvisible particles in therapeutic protein products: Gaps that may compromise product quality. *Journal of Pharmaceutical Sciences*, 98(4): 1201–1205, 2009b.

P. Chakravarty, R. Lee, F. Demarco, and E. Renzi. Ice fog as a means to induce uniform ice nucleation during lyophilization. *BioPharm International*, 25(1):33–38, 2012.

S. Chamow, T. Ryll, H. Lowman, and D. Farson. *Therapeutic Fc-Fusion Proteins*. John Wiley & Sons Ltd, West Sussex, UK, 2013.

K. Chan and P. Rogueda. Formulating biomolecules: Mechanistics insights in molecular interactions. *Advanced Drug Delivery Reviews*, 63(13):1051 – 1052, 2011.

B. Chang and S. Patro. Freeze-drying process development for protein pharmaceuticals. In H. Costantino and M. Pikal, editors, *Lyophilization of biopharmaceuticals*, pages 113–138. American Association of Pharmaceutical Scientists, Arlington, VA, 2004.

B. S. Chang and C. S. Randall. Use of subambient thermal analysis to optimize protein lyophilization. *Cryobiology*, 29(5):632 – 656, 1992.

B. S. Chang and B. Yeung. Physical stability of protein pharmaceuticals. In F. Jameel and S. Hershenson, editors, *Formulation and Process Development Strategies for Manufacturing Biopharmaceuticals*. John Wiley & Sons, Inc., Hoboken, NJ, 2010.

B. S. Chang, B. S. Kendrick, and J. F. Carpenter. Surface-induced denaturation of proteins during freezing and its inhibition by surfactants. *Journal of Pharmaceutical Sciences*, 85(12):1325–1330, 1996.

L. L. Chang and M. J. Pikal. Mechanisms of protein stabilization in the solid state. *Journal of Pharmaceutical Sciences*, 98(9):2886–2908, 2009.

L. L. Chang, D. Shepherd, J. Sun, D. Ouellette, K. L. Grant, X. C. Tang, and M. J. Pikal. Mechanism of protein stabilization by sugars during freeze-drying and storage: Native structure preservation, specific interaction, and/or immobilization in a glassy matrix? *Journal of Pharmaceutical Sciences*, 94(7):1427–1444, 2005a.

L. L. Chang, D. Shepherd, J. Sun, X. C. Tang, and M. J. Pikal. Effect of sorbitol and residual moisture on the stability of lyophilized antibodies: Implications for the mechanism of protein stabilization in the solid state. *Journal of Pharmaceutical Sciences*, 94(7):1445–1455, 2005b.

V. Chester and U. Kuruganti. Trunk kinematics during pediatric gait. In A. J. McGoron, C.-Z. Li, and W.-C. Lin, editors, *25th Southern Biomedical Engineering Conference 2009*, volume 24 of *IFMBE Proceedings*, pages 55–58. Springer Berlin Heidelberg, Berlin, Germany, 2009.

E. Chi, S. Krishnan, T. Randolph, and J. Carpenter. Physical stability of proteins in aqueous solution: Mechanism and driving forces in nonnative protein aggregation. *Pharmaceutical Research*, 20(9):1325–1336, 2003.

M. T. Cicerone and J. F. Douglas. β-relaxation governs protein stability in sugar-glass matrices. *Soft Matter*, 8:2983–2991, 2012.

M. T. Cicerone and C. L. Soles. Fast dynamics and stabilization of proteins: Binary glasses of trehalose and glycerol. *Biophysical Journal*, 86:3836–3845, 2004.

S. Claus, C. Weiler, J. Schiewe, and W. Friess. Optimization of the fine particle fraction of a lyophilized lysozyme formulation for dry powder inhalation. *Pharmaceutical Research*, 30(6):1698–1713, 2013.

J. Cleland, X. Lam, B. Kendrick, J. Yang, T. Yang, D. Overcashier, D. Brooks, C. Hsu, and J. Carpenter. A specific molar ratio of stabilizer to protein is required for storage stability of a lyophilized monoclonal antibody. *Journal of Pharmaceutical Sciences*, 90(3):310–21, 2001.

K. Cook and R. Hartel. Mechanisms of ice crystallization in ice cream production. *Comprehensive Reviews in Food Science and Food Safety*, 9 (2):213–222, 2010.

H. Costantino, J. Andya, S. Shire, and C. Hsu. Fourier-transform infrared spectroscopic analysis of the secondary structure of recombinant humanized immunoglobulin G. *Pharmacy and Pharmacology Communications*, 3(3):121–128, 1997.

H. R. Costantino, K. G. Carrasquillo, R. A. Cordero, M. Mumenthaler, C. C. Hsu, and K. Griebenow. Effect of excipients on the stability and structure of lyophilized recombinant human growth hormone. *Journal of Pharmaceutical Sciences*, 87(11):1412–1420, 1998.

H. R. Costantino, L. Firouzabadian, C. Wu, K. G. Carrasquillo, K. Griebenow, S. E. Zale, and M. A. Tracy. Protein spray freeze drying. 2. effect of formulation variables on particle size and stability. *Journal of Pharmaceutical Sciences*, 91(2):388–395, 2002.

V. Curtin, Y. Amharar, K. H. Gallagher, S. Corcoran, L. Tajber, O. I. Corrigan, and A. M. Healy. Reducing mechanical activation-induced amorphisation of salbutamol sulphate by co-processing with selected carboxylic acids. *International Journal of Pharmaceutics*, 456(2):508 – 516, 2013a.

V. Curtin, Y. Amharar, Y. Hu, A. Erxleben, P. McArdle, V. Caron, L. Tajber, O. I. Corrigan, and A. M. Healy. Investigation of the capacity of low glass transition temperature excipients to minimize amorphization of sulfadimidine on comilling. *Molecular Pharmaceutics*, 10(1):386–396, 2013b.

J. Z. D. Lechuga-Ballesteros, D.P. Miller. Residual water in amorphous solids: measurement and effects on stability. In H. Levine and C. College, editors, *Amorphous Food and Pharmaceutical Systems*, pages 275–316. Royal Society of Chemistry, Cambridge, UK, 2002.

U. Das, G. Hariprasad, A. S. Ethayathulla, P. Manral, T. K. Das, S. Pasha, A. Mann, M. Ganguli, A. K. Verma, R. Bhat, S. K. Chandrayan, S. Ahmed, S. Sharma, P. Kaur, T. P. Singh, and A. Srinivasan. Inhibition of protein aggregation: Supramolecular assemblies of arginine hold the key. *PLoS ONE*, 2(11):e1176, 2007.

J. M. Davis, N. Zhang, R. W. Payne, B. M. Murphy, A. M. Abdul-Fattah, J. E. Matsuura, A. C. Herman, and M. C. Manning. Stability of lyophilized sucrose formulations of an IgG1: subvisible particle formation. *Pharmaceutical Development and Technology*, 18(4):883–896, 2013.

P. Dawson and D. Hockley. Scanning electron microscopy of freeze-dried preparations: relationship of morphology to freeze-drying parameters. *Developments in biological standardization*, 74:185–92, 1992.

Y. De Smet, L. Deriemaeker, and R. Finsy. A simple computer simulation of ostwald ripening. *Langmuir*, 13(26):6884–6888, 1997.

M. S. Dennis, M. Zhang, Y. G. Meng, M. Kadkhodayan, D. Kirchhofer, D. Combs, and L. A. Damico. Albumin binding as a general strategy for improving the pharmacokinetics of proteins. *Journal of Biological Chemistry*, 277(38):35035–35043, 2002.

D. Devineni, C. Gonschorek, M. T. Cicerone, Y. Xu, J. F. Carpenter, and T. W. Randolph. Storage stability of keratinocyte growth factor-2 in lyophilized formulations: Effects of formulation physical properties and protein fraction at the solid-air interface. *European Journal of Pharmaceutics and Biopharmaceutics*, pages –, 2014. In press. Available from http://dx.doi.org/10.1016/j.ejpb.2014.05.012.

K. A. Dill, D. O. V. Alonso, and K. Hutchinson. Thermal stabilities of globular proteins. *Biochemistry*, 28(13):5439–5449, 1989.

D. S. Dimitrov. Therapeutic proteins. In V. Voynov and J. A. Caravella, editors, *Therapeutic Proteins*, volume 899 of *Methods in Molecular Biology*, pages 1–26. Humana Press, Totowa, NJ, 2012.

A. Divan and J. Royds. *Tools and Techniques in Biomolecular Science*. Oxford University Press, Oxford, UK, 2013.

A. Dokoumetzidis and P. Macheras. A century of dissolution research: From noyes and whitney to the biopharmaceutics classification system. *International Journal of Pharmaceutics*, 321(1,2):1–11, 2006.

A. Dong, P. Huang, and W. S. Caughey. Protein secondary structures in water from second-derivative amide I infrared spectra. *Biochemistry*, 29 (13):3303–3308, 1990.

A. Dong, S. J. Prestrelski, S. D. Allison, and J. F. Carpenter. Infrared spectroscopic studies of lyophilization- and temperature-induced protein aggregation. *Journal of Pharmaceutical Sciences*, 84(4):415–424, 1995.

S. Duddu and P. DalMonte. Effect of glass transition temperature on the stability of lyophilized formulations containing a chimeric therapeutic monoclonal antibody. *Pharmaceutical Research*, 14(5):591–595, 1997.

G. H. Dunteman. *Principal Components Analysis*. Number 69 in A Sage Publications. SAGE Publications, Newbury Park, CA, 1989.

D. Ejima, R. Yumioka, K. Tsumoto, and T. Arakawa. Effective elution of antibodies by arginine and arginine derivatives in affinity column chromatography. *Analytical Biochemistry*, 345(2):250 – 257, 2005.

E. Ekenlebie and A. Ingham. *Short Cycle Times for Cost-Efficient Processing in Lyophilized Formulations*. American Pharmaceutical Review, 2011. Online; accessed 10-August-2014.

EMA. *Quality by Design*. European Medicines Agency, 2014. URL `http://www.ema.europa.eu/ema/index.jsp?curl=pages/regulation/document_listing/document_listing_000162.jsp&mid=WC0b01ac058076ed73`. [Online; accessed 20-September-2014].

A. Eon-Duval, H. Broly, and R. Gleixner. Quality attributes of recombinant therapeutic proteins: An assessment of impact on safety and efficacy as part of a quality by design development approach. *Biotechnology Progress*, 28(3):608–622, 2012.

European Medicines Agency. *Refusal assessment report for Cimzia*, 2008. URL `www.ema.europa.eu/docs/en_GB/document_library/EPAR_-_Public_assessment_report/human/000740/WC500070613.pdf`. Online; accessed 21-August-2014.

FDA. *Guidance for Industry PAT-A Framework for Innovative Pharmaceutical Development, Manufacturing, and Quality Assurance*. U.S. Food and Drug Administration, 2004. URL `www.fda.gov/downloads/Drugs/Guidances/ucm070305.pdf`. Online; accessed 22-August-2014.

FDA. *Inactive Ingredient Search for Approved Drug Products*. U.S. Food and Drug Administration, 2013. URL `http://www.accessdata.fda.gov/scripts/cder/iig/`. [Online; accessed 3-August-2014].

FDA. *Drug information (Drugs@FDA)*. U.S. Food and Drug Administration, 2014a. URL `http://www.fda.gov/Drugs`. [Online; accessed 1-July-2014].

FDA. *GRAS Substances (SCOGS) Database*. U.S. Food and Drug Administration, 2014b. URL `http://www.fda.gov/food/ingredientspackaginglabeling/gras/`. [Online; accessed 1-August-2014].

T. A. Felix Franks. Essential physics of low temperature and freezing. In *Freeze-drying of Pharmaceuticals and Biopharmaceuticals: Principles and Practice*, pages 28–53. The Royal Society of Chemistry, cambridge, UK, 2007.

P. Fernandez, L. Otero, B. Guignon, and P. Sanz. High-pressure shift freezing versus high-pressure assisted freezing: Effects on the microstructure of a food model. *Food Hydrocolloids*, 20(4):510–522, 2006.

L. Ferreira, M. H. Gil, A. M. Cabrita, and J. S. Dordick. Biocatalytic synthesis of highly ordered degradable dextran-based hydrogels. *Biomaterials*, 26(23):4707–4716, 2005.

FisherScientific. *Adipic Acid, 99%, ACROS Organics: Physical properties*. Thermo Fisher Scientific Inc, 2014a. URL `http://www.fishersci.com/ecomm/servlet/fsproductdetail_10652_773529__-1_0`. [Online; accessed 3-August-2014].

FisherScientific. *Glutaric Acid, 99%, ACROS Organics: Physical properties*. Thermo Fisher Scientific Inc, 2014b. URL `http://www.fishersci.com/ecomm/servlet/fsproductdetail_10652_619650__-1_0`. [Online; accessed 3-August-2014].

FisherScientific. *Pimelic Acid, 98%, ACROS Organics: Physical properties*. Thermo Fisher Scientific Inc, 2014c. URL http://www.fishersci.com/ecomm/servlet/fsproductdetail_10652_10395202__-1_0. [Online; accessed 3-August-2014].

FisherScientific. *Succinic Acid, 99%, ACROS Organics: Physical properties*. Thermo Fisher Scientific Inc, 2014d. URL http://www.fishersci.com/ecomm/servlet/fsproductdetail_10652_653499__-1_0. [Online; accessed 3-August-2014].

M. C. Flemings. Coarsening in solidification processing. *Materials Transactions*, 46(5):895–900, 2005.

J. Foreman, S. R. Sauerbrunn, and C. L. Marcozzi. *Exploring the Sensitivity of Thermal Analysis Techniques to the Glass Transition*. TA Instruments, 2014. URL http://www.tainstruments.com/library_download.aspx?file=TA082.PDF. Online; accessed 17-August-2014.

K. M. Forney-Stevens, M. J. Pelletier, E. Y. Shalaev, M. J. Pikal, and R. H. Bogner. Optimization of a Raman microscopy technique to efficiently detect amorphous-amorphous phase separation in freeze-dried protein formulations. *Journal of Pharmaceutical Sciences*, 103(9):2749–2758, 2014.

F. Franks. Freeze-drying of bioproducts: putting principles into practice. *European Journal of Pharmaceutics and Biopharmaceutics*, 45(3):221–229, 1998.

F. Franks and R. H. M. Hatley. Stability of proteins at subzero temperatures: thermodynamics and some ecological consequences. *Pure and Applied Chemistry*, 63(10):1367–1380, 1991.

K. Fu, K. Griebenow, L. Hsieh, A. M. Klibanov, and R. Langer. FTIR characterization of the secondary structure of proteins encapsulated within PLGA microspheres. *Journal of Controlled Release*, 58(3):357 – 366, 1999.

Y. Fu, S. Yang, S. H. Jeong, S. Kimura, and K. Park. Orally fast disintegrating tablets: Developments, technologies, taste-masking and clinical studies. *Critical Reviews& trade; in Therapeutic Drug Carrier Systems*, 21(6):433 – 471, 2004.

A. Fujimoto, A. Hirano, and K. Shiraki. Ternary system of solution additives with arginine and salt for refolding of beta-galactosidase. *The Protein Journal*, 29(3):161–166, 2010.

B. J. Fuller. Cryoprotectants: the essential antifreezes to protect life in the frozen state. *Cryoletters*, 25(6):375–388, 2004.

S. Gaisford and M. Saunders. *Essentials of Pharmaceutical Preformulation*. John Wiley & Sons, West Sussex, UK, 2013.

C. Galle. Effect of drying on cement-based materials pore structure as identified by mercury intrusion porosimetry: A comparative study between oven-, vacuum-, and freeze-drying. *Cement and Concrete Research*, 31 (10):1467–1477, 2001.

W. J. Galush, L. N. Le, and J. M. R. Moore. Viscosity behavior of high-concentration protein mixtures. *Journal of Pharmaceutical Sciences*, 101 (3):1012–1020, 2012.

Gamry Instruments. *Raman Spectroelectrochemistry*, 2014. URL `http://www.gamry.com/application-notes/raman-spectroelectrochemistry/`. Online; accessed 14-June-2014.

C. Gao, Y. Wan, C. Yang, K. Dai, T. Tang, H. Luo, and J. Wang. Preparation and characterization of bacterial cellulose sponge with hierarchical pore structure as tissue engineering scaffold. *Journal of Porous Materials*, 18(2):139–145, 2011.

R. Geidobler and G. Winter. Controlled ice nucleation in the field of freeze-drying: Fundamentals and technology review. *European Journal of Pharmaceutics and Biopharmaceutics*, 85(2):214 – 222, 2013.

R. Geidobler, S. Mannschedel, and G. Winter. A new approach to achieve controlled ice nucleation of supercooled solutions during the freezing step in freeze-drying. *Journal of Pharmaceutical Sciences*, 101(12):4409–4413, 2012.

R. Geidobler, I. Konrad, and G. Winter. Can controlled ice nucleation improve freeze-drying of highly-concentrated protein formulations? *Journal of Pharmaceutical Sciences*, 102(11):3915–3919, 2013.

Genentech, Inc. and Novartis Pharmaceuticals Corporation. *How to Prepare & Administer XOLAIR*, 2014. URL `http://www.xolair.com`. [Online; accessed 25-April-2014].

A. Gerhardt, N. R. Mcgraw, D. K. Schwartz, J. S. Bee, J. F. Carpenter, and T. W. Randolph. Protein aggregation and particle formation in prefilled glass syringes. *Journal of Pharmaceutical Sciences*, 103(6):1601–1612, 2014.

H. Goff and R. Hartel. Ice cream and frozen desserts. In Y. Hui, editor, *Handbook of Food Science, Technology, and Engineering*, pages 154.1–154.48. Taylor & Francis, Boca Raton, FL, 2006.

H. Goff and R. Hartel. *Ice Cream*. Springer, New York, NY, 2013.

A. P. Golovanov, G. M. Hautbergue, S. A. Wilson, and L.-Y. Lian. A simple method for improving protein solubility and long-term stability. *Journal of the American Chemical Society*, 126(29):8933–8939, 2004.

J. Goworek. Silica gels: Characterization by physical methods. In P. Somasundaran, editor, *Encyclopedia of Surface and Colloid Science*, number v. 7 in Encyclopedia of Surface and Colloid Science. Taylor & Francis, Boca Raton, FL, 2006.

N. Grasmeijer, M. Stankovic, H. de Waard, H. Frijlink, and W. Hinrichs. Unraveling protein stabilization mechanisms: Vitrification and water replacement in a glass transition temperature controlled system. *Biochimica et Biophysica Acta (BBA) - Proteins and Proteomics*, 1834(4):763 – 769, 2013.

J. J. Gray. The interaction of proteins with solid surfaces. *Current Opinion in Structural Biology*, 14(1):110–115, 2004.

J. L. Green and C. A. Angell. Phase relations and vitrification in saccharide-water solutions and the trehalose anomaly. *The Journal of Physical Chemistry*, 93(8):2880–2882, 1989.

H. Gremlich and B. Yan. *Infrared and Raman Spectroscopy of Biological Materials*. Marcel Dekker Inc., New York, NY, 2001.

I. Grewal. *Emerging Protein Biotherapeutics*. Taylor & Francis, Boca Raton, FL, 2009.

K. Griebenow and A. M. Klibanov. Lyophilization-induced reversible changes in the secondary structure of proteins. *Proceedings of the National Academy of Sciences*, 92(24):10969–10976, 1995.

H. Haas, G. Brezesinski, and H. Mohwald. X-ray diffraction of a protein crystal anchored at the air/water interface. *Biophysical Journal*, 68(1): 312–314, 1995.

T. Haefele and K. Paulus. Confocal Raman microscopy in pharmaceutical development. In T. Dieing, O. Hollricher, and J. Toporski, editors, *Confocal Raman Microscopy: Volume 158 of Springer Series in Optical Sciences*, pages 165–202. Springer-Verlag, Berlin, Germany, 2010.

B. C. Hancock and G. Zografi. Characteristics and significance of the amorphous state in pharmaceutical systems. *Journal of Pharmaceutical Sciences*, 86(1):1–12, 1997.

M. M. Harding, L. G. Ward, and A. D. J. Haymet. Type I 'antifreeze' proteins. *European Journal of Biochemistry*, 264(3):653–665, 1999.

R. H. Hatley and A. Mant. Determination of the unfrozen water content of maximally freeze-concentrated carbohydrate solutions. *International Journal of Biological Macromolecules*, 15(4):227 – 232, 1993.

M. Heller, J. Carpenter, and T. Randolph. Manipulation of lyophilization-induced phase separation: Implications for pharmaceutical proteins. *Biotechnology Progress*, 13(5):590–596, 1997.

M. Heller, J. Carpenter, and T. Randolph. Protein formulation and lyophilization cycle design: Prevention of damage due to freeze-concentration induced phase separation. *Biotechnology and Bioengineering*, 63(2):166–174, 1999.

M. C. Heller, J. F. Carpenter, and T. W. Randolph. Application of a thermodynamic model to the prediction of phase separations in freeze-concentrated formulations for protein lyophilization. *Archives of Biochemistry and Biophysics*, 363(2):191 – 201, 1999a.

M. C. Heller, J. F. Carpenter, and T. W. Randolph. Conformational stability of lyophilized pegylated proteins in a phase-separating system. *Journal of Pharmaceutical Sciences*, 88(1):58–64, 1999b.

S. Hermeling, D. Crommelin, H. Schellekens, and W. Jiskoot. Structure-immunogenicity relationships of therapeutic proteins. *Pharmaceutical Research*, 21(6):897–903, 2004.

R. Hill, G. Bogdan, and R. Dart. Time to reconstitution: purified Fab antivenom vs. unpurified IgG antivenom . *Toxicon*, 39(5):729 – 731, 2001.

A. Hirano, T. Kameda, D. Shinozaki, T. Arakawa, and K. Shiraki. Molecular dynamics simulation of the arginine-assisted solubilization of caffeic acid: Intervention in the interaction. *The Journal of Physical Chemistry B*, 117 (25):7518–7527, 2013.

G. N. Hounsfield. Computerized transverse axial scanning (tomography): Part 1. description of system. *The British Journal of Radiology*, 46(552): 1016–1022, 1973.

L. Hovgaard, S. Frokjaer, and M. van de Weert. *Pharmaceutical Formulation Development of Peptides and Proteins*. CRC Press, Boca Raton, Florida, 2013.

C. C. Hsu, H. M. Nguyen, D. A. Yeung, D. A. Brooks, G. S. Koe, T. A. Bewley, and R. Pearlman. Surface denaturation at solid-void interface-A possible pathway by which opalescent participates form during the storage of lyophilized tissue-type plasminogen activator at high temperatures. *Pharmaceutical Research*, 12(1):69–77, 1995.

J. Huang, G. Kaul, C. Cai, R. Chatlapalli, P. Hernandez-Abad, K. Ghosh, and A. Nagi. Quality by design case study: An integrated multivariate approach to drug product and process development. *International Journal of Pharmaceutics*, 382(1–2):23–32, 2009.

S. Huang and M. Glicksman. Overview 12: Fundamentals of dendritic solidification-II development of sidebranch structure. *Acta Metallurgica*, 29(5):717 –734, 1981.

ICHQ10. *ICH Harmonised Tripartite Guideline: Pharmaceutical Quality System Q10*. International Conference on Harmonisation of Technical Requirements for Registration of Pharmaceuticals for Human Use, 2008. URL `http://www.ich.org/fileadmin/Public_Web_Site/ICH_Products/Guidelines/Quality/Q10/Step4/Q10_Guideline.pdf`. [Online; accessed 2-August-2014].

ICHQ8. *ICH Harmonised Tripartite Guideline: Pharmaceutical Development Q8(R2)*. International Conference on Harmonisation of Technical Requirements for Registration of Pharmaceuticals for Human Use, 2009. URL `http://www.ich.org/fileadmin/Public_Web_Site/ICH_Products/Guidelines/Quality/Q8_R1/Step4/Q8_R2_Guideline.pdf`. [Online; accessed 2-August-2014].

ICHQ9. *ICH Harmonised Tripartite Guideline: Quality Risk Management Q9*. International Conference on Harmonisation of Technical Requirements for Registration of Pharmaceuticals for Human Use, 2005. URL `http://www.ich.org/fileadmin/Public_Web_Site/ICH_Products/Guidelines/Quality/Q9/Step4/Q9_Guideline.pdf`. [Online; accessed 2-August-2014].

N. Inoue, E. Takai, T. Arakawa, and K. Shiraki. Specific decrease in solution viscosity of antibodies by arginine for therapeutic formulations. *Molecular Pharmaceutics*, 11(6):1889–1896, 2014a.

N. Inoue, E. Takai, T. Arakawa, and K. Shiraki. Arginine and lysine reduce the high viscosity of serum albumin solutions for pharmaceutical injection. *Journal of Bioscience and Bioengineering*, 117(5):539 – 543, 2014b.

G. Irvine. Size-exclusion high-performance liquid chromatography of peptides: a review. *Analytica Chimica Acta*, 352(1-3):387 – 397, 1997.

L. Ito, K. Shiraki, T. Matsuura, M. Okumura, K. Hasegawa, S. Baba, H. Yamaguchi, and T. Kumasaka. High-resolution X-ray analysis reveals binding of arginine to aromatic residues of lysozyme surface: implication of suppression of protein aggregation by arginine. *Protein Engineering Design and Selection*, 24(3):269–274, 2011.

K.-I. Izutsu, Y. Fujimaki, A. Kuwabara, and N. Aoyagi. Effect of counterions on the physical properties of L-arginine in frozen solutions and freeze-dried solids. *International Journal of Pharmaceutics*, 301(1–2):161–169, 2005.

K.-i. Izutsu, S. Kadoya, C. Yomota, T. Kawanishi, E. Yonemochi, and K. Terada. Freeze-drying of proteins in glass solids formed by basic amino acids and dicarboxylic acids. *Chemical and Pharmaceutical Bulletin*, 57 (1):43–48, 2009a.

K.-i. Izutsu, S. Kadoya, C. Yomota, T. Kawanishi, E. Yonemochi, and K. Terada. Stabilization of protein structure in freeze-dried amorphous

organic acid buffer salts. *Chemical and Pharmaceutical Bulletin*, 57(11): 1231–1236, 2009b.

K.-i. Izutsu, K. Fujii, C. Katori, C. Yomota, T. Kawanishi, Y. Yoshihashi, E. Yonemochi, and K. Terada. Effects of solute miscibility on the micro- and macroscopic structural integrity of freeze-dried solids. *Journal of Pharmaceutical Sciences*, 99(11):4710–4719, 2010.

K.-i. Izutsu, C. Yomota, H. Okuda, T. Kawanishi, T. W. Randolph, and J. F. Carpenter. Impact of heat treatment on miscibility of proteins and disaccharides in frozen solutions. *European Journal of Pharmaceutics and Biopharmaceutics*, 85(2):177 – 183, 2013.

K.-i. Izutsu, E. Yonemochi, C. Yomota, Y. Goda, and H. Okuda. Studying the morphology of lyophilized protein solids using X-ray micro-CT: Effect of post-freeze annealing and controlled nucleation. *AAPS PharmSciTech*, pages 1–8, 2014.

M. Jackson and H. Mantsch. The use and misuse of FTIR spectroscopy in the determination of protein-structure. *Critical Reviews in Biochemistry and Molecular Biology*, 30(2):95–120, 1995.

F. Jameel and M. Khan. Quality-by-design as applied to the development and manufacturing of a lyophilized protein product. *American Pharmaceutical Review*, 12(7), 2009.

M. Jayaraman, P. M. Buck, A. A. Ignatius, K. R. King, and W. Wang. Agitation-induced aggregation and subvisible particulate formation in model proteins. *European Journal of Pharmaceutics and Biopharmaceutics*, 87(2):299 – 309, 2014.

R. Johnson and L. Lewis. Freeze-drying protein formulations above their collapse temperatures: Possible issues and concerns. *American Pharmaceutical Review*, 14(3), 2011.

R. E. Johnson, M. E. Oldroyd, S. S. Ahmed, H. Gieseler, and L. M. Lewis. Use of manometric temperature measurements (MTM) to characterize the freeze-drying behavior of amorphous protein formulations. *Journal of Pharmaceutical Sciences*, 99(6):2863–2873, 2010.

I. Jolliffe. *Principal Component Analysis*. Springer-Verlag New York Inc., New York, NY, 2002.

L. S. Jones, T. W. Randolph, U. Kohnert, A. Papadimitriou, G. Winter, M.-L. Hagmann, M. C. Manning, and J. F. Carpenter. The effects of tween 20 and sucrose on the stability of anti-L-selectin during lyophilization and reconstitution. *Journal of Pharmaceutical Sciences*, 90(10):1466–1477, 2001.

S. Joshi, A. Bhambhani, Y. Zeng, and C. R. Middaugh. An empirical phase diagram–high-throughput screening approach to the characterization and formulation of biopharmaceuticals. In F. Jameel and S. Hershenson, editors, *Formulation and Process Development Strategies for Manufacturing Biopharmaceuticals*. John Wiley & Sons, Inc., Hoboken, NJ, 2010.

J. M. Juran. *Juran on Quality by Design: The New Steps for Planning Quality Into Goods and Services*. Free Press, New York, NY, 1992.

L. D. Kaale and T. M. Eikevik. The development of ice crystals in food products during the superchilling process and following storage, a review. *Trends in Food Science & Technology*, 2014. In press. Available from http://dx.doi.org/10.1016/j.tifs.2014.07.004.

S. Kadoya, K.-i. Izutsu, E. Yonemochi, K. Terada, C. Yomota, and T. Kawanishi. Glass-state amorphous salt solids formed by freeze-drying of amines and hydroxy carboxylic acids: Effect of hydrogen-bonding and electrostatic interactions. *Chemical and Pharmaceutical Bulletin*, 56(6): 821–826, 2008.

C. Kalonia, O. S. Kumru, J. H. Kim, C. R. Middaugh, and D. B. Volkin. Radar chart array analysis to visualize effects of formulation variables on IgG1 particle formation as measured by multiple analytical techniques. *Journal of Pharmaceutical Sciences*, 102(12):4256–4267, 2013.

T. J. Kamerzell, R. Esfandiary, S. B. Joshi, C. R. Middaugh, and D. B. Volkin. Protein-excipient interactions: Mechanisms and biophysical characterization applied to protein formulation development. *Advanced Drug Delivery Reviews*, 63(13):1118 – 1159, 2011.

D. Kammer and P. Voorhees. The morphological evolution of dendritic microstructures during coarsening. *Acta Materialia*, 54(6):1549 – 1558, 2006.

A. Kar. *Pharmaceutical Drug Analysis*. New Age International (P) Ltd., New Delhi, India, 2005.

J. C. Kasper and W. Friess. The freezing step in lyophilization: Physico-chemical fundamentals, freezing methods and consequences on process performance and quality attributes of biopharmaceuticals. *European Journal of Pharmaceutics and Biopharmaceutics*, 78(2):248 – 263, 2011.

J. C. Kasper, D. Schaffert, M. Ogris, E. Wagner, and W. Friess. Development of a lyophilized plasmid/lpei polyplex formulation with long-term stability - a step closer from promising technology to application. *Journal of Controlled Release*, 151(3):246 – 255, 2011.

J. C. Kasper, C. Troiber, S. KÃijchler, E. Wagner, and W. Friess. Formulation development of lyophilized, long-term stable

siRNA/oligoaminoamide polyplexes. *European Journal of Pharmaceutics and Biopharmaceutics*, 85(2):294 – 305, 2013a.

J. C. Kasper, G. Winter, and W. Friess. Recent advances and further challenges in lyophilization. *European Journal of Pharmaceutics and Biopharmaceutics*, 85(2):162–169, 2013b.

J. K. Kaushik and R. Bhat. A mechanistic analysis of the increase in the thermal stability of proteins in aqueous carboxylic acid salt solutions. *Protein Science*, 8(1):222–233, 1999.

O. Kayser and H. Varzecha. *Pharmaceutical biotechnology: drug discovery and clinical applications*. Wiley-VCH Verlag, Weinheim, Germany, 2012.

B. S. Kendrick, A. Dong, S. D. Allison, M. C. Manning, and J. F. Carpenter. Quantitation of the area of overlap between second-derivative amide I infrared spectra to determine the structural similarity of a protein in different states. *Journal of Pharmaceutical Sciences*, 85(2):155–158, 1996.

B. A. Kerwin, M. C. Heller, S. H. Levin, and T. W. Randolph. Effects of tween 80 and sucrose on acute short-term stability and long-term storage at -20 °C of a recombinant hemoglobin. *Journal of Pharmaceutical Sciences*, 87(9):1062–1068, 1998.

S. Kiese, A. Pappenberger, W. Friess, and H.-C. Mahler. Equilibrium studies of protein aggregates and homogeneous nucleation in protein formulation. *Journal of Pharmaceutical Sciences*, 99(2):632–644, 2010.

K. H. Kim, Z. Akase, T. Suzuki, and D. Shindo. Charging effects on SEM/SIM contrast of metal/insulator system in various metallic coating conditions. *Materials Transactions*, 51(6):1080–1083, 2010.

Y. Kita, T. Arakawa, T.-Y. Lin, and S. N. Timasheff. Contribution of the surface free energy perturbation to protein-solvent interactions. *Biochemistry*, 33(50):15178–15189, 1994.

M. Kobayashi. Development of new refrigeration system and optimum geometry of the vapor condenser for pharmaceutical freeze dryers. In R. Toei and A. S. Mujumdar, editors, *Drying '85*, pages 281–288. Springer-Verlag, Berlin, Germany, 1985.

J. Kong and S. Yu. Fourier transform infrared spectroscopic analysis of protein secondary structures. *Acta Biochimica et Biophysica Sinica*, 39 (8):549–559, 2007.

A. K. Konstantinidis, W. Kuu, L. Otten, S. L. Nail, and R. R. Sever. Controlled nucleation in freeze-drying: Effects on pore size in the dried product layer, mass transfer resistance, and primary drying rate. *Journal of Pharmaceutical Sciences*, 100(8):3453–3470, 2011.

E. H. Koo, P. T. Lansbury, and J. W. Kelly. Amyloid diseases: Abnormal protein aggregation in neurodegeneration. *Proceedings of the National Academy of Sciences*, 96(18):9989–9990, 1999.

M. Kramer, B. Sennhenn, and G. Lee. Freeze-drying using vacuum-induced surface freezing. *Journal of Pharmaceutical Sciences*, 91(2):433–443, 2002.

M. Krokida, V. Karathanos, and Z. Maroulis. Effect of freeze-drying conditions on shrinkage and porosity of dehydrated agricultural products. *Journal of Food Engineering*, 35(4):369 – 380, 1998.

W. Y. Kuu, K. R. O'Bryan, L. M. Hardwick, and T. W. Paul. Product mass transfer resistance directly determined during freeze-drying cycle runs using tunable diode laser absorption spectroscopy (TDLAS) and pore diffusion model. *Pharmaceutical Development and Technology*, 16 (4):343–357, 2011.

P. Laity, M. Mantle, L. Gladden, and R. Cameron. Magnetic resonance imaging and X-ray microtomography studies of a gel-forming tablet formulation. *European Journal of Pharmaceutics and Biopharmaceutics*, 74 (1):109–119, 2010.

C. Lange and R. Rudolph. Suppression of protein aggregation by L-arginine. *Current Pharmaceutical Biotechnology*, 10:13426–38, 2009.

I. Langmuir. The adsorption of gases on plane surfaces of glass, mica and platinum. *Journal of the American Chemical Society*, 40(9):1361–1403, 1918.

P. Larkin. *IR and Raman spectroscopy: principals and spectral interpretation.* Elsevier Inc., Waltham, MA, 1997.

B. Leader, Q. J. Baca, and D. E. Golan. Protein therapeutics: a summary and pharmacological classification. *Nature Reviews Drug Discovery*, 7: 21–39, 2008.

J. Lee and S. Timasheff. The stabilization of proteins by sucrose. *The Journal of Biological Chemistry*, 256:7193–7201, 1981.

C. Leuner and J. Dressman. Improving drug solubility for oral delivery using solid dispersions. *European Journal of Pharmaceutics and Biopharmaceutics*, 50(1):47 – 60, 2000.

S. G. Levesque, R. M. Lim, and M. S. Shoichet. Macroporous interconnected dextran scaffolds of controlled porosity for tissue-engineering applications. *Biomaterials*, 26(35):7436–7446, 2005.

X. Liao, R. Krishnamurthy, and R. Suryanarayanan. Influence of the active pharmaceutical ingredient concentration on the physical state of mannitol–implications in freeze-drying. *Pharmaceutical Research*, 22(11): 1978–1985, 2005.

I. Lifshitz and V. Slyozov. The kinetics of precipitation from supersaturated solid solutions. *Journal of Physics and Chemistry of Solids*, 19(1–2):35–50, 1961.

K. H. Liland and B.-H. Mevik. *baseline: Baseline Correction of Spectra*, 2012. URL `http://CRAN.R-project.org/package=baseline`. R package version 1.1-0.

H.-M. Lin, H.-Y. Tien, Y.-T. Hone, and M.-J. Lee. Solubility of selected dibasic carboxylic acids in water, in ionic liquid of [Bmim][BF4], and in aqueous [Bmim][BF4] solutions. *Fluid Phase Equilibria*, 253(2):130 – 136, 2007.

J. L. Lippert, D. Tyminski, and P. J. Desmeules. Determination of the secondary structure of proteins by laser Raman spectroscopy. *Journal of the American Chemical Society*, 98(22):7075–7080, 1976.

K. Lippert and E. A. Galinski. Enzyme stabilization be ectoine-type compatible solutes: protection against heating, freezing and drying. *Applied Microbiology and Biotechnology*, 37(1):61–65, 1992.

J. Liu. Physical characterization of pharmaceutical formulations in frozen and freeze-dried solid states: Techniques and applications in freeze-drying development. *Pharmaceutical Development and Technology*, 11(1):3–28, 2006.

L. Liu, T. W. Randolph, and J. F. Carpenter. Particles shed from syringe filters and their effects on agitation-induced protein aggregation. *Journal of Pharmaceutical Sciences*, 101(8):2952–2959, 2012.

L. Liu, W. Qi, D. K. Schwartz, T. W. Randolph, and J. F. Carpenter. The effects of excipients on protein aggregation during agitation: An interfacial shear rheology study. *Journal of Pharmaceutical Sciences*, 102 (8):2460–2470, 2013a.

R. Liu, X. Yin, H. Li, Q. Shao, P. York, Y. He, T. Xiao, and J. Zhang. Visualization and quantitative profiling of mixing and segregation of granules using synchrotron radiation X-ray microtomography and three dimensional reconstruction. *International Journal of Pharmaceutics*, 445(1–2): 125–133, 2013b.

K. Lobmann, H. Grohganz, R. Laitinen, C. Strachan, and T. Rades. Amino acids as co-amorphous stabilizers for poorly water soluble drugs — part 1: Preparation, stability and dissolution enhancement. *European Journal of Pharmaceutics and Biopharmaceutics*, 85(3, Part B):873–881, 2013.

B. Lueckel, B. Helk, D. Bodmer, and H. Leuenberger. Effects of formulation and process variables on the aggregation of freeze-dried interleukin-6 (IL-6) after lyophilization and on storage. *Pharmaceutical Development and Technology*, 3(3):337–346, 1998.

S. Luthra, D. S. Kalonia, and M. J. Pikal. Effect of hydration on the secondary structure of lyophilized proteins as measured by fourier transform infrared (FTIR) spectroscopy. *Journal of Pharmaceutical Sciences*, 96 (11):2910–2921, 2007.

M. Nasr. *FDA's Quality Initiatives: An Update*. U.S. Food and Drug Administration, 2006. URL `http://www.gmp-compliance.com/daten/download/FDAs_Quality_Initiative.pdf`. [Online; accessed 2-August-2014].

H.-C. Mahler, W. Friess, U. Grauschopf, and S. Kiese. Protein aggregation: Pathways, induction factors and analysis. *Journal of Pharmaceutical Sciences*, 98(9):2909–2934, 2009.

D. Mahlin, J. Wood, N. Hawkins, J. Mahey, and P. G. Royall. A novel powder sample holder for the determination of glass transition temperatures by DMA. *International Journal of Pharmaceutics*, 371(1-2):120 –125, 2009.

P. E. Mason, G. W. Neilson, C. E. Dempsey, A. C. Barnes, and J. M. Cruickshank. The hydration structure of guanidinium and thiocyanate ions: Implications for protein stability in aqueous solution. *Proceedings of the National Academy of Sciences*, 100(8):4557–4561, 2003.

S. Matheus, W. Friess, and H.-C. Mahler. FTIR and nDSC as analytical tools for high-concentration protein formulations. *Pharmaceutical Research*, 23(6):1350–1363, 2006.

M. Mattern, G. Winter, U. Kohnert, and G. Lee. Formulation of proteins in vacuum-dried glasses. II. process and storage stability in sugar-free amino acid systems. *Pharmaceutical Development and Technology*, 4(2): 199–208, 1999.

S. B. Mehta, J. S. Bee, T. W. Randolph, and J. F. Carpenter. Partial unfolding of a monoclonal antibody: Role of a single domain in driving protein aggregation. *Biochemistry*, 53(20):3367–3377, 2014.

E. Meister and H. Gieseler. Freeze–dry microscopy of protein/sugar mixtures: Drying behavior, interpretation of collapse temperatures and a comparison to corresponding glass transition data. *Journal of Pharmaceutical Sciences*, 98(9):3072–3087, 2009.

K. Menard. *Dynamic Mechanical Analysis: A Practical Introduction, Second Edition*. Taylor & Francis, Boca Raton, FL, 2008.

E. Merisko-Liversidge, G. G. Liversidge, and E. R. Cooper. Nanosizing: a formulation approach for poorly-water-soluble compounds. *European Journal of Pharmaceutical Sciences*, 18(2):113 – 120, 2003.

Mettler Toledo. *Good Titration Practice in Karl Fisher Titration*, 2011. URL `http://uk.mt.com/gb/en/home/supportive_content/know_how/GTP_in_KF.html`. Online; accessed 9-August-2014.

M. A. Miller, M. A. Rodrigues, M. A. Glass, S. K. Singh, K. P. Johnston, and J. A. Maynard. Frozen-state storage stability of a monoclonal antibody: Aggregation is impacted by freezing rate and solute distribution. *Journal of Pharmaceutical Sciences*, 102(4):1194–1208, 2013.

T. Miller-Livney and R. W. Hartel. Ice recrystallization in ice cream: Interactions between sweeteners and stabilizers. *Journal of Dairy Science*, 80(3):447–456, 1997.

L. Mockus, D. LeBlond, P. Basu, R. Shah, and M. Khan. A QbD case study: Bayesian prediction of lyophilization cycle parameters. *AAPS PharmSciTech*, 12(1):442–448, 2011a.

L. N. Mockus, T. W. Paul, N. A. Pease, N. J. Harper, P. K. Basu, E. A. Oslos, G. A. Sacha, W. Y. Kuu, L. M. Hardwick, J. J. Karty, M. J. Pikal, E. Hee, M. A. Khan, and S. L. Nail. Quality by design in formulation and process development for a freeze-dried, small molecule parenteral product: a case study. *Pharmaceutical Development and Technology*, 16 (6):549–576, 2011b.

S. Mori and H. G. Barth. *Size Exclusion Chromatography*. Springer-Verlag, Berlin, Germany, 1999.

K. Murayama and M. Tomida. Heat-induced secondary structure and conformation change of bovine serum albumin investigated by fourier transform infrared spectroscopy. *Biochemistry*, 43(36):11526–11532, 2004.

K. Murphy. *Janeway's Immunobiology*. Garland Science, New York, NY, 2011.

H. Nagendra, N. Sukumar, and M. Vijayan. Role of water in plasticity, stability, and action of proteins: The crystal structures of lysozyme at very low levels of hydration. *Proteins: Structure, Function, and Bioinformatics*, 32(2):229–240, 1998.

P. Nagle, C. Nicita, L. Gerdes, and C. Schmeichel. Characteristics of and trends in the late-stage biopharmaceutical pipeline. *The American Journal of Managed Care*, 14(4):226–229, 2008.

K. Nakagawa, A. Hottot, S. Vessot, and J. Andrieu. Influence of controlled nucleation by ultrasounds on ice morphology of frozen formulations for pharmaceutical proteins freeze-drying. *Chemical Engineering and Processing: Process Intensification*, 45(9):783–791, 2006.

K. Nakagawa, A. Hottot, S. Vessot, and J. Andrieu. Modeling of freezing step during freeze-drying of drugs in vials. *AIChE Journal*, 53(5):1362–1372, 2007.

A. Nayak, J. Colandene, V. Bradford, and M. Perkins. Characterization of subvisible particle formation during the filling pump operation of a monoclonal antibody solution. *Journal of Pharmaceutical Sciences*, 100 (10):4198–4204, 2011.

A. L. Nelson, E. Dhimolea, and J. M. Reichert. Development trends for human monoclonal antibody therapeutics. *Nature Reviews Drug Discovery*, 9:767–774, 2010.

S. Noguchi, R. Kajihara, Y. Iwao, Y. Fujinami, Y. Suzuki, Y. Terada, K. Uesugi, K. Miura, and S. Itai. Investigation of internal structure of fine granules by microtomography using synchrotron X-ray radiation. *International Journal of Pharmaceutics*, 445(1–2):93 – 98, 2013.

S. Ohtake and Y. J. Wang. Trehalose: Current use and future applications. *Journal of Pharmaceutical Sciences*, 100(6):2020–2053, 2011.

S. Ohtake, Y. Kita, and T. Arakawa. Interactions of formulation excipients with proteins in solution and in the dried state. *Advanced Drug Delivery Reviews*, 63(13):1053 – 1073, 2011.

D. Overcashier, T. Patapoff, and C. Hsu. Lyophilization of protein formulations in vials: Investigation of the relationship between resistance to vapor flow during primary drying and small-scale product collapse. *Journal of Pharmaceutical Sciences*, 88(7):688–695, 1999.

A. M. Padilla and M. J. Pikal. The Study of Phase Separation in Amorphous Freeze-Dried Systems, Part 2: Investigation of Raman Mapping as a Tool for Studying Amorphous Phase Separation in Freeze-Dried Protein Formulations. *Journal of Pharmaceutical Sciences*, 100(4):1467–1474, 2011.

A. M. Padilla, I. Ivanisevic, Y. Yang, D. Engers, R. H. Bogner, and M. J. Pikal. The study of phase separation in amorphous freeze-dried systems. part I: Raman mapping and computational analysis of xrpd data in model polymer systems. *Journal of Pharmaceutical Sciences*, 100(1):206–222, 2011.

PANalytical B.V. *X'PERT3 Powder: Dedication in X-ray powder diffraction*, 2014. URL `www.panalytical.com/web/file?uuid=39e17912-5796-4b99-bf95-e5a6ea94b646&owner=ce090ecb-1fc6-4295-ab98-fb45920410c2&contentid=4078`. Online; accessed 13-August-2014.

J. Park, K. Nagapudi, C. Vergara, R. Ramachander, J. Laurence, and S. Krishnan. Effect of ph and excipients on structure, dynamics, and long-term

stability of a model IgG1 monoclonal antibody upon freeze-drying. *Pharmaceutical Research*, 30(4):968–984, 2013.

A. Parker, S. Rigby-Singleton, M. Perkins, D. Bates, D. Le Roux, C. J. Roberts, C. Madden-Smith, L. Lewis, D. L. Teagarden, R. E. Johnson, and S. S. Ahmed. Determination of the influence of primary drying rates on the microscale structural attributes and physicochemical properties of protein containing lyophilized products. *Journal of Pharmaceutical Sciences*, 99(11):4616–4629, 2010.

F. Parker. *Applications of Infrared, Raman, and Resonance Raman Spectroscopy in BioChemistry*. Plenum Press, New York, NY, 1983.

S. Passot, F. Fonseca, N. Barbouche, M. Marin, M. Alarcon-Lorca, D. Rolland, and M. Rapaud. Effect of product temperature during primary drying on the long-term stability of lyophilized proteins. *Pharmaceutical Development and Technology*, 12(6):543–553, 2007.

S. Patel, B. Lobo, and A. Shah. Practical considerations for freeze-drying process design, development and scale-up. *American Pharmaceutical Review*, 16(6), 2013.

S. M. Patel and M. J. Pikal. Lyophilization process design space. *Journal of Pharmaceutical Sciences*, 102(11):3883–3887, 2013.

S. M. Patel, C. Bhugra, and M. J. Pikal. Reduced pressure ice fog technique for controlled ice nucleation during freeze-drying. *AAPS PharmSciTech*, 10(4):1406–1411, 2009.

S. M. Patel, T. Doen, and M. J. Pikal. Determination of End Point of Primary Drying in Freeze-Drying Process Control. *AAPS PharmSciTech*, 11(1):73–84, 2010.

R. Patil. Contrast agents. In A. Ghom, editor, *Textbook of Oral Radiology*. Elsevier, New Delhi, India, 2008.

J. T. Pelton and L. R. McLean. Spectroscopic methods for analysis of protein secondary structure. *Analytical Biochemistry*, 277(2):167 – 176, 2000.

Z. Peng, K. Hidajat, and M. Uddin. Adsorption of bovine serum albumin on nanosized magnetic particles. *Journal of Colloid and Interface Science*, 271(2):277–283, 2004.

B.-H. Peters, F. Molnar, and J. Ketolainen. Structural attributes of model protein formulations prepared by rapid freeze-drying cycles in a microscale heating stage. *European Journal of Pharmaceutics and Biopharmaceutics*, 87(2):347 – 356, 2014.

T. Peters Jr. Serum albumin. *Advances in Protein Chemistry*, 37:161–245, 1985.

A. Petersen, H. Schneider, G. Rau, and B. Glasmacher. A new approach for freezing of aqueous solutions under active control of the nucleation temperature. *Cryobiology*, 53(2):248–257, 2006.

G. Petzold and J. M. Aguilera. Ice morphology: Fundamentals and technological applications in foods. *Food Biophysics*, 4(4):378–396, 2009.

Ph. Eur. method 2.2.1. *Appendix IV A. Clarity of Solution*. British Pharmacoepia Online, 2013. Online; accessed 29-April-2014.

Ph. Eur. method 2.9.19. *Appendix XIII Particulate Contamination*. British Pharmacoepia Online, 2013. Online; accessed 15-August-2014.

M. Pikal and R. R. Rambhatla. The impact of the freezing stage in lyophilization: effects of the ice nucleation temperature on process design and product quality. *American Pharmaceutical Review*, 5:48–53, 2002.

M. Pikal, S. Shah, M. Roy, and R. Putman. The secondary drying stage of freeze drying: drying kinetics as a function of temperature and chamber pressure. *International Journal of Pharmaceutics*, 60(3):203–217, 1990.

M. J. Pikal and D. Rigsbee. The stability of insulin in crystalline and amorphous solids: Observation of greater stability for the amorphous form. *Pharmaceutical Research*, 14(10):1379–1387, 1997.

M. J. Pikal and S. Shah. The collapse temperature in freeze drying: Dependence on measurement methodology and rate of water removal from the glassy phase. *International Journal of Pharmaceutics*, 62(2,3):165 – 186, 1990.

M. J. Pikal, W. J. Mascarenhas, H. U. Akay, S. Cardon, C. Bhugra, F. Jameel, and S. Rambhatla. The nonsteady state modeling of freeze drying: In-process product temperature and moisture content mapping and pharmaceutical product quality applications. *Pharmaceutical Development and Technology*, 10(1):17–32, 2005.

M. J. Pikal, D. Rigsbee, and M. Roy. Solid state chemistry of proteins: I. glass transition behavior in freeze dried disaccharide formulations of human growth hormone (hGH). *Journal of Pharmaceutical Sciences*, 96 (10):2765–2776, 2007.

M. J. Pikal, D. Rigsbee, M. L. Roy, D. Galreath, K. J. Kovach, B. S. Wang, J. F. Carpenter, and M. T. Cicerone. Solid state chemistry of proteins: II. the correlation of storage stability of freeze-dried human growth hormone (hGH) with structure and dynamics in the glassy solid. *Journal of Pharmaceutical Sciences*, 97(12):5106–5121, 2008.

S. Porter. Human immune response to recombinant human proteins. *Journal of Pharmaceutical Sciences*, 90(1):1–11, 2001.

G. Prasad and M. Vijayan. X-ray studies on crystalline complexes involving amino acids and peptides. XIX. effects of change in chirality in the complexes of succinic acid with DL- and L-arginine. *International Journal of Peptide and Protein Research*, 35(4):357–364, 1990.

S. Prestrelski, N. Tedeschi, T. Arakawa, and J. F. Carpenter. Dehydration-induced conformational transitions in proteins and their inhibition by stabilizers. *Biophysical Journal*, 65(2):661–671, 1993.

ProteinSimple. *See sub-visible particles. Micro-Flow Imaging*, 2014. URL `http://www.proteinsimple.com/literature_download.html?docid=565`. Online; accessed 13-August-2014.

R Core Team. *R: A Language and Environment for Statistical Computing*. R Foundation for Statistical Computing, Vienna, Austria, 2012. URL `http://www.R-project.org/`. ISBN 3-900051-07-0.

S. Rambhatla and M. J. Pikal. Heat and mass transfer scale-up issues during freeze-drying, I: Atypical radiation and the edge vial effect. *AAPS PharmSciTech*, 4(2):22–31, 2003.

S. Rambhatla and M. J. Pikal. Heat and mass transfer issues in freeze-drying process development. In H. Costantino and M. Pikal, editors, *Lyophilization of biopharmaceuticals*, pages 75–109. American Association of Pharmaceutical Scientists, Arlington, VA, 2004.

S. Rambhatla, R. Ramot, C. Bhugra, and M. J. Pikal. Heat and mass transfer scale-up issues during freeze-drying, II: Control and characterization of the degree of supercooling. *AAPS PharmSciTech*, 5(4):54–62, 2004.

S. Rambhatla, J. Obert, S. Luthra, C. Bhugra, and M. Pikal. Cake shrinkage during freeze drying: A combined experimental and theoretical study. *Pharmaceutical Development and Technology*, 10(1):33–40, 2005.

T. W. Randolph. Phase separation of excipients during lyophilization: Effects on protein stability. *Journal of Pharmaceutical Sciences*, 86(11): 1198–1203, 1997.

A. Rathore and H. Winkle. Quality by design for biopharmaceuticals. *Nature Biotechnology*, 27(1):26–34, 2009.

A. S. Rathore. Roadmap for implementation of quality by design (QbD) for biotechnology products. *Trends in Biotechnology*, 27(9):546–553, 2009.

R. C. Reddy K., H. Lilie, R. Rudolph, and C. Lange. L-arginine increases the solubility of unfolded species of hen egg white lysozyme. *Protein Science*, 14(4):929–935, 2005.

J. M. Reichert. Monoclonal antibodies as innovative therapeutics. *Current Pharmaceutical Biotechnology*, 9(6):423–430, 2008.

L. Reimer. *Scanning Electron Microscopy: Physics of Image Formation and Microanalysis*. Springer-Verlag, Berlin, Germany, 1998.

G. S. Rohrer. Influence of interface anisotropy on grain growth and coarsening. *Annual Review of Materials Research*, 35(1):99–126, 2005.

G. S. Rohrer, C. L. Rohrer, and W. W. Mullins. Coarsening of faceted crystals. *Journal of the American Ceramic Society*, 85(3):675–682, 2002.

E. Romero and P. H. Simms. Microstructure investigation in unsaturated soils: A review with special attention to contribution of mercury intrusion porosimetry and environmental scanning electron microscopy. *Geotechnical and Geological Engineering*, 26(6):705–727, 2008.

C. A. Ross and M. A. Poirier. Protein aggregation and neurodegenerative disease. *Nature Medicine*, 10:S10–S17, 2004.

S. Roy, D. D. Singh, and M. Vijayan. X-ray studies on crystalline complexes involving amino acids and peptides. XLII. Adipic acid complexes of L- and DL-arginine and supramolecular association in arginine–dicarboxylic acid complexes. *Acta Crystallographica Section B*, 61(1):89–95, 2005.

P. G. Royall, C.-y. Huang, S.-w. J. Tang, J. Duncan, G. Van-de Velde, and M. B. Brown. The development of DMA for the detection of amorphous content in pharmaceutical powdered materials. *International Journal of Pharmaceutics*, 301(1–2):181–191, 2005.

RSC. *The Merck Index Online*. Royal Society of Chemistry, 2014. URL `https://www.rsc.org/merck-index`. [Online; accessed 2-August-2014].

R. Salaman, W. Burton, and J. Hawkes. *The History and Social Influence of the Potato*. Cambridge University Press, Cambridge, UK, 1985.

S. Sane and C. Hsu. Considerations for successful lyophilization process scale-up, technology transfer and routine production. In F. Jameel and S. Hershenson, editors, *Formulation and Process Development Strategies for Manufacturing Biopharmaceuticals*. John Wiley & Sons, Inc., Hoboken, NJ, 2010.

T. Sano and G. S. Rohrer. Experimental evidence for the development of bimodal grain size distributions by the nucleation-limited coarsening mechanism. *Journal of the American Ceramic Society*, 90(1):211–216, 2007.

P. Sarangapani, S. Hudson, K. Migler, and J. Pathak. The limitations of an exclusively colloidal view of protein solution hydrodynamics and rheology. *Biophysical Journal*, 105(10):2418–2426, 2013. [Supplementary information].

N. T. Saraswathi and M. Vijayan. X-ray studies on crystalline complexes involving amino acids and peptides. XXXVIII. crystal structures of the complexes of L-arginine and L-histidine with glutaric acid and a comparative study of amino acid–glutaric acid complexes. *Acta Crystallographica Section B*, 57(6):842–849, 2001.

N. T. Saraswathi, S. Roy, and M. Vijayan. X-ray studies on crystalline complexes involving amino acids and peptides. XLI. Commonalities in aggregation and conformation revealed by the crystal structures of the pimelic acid complexes of L-arginine and DL-lysine. *Acta Crystallographica Section B*, 59(5):641–646, 2003.

J. Sarciaux, S. Mansour, M. Hageman, and S. Nail. Effects of buffer composition and processing conditions on aggregation of bovine IgG during freeze-drying. *Journal of Pharmaceutical Sciences*, 88(12):1354–1361, 1999.

M. Saunders and P. Gabbott. Thermal analysis -conventional techniques. In R. Storey and I. Ymen, editors, *Solid State Characterization of Pharmaceuticals*, pages 135–186. Blackwell Publishing, West Sussex, UK, 2011.

K. Schersch, O. Betz, P. Garidel, S. Muehlau, S. Bassarab, and G. Winter. Systematic investigation of the effect of lyophilizate collapse on pharmaceutically relevant proteins I: Stability after freeze-drying. *Journal of Pharmaceutical Sciences*, 99(5):2256–2278, 2010.

J. Schindelin, I. Arganda-Carreras, E. Frise, V. Kaynig, M. Longair, T. Pietzsch, S. Preibisch, C. Rueden, S. Saalfeld, B. Schmid, J.-Y. Tinevez, D. J. White, V. Hartenstein, K. Eliceiri, P. Tomancak, and A. Cardona. Fiji: an open-source platform for biological-image analysis. *Nature Methods*, 9 (7):676–682, 2012.

C. P. Schneider, D. Shukla, and B. L. Trout. Arginine and the hofmeister series: The role of ion-ion interactions in protein aggregation suppression. *The Journal of Physical Chemistry B*, 115(22):7447–7458, 2011.

J. Searles, J. Carpenter, and T. Randolph. Annealing to optimize the primary drying rate, reduce freezing-induced drying rate heterogeneity, and determine Tg′ in pharmaceutical lyophilization. *Journal of Pharmaceutical Sciences*, 90(7):872–887, 2001a.

J. A. Searles, J. F. Carpenter, and T. W. Randolph. The ice nucleation temperature determines the primary drying rate of lyophilization for samples frozen on a temperature-controlled shelf. *Journal of Pharmaceutical Sciences*, 90(7):860–871, 2001b.

D. Shah, A. R. Shaikh, X. Peng, and R. Rajagopalan. Effects of arginine on heat-induced aggregation of concentrated protein solutions. *Biotechnology Progress*, 27(2):513–520, 2011.

D. Shah, J. Li, A. R. Shaikh, and R. Rajagopalan. Arginine-aromatic interactions and their effects on arginine-induced solubilization of aromatic solutes and suppression of protein aggregation. *Biotechnology Progress*, 28(1):223–231, 2012.

D. K. Sharma, P. Oma, M. J. Pollo, and M. Sukumar. Quantification and characterization of subvisible proteinaceous particles in opalescent mab formulations using micro-flow imaging. *Journal of Pharmaceutical Sciences*, 99(6):2628–2642, 2010.

V. K. Sharma and D. S. Kalonia. Experimental detection and characterization of protein aggregates. In W. Wang and C. J. Roberts, editors, *Aggregation of Therapeutic Proteins*, pages 205–256. John Wiley & Sons, Inc., Hoboken, NJ, 2010.

S. J. Shire, Z. Shahrokh, and J. Liu. Challenges in the development of high protein concentration formulations. *Journal of Pharmaceutical Sciences*, 93(6):1390–1402, 2004.

S. J. Shire, W. Gombotz, K. Bechtold-Peters, and J. Andya. *Current Trends in Monoclonal Antibody Development and Manufacturing*. American Association of Pharmaceutical Scientists, Arlington, VA, 2010.

D. Shukla and B. L. Trout. Interaction of arginine with proteins and the mechanism by which it inhibits aggregation. *The Journal of Physical Chemistry B*, 114(42):13426–13438, 2010.

D. Shukla and B. L. Trout. Understanding the synergistic effect of arginine and glutamic acid mixtures on protein solubility. *The Journal of Physical Chemistry B*, 115(41):11831–11839, 2011.

D. Shukla, C. P. Schneider, and B. L. Trout. Complex interactions between molecular ions in solution and their effect on protein stability. *Journal of the American Chemical Society*, 133(46):18713–18718, 2011a.

D. Shukla, L. Zamolo, C. Cavallotti, and B. L. Trout. Understanding the role of arginine as an eluent in affinity chromatography via molecular computations. *The Journal of Physical Chemistry B*, 115(11):2645–2654, 2011b.

M. L. Shulman, M. C. Jacobson, R. J. Carlson, R. E. Synovec, and T. E. Young. Dissolution behavior and surface tension effects of organic compounds in nucleating cloud droplets. *Geophysical Research Letters*, 23(3): 277–280, 1996.

Sigma-Aldrich. *Bovine Serum Albumins*. Sigma-Aldrich Co. LLC., 2014. URL `http://www.sigmaaldrich.com/life-science/biochemicals/biochemical-products.html?TablePage=103994915`. [Online; accessed 19-September-2014].

B. R. Simler, G. Hui, J. E. Dahl, and B. Perez-Ramirez. Mechanistic complexity of subvisible particle formation: Links to protein aggregation are highly specific. *Journal of Pharmaceutical Sciences*, 101(11):4140–4154, 2012.

K. S. W. Sing, D. H. Everett, R. A. W. Haul, L. Moscou, R. A. Pierotti, and T. Rouquerol, J.and Siemieniewska. Reporting physisorption data for gas/solid systems with special reference to the determination of surface area and porosity (recommendations 1984). *Pure and Applied Chemistry*, 57(4):603–619, 1985.

S. K. Singh. Impact of product-related factors on immunogenicity of biotherapeutics. *Journal of Pharmaceutical Sciences*, 100(2):354–387, 2011.

S. K. Singh, P. Kolhe, W. Wang, and S. Nema. Large-scale freezing of biologics. A practitioner's review, part one: Fundamental aspects. *BioProcess International*, 7(10):34–42, 2009.

B. Sivasankar. Finishing operations and formulation. In *Bioseparations: Principals and Techniques*. PHI Learning, New Delhi, India, 2005.

B. Sixou, A. Faivre, L. David, and G. Vigier. Intermolecular and intramolecular contributions to the relaxation process in sorbitol and maltitol. *Molecular Physics*, 99(22):1845–1850, 2001.

W. Stacklies, H. Redestig, M. Scholz, D. Walther, and J. Selbig. pcaMethods – a Bioconductor package providing PCA methods for incomplete data. *Bioinformatics*, 23:1164–1167, 2007.

S. Stock. *MicroComputed Tomography: Methodology and Applications*. Taylor & Francis, Boca Raton, FL, 2008.

H. Stoker. *Organic and Biological Chemistry*. Cengage Learning, Belmont, CA, 2009.

G. Strambini and E. Gabellieri. Proteins in frozen solutions: evidence of ice-induced partial unfolding. *Biophysical Journal*, 70(2):971–976, 1996.

R. Strehl, V. Rombach-Riegraf, M. Diez, K. Egodage, M. Bluemel, M. Jeschke, and A. V. Koulov. Discrimination between silicone oil droplets and protein aggregates in biopharmaceuticals: A novel multiparametric image filter for sub-visible particles in microflow imaging analysis. *Pharmaceutical Research*, 29(2):594–602, 2012.

W. Q. Sun, P. Davidson, and H. S. Chan. Protein stability in the amorphous carbohydrate matrix: relevance to anhydrobiosis. *Biochimica et Biophysica Acta (BBA) - General Subjects*, 1425(1):245 – 254, 1998.

J. Sundaram, C. C. Hsu, Y.-H. M. Shay, and S. U. Sane. Design space development for lyophilization using doe and process modeling. *BioPharm International*, 23(9), 2010.

P. Sundaramurthi and R. Suryanarayanan. Influence of crystallizing and non-crystallizing cosolutes on trehalose crystallization during freeze-drying. *Pharmaceutical Research*, 27(11):2384–2393, 2010.

P. Sundaramurthi and R. Suryanarayanan. Calorimetry and complementary techniques to characterize frozen and freeze-dried systems. *Advanced Drug Delivery Reviews*, 64(5):384 – 395, 2012.

TA Instruments. *Q200 Product Brochure*, 2014. URL `http://www.tainstruments.com/product.aspx?id=16&n=1&siteid=11`. Online; accessed 13-August-2014.

K. Talley and E. Alexov. On the pH-optimum of activity and stability of proteins. *Proteins: Structure, Function, and Bioinformatics*, 78(12): 2699–2706, 2010.

X. Tang, S. L. Nail, and M. J. Pikal. Evaluation of manometric temperature measurement, a process analytical technology tool for freeze-drying: Part I, product temperature measurement. *AAPS PharmSciTech*, 7(1):E95–E103, 2006.

X. C. Tang and M. Pikal. Design of freeze-drying processes for pharmaceuticals: Practical advice. *Pharmaceutical Research*, 21(2):191–200, 2004.

S. N. Telikepalli, O. S. Kumru, C. Kalonia, R. Esfandiary, S. B. Joshi, C. R. Middaugh, and D. B. Volkin. Structural characterization of IgG1 mAb aggregates and particles generated under various stress conditions. *Journal of Pharmaceutical Sciences*, 103(3):796–809, 2014.

L. Thomas. *Modulated DSC Paper 8 Use Of Quasi-isothermal Mode for Improved Understanding of Structure Change*. TA Instruments, 2005. URL `http://www.tainstruments.com/main.aspx?n=2&id=181&main_id=898&siteid=18`. Online; accessed 15-August-2014.

F. Tian, S. Sane, and J. H. Rytting. Calorimetric investigation of protein/amino acid interactions in the solid state. *International Journal of Pharmaceutics*, 310(1–2):175–186, 2006.

E. Trappler. Lyophilization equipment. In H. Costantino and M. Pikal, editors, *Lyophilization of biopharmaceuticals*, pages 3–41. American Association of Pharmaceutical Scientists, Arlington, VA, 2004.

D. Troy, J. Remington, and P. Beringer. *Remington: The Science and Practice of Pharmacy*. Lippincott Williams & Wilkins, Philadelphia, PA, 2006.

K. Tsumoto, M. Umetsu, I. Kumagai, D. Ejima, J. S. Philo, and T. Arakawa. Role of arginine in protein refolding, solubilization, and purification. *Biotechnology Progress*, 20(5):1301–1308, 2004.

USP <1787>. *In-Process Revision: <1787> Measurement of Subvisible Particulate Matter in Therapeutic Protein Injections*. Pharmacopeial Forum 39(6), 2013. Online; accessed 12-May-2014.

V. Vagenende, A. X. Han, M. Mueller, and B. L. Trout. Protein-associated cation clusters in aqueous arginine solutions and their effects on protein stability and size. *ACS Chemical Biology*, 8(2):416–422, 2013.

P. Varlashkin. Approaches to quantification of amorphous content in crystalline drug substance by powder X-ray diffraction. *American Pharmaceutical Review*, 14(1), 2011.

S. A. Velardi and A. A. Barresi. Development of simplified models for the freeze-drying process and investigation of the optimal operating conditions. *Chemical Engineering Research and Design*, 86(1):9–22, 2008.

C. Wagner. Theorie der Alterung von Niederschlägen durch Umlösen (Ostwald-Reifung). *Zeitschrift für Elektrochemie, Berichte der Bunsengesellschaft für physikalische Chemie*, 65(7–8):581–591, 1961.

G. Walsh. *Pharmaceutical Biotechnology: Concepts and Applications*. John Wiley & Sons, West Sussex, UK, 2007.

R. H. Walters, B. Bhatnagar, S. Tchessalov, K.-I. Izutsu, K. Tsumoto, and S. Ohtake. Next generation drying technologies for pharmaceutical applications. *Journal of Pharmaceutical Sciences*, 103(9):2673–2695, 2014.

B. Wang and M. J. Pikal. The impact of thermal treatment on the stability of freeze dried amorphous pharmaceuticals: I. dimer formation in sodium ethacrynate. *Journal of Pharmaceutical Sciences*, 99(2):663–682, 2010.

B. Wang, S. Tchessalov, M. T. Cicerone, N. W. Warne, and M. J. Pikal. Impact of sucrose level on storage stability of proteins in freeze-dried solids: II. correlation of aggregation rate with protein structure and molecular mobility. *Journal of Pharmaceutical Sciences*, 98(9):3145–3166, 2009.

B. Wang, M. T. Cicerone, Y. Aso, and M. J. Pikal. The impact of thermal treatment on the stability of freeze-dried amorphous pharmaceuticals: II. aggregation in an IgG1 fusion protein. *Journal of Pharmaceutical Sciences*, 99(2):683–700, 2010.

W. Wang. Instability, stabilization, and formulation of liquid protein pharmaceuticals. *International Journal of Pharmaceutics*, 185(2):129–188, 1999.

W. Wang. Lyophilization and development of solid protein pharmaceuticals. *International Journal of Pharmaceutics*, 203(1-2):1 – 60, 2000.

W. Wang. Protein aggregation and its inhibition in biopharmaceutics. *International Journal of Pharmaceutics*, 289(1–2):1–30, 2005.

Y. Wang, H. Yu, X. Shi, Z. Luo, D. Lin, and M. Huang. Structural mechanism of ring-opening reaction of glucose by human serum albumin. *Journal of Biological Chemistry*, 288(22):15980–15987, 2013.

E. W. Washburn. The dynamics of capillary flow. *Physical Review*, 17: 273–283, 1921a.

E. W. Washburn. Note on a method of determining the distribution of pore sizes in a porous material. *Proceedings of the National Academy of Sciences*, 7(4):115–116, 1921b.

D. G. Watson. *Pharmaceutical Analysis, A Textbook for Pharmacy Students and Pharmaceutical Chemists,3: Pharmaceutical Analysis*. Elsevier Ltd., London, UK, 2012.

P. Webb and C. Orr. *Analytical Methods in Fine Powder Particle Technology*. Micromeritics Instrument Corp., Norcross, GA, 1997.

S. Webb, J. Cleland, J. Carpenter, and T. Randolph. Effects of annealing lyophilized and spray-lyophilized formulations of recombinant human interferon-γ. *Journal of Pharmaceutical Sciences*, 92(4):715–729, 2003.

S. D. Webb, J. L. Cleland, J. F. Carpenter, and T. W. Randolph. A new mechanism for decreasing aggregation of recombinant human interferon-γ by a surfactant: Slowed dissolution of lyophilized formulations in a solution containing 0.03% polysorbate 20. *Journal of Pharmaceutical Sciences*, 91(2):543–558, 2002a.

S. D. Webb, S. L. Golledge, J. L. Cleland, J. F. Carpenter, and T. W. Randolph. Surface adsorption of recombinant human interferon-γ in lyophilized and spray-lyophilized formulations. *Journal of Pharmaceutical Sciences*, 91(6):1474–1487, 2002b.

R. Weissleder and S. Gambhir. *Molecular Imaging: Principles and Practice*. Molecular Imaging: Principles and Practice. People's Medical Publishing House, Shelton, CT, 2010.

J. Wells. *Pharmaceutical Preformulation. The Physicochemical Propoerties of Drug Substances*. John Wiley & Sons, Chichester, UK, 1988.

D. Whitford. *Proteins: Structure and Function*. John Wiley & Sons, Chichester, UK, 2005.

A. Wierzbicki, P. Dalal, T. E. Cheatham, J. E. Knickelbein, A. D. J. Haymet, and J. D. Madura. Antifreeze proteins at the ice/water interface: Three calculated discriminating properties for orientation of type I proteins. *Biophysical Journal*, 93(5):1442–1451, 2007.

R. J. Williams and D. E. Bause. Elemental and chemical analysis. In J. P. Sibilia, editor, *A guide to materials characterization and chemical analysis*, pages 115–166. Wiley-VCH, Inc., New York, NY, 1996.

T. Wu and L. Yu. Surface crystallization of indomethacin below Tg. *Pharmaceutical Research*, 23(10):2350–2355, 2006.

Q. Xie, T. Guo, J. Lu, and H.-M. Zhou. The guanidine like effects of arginine on aminoacylase and salt-induced molten globule state. *The International Journal of Biochemistry & Cell Biology*, 36(2):296 – 306, 2004.

Y. Xu, J. F. Carpenter, M. T. Cicerone, and T. W. Randolph. Contributions of local mobility and degree of retention of native secondary structure to the stability of recombinant human growth hormone (rhGH) in glassy lyophilized formulations. *Soft Matter*, 9:7855–7865, 2013.

Y. Xu, P. Grobelny, A. Von Allmen, K. Knudson, M. Pikal, J. F. Carpenter, and T. W. Randolph. Protein quantity on the air-solid interface determines degradation rates of human growth hormone in lyophilized samples. *Journal of Pharmaceutical Sciences*, 103(5):1356–1366, 2014.

T. Yamaki, R. Ohdate, E. Nakadai, Y. Yoshihashi, E. Yonemochi, K. Terada, H. Moriyama, K.-i. Izutsu, C. Yomota, H. Okuda, and T. Kawanishi. Component crystallization and physical collapse during freeze-drying of L-arginine-citric acid mixtures. *Chemical and Pharmaceutical Bulletin*, 60(9):1176–1181, 2012.

L. Yin. X-ray computerized microtomography. In G. W. Padua and Q. Wang, editors, *Nanotechnology Research Methods for Food and Bioproducts*, pages 215–234. John Wiley & Sons, West Sussex, UK, 2012.

S. Yoshioka and Y. Aso. A quantitative assessment of the significance of molecular mobility as a determinant for the stability of lyophilized insulin formulations. *Pharmaceutical Research*, 22(8):1358–1364, 2005.

S. Yoshioka and Y. Aso. Correlations between molecular mobility and chemical stability during storage of amorphous pharmaceuticals. *Journal of Pharmaceutical Sciences*, 96(5):960–981, 2007.

S. Yoshioka, Y. Aso, and S. Kojima. Usefulness of the kohlrausch-williams-watts stretched exponential function to describe protein aggregation in lyophilized formulations and the temperature dependence near the glass transition temperature. *Pharmaceutical Research*, 18(3):256–260, 2001.

S. Yoshioka, T. Miyazaki, Y. Aso, and T. Kawanishi. Significance of local mobility in aggregation of β-galactosidase lyophilized with trehalose, sucrose or stachyose. *Pharmaceutical Research*, 24(9):1660–1667, 2007.

L. Yu. Amorphous pharmaceutical solids: preparation, characterization and stabilization. *Advanced Drug Delivery Reviews*, 48(1):27–42, 2001.

X. Yu, S. Kappes, L. Bello-Perez, and S. Schmidt. Investigating the moisture sorption behavior of amorphous sucrose using a dynamic humidity generating instrument. *Journal of Food Science*, 73(1):E25–E35, 2008.

J. G. Zeikus, M. K. Jain, and P. Elankovan. Biotechnology of succinic acid production and markets for derived industrial products. *Applied Microbiology and Biotechnology*, 51(5):545–552, 1999.

L. Zhu, L. Wong, and L. Yu. Surface-enhanced crystallization of amorphous nifedipine. *Molecular Pharmaceutics*, 5(6):921–926, 2008.

L. Zhu, J. Jona, K. Nagapudi, and T. Wu. Fast surface crystallization of amorphous griseofulvin below Tg. *Pharmaceutical Research*, 27(8):1558–1567, 2010.

A. S. Zidan, O. A. Sammour, M. A. Hammad, N. A. Megrab, M. J. Habib, and M. A. Khan. Quality by design: Understanding the formulation variables of a cyclosporine a self-nanoemulsified drug delivery systems by Box-Behnken design and desirability function. *International Journal of Pharmaceutics*, 332(1–2):55–63, 2007.

S. Zölls, M. Gregoritza, R. Tantipolphan, M. Wiggenhorn, G. Winter, W. Friess, and A. Hawe. How subvisible particles become invisible-relevance of the refractive index for protein particle analysis. *Journal of Pharmaceutical Sciences*, 102(5):1434–1446, 2013a.

S. Zölls, D. Weinbuch, M. Wiggenhorn, G. Winter, W. Friess, W. Jiskoot, and A. Hawe. Flow imaging microscopy for protein particle analysis - a comparative evaluation of four different analytical instruments. *The AAPS Journal*, 15(4):1200–1211, 2013b.

J.-G. Zuo, T.-C. Hua, B.-L. Liu, and G.-Y. Zhou. Thermal analysis of tertiary butyl alcohol/sucrose/water ternary system. *Cryoletters*, 26(5): 289–296, 2005.